AD-A188 724 STIMULATED EMISSION OF ENERGETIC PARTICLES (SEEP)(U) 1/3
LOCKHEED MISSILES AND SPACE CO INC PALO ALTO CA PALO
ALTO RESEARCH LAB W L IMHOF ET AL. 30 NOV 87
UNCLASSIFIED LMSC/D060456 N00014-79-C-0024 F/G 4/1 NL

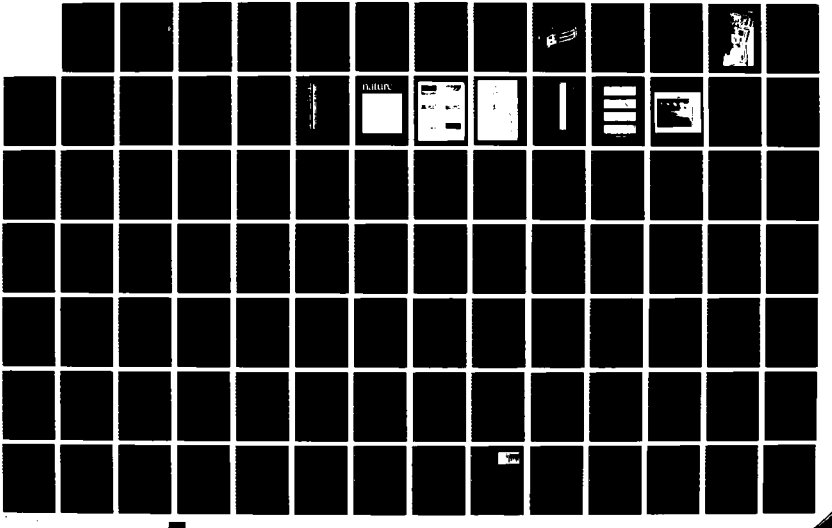

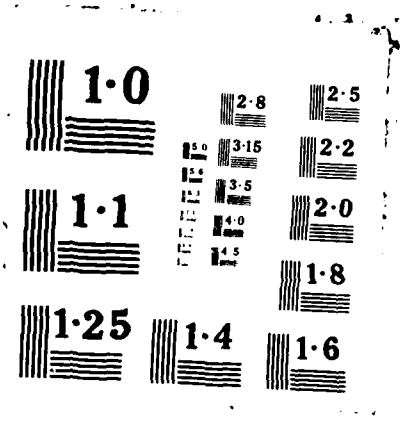
1·0
1·1
1·25
1·4
1·6
1·8
2·0
2·2
2·5
2·8
3·15
3·5
4·0
4·5

AD-A188 724

LMSC/D068456

(4)

FINAL REPORT

For Period Ending 30 September 1987

Contract N00014-79-C-0824

DTIC FILE COPY

STIMULATED EMISSION OF ENERGETIC PARTICLES (SEEP)

*Original contains color plates: All DTIC reproductions will be in black and white.

W. L. IMHOF
H. D. VOSS
J. MOBILIA
D. W. DATLOWE
E. E. GAINES

DTIC
ELECTE
DEC 09 1987
S D

Lockheed Palo Alto Research Laboratory
3251 Hanover Street
Palo Alto, California 94304

UNLIMITED DISTRIBUTION ; CLEARED FOR PUBLIC RELEASE AND SALE

30 November 1987

Final Report
Contract N00014-79-C-0824

Prepared for:
Office of Naval Research
800 North Quincy Street
Arlington, Virginia 22217

87 12 1 015

LMSC/D068456

FINAL REPORT

For Period Ending 30 September 1987

Contract N00014-79-C-0824

STIMULATED EMISSION OF ENERGETIC PARTICLES (SEEP)

W. L. IMHOF
H. D. VOSS
J. MOBILIA
D. W. DATLOWE
E. E. GAINES

Lockheed Palo Alto Research Laboratory
3251 Hanover Street
Palo Alto, California 94304

UNLIMITED DISTRIBUTION ; CLEARED FOR PUBLIC RELEASE AND SALE

30 November 1987

Final Report
Contract N00014-79-C-0824

Prepared for:
Office of Naval Research
800 North Quincy Street
Arlington, Virginia 22217

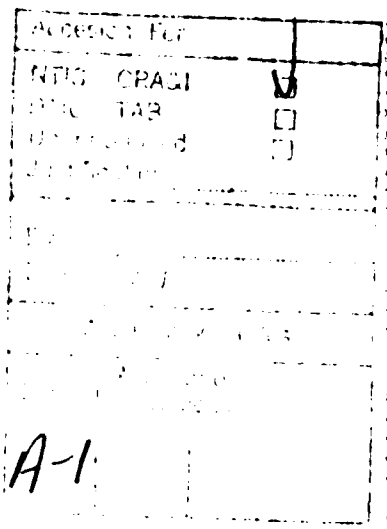

FINAL REPORT

(For Period Ending 30 September 1987)

Contract N00014-79-C-0824

STIMULATED EMISSION OF ENERGETIC PARTICLES (SEEP)

Contractor: Lockheed Missiles and Space Company

Principal Investigator: W. L. Imhof

(415) 424-3252

Conclusion Date of Contract: 30 September 1987

Contract Amount: $2,016,682

Sponsored by Office of Naval Research

30 November 1987

SEEP FINAL REPORT

SECURITY CLASSIFICATION OF THIS PAGE

REPORT DOCUMENTATION PAGE

Form Approved OMB No. 0704-0188

AD-A188 724

1a. REPORT SECURITY CLASSIFICATION UNCLASSIFIED	1b. RESTRICTIVE MARKINGS
2a. SECURITY CLASSIFICATION AUTHORITY	3. DISTRIBUTION/AVAILABILITY OF REPORT Unlimited; cleared for public release and sale.
2b. DECLASSIFICATION/DOWNGRADING SCHEDULE	
4. PERFORMING ORGANIZATION REPORT NUMBER(S) LMSC/D068456	5. MONITORING ORGANIZATION REPORT NUMBER(S)
6a. NAME OF PERFORMING ORGANIZATION LOCKHEED PALO ALTO RESEARCH LABORATORY 6b. OFFICE SYMBOL (If applicable)	7a. NAME OF MONITORING ORGANIZATION
6c. ADDRESS (City, State, and ZIP Code) 3251 HANOVER STREET, BUILDING 255 PALO ALTO, CALIFORNIA 94304	7b. ADDRESS (City, State, and ZIP Code)
8a. NAME OF FUNDING/SPONSORING OFFICE OF NAVAL RESEARCH DEPARTMENT OF THE NAVY 8b. OFFICE SYMBOL (If applicable) Code 1114	9. PROCUREMENT INSTRUMENT IDENTIFICATION NUMBER CONTRACT N00014-79-C-0824
8c. ADDRESS (City, State, and ZIP Code) 800 NORTH QUINCY STREET ARLINGTON, VIRGINIA 22217-5000	10. SOURCE OF FUNDING NUMBERS PROGRAM ELEMENT NO. 61153N; PROJECT NO.; TASK NO; WORK UNIT ACCESSION NO NR089-138

11. TITLE (Include Security Classification)
STIMULATED EMISSION OF ENERGETIC PARTICLES (SEEP)

12. PERSONAL AUTHOR(S)
Imhof, William L.; Voss, Henry D.; Mobilia, Joseph; Datlowe, Dayton W.; Gaines, Edward E.

13a. TYPE OF REPORT	13b. TIME COVERED	14. DATE OF REPORT (Year, Month, Day)	15. PAGE COUNT
FINAL REPORT	FROM 1 Aug 79 TO 30 Nov 87	1987, November 30	

16. SUPPLEMENTARY NOTATION

17. COSATI CODES			18. SUBJECT TERMS (Continue on reverse if necessary and identify by block number)
FIELD	GROUP	SUB-GROUP	Satellite Payload; Electron Precipitation; Satellite Flight; Modulation of VLF Transmitters; Active Experiment
17	02	0.1	
20	14		

19. ABSTRACT (Continue on reverse if necessary and identify by block number)

An active satellite-ground coordinated space plasma experiment was conducted from May to December, 1982, in which electrons were precipitated from the radiation belts into the ionosphere by the controlled injection of VLF signals from ground-based transmitters. In this experiment Stimulated Emission of Energetic Particles (SEEP), the U. S. Navy operational VLF transmitters at Cutler, Maine (NAA); Annapolis, Maryland (NSS); and Jim Creek, Washington (NLK) and the Stanford University research VLF transmitter at Siple Station, Antarctica, were operated in special controlled formats at times of overpasses of the low-altitude polar-orbiting satellite S81-1. The results confirm the hypothesis that electrons can be precipitated from the radiation belts by ground-based VLF transmitters, and they provide information relating to the effects of such precipitation on the ionosphere. In addition, the precipitation of electrons by VLF waves associated with lightning was measured for the first time from a satellite. Many other important findings were made with the SEEP data. These include the following: 1) An assessment was made of the relative contributions of hiss,

(see reverse side)

20. DISTRIBUTION/AVAILABILITY OF ABSTRACT ☐ UNCLASSIFIED/UNLIMITED ☒ SAME AS RPT ☐ DTIC USERS	21. ABSTRACT SECURITY CLASSIFICATION UNCLASSIFIED
22a. NAME OF RESPONSIBLE INDIVIDUAL	22b. TELEPHONE (Include Area Code) / 22c. OFFICE SYMBOL

DD Form 1473, JUN 86 — Previous editions are obsolete — SECURITY CLASSIFICATION OF THIS PAGE

19. Abstract (continued)

lightning and VLF transmitter waves to electron precipitation from the slot region, 2) discovery of the frequent occurrence of multiple peaks in the energy spectra of electrons trapped at low altitudes, 3) observation of electron pulsations near the trapping boundary and 4) discovery of bremsstrahlung x-ray images of small isolated patches of energetic electron precipitation at high latitude.

TABLE OF CONTENTS

SEEP FINAL REPORT

I. OBJECTIVES OF THE SEEP PROGRAM

The SEEP (Stimulated Emission of Energetic Particles) program had important military and scientific objectives. These are summarized as follows:

Military:

- o Investigate the potential of controlled, transmitter-stimulated wave-particle interactions in the magnetosphere as techniques for:
  - (1) Degrading/blacking out critical U.S. Navy Communication and Navigation Links Operating at HF, VLF and ELF through the selective precipitation of energetic electrons from the earth's radiation belts.
  - (2) Jamming of VLF commnunications with ground-or satellite-based VLF transmitter signals that are amplified in the magnetosphere.
  - (3) Depleting the intense trapped radiation belts created by a high altitude nuclear burst.

Scientific:

- o Test the theory predicting that ground-based VLF transmissions can precipitate radiation belt particles into the ionosphere/atmosphere.
- o Establish experimentally the detailed relationship between ground-based VLF transmitter activity (i.e. operating frequency, signal strength, pulse duration and duty cycle) and the characteristics of the resulting precipitation (intensity, energy and pitch angle distribution).

The experiment concept is illustrated schematically in Figure 1. The locations of the VLF transmitters are indicated along with a representation of the satellite paths during three successive passes. In addition, the

SEEP EXPERIMENT CONCEPT

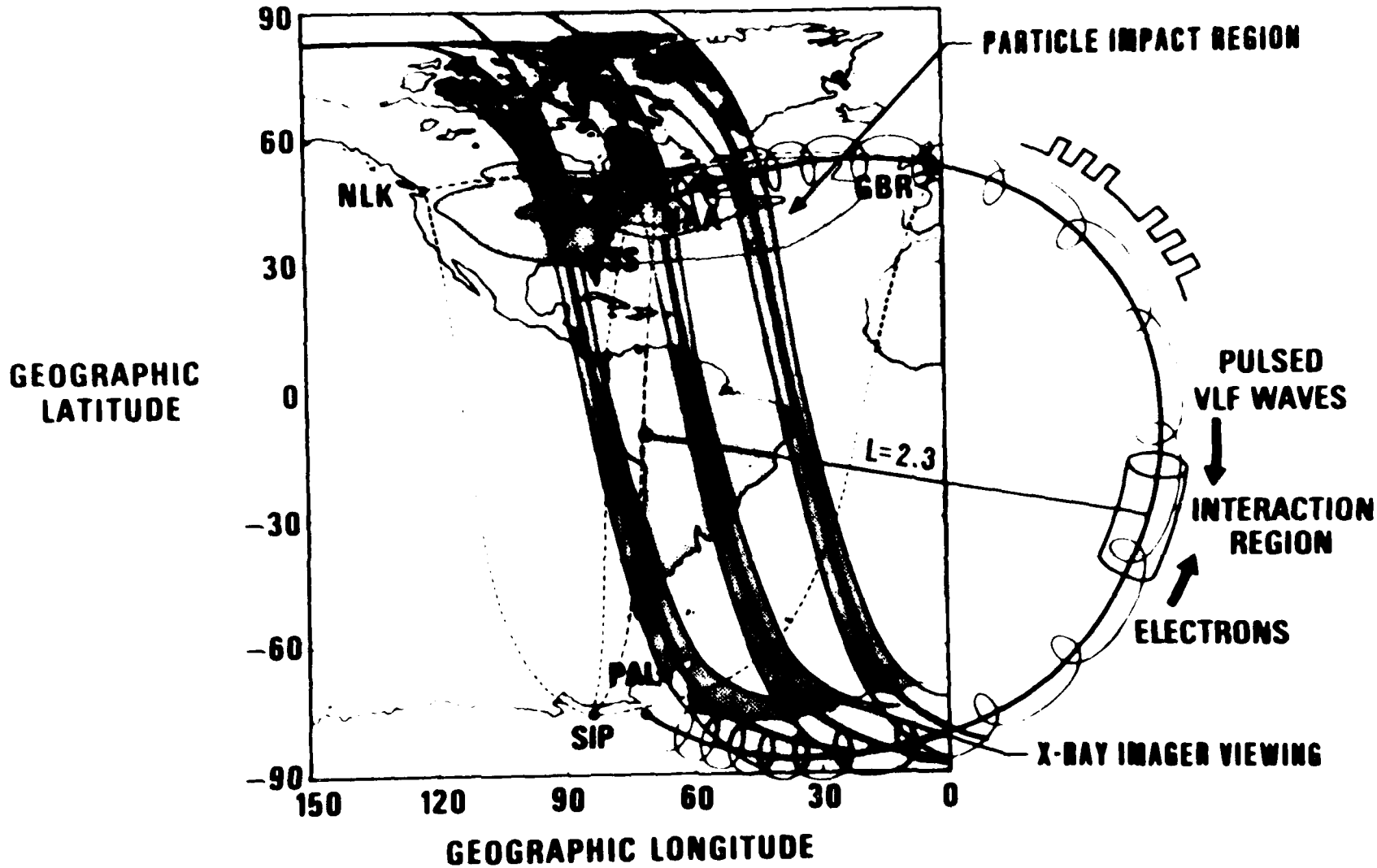

Figure 1

modulated VLF waves and their regions of interaction with the trapped electrons are also shown.

II. HISTORY OF THE SEEP PROGRAM

The SEEP experiment was conducted on the S81-1 spacecraft. The history of the program is briefly summarized as follows:

Early 77	SEEP experiment proposed
Mid 77	Designated ONR-804
Aug 77	Rated category 1 by USN
Nov 77	Rated category 1 by DOD
Oct 78	SEEP study initiated
May 79	Piggy-back flight opportunity identified
Aug 79	USAF STP recommended merger with ONR-602
Sept 79	S81-1 mission combining ONR-804 and ONR-602 approved; flight assigned; design phase initiated
Oct 79	Integration go-ahead through HVIC (ECP 142)
Jan 80	S81-1 design review conducted; fabrication phase initiated
Feb 80	Interface control document with ONR-602 and with host vehicle signed
July 80	Integration and test phase initiated
Oct 80	HV interface verified at module test lab
Dec 80	EMC test with HV completed
Feb 81	Box-level environmental test program completed
Apr 81	Acceptance testing of integrated payload completed (thermal-vacuum and acoustic vibration)
May 81	Payload placed in storage, instruments returned to investigators
July 81	EFROP approved
Aug 81	Acceptance review conducted
Sept 81	Payload taken out of storage
Oct 81	Reintegration of instruments
Nov 81	Integrated pallet tests
Dec 81	Call-up readiness review
Jan 82	Payload delivery
May 82	Launch activities completed
May-Dec 82	On-orbit operations
82-87	Data analysis and interpretation

III. INSTRUMENT DEVELOPMENT

In order to investigate the relationship between radio waves from high power VLF transmitters and energetic particles in the magnetosphere, the intensities, energy spectra and pitch angle distributions of electrons over a wide range of energies were measured in the vicinity of several transmitters. Both electrons and ions were measured with an array of charged particle detectors that were developed specifically to achieve a high sensitivity. The characteristics of these detectors are summarized in Table 1.

Since electrons may be precipitated by VLF transmitters in narrow ducted regions over a large area it was considered important to detect electron precipitation by remote sensing techniques. For this purpose an airglow photometer was flown to sense emissions from the atmosphere at 391.4 nm and at 630 nm. In addition, an x-ray imaging spectrometer (XRIS) was included in the payload to map the production of bremsstrahlung x-rays (4 to 40 keV) by electrons precipitating into the atmosphere. Some of the key specifications of these instruments are listed in Table 1. A photograph of the instruments mounted on the payload pallet is provided in Figure 2.

Arrangements were made to modulate the U. S. Navy operational VLF transmitters at Cutler, Maine (NAA), Annapolis, Maryland (NSS); and Jim Creek, Washington (NLK) and the Stanford University research VLF transmitter at Siple Station, Antarctica in special controlled formats. These formats were operated at the times of overpass of the S81-1 satellite.

More detailed descriptions of these instruments are provided in the various reprints included in this report.

SPACE TEST PROGRAM S81-1 PAYLOAD

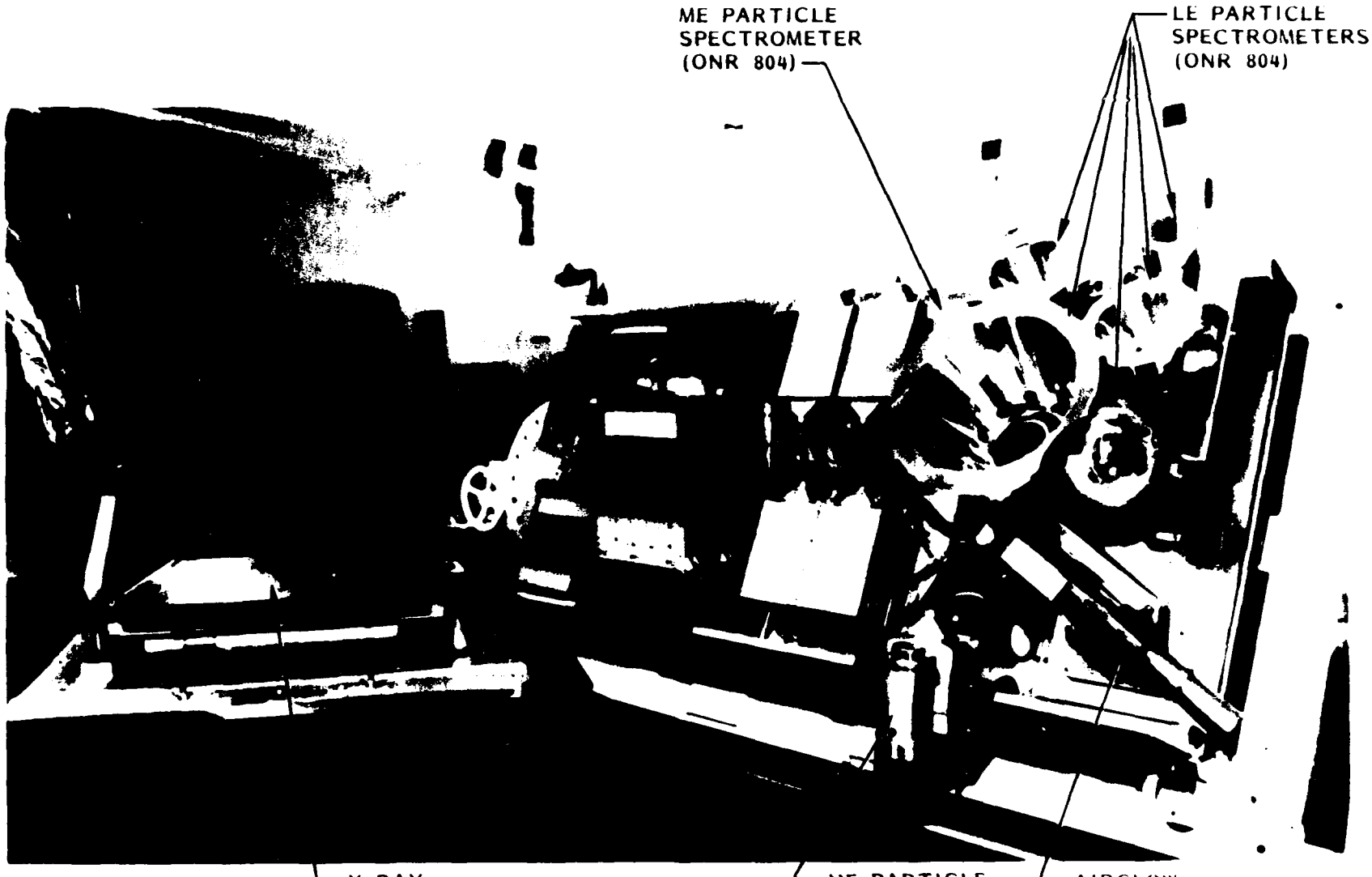

Figure 2

TABLE I
SEEP INSTRUMENTATION

Detector	Measurement	Range (keV)	Energy Channels	Energy Resolution (keV FWHM)	Temporal Resolution (sec)	Det Area (cm^2)	Field of View (deg)	Geometrical Factor ($cm^2 sr$)	Pointing from Zenith
ME1	Electrons Protons	45-1000 450-1500	256	14	.063	4.5	±30	2.47	0°
LE1	Electrons Protons	10-200 30-200	16-256	4	.128	1.5	±20	0.51	10°
LE2	Electrons Protons	6-200 10-200	16-256	2.1	.128	0.5	±20	0.17	50°
LE4	Electrons Protons	Magnet 20-200	16-256	4	.128	0.5	±6	0.1	50°
LE5	Electrons Protons	2-200 30-200	16-256	1	.128	0.5	±20	0.17	50°
TE1	Electrons Protons	3-180 30-180	16-256	1.3	.128	0.5	±20	0.17	90°
TE2	Electrons Protons	6-925 30-950	256	1.3	.063	0.5	±20	0.17	90°
ME2	Electrons Protons	45-1000 450-1500	256	20	.063	4.5	±30	2.47	180°
AI	Photometer	391.4 nm 391.4 nm 630.0 nm	1 1 1	0.8 nm 2.4 nm 1.2 nm	.245	3.0	±8	-	125°
APP	Plasma	10^2-$10^5 cm^{-3}$	-	-	.063	2.0	-	-	35°
XRTS	X-rays	4-40	24	21%	.031	590	±90	6.0	125°

IV. ON-ORBIT OPERATIONS

Soon after launch, the SEEP payload checkout was completed without problems, and the payload continued to perform very well on-orbit. During much of the time from May until early December 1982, the data coverage was maintained at about 70 percent, in accordance with the available power and the recorder read-in constraints. All temperatures were within specifications, and all orbital transients matched the expected values.

All of the instruments in the SEEP payload checked out as planned. The particle spectrometers performed well and returned excellent data. The airglow photometer also operated well. The XRIS spectrometer provided positional mapping information only from May until July 1, 1982, but after the latter date it continued to provide good counting rate and spectral data throughout the mission.

During passes of the SEEP payload over the U.S. Navy VLF transmitters the transmitters were typically run in one of ten selectable formats for on-off operation. These formats are indicated in Figure 3. The output signals were received and monitored at the Lockheed Palo Alto Research Laboratory.

V. ANALYSES AND INTERPRETATIONS OF THE FLIGHT DATA

The primary objective of the SEEP mission was accomplished by achieving the first direct measurements of electron precipitation by the controlled wave modulation of a VLF transmitter. In addition, the precipitation of electrons by VLF waves associated with lightning was measured for the first time from a satellite. The accomplishments are briefly described below and reprints of published articles describing the findings are provided in section XI. With the SEEP data many other important findings have been made. These include the

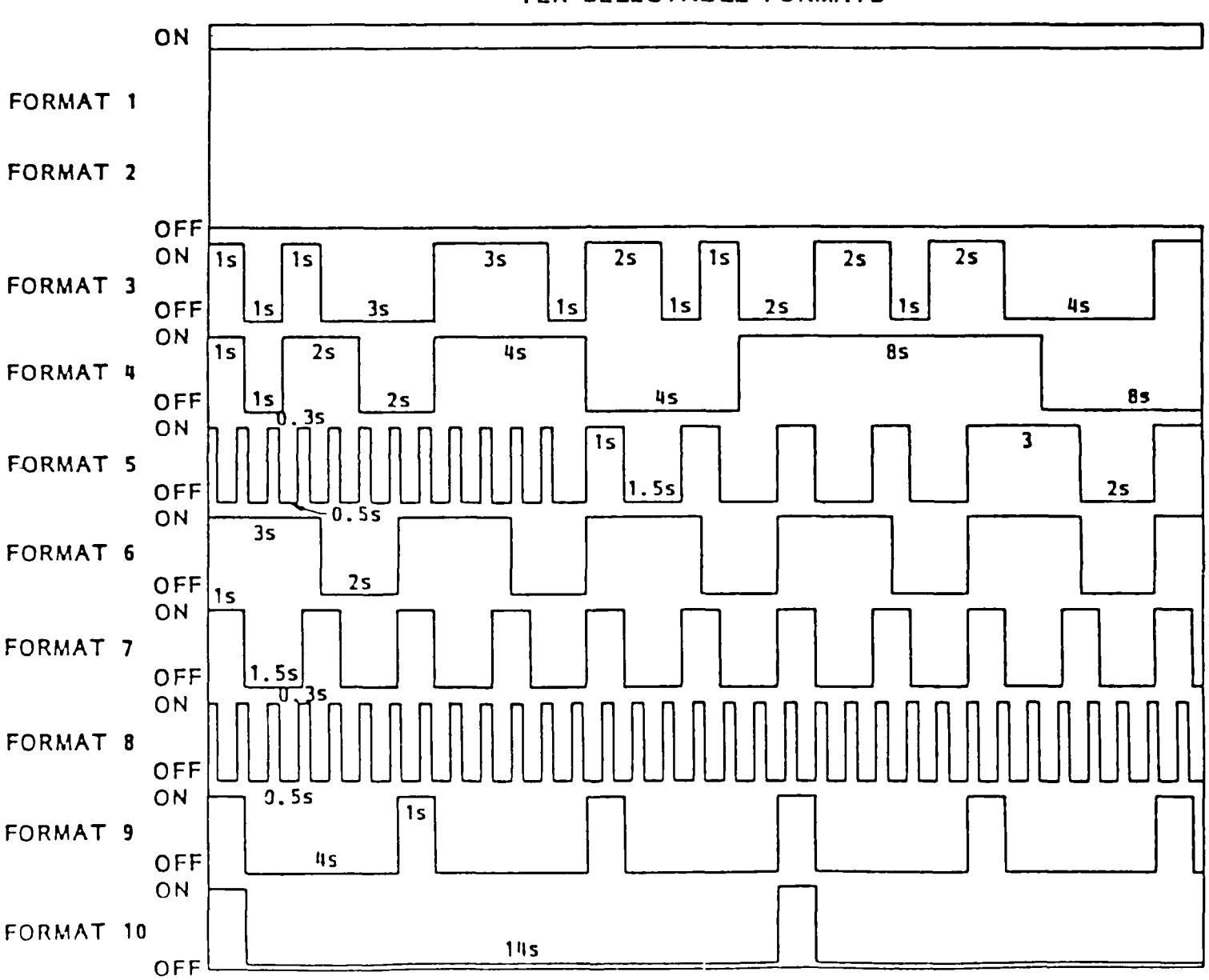
TEN SELECTABLE FORMATS
ON
FORMAT 1
FORMAT 2
OFF
ON
FORMAT 3
OFF
1s
1s
1s
3s
3s
1s
2s
1s
1s
2s
2s
1s
2s
4s
ON
FORMAT 4
OFF
1s
2s
1s
2s
4s
4s
8s
8s
ON
FORMAT 5
OFF
0.3s
1s
1.5s
3
2s
0.5s
ON
FORMAT 6
OFF
3s
2s
1s
ON
FORMAT 7
OFF
1.5s
0.3s
ON
FORMAT 8
OFF
ON
FORMAT 9
OFF
0.5s
1s
4s
ON
FORMAT 10
OFF
14s

Figure 3

following: 1) an assessment was made of the relative contributions of hiss, lightning and VLF transmitter waves to electron precipitation from the slot region ($2 \leq L \leq 3.5$) 2) discovery of the frequent occurrence of multiple peaks in the energy spectra of electrons trapped at low altitudes, 3) observation of electron pulsations near the trapping boundary and 4) discovery of bremsstrahlung x-ray images of small isolated patches of energetic electron precipitation at high latitude.

A good example of electron flux modulations in correlation with the transmitter on-off signals occurred on August 17, 1982 at 8680-8740 seconds UT when the SEEP payload was passing near the NAA transmitter as it was being modulated with a 3-s on and 2-s off pattern. In Figure 4, the electron fluxes measured at various zenith angles are plotted as a function of time. A modulation period of 5 ± 0.1 s is clearly seen for 12 consecutive cycles. For reference, the measured on times of the transmitter at NAA are indicated. The risetime of the electron flux and the observed delay in decay time of ~1.5 s are now understood [Inan et al., 1985] in terms of the pitch angle dependence of the particle distribution near the edge of the loss cone and by the multiple interaction of the particles with the waves due to significant atmospheric backscatter.

From surveys of the SEEP data five electron modulation events were found from the 65 passes of the satellite when one of the transmitters was being modulated in a special 3-s on and 2-s off format. No such events were found in the 175 passes when neither the NAA nor the NSS transmitter was being modulated in one of the special SEEP formats. All of the time profiles for the events displayed a similar pattern in which the fluxes increased rather slowly after start of the on period and reached a maximum about 2 s later. The temporal profile and the absolute counting rates of the observed fluxes

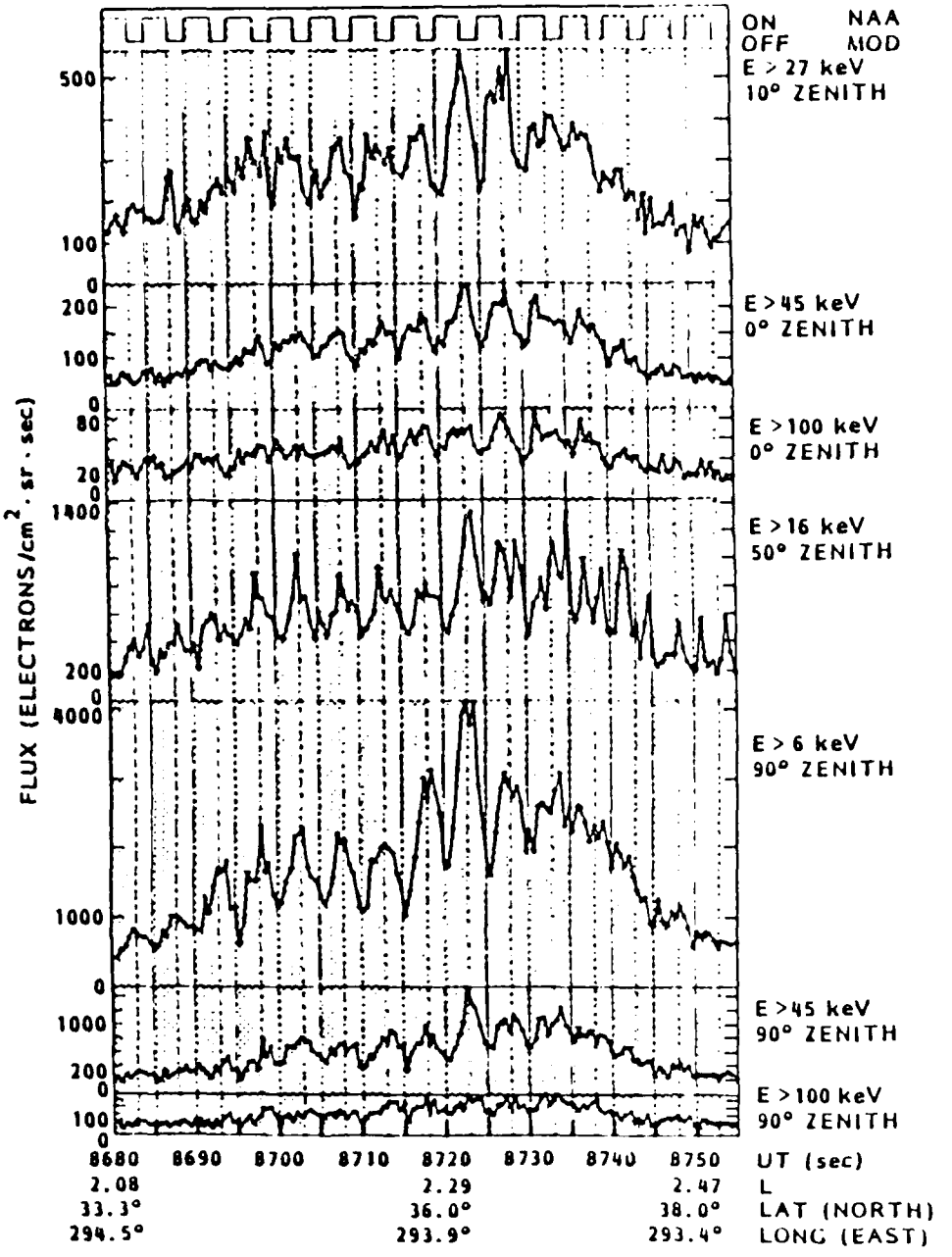
ON NAA
OFF MOD
E > 27 keV
10° ZENITH
E > 45 keV
0° ZENITH
E > 100 keV
0° ZENITH
E > 16 keV
50° ZENITH
E > 6 keV
90° ZENITH
E > 45 keV
90° ZENITH
E > 100 keV
90° ZENITH
FLUX (ELECTRONS/cm^2 · sr · sec)
500
100
0
200
100
0
80
20
0
1400
200
0
4000
1000
0
1000
200
0
100
0
8680 8690 8700 8710 8720 8730 8740 8750
UT (sec)
2.08 2.29 2.47
L
33.3° 36.0° 38.0°
LAT (NORTH)
294.5° 293.9° 293.4°
LONG (EAST)

Figure 4

were found to be in good agreement with the predictions of an extended test particle model of the wave-particle interaction in the magnetosphere [Inan et al., 1985].

For the first time measurements were made of the intensities and energy spectra of electrons precipitated by the VLF radiation from lightning. Seven lightning-induced electron precipitation (LEP) events recorded on 9 September 1982 with the SEEP experiment are shown in Figure 5. In the strong LEP events A, D, and E, electron fluxes are observed to increase rapidly in strength, about 100 times background in less than 0.2 second. The observations of LEP events have provided direct evidence of an important coupling mechanism between terrestrial lightning and relativistic radiation belt electron precipitation. An energy versus time spectrogram of these events was published on the cover of Nature magazine and is provided in Figure 6. Since initial discovery of these events approximately 200 short duration electron precipitation bursts, many very similar in characteristic to the 9 September 1982 LEP events, have been and are still being studied.

Examples of the bremsstrahlung x-ray images obtained at high latitudes are shown in Figure 7. Some of the stronger arc shaped images are provided in Figure 8. During certain passes of the S81-1 satellite, as illustrated in Figure 9, isolated patches of x-rays were observed poleward of the auroral zone. Other examples of these patches are shown in Figure 10.

The frequent occurrence of multiple peaks in the energy spectra of electrons trapped at low altitudes is illustrated in Figure 11. Here is shown an energy-time spectrogram of electrons obtained during a portion of one orbit of the S81-1 satellite.

The above examples of the SEEP data are discussed in much more detail in section XI.

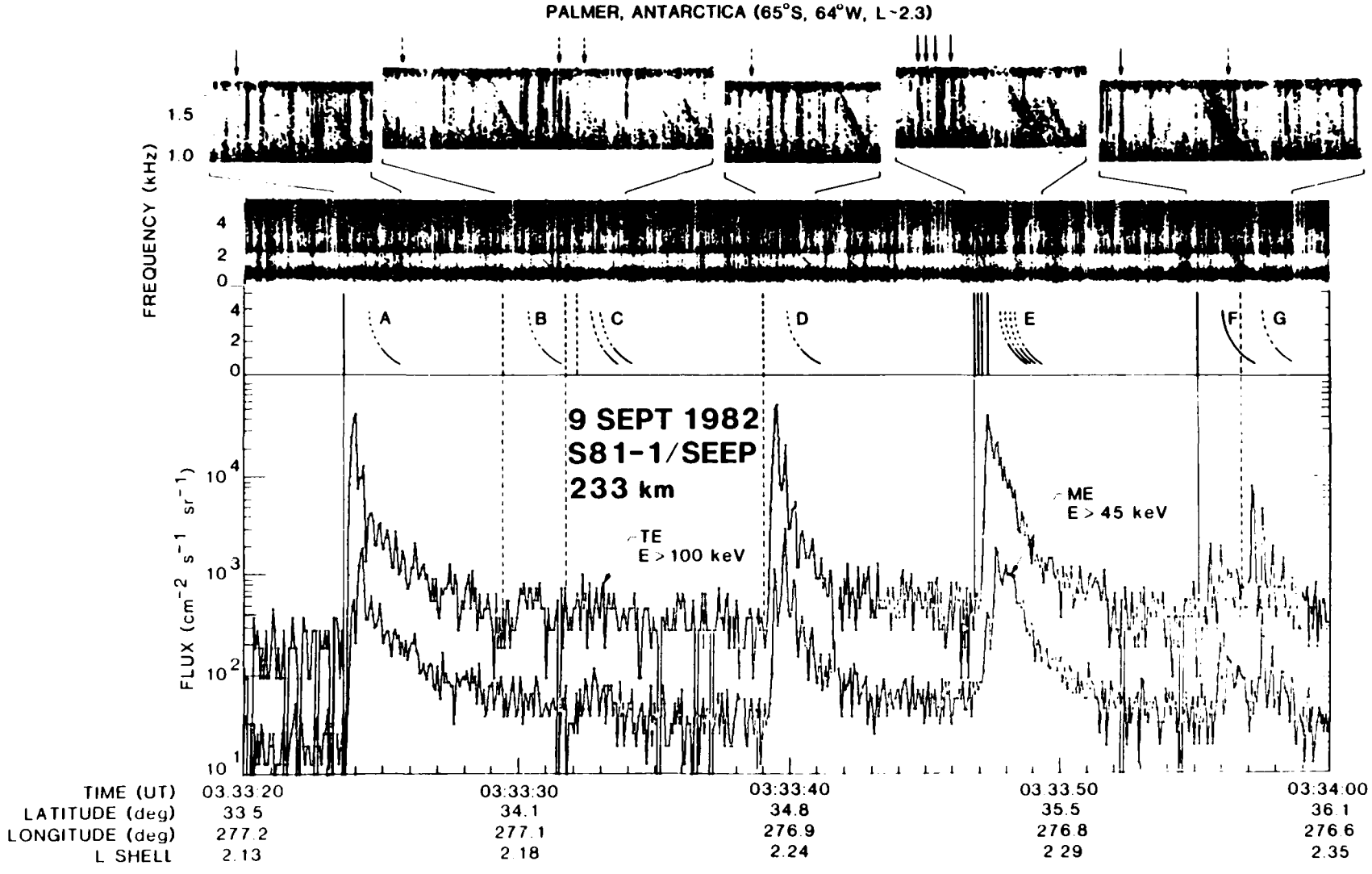
PALMER, ANTARCTICA (65°S, 64°W, L~2.3)
FREQUENCY (kHz)
1.5
1.0
4
2
0
A
B
C
D
E
F
G
9 SEPT 1982
S81-1/SEEP
233 km
TE
E > 100 keV
ME
E > 45 keV
FLUX (cm⁻² s⁻¹ sr⁻¹)
TIME (UT) 03:33:20 03:33:30 03:33:40 03:33:50 03:34:00
LATITUDE (deg) 33.5 34.1 34.8 35.5 36.1
LONGITUDE (deg) 277.2 277.1 276.9 276.8 276.6
L SHELL 2.13 2.18 2.24 2.29 2.35

Figure 5

nature
INTERNATIONAL WEEKLY JOURNAL OF SCIENCE

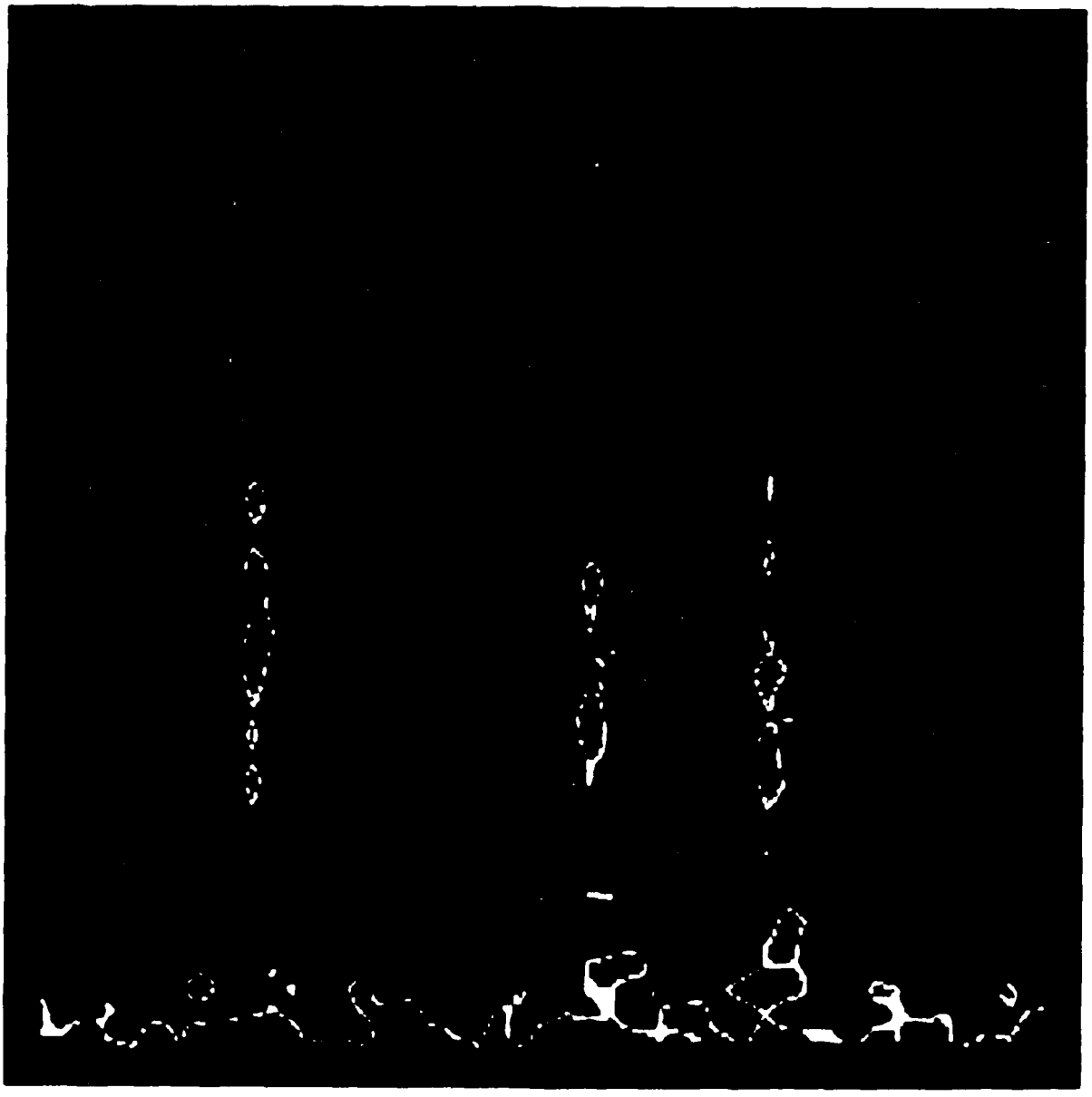

LIGHTNING-INDUCED ELECTRON PRECIPITATION

Figure 6

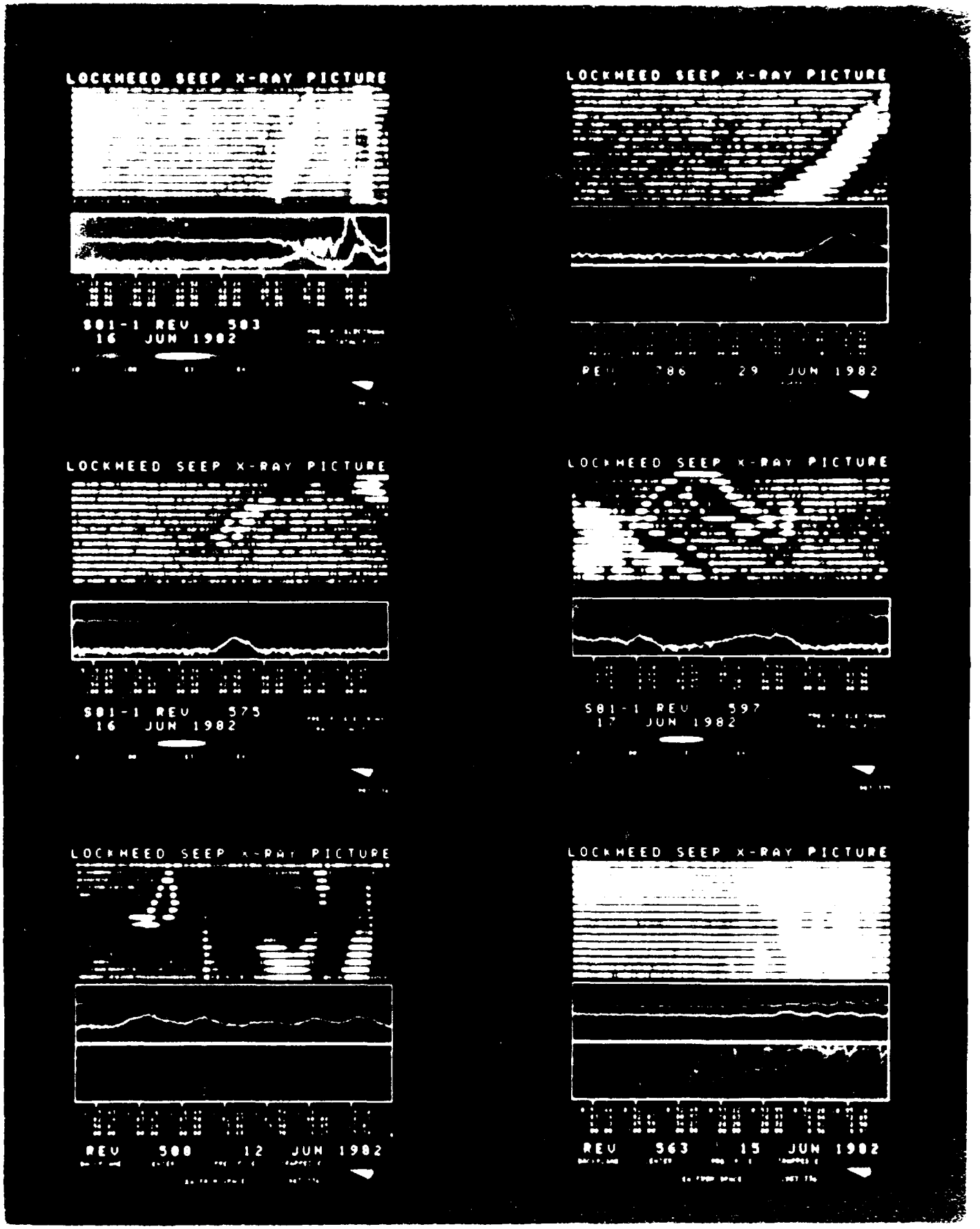
LOCKHEED SEEP X-RAY PICTURE
S81-1 REV 503
16 JUN 1982
LOCKHEED SEEP X-RAY PICTURE
REV 586 29 JUN 1982
LOCKHEED SEEP X-RAY PICTURE
S81-1 REV 575
16 JUN 1982
LOCKHEED SEEP X-RAY PICTURE
S81-1 REV 597
17 JUN 1982
LOCKHEED SEEP X-RAY PICTURE
REV 508 12 JUN 1982
LOCKHEED SEEP X-RAY PICTURE
REV 563 15 JUN 1982

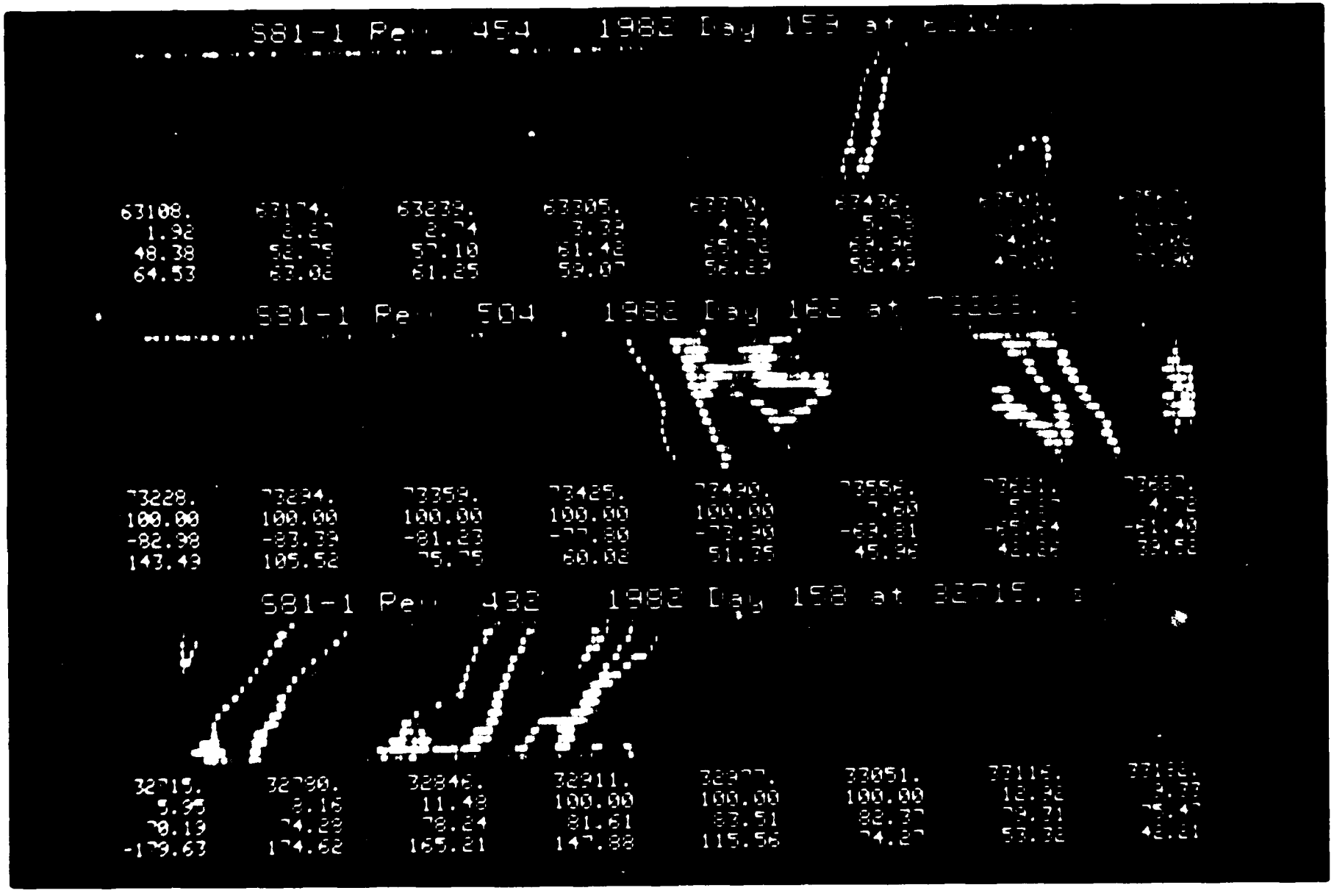
581-1 Per 454 1982 Day 158 at
63108. 63174. 63239. 63305. 63370. 63436.
1.92 2.74 3.33 4.34
48.38 52.75 57.10 61.42
64.53 63.02 61.25 58.07
581-1 Per 504 1982 Day 158 at
73228. 73294. 73359. 73425. 73490. 73556.
100.00 100.00 100.00 100.00 100.00
-82.98 -83.33 -81.23 -77.80 -73.90 -69.81
143.43 105.52 75.75 60.02 51.39 45.98
581-1 Per 432 1982 Day 158 at
32715. 32780. 32846. 32911. 32977. 33051.
5.95 8.16 11.48 100.00 100.00 100.00
70.19 74.28 78.24 81.61 83.51 82.37
-179.63 174.62 165.21 147.88 115.56 74.27

Figure 8

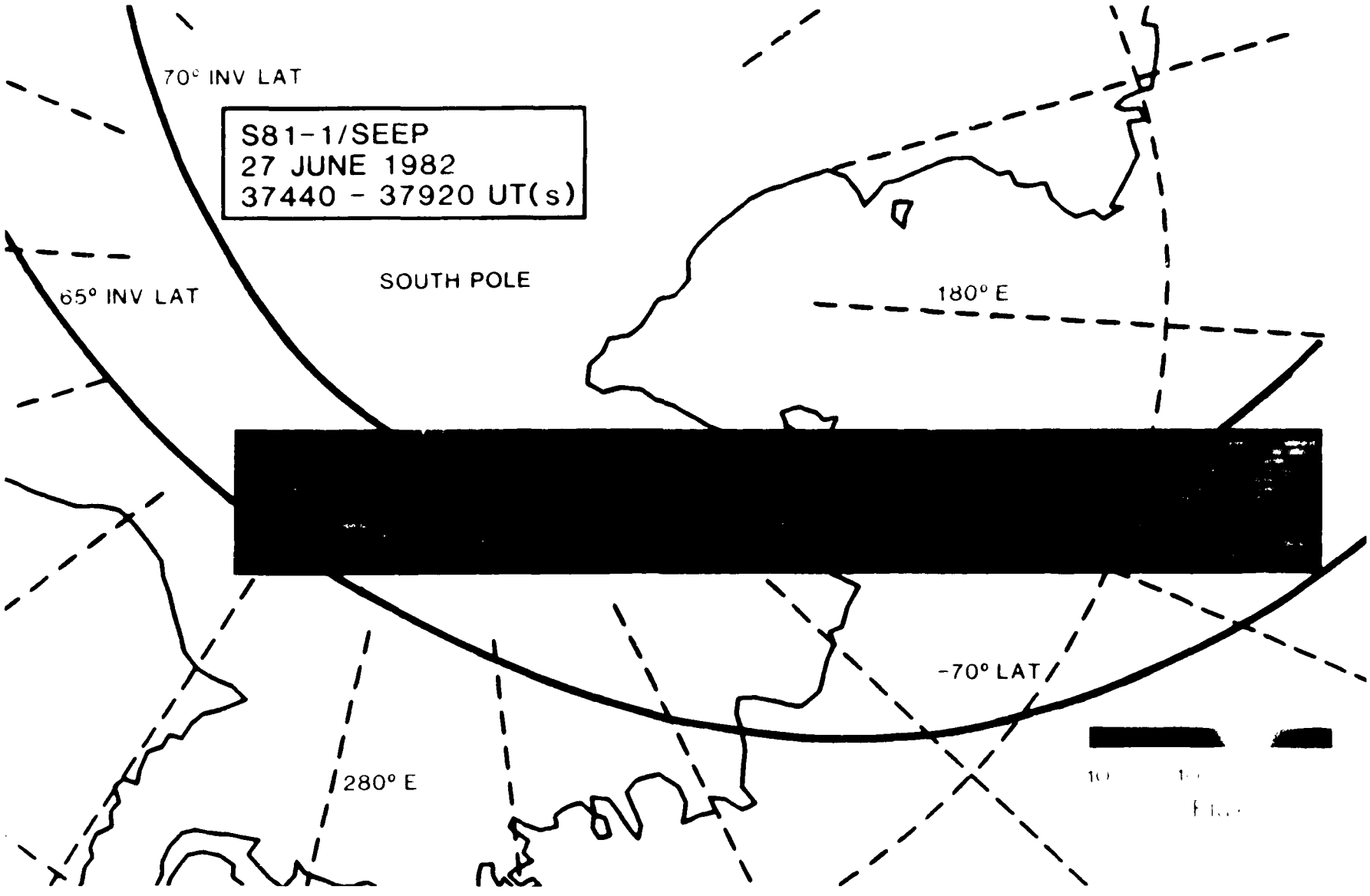
70° INV LAT
S81-1/SEEP
27 JUNE 1982
37440 - 37920 UT(s)
65° INV LAT
SOUTH POLE
180° E
-70° LAT
280° E

Figure 9

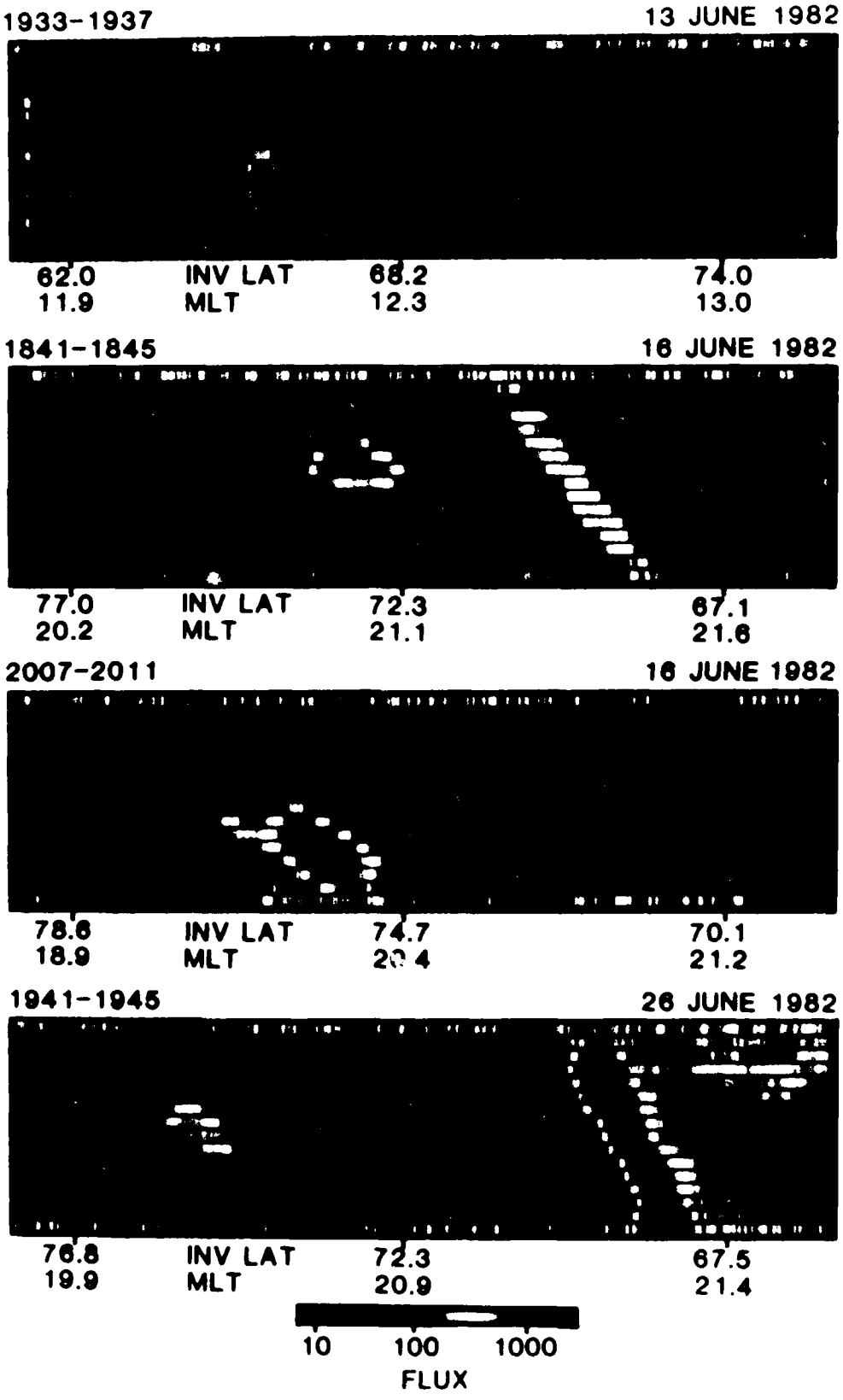
1933-1937
13 JUNE 1982
62.0
11.9
INV LAT
MLT
68.2
12.3
74.0
13.0
1841-1845
16 JUNE 1982
77.0
20.2
INV LAT
MLT
72.3
21.1
67.1
21.6
2007-2011
16 JUNE 1982
78.6
18.9
INV LAT
MLT
74.7
20.4
70.1
21.2
1941-1945
26 JUNE 1982
76.8
19.9
INV LAT
MLT
72.3
20.9
67.5
21.4
10
100
1000
FLUX

Figure 10

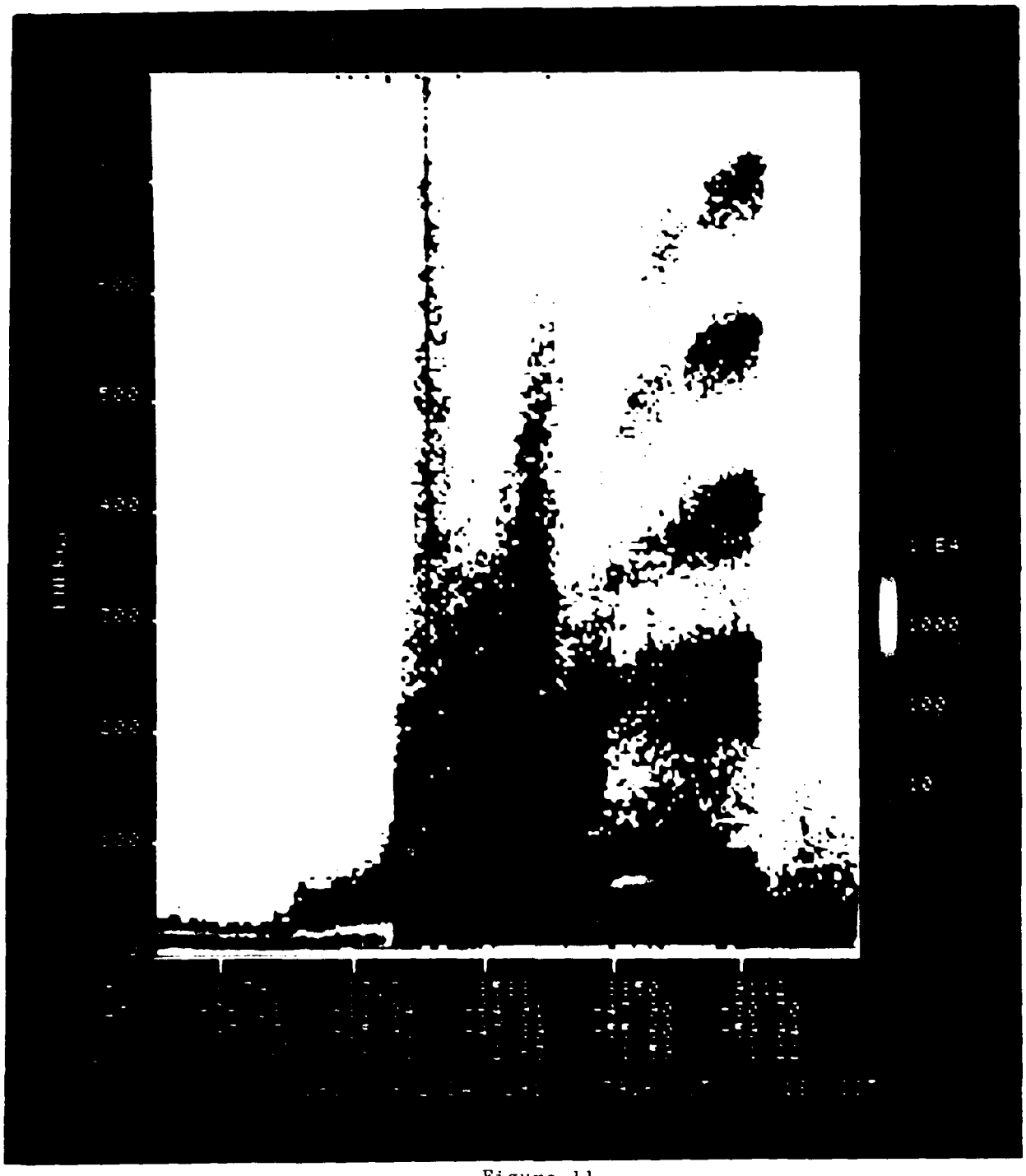

Figure 11

VI. ACKNOWLEDGMENT

Launch and orbital support were provided by the USAF Space Test Program Office. Appreciation is extended to the ONR program manager, R. G. Joiner, to the payload system engineer, S. J. Battel, to J. B. Reagan and D. P. Cauffman for their program management of the satellite payload development, to J. C. Bakke for his significant role in the instrument development, to R. R. Vondrak for helpful consultations, and to J. P. McGlennon for his contribution to the data analysis.

VII. FIGURE CAPTIONS

Figure 1. Schematic illustration of the SEEP experiment concept. The locations of the pertinent VLF transmitters are indicated along with a representation of the satellite paths during three successive passes. Also shown are modulated VLF waves and the region of wave-particle interactions.

Figure 2. Photograph of the SEEP instruments mounted on the S81-1 payload pallet.

Figure 3. The ten selectable formats for operation of U. S. Navy transmitters.

Figure 4. Electron fluxes on August 17, 1982 plotted as a function of time. Also shown are the ON and OFF times of the NAA transmitter.

Figure 5. Energetic electron measurements obtained with the SEEP payload on 9 September 1982 are correlated one-to-one with concurrent ground-based VLF whistlers at Palmer Station, Antarctica. The uppermost insets show the Palmer VLF data with an expanded time scale for the seven lightning-induced electron precipitation events.

Figure 6. An energy-time spectrogram of lightning-induced electron precipitation from the radiation belts, as observed in the SEEP payload on the S81-1 satellite. The color scale indicates the electron flux, with red being most intense, and the vertical and horizontal axes represent energy and time, respectively.

Figure 7. Six different x-ray images acquired at high latitudes with the SEEP payload.

Figure 8. Some arc-shaped images measured at high latitudes with the SEEP payload.

Figure 9. The x-ray image obtained during a pass of the SEEP payload across the southern polar region. An isolated x-ray patch is evident at about a third of the distance from the right hand edge of the image.

Figure 10. Mappings of the x-ray intensities (4-40 keV) observed at high latitudes. In each of these images an isolated x-ray patch is evident.

Figure 11. Two-dimensional display of electron spectra versus time. Energies run from 6 keV (bottom) to 1 MeV (top), and time runs from left to right. The electron counting rate is indicated by colors.

VIII. LIST OF PUBLICATIONS

Cauffman, D. P., Electron spectra from satellite x-ray images: practical considerations, Proceedings of the IAGA Edinburgh Assembly, Aug. 81.

Calvert, W., H. D. Voss, and T. C. Sanders, A satellite imager for atmospheric x-rays, IEEE Trans. NS Vol. NS-32 1985, pp.112-118.

Datlowe, D. W., W. L. Imhof, H. D. Voss, J. R. Kilner, J. Mobilia, J. B. Reagan, and W. Calvert, Coordinated measurements of auroral zone x-rays from two satellites, EOS Vol. 64 1983, p.294.

Datlowe, D. W., W. L. Imhof, H. D. Voss, E. E. Gaines, and J. B. Reagan, Observation of multiple peaks in the spectrum of trapped electrons from low earth orbit, EOS Vol. 64 1983, p.809.

Datlowe, D. W., W. L. Imhof, and E. E. Gaines, Ovservation of multiple peaks in the spectrum of trapped electrons in the inner belt, EOS Vol. 65 1984, p.1044.

Datlowe, D. W., W. L. Imhof, and E. E. Gaines, Probing the equatorial plasma density at L = 1.5 - 2.0 by cyclotron resonance precipitation of energetic electrons, EOS Vol. 66 1985, p.1039.

Datlowe, D. W., W. L. Imhof, E. E. Gaines, and H. D. Voss, Multiple peaks in the spectrum of inner belt electrons, JGR Vol. 90 1985, p.8333.

Datlowe, D. W., W. L. Imhof, and H. D. Voss, Spectral mapping of precipitating electrons with x-rays images, EOS Vol. 67 1986, pp.1169-70.

Datlowe, D. W., W. L. Imhof, and H. D. Voss, X-ray imaging of the auroral zone by the S81-1 satellite, IUGG XIX General Assembly, 1987.

Datlowe, D. W., W. L. Imhof, and H. D. Voss, Spectral mapping of precipitating electrons with x-ray images from a satellite, EOS Vol. 68, 1987, p.1435.

Datlowe, D. W., W. L. Imhof, and H. D. Voss, Spectral images of energetic electrons precipitating in the auroral zone, submitted to JGR.

Gaines, E. E., W. L. Imhof, J. B. Reagan, and H. D. Voss, High resolution measurements of peaks in the spectra of electrons precipitating from the inner radiation Belt, EOS Vol. 63 1982, p.1072.

Gaines, E. E., W. L. Imhof, J. B. Reagan, and H. D. Voss, Wave particle interactions in the magnetosphere as detected by the SEEP electron spectrometers, Chapman Conference 1983.

Imhof, W. I., J. B. Reagan, H. D. Voss, E. E. Gaines, R. A. Helliwell, U. S. Inan, J. P. Katsufrakis, and R. G. Joiner, Active wave-particle experiment involving a satellite and ground-based transmitters, EOS Vol. 63 1982, p.404.

Imhof, W. I., J. B. Reagan, E. E. Gaines, H. D. Voss, D. W. Datlowe, J. Mobilia, R. A. Helliwell, U. S. Inan, and J. P. Katsufrakis, The effects of modulated VLF transmitters on the precipitation of energetic electrons from the outer radiation belt, EOS Vol. 63 1982, p.1072.

Imhof, W. I., J. B. Reagan, H. D. Voss, E. E. Gaines, D. W. Datlowe, J. Mobilia, R. Helliwell, U. S. Inan, Katsufrakis, and R. G. Joiner, The precipitation of electrons from the radiation belts by controlled VLF signals from ground- based transmitters, Nat. Rad. Sci. Meeting, 1983.

Imhof, W. I., J. B. Reagan, H. D. Voss, E. E. Gaines, D. W. Datlowe, J. Mobilia, R. A. Helliwell, U. S. Inan, J. Katsufrakis, and R. G. Joiner, A statistical study of modulated electron precipitation events induced by controlled signals from VLF transmitters, EOS Vol. 64 1983, p.301.

Imhof, W. I., J. B. Reagan, H. D. Voss, D. W. Datlowe, J. R. Kilner, E. E. Gaines, J. Mobilia, T. J. Rosenberg, and R. G. Joiner, Coordinated satellite and ground-based studies of intense magnetospheric electron

precipitation events, EOS Vol. 64 1983, p.810.

Imhof, W. I., J. B. Reagan, H. D. Voss, E. E. Gaines, D. W. Datlowe, J. Mobilia, R. A. Helliwell, U. S. Inan, J. Katsufrakis, and R. G. Joiner, Direct observation of radiation belt electrons precipitated by the controlled injection of VLF signals from a ground-based transmitter, GRL Vol. 10 1983, pp.361-364.

Imhof, W. I., J. B. Reagan, H. D. Voss, E. E. Gaines D. W. Datlowe, J. Mobilia, R. A. Helliwell, U. S. Inan, J. Katsufrakis, and R. G. Joiner, The modulated precipitation of radiation belt electrons by controlled signals from VLF transmitters, GRL Vol. 10 1983, pp.615-618.

Imhof, W. I., J. B. Reagan, H. D. Voss, e. E. Gaines, and J. Mobilia, Coordinated satellite measurements of particle precipitation during the storm of July 13, 1982, IAGA Meeting 1983.

Imhof, W. I., J. B. Reagan, E. E. Gaines, H. D. Voss, D. W. Datlowe, J. Mobilia, Helliwell, Inan, and Katsufrakis, The effects of modulated VLF transmitters on the precipitation of energetic electrons from the radiation belts, Chapman Conference 1983.

Imhof, W. I., J. B. Reagan, H. D. Voss, D. W. Datlowe, E. E. Gaines, and J. Mobilia, The simultaneous energy selective precipitation of electrons and ions from narrow regions of the outer radiation belt, EOS Vol. 65 1984, p.1044.

Imhof, W. I., T. J. Rosenberg, L. J. Lanzerotti, J. B. Reagan, H. D. Voss, D. W. Datlowe, J. R. Kilner, E. E. Gaines, J. Mobilia, and R. G. Joiner, A coordinated satellite and ground-based study of an intense electron precipitation spike over the southern polar cap, JGR Vol. 89 1984, pp.10,837-10,846.

Imhof, W. I., J. B. Reagan, H. D. Voss, E. E. Gaines, D. W. Datlowe, and J.

Mobilia, Results from the SEEP active plasma experiment, Proceedings of IES 1984.

Imhof, W. I., H. D. Voss, M. Walt, E. E. Gaines, J. Mobilia, and D. W. Datlowe, The role of lightning in precipitating electrons from the slot region of the radiation belt, EOS Vol. 66 1985, p.350.

Imhof, W. I., H. D. Voss, J. Mobilia, and D. S. Evans, The spatial extent of lightning and chorus electron precipitation bursts in the slot region; EOS Vol. 66 1985, p.1039.

Imhof, W. I., and H. D. Voss, Observations of auroral bremsstrahlung x-rays, EOS Vol. 66 1985, p.1047.

Imhof, W. I., H. D. Voss, J. B. Reagan, D. W. Datlowe, and J. Mobilia, Localized electron precipitation events at high latitudes studied with x-ray imagery from a satellite, Adv. Space Res. Vol. 5 1985, pp.69-72.

Imhof, W. I., E. E. Gaines, H. D. Voss, J. B. Reagan, D. W. Datlowe, J. Mobilia, R. A. Helliwell, U. S. Inan, J. Katsufrakis, and R. G. Joiner, Results from the SEEP active space plasma experiment: effects on the ionosphere, Rad.Sci Vol. 20 1985, pp.511-518.

Imhof, W. I., H. D. Voss, D. W. Datlowe, and J. Mobilia, Bremsstrahlung x-ray images of isolated electron patches at high latitudes, JGR Vol. 90 1985, pp.6515-6524.

Imhof, W. I., H. D. Voss, M. Walt, E. E. Gaines, J. Mobilia, and D. W. Datlowe, The precipitation of radiation belt electrons by VLF transmitters, by plasmaspheric hiss, and by lightning whistlers, URSI N. American Rad. Sci. Meeting 1985, p.539.

Imhof, W. I., H. D. Voss, D. W. Datlowe, and J. Mobilia, Electron precipitation at high latitudes, EOS Vol. 67 1986, p.1158.

Imhof, W. I., H. D. Voss, J. B. Reagan, D. W. Datlowe, E. E. Gaines, J. Mobilia,

and D. S. Evans, Relativistic electron and energetic ion precipitation spikes near the plasmapause, JGR Vol. 91 1986, pp.3077-3088.

Imhof, W. I., H. D. Voss, M. Walt, E. E. Gaines, J. Mobilia, D. W. Datlowe, and J. B. Reagan, Slot region electron precipitation by lightning, VLF chorus, and plasmaspheric hiss, JGR Vol. 91 1986, pp.8883-8894.

Imhof, W. I., H. D. Voss, J. Mobilia, E. E. Gaines, and D. S. Evans, Electron precipitation bursts in the nighttime slot region measured simultaneously from two satellites, JGR Vol. 92 1987, pp.4515-4524.

Imhof, W. I., H. D. Voss, D. W. Datlowe, and J. Mobilia, Isolated electron precipitation regions at high latitudes, submitted to JGR.

Imhof, W. I., H. D. Voss, M. Walt, J. Mobilia, D. W. Datlowe, and E. E. Gaines, Fast time variations in the energy spectra of electron precipitation bursts from the radiation belts, EOS Vol. 68 1987, p. 1440.

Mobilia, J., H. D. Voss, W. L. Imhof, J. B. Reagan, and K. L. Miller, Satellite observations of periodic F-region gradients during the stimulated emission of energetic particles (SEEP) experiment, EOS Vol. 64 1983, p.289.

Mobilia, J., W. L. Imhof, J. B. Reagan, H. D. Voss, E. E. Gaines, D. W. Datlowe, R. A. Helliwell U. S. Inan, J. Katsufrakis, and R. G. Joiner, Study of the effects of VLF transmitter operation on the fluxes of precipitating electrons, EOS Vol. 64 1983, p.814.

Mobilia, J., H. D. Voss, and W. L. Imhof, Nighttime satellite observations of lightning flashes correlated with electron precipitation, EOS Vol. 65 1984, p.1060.

Mobilia, J., H. D. Voss, W. L. Imhof, and S. J. Goodman, Lightning observations from the Seep/S81-1 satellite, EOS Vol. 66 1985, p.1001.

Mobilia, J., H. D. Voss, and W. L. Imhof, Global distribution of LEP bursts, EOS Vol. 67 1986, p.1168.

Reagan, J. B., and W. L. Imhof, The phenomenology of energetic particle precipitation in the magnetosphere, EOS vol. 63 1982. p.402.

Reagan, J. B., W. L. Imhof, R. A. Helliwell, U. S. Inan, J. Katsufrakis, and R. G. Joiner, The stimulated emission of energetic particles experiment, EOS Vol. 63 1982, p.1071-1072.

Reagan, J. B., W. L. Imhof, H. D. Voss, E. E. Gaines, R. A. Helliwell, U. S. Inan, J. Katsufrakis, and R.G. Joiner, Modification of the lower ionosphere by transmitter-induced electron precipitation, IAGA, Aug. 83.

Reagan, J. B., W. L. Imhof, H. D. Voss, E. E. Gaines, R. A. Helliwell, U. S. Inan, J. Katsufrakis, and R. G. Joiner, Effects of transmitter-induced precipitation on the ionosphere, EOS Vol. 64 1983, p.302.

Spear, K. A., H. D. Voss, and W. L. Imhof, Airglow response to energetic electron precipitation compared with satellite observations, EOS Vol. 67 1986, p.1140.

Voss, H. D., W. L. Imhof, J. B. Reagan, E. E. Gaines, S. B. Mende, R. R. Vondrak, D. W. Datlowe, and J. Mobilia, Simultaneous x-ray, airglow and energetic particle measurements using the SEEP payload high sensitivity spectrometers, EOS Vol. 63 1982, p. 1072.

Voss, H. D., J. B. Reagan, W. L. Imhof, D. O. Murray, D. A. Simpson, D. P. Cauffman, and J. C. Bakke, Low temperature characteristics of solid state detectors for energetic x-ray, ion and electron spectrometers, IEEE Trans. NS Vol. NS-19 1982, p.164.

Voss, H. D., J. C. Bakke, and S. N. Roselle, A spacecraft multichannel analyzer for a multidetector solid state detector array, IEEE Trans. N.S. Vol. NS-29 1982, pp.173-177.

Voss, H. D., W. L. Imhof, J. B. Reagan, R. R. Vondrak, M. Walt, D. W. Datlowe, J. Mobilia, D. P. Cauffman, and W. Calvert, Preliminary results from the

S81-1 SEEP satellite x-ray imaging spectrometer (XRIS), EOS Vol. 64 1983, p.302.

Voss, H. D., W. L. Imhof, J. B. Reagan, R. R. Vondrak, M. Walt, J. Mobilia, D. W. Datlowe, D. P. Cauffman, W. Calvert, and R. G. Joiner, SEEP x-ray imagery of the earth's aurora, EOS Vol. 64 1983, p.792.

Voss, H. D., COVER PHOTO; EOS Vol. 64 1983; cover page(p.952)

Voss, H. D., W. L. Imhof, J. B. Reagan, and E. E. Gaines, Rapid spectral snapshots of short-duration particle precipitation events using the SEEP payload high sensitivity spectrometers, Chapman Conference 1983.

Voss, H. D., W. L. Imhof, J. B. Reagan, K. L. Miller, and J. Mobilia, TID's above thunderstorms associated with the efficient transmission of VLF Energy Through the ionosphere, EOS Vol. 65 1984; p.267.

Voss, H. D., W. L. Imhof, M. Walt, E. E. Gaines, J. Mobilia, U. S. Inan, R. A. Helliwell, and D. L. Carpenter, Lightning-induced electron precipitation, EOS Vol. 65 1984; p.1059.

Voss, H. D., W. L. Imhof, M. Walt, J. Mobilia, E. E. Gaines, J. B. Reagan, U. S. Inan, R. A. Helliwell, D. L. Carpenter, J. P. Katsufrakis, and H. C. Chang, Lightning-induced electron precipitation, Nature Vol. 312 1984; pp. 740-742.

Voss, H. D., W. L. Imhof, and J. Mobilia, Satellite observations of energetic ions and neutrals in the equatorial precipitation zone, Proceedings Yosemite '84: Planetary Plasma Environments: A Comparative View, pp.95-6.

Voss, H. D., E. E. Gaines, J. B. Reagan, W. L. Imhof, D. P. Cauffman, D. O. Murray, and S. Roselle, The cooled solid state energetic particle spectrometer array for the S81-1 satellite, Nuc. Sci. Meeting 1984.

Voss, H. D., The plasma probe environment monitor for the S81-1 satellite, Nuc. Sci. Meeting 1984.

Voss, H. D., W. L. Imhof, J. B. Reagan, D. P. Cauffman, and J. C. Bakke, The atmospheric x-ray imaging instrument for the S81-1 satellite: final design, calibration and flight performance., Nuc. Sci. Meeting 1984.

Voss, H. D., and S. B. Mende, The quadrant photometer for the S81-1 satellite, Nuc. Sci. Meeting 1984.

Voss, H. D., W. L. Imhof, M. Walt, J. Mobilia, E. E. Gaines, U. S. Inan, R. A. Helliwell, and D. L. Carpenter, Energy and time structure of lightning-induced electron precipitation, EOS Vol. 66 1985, p.350.

Voss, H. D., W. L. Imhof, and J. Mobilia, Thunderstorm effects in space observed with the SEEP/S81-1 satellite, EOS Vol. 66 1985, p.1039.

Voss, H. D., W. L. Imhof, and J. Mobilia, Satellite observations of lightning associated electron precipitation, IAGA/IAMAP Fifth Gen. Ass. 1985, p.248.

Voss, H. D., W. L. Imhof, and R. R. Vondrak, Simultaneous x-ray imagery, optical and energetic particle observations of the earth's aurora, IAGA/IAMAP Fifth Gen. Ass. 1985, p.252.

Voss, H. D., W. L. Imhof, J. Mobilia, E. E. Gaines, and J. B. Reagan, Energetic particles in the nighttime middle and low latitude ionosphere, Adv. Space Res. Vol. 5 1985, pp.175-178.

Voss, H. D., J. Mobilia, D. W. Datlowe, and S. N. Roselle, The ground support computer and in-orbit survey data analysis program for the SEEP experiment, IEEE Trans. NS Vol. NS-32 1985, pp.168-173.

Voss, H. D., W. L. Imhof, M. Walt, J. Mobilia, Y. T. Chiu, E. E. Gaines, and D. W. Datlowe, Satellite observation of lightning-induced electron precipitation, URSI N. American Rad. Sci. Meeting 1985, p.540.

Voss, H. D., W. L. Imhof, G. T. Davidson, and J. Mobilia, Pulsating electron precipitation at the trapping boundary, EOS Vol. 67 1986, p.345.

Voss, H. D., W. L. Imhof, Y. T. Chiu, and J. Mobilia, Satellite observations of

lightning-induced electric fields, EOS Vol. 67 1986, p. 1166.

Voss, H. D., W. L. Imhof, and J. Mobilia, X-ray imagery, optical and energetic particle observations over antarctica in June 1982, Abstract for SCAR Upper Atmosphere Physics Working Group Meeting 18 June 1986.

Voss, H. D., W. L. Imhof, W. Calvert, J. B. Reagan, D. P. Cauffman, T. C. Sanders, and J. C. Bakke, The atmospheric x-ray imaging spectrometer (XRIS) for the S81-1/SEEP satellite: calibration and flight performance, submitted to IEEE Trans. on Geoscience and Remote Sensing.

IX. SUMMARY OF SEEP PUBLICATIONS

Papers given at AGU meeting: 35

Papers given at other meeting: 20

Publication in JGR: 6

Publications in IEEE: 4

Publications in GRL: 2

Publications in COSPAR proceedings: 2

Publication in Radioscience: 1

Publication in Nature: 1

Publication on cover of Nature: 1

Publication on cover of EOS: 1

X. Abstracts of Papers Presented at Scientific Meetings

Active Wave-Particle Experiment Involving a Satellite and Ground-Based Transmitters

W. L. IMHOF, J. B. REAGAN, H. D. VOSS, and E. E. GAINES (all at Lockheed Palo Alto Research Laboratory, 3251 Hanover Street, Building 255, Palo Alto, California 94304)
R. A. HELLIWELL, U. S. INAN, and J. P. KATSUFRAKIS (all at Stanford University, Calif. 94305)
R. G. JOINER (The Office of Naval Research, Arlington, Virginia 22217)

An active wave-particle experiment is scheduled to begin in 1982 to investigate the effects of ground-based VLF transmitters on the precipitation of energetic electrons from the magnetosphere into the upper atmosphere/ionosphere system. The Stimulated Emission of Energetic Particles Experiment (SEEP) involves a low-altitude satellite payload with an array of cooled silicon solid state detectors to measure precipitated electrons > 2 keV directly, an imaging x-ray proportional counter to map bremsstrahlung x-rays (> 3 keV) and an airglow photometer to measure optical emissions. For the first time, high sensitivity measurements of precipitating electrons will be performed in coordination with the programmed modulation of selected U. S. Navy VLF transmitters and the research VLF transmitter operated by Stanford University at Siple Station Antarctica in characteristic patterns so as to provide a unique correlation capability for cause and effect studies. The VLF data will be recorded at various ground stations and on satellites containing VLF receivers. The coordinated satellite-transmitter operations will be reviewed with respect to the sensitivities for detecting wave-particle interactions, and available preliminary data presented. The possibilities for other coordinated ground-based, balloon, rocket and satellite measurements of waves and particles will also be discussed and encouraged.

EOS Vol. 63 #18, p.404, May 4, 1982

The Phenomenology of Energetic Particle Precipitation in the Magnetosphere

J. B. REAGAN
W. L. IMHOF (both at Lockheed Palo Alto Research Laboratory, 3251 Hanover Street, Bldg. 255, Palo Alto, California, 94304)

The phenomenology of energetic particle precipitation within the magnetosphere will be reviewed. Our present knowledge of the features of the precipitation as a function of latitude, longitude, local time, and magnetic activity will be discussed. The distinctions between bounce and drift loss cone precipitation will be highlighted. The role of natural and man-made waves in the precipitation processes will be emphasized. The occurrence frequency and duration of events, including transient phenomena, will be discussed in terms of their impact on the atmospheric/ionospheric system. The known effects of these precipitations on the neutral, ionized, and electrical components of the atmosphere/ionosphere will be summarized. The limitations of our current knowledge will be delineated and approaches to overcoming these limitations will be proposed.

EOS Vol 63 #18, p.402, May 4, 1982

The Phenomenology of Energetic Particle Precipitation in the Magnetosphere

J. B. REAGAN
W. L. IMHOF (both at Lockheed Palo Alto Research Laboratory, 3251 Hanover Street, Bldg. 255, Palo Alto, California, 94304)

The phenomenology of energetic particle precipitation within the magnetosphere will be reviewed. Our present knowledge of the features of the precipitation as a function of latitude, longitude, local time, and magnetic activity will be discussed. The distinctions between bounce and drift loss cone precipitation will be highlighted. The role of natural and man-made waves in the precipitation processes will be emphasized. The occurrence frequency and duration of events, including transient phenomena, will be discussed in terms of their impact on the atmospheric/ionospheric system. The known effects of these precipitations on the neutral, ionized, and electrical components of the atmosphere/ionosphere will be summarized. The limitations of our current knowledge will be delineated and approaches to overcoming these limitations will be proposed.

EOS Vol. 63 #8, p. 402 May 4, 1982

High Resolution Measurements of Peaks in the Spectra of Electrons Precipitating from the Inner Radiation Belt

E. E. GAINES, W. L. IMHOF, J. B. REAGAN and H. D. VOSS (Lockheed Palo Alto Research Laboratory, Palo Alto, Calif. 94304)

Peaks in the energy spectra of inner belt electrons in the drift loss cone have been shown to be consistent with cyclotron resonance interactions with narrow band waves from VLF transmitters (Imhof et al., JGR, 86, 11225, 1981). Recent measurements with a very high resolution spectrometer on board the S81-1 spacecraft have extended the measurement of these L-dependent peaks to lower energies (~10 keV) and with better resolution (≤ 2 keV FWHM) than previous studies. These new data reveal peaks with resolutions as narrow as 15 keV FWHM placing even more stringent limitations on the region along the field line in which the wave-particle interactions must take place. The peaks have been followed to higher L shell values with correspondingly lower energies than was previously possible. On occasion the peaks rapidly decrease in amplitude at the higher L values. Representative spectra and the L shell dependence of the peaks will be presented along with evaluations of the wave-particle interaction region restrictions and possible VLF wave sources.

EOS Vol. 63 #45, p.1072, November 9, 1982

The Effects of Modulated VLF Transmitters on the Precipitation of Energetic Electrons from the Outer Radiation Belt

W. L. IMHOF, J. B. REAGAN, E. E. GAINES, H. D. VOSS, D. W. DATLOWE and J. MOBILIA (Lockheed Palo Alto Research Laboratory, Palo Alto, Calif. 94304)

R. A. HELLIWELL, U. S. INAN and J. P. KATSUFRAKIS (Radioscience Laboratory, Stanford University, Stanford, Calif. 94305)

From the SEEP payload on the S81-1 spacecraft an investigation is being made of the precipitation of energetic electrons induced by VLF waves generated from U.S. Navy and Siple VLF transmitters. The transmitters at Annapolis, Maryland (21.4 kHz), at Cutler, Maine (17.8 kHz), and at Jim Creek, Washington (24.8 kHz), are modulated at selected times with characteristic patterns which are searched for in the satellite data. The satellite measures both direct electron precipitation down to energies of ~ 2 keV and bremsstrahlung x-rays from the atmosphere. Electron bursts have been observed over a range of L values down to the inner belt and with periods in the few second range. Some of these events originate in natural microbursts, but periodic pulses of precipitating electrons have been seen during satellite passes over transmitter sites. These data have been analyzed to separate natural events from induced precipitation.

EOS Vol. 63 #45, p.1072, November 9, 1982

The Stimulated Emission of Energetic Particles Experiment

J. B. REAGAN and W. L. IMHOF (Space Sciences Laboratory, Lockheed Palo Alto Research Laboratory, Palo Alto, California 94304
R. A. HELLIWELL, U. S. INAN, and J. KATSUFRAKIS (Radiosciences Laboratory, Stanford University, Stanford, California 94305)
R. G. JOINER (Office of Naval Research, Arlington, Virginia 22217)

Since May 1982 an experiment has been conducted to stimulate the precipitation of energetic electrons from the magnetosphere into the atmosphere through resonant wave-particle-interaction processes. The U. S. Navy operational VLF transmitters at Cutler, Maine, Annapolis, Md., and Seattle, Wash. have been operated in pulsed CW modes at the times of overpasses of the low-altitude polar-orbiting satellite S81-1. The Stanford Univ. VLF transmitters at Siple, Antarctica has also been operated in pulsed mode at the time of the satellite overpasses. Aboard the satellite are cooled silicon detectors having very high sensitivity for the detection of electrons in the 2 to 2000 keV energy range as well as an optical photometer and an x-ray imager that view the atmosphere. Waves from the transmitters are measured at several points in the earth's ionospheric wave guide as well as in the magnetosphere by satellites. The objective of the experiment is to uniquely identify the characteristic bursts of electrons in the direct and bounce loss cones associated with the modulated VLF waves. The details of the various experimental elements will be described along with some of the results obtained to date.

EOS Vol. 63 #45, p.1071, November 9, 1982

Simultaneous X-Ray, Airglow and Energetic Particle Measurements Using the SEEP Payload High Sensitivity Spectrometers

H. D. VOSS, W. L. IMHOF, J. B. REAGAN, E. E. GAINES, S. B. MENDE, R. R. VONDRAK, D. W. DATLOWE and J. MOBILIA (Lockheed Palo Alto Research Laboratory, Palo Alto, Calif. 94304)

Unique instrumentation onboard the S81-1 low altitude (170-250 km) satellite is being used to comprehensively analyze numerous energetic particle precipitation events. High resolution (1 keV FWHM) in situ measurements of energetic particles are being made with an array of passively cooled (150°K) silicon solid state detectors (geometrical factors of 0.2 to 0.6 cm^2 ster) which are sensitive to electrons ($E \geq 2$ keV) and ions ($E \geq 15$ keV). Remote sensing of this precipitation is accomplished using a 16 pixel wide imaging proportional counter to map bremsstrahlung x-rays ($3 < E < 30$ keV) in concert with a quadrant airglow photometer sensitive to 391.4 nm (0.8 and 2.4 nm FWHM) and 630 nm (1.2 nm FWHM) wavelengths. Examples are given illustrating the advantages of simultaneous remote and in situ measurements of energetic particle precipitation on a global basis during relatively quiet and disturbed conditions (i.e. middle and low latitude precipitation and various auroral features). Details of the orbital data base coverage are presented with considerations for possible coordinated analysis with ground based and satellite measurements.

EOS Vol. 63 #45, p.1072, November 9, 1982

COORDINATED SATELLITE MEASUREMENTS OF PARTICLE PRECIPITATION DURING THE STORM OF JULY 13, 1982

W. L. IMHOF, J. B. REAGAN, H. D. VOSS, E. E. GAINES, AND J. MOBILIA (SPACE SCIENCES LABORATORY, LOCKHEED PALO ALTO RESEARCH LABORATORY, PALO ALTO, CA 94304)

DURING THE MAJOR MAGNETIC STORM OF JULY 13, 1982 AND THE ASSOCIATED SOLAR PARTICLE EVENT, HIGH FLUXES OF PRECIPITATING PARTICLES WERE MEASURED WITH AN ARRAY OF SPECTROMETERS ON THREE LOW ALTITUDE POLAR-ORBITING SATELLITES IN DIFFERENT LOCAL TIME REGIMES; P72-1 (4 AM - 4 PM), P78-1 (NOON - MIDNIGHT) AND S81-1 (10:30 AM - 10:30 PM) IN THE U. S. AIR FORCE TEST PROGRAM. IN ADDITION TO A VARIETY OF ELECTRON/PROTON SPECTROMETERS ON ALL THREE VEHICLES, BREMSSTRAHLUNG X-RAY DETECTORS WERE PLACED ON THE LATTER TWO SATELLITES AND AN AIRGLOW PHOTOMETER WAS CONTAINED IN THE SEEP PAYLOAD ON THE S81-1 SPACECRAFT. LARGE FLUXES OF PRECIPITATING ENERGETIC PROTONS WERE MEASURED OVER THE POLAR CAP IN ADDITION TO HIGH FLUXES OF ELECTRONS THAT WERE PRECIPITATING AT LOWER LATITUDES. INSTANTANEOUS LOCAL TIME DISTRIBUTIONS IN THE ELECTRON PRECIPITATION OVER A BROAD INTERVAL WERE OBTAINED FROM THE X-RAY DETECTORS ON P78-1. THE TRAPPING BOUNDARY LOCATIONS AND THEIR RELATIONSHIP TO THE SOLAR PARTICLE CUTOFFS WERE ALSO MEASURED AND WILL BE REPORTED IN ADDITION TO THE ENERGY SPECTRA AND SPATIAL DISTRIBUTION OF PRECIPITATING ELECTRONS.

IAGA Meeting 1983

Rapid Spectral Snapshots of Short-Duration Particle Precipitation Events Using the SEEP Payload High Sensitivity Spectrometers

H. D. VOSS, W. L. IMHOF, J. B. REAGAN, and E. E. GAINES (Lockheed Palo Alto Research Laboratory, Palo Alto, Calif. 94304)

Unique instrumentation on board the stabilized S81-1 low altitude (~ 200 km) satellite is being used to comprehensively analyze numerous VLF associated natural and man-made particle precipitaton events. High resolution electron measurements (1 keV FWHM, E > 2 keV) are being made of these events with an array of passively cooled ($150^{o}K$) silicon solid state detectors (geometrical factors of 0.2 to 0.6 cm^{2} ster). The accompanying multidetector-multichannel pulse height analyzer features controllable energy (16 to 256 channels) and time resolution (60 to 1000 ms) for detailed investigation of the time-energy dispersion microphysics. Based on an observed spectral succession of an individual pulse the gyroresonant wave-particle interaction region is remotely sensed. These measurements are compared with theoretical predictions. Details of the orbital data base coverage are presented with consideration for possible coordinated analysis.

Chapman Conference on "Waves in Magnetospheric Plasmas" 1983

Coordinated Measurements of Auroral Zone X-rays from Two Satellites

D. W. DATLOWE, (Lockheed Palo Alto Research Laboratory, Palo Alto, CA 94304), W. L. IMHOF, H. D. VOSS, J. R. KILNER, J. MOBILIA, and J. B. REAGAN
W. CALVERT, (University of Iowa, Iowa City, Iowa 52243)

We report on studies of the spatial distribution of X-ray emission from the Auroral zone during geomagnetically disturbed times. The coordinated observations come from two low altitude polar orbiting satellites, P78-1 and S81-1. P78-1 contains six collimated Cadmium Telluride spectrometers with 21 keV thresholds. The detector fields of view are at selected angles with respect to the satellite spin axis. At the ~ 600 km altitude of the satellite the field of view circle has a radius of ~ 3000 km. The S81-1 satellite contains a position sensitive proportional counter with a 4 keV threshold. The satellite is 3-axis stabilized and at the ~ 220 km altitude of observation each pixel covers a spatial extent of ~ 30 km. Spatially resolved data from these instruments give a picture of the distribution of bremsstahlung emitting electrons. Distributions of electron precipitation in magnetic local time during major events in June, 1982, will be presented.

EOS Vol. 64 #18, p. 294 May 3, 1983

A Statistical Study of Modulated Electron Precipitation Events Induced by Controlled Signals from VLF Transmitters

W. L. IMHOF, (Lockheed Palo Alto Research Laboratory, Palo Alto, CA 94304), J. B. REAGAN, H. D. VOSS, E. E. GAINES, D. W. DATLOWE, J. MOBILIA
R. A. HELLIWELL, (Stanford University), U. S. INAN, J. KATSUFRAKIS
R. G. JOINER, (Office of Naval Research)

The first direct observation of the precipitation of radiation belt electrons by the controlled injection of VLF signals from a ground-based transmitter was recently reported from data in the SEEP (Stimulated Emission of Energetic Particles) experiment (Imhof et al., GRL, 1983). Subsequently, more examples of time-correlated wave and electron data have been found in the data set taken during many passes of the low altitude satellite S81-1 over one of the U. S. Navy VLF transmitters at Cutler, Maine, Annapolis, Maryland, and at Jim Creek, Washington when it was being modulated in a 3s ON/2s OFF format. In several events the fluxes of precipitating electrons displayed a similar time behavior with respect to the transmitter modulation: a relatively slow rate of increase after start of the ON period leading to a maximum about 2 seconds later. Details of these time profiles and their frequencies of occurrence will be presented, along with a comparison of the absolute fluxes of precipitating electrons observed under various conditions of transmitter operation.

EOS Vol. 64 #18, p. 301 May 3, 1983

Effects of Transmitter-Induced Precipitation on the Ionosphere

J. B. REAGAN, W. L. Imhof, H. D. Voss, E. E. Gaines (Space Sciences Laboratory, Lockheed Palo Alto Research Laboratory, Palo Alto, CA 94304)
R. A. HELLIWELL, U. S. Inan and J. Katsufrakis (STAR Laboratory, Stanford University, Stanford, CA 94305)
R. G. JOINER (Office of Naval Research, Arlington, VA 22217)

From May to Dec 1982 an experiment called SEEP was conducted in which energetic electrons were precipitated from the radiation belt by powerful, ground-based VLF transmitters. Unique ON/OFF modulation patterns were employed at the times that the S81-1 satellite was overpassing the transmitter sites. Beams of electrons with good signal-to-background ratios and with the same modulation timing as the transmitter were observed on several occasions to be precipitating into the atmosphere. The most outstanding case occurred on 17 August 1982 when 12 successive beams were observed. High sensitivity sensors aboard the satellite provided direct and detailed measurement of the spectra of the precipitating electrons. The precipitation spectra can be described by an exponential continuum plus the addition of an L-dependent energy peak. The relative intensities of the continuum and the energy peaks varied throughout the interaction region on 17 August. The measured electron spectra have been used as input to an atmospheric deposition computer program to obtain the energy deposition profile and the enhanced ionization rates. Electron density profiles have been derived using available nighttime effective recombination rate coefficients. Near the peak in precipitation the transmitter-induced electron density at 80 km altitude was calculated to be a factor of 6 higher than ambient nighttime conditions. Riometer absorption at 20 and 30 MHz was estimated to be 0.13 and 0.06 db, respectively. Details of the precipitating spectra and the effects on the lower ionosphere will be presented.

EOS Vol. 64 #18, p. 302 May 3, 1983

Preliminary Results from the S81-1 SEEP Satellite X-Ray Imaging Spectrometer (XRIS)

H. D. VOSS, W. L. IMHOF, J. B. REAGAN, R. R. VONDRAK, M. WALT, D. W. DATLOWE, J. MOBILIA, D. P. CAUFFMAN, W. CALVERT* (all of Lockheed Palo Alto Research Laboratory, Palo Alto, CA 94304)
*(now at the University of Iowa, Iowa City, Iowa 52243)

Simultaneous x-ray, airglow and energetic particle measurements have been made onboard the SEEP (S81-1) satellite. SEEP is a 3-axis stabilized satellite in polar orbit at low altitude (170-280 km). The SEEP x-ray imaging spectrometer (XRIS) measures x-rays from the atmosphere with a large area imaging proportional counter sensitive over the energy range of 4 to 40 keV. The XRIS field-of-view is divided into 16 pixels in the direction perpendicular to the satellite trajectory. This enables the remote sensing of electron precipitation over a large area with fine spatial (30 km) and temporal (0.13 sec) resolution. XRIS images are presented for various auroral features: pulsating aurora, discrete arcs, polar-cap events and auroral patches. These x-ray images are compared to the nearly simultaneous airglow (391.4 and 630 nm) and energetic particle (E > 2 keV) measurements. The observed x-ray fluxes and energy distributions can be used to compute the precipitated energetic electron spectra, energy inputs, ionospheric electron densities, and upper atmospheric conductivities.

EOS Vol. 64 #18, p. 302 May 3, 1983

Satellite Observations of Periodic F-Region Gradients During the Stimulated Emission of Energetic Particles (SEEP) Experiment

J. MOBILIA, H. D. VOSS, W. I. IMHOF, J. B. REAGAN, K. L. MILLER (all of Lockheed Palo Alto Research Laboratory, Palo Alto, CA 94304)

Satellite observations of large-scale F-region plasma gradients are reported that accompany manmade precipitation of radiation belt electrons. The radiation-belt precipitation was accomplished by the controlled injection of 17.8 kHz VLF signals from a ground-based transmitter (NAA). Strong F-region electron-density variations having horizontal wavelength of ~200 km have been observed during two of the strongest transmitter-induced precipitation events with the SEEP plasma probe at an altitude of about 220 km. The location and infrequent occurrence of such large density variations suggest they may be responsible for efficient coupling of ground-based VLF energy into selected regions of the magnetosphere. Ionosonde measurements from Wallops Island support the satellite measurements and are used to obtain the vertical density profile. The known properties of internal gravity waves at these latitudes and the satellite observations are used to estimate the spatial distribution of electron density with latitude and altitude.

EOS Vol. 64 #18, p. 289 May 5, 1983

COORDINATED SATELLITE MEASUREMENTS OF PARTICLE PRECIPITATION DURING THE STORM OF JULY 13, 1982

W. L. IMHOF, J. B. Reagan, H. D. Voss, E. E. Gaines, and J. Mobilia (Space Sciences Laboratory, Lockheed Palo Alto Research Laboratory, Palo Alto, CA 94304)

During the major magnetic storm of July 13, 1982 and the associated solar particle event, high fluxes of precipitating particles were measured with an array of spectrometers on three low altitude polar-orbiting satellites in different local time regimes; P72-1 (4 am - 4 pm), P78-1 (noon - midnight) and S81-1 (10:30 am - 10:30 pm) in the U. S. Air Force Test Program. In addition to a variety of electron/proton spectrometers on all three vehicles, bremsstrahlung x-ray detectors were placed on the latter two satellites and an airglow photometer was contained in the SEEP payload on the S81-1 spacecraft. Large fluxes of precipitating energetic protons were measured over the polar cap in addition to high fluxes of electrons that were precipitating at lower latitudes. Instantaneous local time distributions in the electron precipitation over a broad interval were obtained from the x-ray detectors on P78-1. The trapping boundary locations and their relationship to the solar particle cutoffs were also measured and will be reported in addition to the energy spectra and spatial distribution of precipitating electrons.

1. Dr. William L. Imhof
   Lockheed Palo Alto Research Laboratory
   D/52-12, B-255
   3251 Hanover Street
   Palo Alto, California 94304
2. Session G3 General Contributions to Division III on Magnetospheric Phenomena
3. Dr. N. Fukushima
   Dr. A. Nishida, Convener
4. Category of this paper (a) oral presentation highly preferred
5. Special Requests: None; 35 mm slides will be used

IAGA 17th General Ass. of IUGG August 1983

Observation of Multiple Peaks in the Spectrum of Trapped Electrons from Low Earth Orbit

D. W. DATLOWE, W. L. IMHOF, H. D. VOSS, E.E. GAINES, AND J. B. REAGAN, (Lockheed Palo Alto Research Laboratory, Palo Alto, Ca. 94304)

We report on measurements of trapped electron spectra made by the S81-1 spectrometer in the energy range 6 keV to 1 Mev. In many cases the spectra exhibit multiple peaks. The peaks have been observed in the longitude range 300° - 360°E and for magnetic L parameters 1.2 to 1.8. At the 250km observing altitude of the S81-1 instrument, peaks are routinely observed at southern latitudes in this L-range. Correlated observations with the P78-1 satellite at 600 km show that the phenomenon occurs in both hemispheres. The energies at which the peaks occur decreases linearly with increasing magnetic L parameter and changes with longitude. The general characteristics of these spectra will be presented.

EOS Vol. 64 #45, p. 809 November 8, 1983

Coordinated Satellite and Ground-Based Studies of Intense Magnetospheric Electron Precipitation Events

W. L. IMHOF, J. B. REAGAN, H. D. VOSS, D. W. DATLOWE, J. R. KILNER, E. E. GAINES, AND J. MOBILIA, (Lockheed Palo Alto Research Laboratory, Palo Alto, CA 94304)
T. J. ROSENBERG, (Inst. for Phy. Sci. & Tech., University of Maryland, College Park, MD 20742)
R. G. JOINER, (Office of Naval Research, Arlington, VA 22217

The precipitation of energetic electrons (tens of keV and greater) during strong precipitation events has been investigated using both direct electron and bremsstrahlung x-ray observations from two satellites and riometer and magnetometer measurements at Antarctic stations. The riometer absorption during an event at ~ 2300 UT on 27 June 1982 was > 10 db at 30 MHz, the highest recorded at South Pole in 1982 associated with an isolated substorm. Near the time of maximum absorption the P78-1 satellite was over the Southern polar cap and bremsstrahlung x-ray mappings > 21 keV were performed with an array of cadmium telluride spectrometers that overlapped the South Pole station. The x-ray mappings indicated that the position of maximum electron precipitation was close to the South Pole. Nearly simultaneous direct electron and bremsstrahlung x-ray measurements were also performed over the North polar cap with the SEEP payload on the S81-1 spacecraft and these provide the opportunity to study conjugacy effects. At the time of the SSC near 1618 UT on 13 July 1982 the fluxes of bremsstrahlung x-rays > 21 keV recorded from the P78-1 satellite were the highest noted in over four years of on-orbit operation. During this event riometer absorption of > 10 db at 30 MHz was recorded at South Pole, comparable to that observed on 27 June 1982.

EOS Vol. 64 #45, p. 810 November 8, 1983

Coordinated Satellite and Ground-Based Studies of Intense Magnetospheric Electron Precipitation Events

W. L. IMHOF, J. B. REAGAN, H. D. VOSS, D. W. DATLOWE, J. R. KILNER, E. E. GAINES, AND J. MOBILIA, (Lockheed Palo Alto Research Laboratory, Palo Alto, CA 94304)
T. J. ROSENBERG, (Inst. for Phy. Sci. & Tech., University of Maryland, College Park, MD 20742)
R. G. JOINER, (Office of Naval Research, Arlington, VA 22217

The precipitation of energetic electrons (tens of keV and greater) during strong precipitation events has been investigated using both direct electron and bremsstrahlung x-ray observations from two satellites and riometer and magnetometer measurements at Antarctic stations. The riometer absorption during an event at ~ 2300 UT on 27 June 1982 was > 10 db at 30 MHz, the highest recorded at South Pole in 1982 associated with an isolated substorm. Near the time of maximum absorption the P78-1 satellite was over the Southern polar cap and bremsstrahlung x-ray mappings > 21 keV were performed with an array of cadmium telluride spectrometers that overlapped the South Pole station. The x-ray mappings indicated that the position of maximum electron precipitation was close to the South Pole. Nearly simultaneous direct electron and bremsstrahlung x-ray measurements were also performed over the North polar cap with the SEEP payload on the SBI-1 spacecraft and these provide the opportunity to study conjugacy effects. At the time of the SSC near 1618 UT on 13 July 1982 the fluxes of bremsstrahlung x-rays > 21 keV recorded from the P78-1 satellite were the highest noted in over four years of on-orbit operation. During this event riometer absorption of > 10 db at 30 MHz was recorded at South Pole, comparable to that observed on 27 June 1982.

EOS Vol. 64 #45, p. 810 November 8, 1983

Study of the Effects of VLF Transmitter Operation on the Fluxes of Precipitating Electrons

J. MOBILIA, W. L. IMHOF, J. B. REAGAN, H. D. VOSS, E. E. GAINES, AND D. W. DATLOWE, (Palo Alto Research Laboratory, Palo Alto, California 94304)
R. A. HELLIWELL, U. S. INAN, AND J. KATSUFRAKIS, (STAR Laboratory, Stanford University, Stanford, CA 94305)
R. G. JOINER, (Office of Naval Research, Arlington, VA 22217)

Examples of the direct precipitation of radiation belt electrons by the controlled injection of VLF signals from a ground based transmitter have been recently reported from data acquired on the SEEP (Stimulated Emission of Energetic Particles) experiment. During each of the events the fluxes of precipitating electrons were observed repeatedly to display a characteristic time behavior with respect to the transmitter modulation. Now, detailed comparisons have been made of the absolute fluxes of precipitating electrons observed during normal operation of the U. S. Navy VLF transmitters at Cutler, Maine, at Annapolis, Maryland and at Jim Creek, Washington with those recorded when one of these transmitters was modulated in a special 3s ON/2s OFF format. The data in the longitude interval 220° - 310°E were acquired during a total of ~ 400 passes of the satellite, ~ 100 of which were taken during times of the special transmitter modulation. Large variations in the fluxes of precipitating electrons from one satellite pass to another are observed at a variety of L shells and over a broad range of longitudes. Both the normally occurring precipitation and any changes associated with the special transmitter operation will be discussed.

EOS Vol. 64 #45, p. 814 November 8, 1983

SEEP X-Ray Imagery of the Earth's Aurora

H. D. VOSS, W. L. IMHOF, J. B. REAGAN, R. R. VONDRAK, M. WALT, J. MOBILIA, D. W. DATLOWE AND D. P. CAUFFMAN (Lockheed Palo Alto Research Laboratory, Palo Alto, California 94304)
W. CALVERT (University of Iowa, Iowa City 52243)
R. G. JOINER, (The Office of Naval Research, Arlington, Virginia 22217)

X-ray imagery of the Earth's aurora in the 4 to 40 keV energy range was obtained during the S81-1 SEEP mission. S81-1 was a 3-axis stabilized satellite in polar orbit at low altitude (170 - 280 km). The SEEP x-ray imaging spectrometer (XRIS) remotely sensed bremsstrahlung x-rays from the atmosphere over a large area along the orbit cross-track with fine spatial (30 km) and temporal (0.13 sec) resolution. Currently over 250 well defined x-ray events have been identified during the month of June, 1982 and are being quantitatively analyzed to obtain absolute intensities for comparison with the simultaneous airglow (391.4 and 630.0 nm) and energetic particle ($E > 2$ keV) measurements made concurrently onboard the SEEP satellite. The x-ray images have been catalogued and have provided new details of the spatial distributions and energy variations of various auroral features: pulsating aurora (periods < 10 sec), daytime arcs, polar-cap events and auroral patches. The observed x-ray fluxes and energy distributions can be used to compute the precipitated energetic electron spectra, energy inputs, and ionospheric conductivities for comparison with groundbased measurements and theoretical models.

EOS Vol. 64 #45, p. 292 November 8,1983

Satellite Observations of Energetic Ions and Neutrals in the Equatorial Precipitation Zone

H. D. Voss , W. L. Imhof, and J. Mobilia
Lockheed Palo Alto Research Laboratory
3251 Hanover St., Building 255
Palo Alto, California 94304

From the SEEP payload on the S81-1 spacecraft an investigation is being made of energetic ions and neutrals observed in the equatorial precipitation zone. SEEP is a 3-axis stablized satellite in polar orbit at low altitude (170-280 km). High resolution energetic electron (E > 2 keV) and ion (E > 20 keV for hydrogen) measurements were made with an array of passively cooled (150^0K) silicon solid state detectors (geometrical factors of 0.2 to 0.6 cm^2 sr). Remote sensing of the ion and neutral precipitation was accomplished using a quadrant airglow photometer sensitive to 391.4 nm (0.8 and 2.4 nm FWHM) and 630.0 nm wavelengths. Also included in the payload was a plasma diagnostic probe operated as a Langmuir probe.

During the 13 July 1982 magnetic storm (Dst = -328) high fluxes (10^5 cm^{-2} s^{-1} sr^{-1}) of energetic neutrals and ions were observed about the geomagnetic equator. At an altitude of 175 km the flux is observed to dip at the geomagnetic equator. On either side of this minimum an almost mirror image of the flux latitude variation is observed with a maximum intensity located near ± 10 degrees about the geomagnetic equator. Also measured was the location of the plasma trough (i.e. the compression of the magnetosphere) with the plasma probe during the various phases of the magnetic storm. With the energetic particle spectrometers and an airglow photometer strong energetic ion and electron precipitation was observed on midlatitude L-shells associated with the ring current.

The explanation of this equatorial precipitation zone is believed to be a double-charge-exchange process of ions originating in the ring current [Moritz, 1972, Tinsley, 1978, Voss and Smith, 1980a]. By charge exchange with thermal hydrogen atoms, the protons of the ring current become high velocity hydrogen atoms which for those directed toward the earth are focussed in the equatorial atmosphere where they again become protons by ionization collisions. A similar process occurs for energetic helium and oxygen; however, the loss rate from the ring current is smaller than that for protons and consequently the energetic helium and oxygen are more important in the later recovery phase of a magnetic storm. The charge-exchange mechanism is consistent with the measured particle altitude profile, energy spectrum, and pitch-angle distribution [Moritz, 1972; Mizera and Blake, 1973; Voss and Smith, 1977, 1980b] and provides a good explanation of the rapid drift of energetic particles in a direction perpendicular to the magnetic field lines.

The low altitude particle zone is therefore a mapping of the internal composition, spatial geometry and temporal changes of the ring-current particles, weighted by the appropriate cross sections and neutral hydrogen density; it provides a powerful method of studying the ring current.

Based on the satellite observations and the theoretical predictions of the ring current source it is proposed that a multidetector sensor which measures the energetic neutrals might be able to image, in a limited fashion, the integral ion intensities of the ring current as a function of latitude and longitude about the geomagnetic equator (e.g. during one raster scan or spin period of a satellite).

Proc. Yosemite '84: Planetary Plasma Environments : A Comparative View, p.95-96

TID's Above Thunderstorms Associated with the Efficient Transmission of VLF Energy Through the Ionosphere

H. D. VOSS, W. L. Imhof, J. B. Reagan, K. L. Miller, and J. Mobilia, (Lockheed Palo Alto Research Laboratory, Palo Alto, CA. 94304)

The precipitation of energetic electrons from the radiation belts by the controlled injection of 17.8 kHz VLF signals from the NAA transmitter has previously been reported. During two of the strongest transmitter-induced precipitation events measured with the SEEP S81-1 satellite, simultaneous in situ measurements of strong F-region electron density variations were made with the SEEP plasma probe at an altitude of about 220 km. The electron density variations had a horizontal wavelength of about 200 km and are consistent with being classified as traveling-ionospheric-disturbances (TID). Thunderstorm weather fronts have been identified from weather satellite maps as being located directly beneath these two TID's and adjacent to the particle precipitation region. The plasma density gradients associated with TID's are known to extend from the lower D-region into the magnetosphere. It is suggested that the TID's, which may be initiated by the thunderstorms beneath, are responsible for the efficient coupling of VLF waves into the magnetosphere where interaction with the energetic electrons occurs. In all of the sixteen cases of transmitter modulations studied to date in which there were no observed particle precipitation, there was also no evidence of TID activity. Data on the plasma density variations and this correlation with the thunderstorm fronts will be presented.

EOS Vol. 65 #16, p. 267 April 17, 1984

Observation of Multiple Peaks in the Spectrum of Trapped Electrons in the Inner Belt

D. W. DATLOWE, W. L. IMHOF, R. E. GAINES (Lockheed Palo Alto Research Laboratory, Palo Alto, Ca. 94304)

We report on correlated measurements of peaks in the energy spectra of geomagnetically trapped electrons in the range 100 keV to 1 Mev. The peaks are observed in the region of the South Atlantic anomaly at $L \leq 2$. The data have been selected from measurements by an electron spectrometer on the P78-1 satellite from 1979 to 1983. Double spectral peaks were observed several times in conjunction with high geomagnetic activity, but they were not a routine occurrence. Spectra with up to six peaks were seen on some occasions. Coordinated spectral measurements were made with the S81-1 satellite during the fall of 1982. At S81-1's lower altitude (smaller equatorial pitch angle) the spectra tended to have more prominent peaks.

EOS Vol. 65 #45, p. 1044 November 6, 1984

The Simultaneous Energy Selective Precipitation of Electrons and Ions From Narrow Regions of the Outer Radiation Belt

W. L. IMHOF, J. B. REAGAN, H. D. VOSS, D. W. DATLOWE, E. E. GAINES, and J. MOBILIA (Lockheed Palo Alto Research Laboratory, Palo Alto, California 94304)

An investigation has been made of simultaneous large and spatially-narrow enhancements in the fluxes of electrons (68 keV - > 4 MeV) and ions (60 keV - 900 keV) precipitating in the drift loss cone at L ≃ 4 - 5. The events show greater enhancements at higher energies. The electron and ion flux increases observed from low altitude polar orbiting satellites are sometimes co-located and enhancements with widths of ~ 0.1 units in L have been observed on occasion for both electrons and ions. Since electrons and ions longitude drift in opposite directions, on those occasions wher similar flux profiles are seen the interaction may be occurring close to the point of observation. The measurements are interpreted in terms of wave-particle interactions, with the narrow widths in L perhaps being associated with fine structure in the cold plasma density profiles. Possible combinations of electromagnetic ion-cyclotron wave frequency and cold plasma density are invoked to interpret the nearly simultaneous electron and proton precipitation.

EOS Vol. 65 #45, p. 1044 November 6, 1984

Nighttime Satellite Observations of Lightning Flashes Correlated with Electron Precipitation

J. MOBILIA, H. D. VOSS, AND W. L. IMHOF (Lockheed Palo Alto Research Laboratory, Palo Alto, CA 94304)

During the period from May 28 to December 5, 1982 over 200 intense terrestrial lightning events with multiflash bursts were observed with the cooled airglow photometer on-board the low altitude and 3-axis stabilized S81-1 satellite (SEEP payload). Three quadrants of the photometer had center filter wavelengths of 391.4, 390.8 and 630.3 nm. with bandwidths of 0.8, 2.4, and 1.2 nm. respectively. The fourth channel was sealed light tight. The N^+ excitation line (391.4 nm) is well known from ground-based studies to be a significant component of lightning spectra. The geographic distribution of the lightning flash events are found to be consistent with the location of major thunderstorm centers. Also included on the SEEP payload was a fine resolution and high sensitivity (0.17 to 0.51 cm^2 sr) cooled solid state particle spectrometer array. During lightning flash events observed with the photometer numerous Lightning-induced Electron Precipitation (LEP) events were also present. Some of these LEP events were directly associated with observed 391.4 nm lightning flashes. The SEEP energetic electron data base, covering L shells of 2.0 - 3.0 in the longitude interval 200^0 - 310^0 E, is compared with the lightning data base. Strong electron precipitation and LEP events are observed to intensify four to five days after the strong magnetic storms of 13 July and 6 September 1982.

EOS Vol. 65 #45, p. 1060 November 6, 1984

Lightning-Induced Electron Precipitation

H. D. VOSS, W. L. IMHOF, M. WALT, E. E. GAINES, and J. MOBILIA, (Lockheed Palo Alto Research Laboratory, Palo Alto, CA 94304)

U. S. INAN, R. A. HELLIWELL, and D. L. CARPENTER, (STAR Laboratory, Stanford University, Stanford, CA 94305)

Energetic electron precipitation bursts (E ~ 150 keV at L = 2.1) from the earth's radiation belts have been observed with the S81-1 satellite in association with terrestrial lightning flashes. The measured energy deposition (~ 10^{-3} ergs cm^{-2}) of a single Lightning-induced Electron Precipitation (LEP) burst is sufficient to empty about .001% of the radiation belt at L = 2.3 (assuming 10^{8} electrons cm^{-2} q^{-1} and E > 100 keV) in the region covered by the burst magnetic field lines. A one-to-one correlation is found between whistlers observed at Palmer, Antarctica and LEP bursts. In one case, a Trimpi event observed at Palmer is correlated with an LEP event observed 2000 km away in longitude at the S81-1 satellite. Whistler waves (1-6 kHz) that undergo cyclotron resonance with radiation belt electrons are believed to cause the first electron precipitation pulse of the LEP event. This pulse has a broadly peaked energy spectrum (100 < E < 200 keV at L = 2.3) and at 200 km altitude a narrow pitch angle distribution near 90°. Subsequent reflections and backscatterings in the northern and southern hemispheres produce a train of pulses (~ 320 ms period) of diminishing intensity which make up the individual LEP event. The observed LEP peak resonant energies decrease with increasing L consistent with the variation in the equatorial cold plasma density and radiation belt spectra.

EOS Vol. 65 #45, p. 1059 November 6, 1984

Lightning-Induced Electron Precipitation

H. D. VOSS, W. L. IMHOF, M. WALT, E. E. GAINES, and J. MOBILIA, (Lockheed Palo Alto Research Laboratory, Palo Alto, CA 94304)

U. S. INAN, R. A. HELLIWELL, and D. L. CARPENTER, (STAR Laboratory, Stanford University, Stanford, CA 94305)

Energetic electron precipitation bursts (E ~ 150 keV at L = 2.1) from the earth's radiation belts have been observed with the S81-1 satellite in association with terrestrial lightning flashes. The measured energy deposition (~ 10^{-3} ergs cm^{-2}) of a single Lightning-induced Electron Precipitation (LEP) burst represents a reduction of 0.01 - .001% of the radiation belt population at L = 2.3 in the region covered by the burst magnetic field lines. A one-to-one correlation is found between whistlers observed at Palmer, Antarctica and LEP bursts observed on the satellite. In one case, a precipitation-induced subionospheric VLF signal perturbation observed at Palmer is correlated with an LEP event observed 2000 km away in longitude at the S81-1 satellite. Whistler waves (1-6 kHz) that undergo cyclotron resonance with radiation belt electrons are believed to cause the first electron precipitation pulse of the LEP event. This pulse has a broadly peaked energy spectrum (100 < E < 200 keV at L = 2.3) and at 200 km altitude a narrow pitch angle distribution near 90°. Subsequent reflections and backscatterings in the northern and southern hemispheres produce a train of pulses (~ 320 ms period) of diminishing intensity which make up the individual LEP event. The observed LEP peak resonant energies decrease with increasing L consistent with the variation in the equatorial cold plasma density in accordance with cyclotron resonance as well as the radiation belt spectra.

EOS Vol.65 #45, p.1059, Nov. 6, 1984

The Role of Lightning in Precipitating Electrons From the Slot Region of the Radiation Belt

W. L. IMHOF, H. D. VOSS, M. WALT, E. E. GAINES, J. MOBILIA, and D. W. DATLOWE, (Lockheed Palo Alto Research Laboratory, Palo Alto, CA 94304)

An evaluation is made of the contribution of VLF waves generated by lightning in precipitating energetic electrons from the slot region of the radiation belts. This investigation is based on differences between the energy spectra of the electrons in the drift loss cone and the energy spectra of lightning-induced electron precipitation events. The spectra of energetic electrons normally observed in the drift loss cone frequently display pronounced maxima and have sometimes significant flux extending above 500 keV. On the other hand electrons precipitated by lightning often display less pronounced and broad peaks that rarely extend above 250 keV. These upper energy limits are consistent with the wave frequencies associated with lightning and with VLF hiss, assuming that the precipitation results from first order cyclotron resonance of the trapped electrons with VLF waves. In the drift loss cone the spectral information combined with pitch angle distributions allow a determination of the total loss rates from the radiation belts.

EOS Vol. 66 #18, p. 350 April 30, 1985

Energy and Time Structure of Lightning-Induced Electron Precipitation

H. D. Voss, W. L. Imhof, M. Walt, J. Mobilia, and E. E. Gaines (Lockheed Palo Alto Research Laboratory, Palo Alto, California 94304)

U. S. Inan, R. A. Helliwell, and D. L. Carpenter (STAR Laboratory, Stanford University, Stanford, CA 94305)

Lightning-induced electron precipitation (LEP) from the earth's radiation belt has been observed with the SEEP Payload on the low-altitude SR1-1 satellite. The events occurred on a one-to-one basis with the observation of one-hop whistlers at Palmer, Antarctica. The energies ($6 < E < 1000$ keV) of individual electrons were recorded every 4 ms during the LEP bursts and the increase of electron energy with time follows directly the cyclotron resonant frequency of a 1 2 hop whistler at the geomagnetic equator. The observed multipulse time structure (~ 0.33 s period at $L = 2.2$) within LEP burst events is understood to be caused by bunches of magnetically guided 100-200 keV electrons which are repeatedly scattered off the magnetic field line. Additionally, in some cases the burst events repeat after a delay of 1.3 s, suggesting that an echoing whistler may initiate LEP bursts each time it traverses the geomagnetic equator. Near the time of interest VLF measurements on the ISIS satellite and on the ground provide substantial evidence of second and third-hop whistler echoing activity, both in ducted and non-ducted modes. The energy-time structure of the LEP bursts is compared with the whistler-particle interaction model.

EOS Vo. 66 #18, p. 350 April 30, 1985

THE PRECIPITATION OF RADIATION BELT ELECTRONS BY VLF TRANSMITTERS, BY PLASMASPHERIC HISS, AND BY LIGHTNING WHISTLERS

W. L. Imhof, H. D. Voss, M. Walt, E. E. Gaines, J. Mobilia, and D. W. Datlowe
Lockheed Palo Alto Research Laboratory
Palo Alto, California 94304

The frequency of occurrence of the various processes by which VLF waves precipitate geomagnetic electrons can be studied by the characteristic energy spectra of the precipitated electrons. In the inner radiation belt and the slot region it has been clearly demonstrated that ground-based transmitters precipitate electrons with narrowly peaked spectra, and that the energy of the peaks decreases rapidly with increasing L. In the slot region electrons are often precipitated by wave bands associated with plasmaspheric hiss and lightning whistlers. The resulting energy spectra of the precipitated electrons have broad peaks with a similar L-dependence to those associated with transmitters. Using data from electron spectrometers on two low altitude satellites, we will show spectra attributed to each of these processes. The data provide a measure of the relative importance of the various loss mechanisms as a function of L, local time and geomagnetic activity.

URSI 1985 North American Radioscience Meeting
p. 539 June 1985

SATELLITE OBSERVATION OF LIGHTNING-INDUCED ELECTRON PRECIPITATION

H. D. Voss, W. L. Imhof, M. Walt, J. Mobilia, T. T. Chiu,
E. E. Gaines, and D. W. Datlowe
Lockheed Palo Alto Research Laboratory
Palo Alto, California 94304

Energetic electron precipitation bursts ($100 \lesssim E \lesssim 1000$ keV) from the earth's radiation belts have been observed with the low-altitude S81-1 satellite in association with terrestrial lightning flashes. The measured energy deposition ($\sim 10^{-3}$ ergs cm^{-2}) of a single Lightning-induced Electron Precipitation (LEP) burst represents a reduction of 0.01 - .001% of the radiation belt population at L = 2.3 in the region covered by the burst magnetic field lines. A strong correlation is found between thunderstorm lightning flash events observed with the S81-1 391.4 nm photometer and the LEP bursts. A one-to-one correlation is found between whistlers observed at Palmer, Antarctica and LEP bursts observed on the satellite. In one case, a precipitation-induced subionospheric VLF signal perturbation observed at Palmer is correlated with an LEP event observed 2000 km away in longitude at the S81-1 satellite (Voss et al., Nature, 312, 740-742, 1984).

Whistler waves (1-6 kHz) that undergo cyclotron resonance with radiation-belt electrons are believed to cause the first electron precipitation pulse of the LEP event. This pulse has a broadly peaked energy spectrum ($100 < E < 200$ keV at L = 2.3) and at 200 km altitude a narrow pitch angle distribution near 90°. Subsequent reflections and backscatterings in the northern and southern hemisphere produce a train of pulses ($\sim$ 320 ms period) of diminishing intensity which make up the individual LEP event.

The observed LEP peak resonance energies decrease with increasing L consistent with the variation in the equatorial cold plasma density in accordance with cyclotron resonance as well as the radiation-belt spectra. A study of the latitude variation of LEP events over North America indicates a maximum occurance frequency near L = 2.3 with a rather sharp equatorward cutoff at L = 2. This L-shell region of frequently observed LEP burst is found to be similar to the radiation belt slot region, the midlatitude electron zone and the region of efficient VLF transmitter-induced electron precipitation.

In addition to the satellite observation of optical lightning flashes and LEP bursts in the vicinity of thunderstorms the satellite plasma probe also observed associated F-region irregularities, TID variations ($\lambda \sim 200$ km) and transient displacement currents that are thought to be induced by the transient lightning-induced electromagnetic electric field. The lightning associated transient electric fields are observed to have rise times faster than the instrument resolution of 64 msec and recovery times of several seconds.

URSI 1985 North American Radio Science Meeting
p. 540 June 1985

02.04.08 SATELLITE OBSERVATIONS OF LIGHTNING AND ASSOCIATED ELECTRON PRECIPITATION

H D Voss, W L Imhof, J Mobilia

Lightning-induced electron precipitation (LEP) from the earth's radiation belt has been observed with the SEEP Payload on the low-altitude (F region) S81-1 satellite. The LEP events occurred on a one-to-one basis with the observation of one-hop whistlers at Palmer-Antarctica and in association with lightning flashes observed with the SEEP 391.4 nm photometer. In addition, the SEEP plasma probe observed Traveling Ionospheric Distrubances (TIDs) and transient displacement currents in the vicinity of thunderstorms. The observed current transient is thought to be induced by the transient lightning electric field.

IAGA/IAMAP 5th Gen. Ass., p. 248, August 1985

02.07.06 SIMULTANEOUS X-RAY IMAGERY, OPTICAL AND ENERGETIC PARTICLE OBSERVATIONS OF THE EARTH'S AURORA

H D Voss, W L Imhof, R R Vondrak

X-ray images of the earth's aurora in the 4-40 keV energy range were acquired with the SEEP payload on the low-altitude (F region) S81-1 satellite. The x-ray imaging spectrometer (XRIS) remotely sensed bremsstrahlung x rays from the atmosphere over a large area along the orbit cross-track (~ 700 km long) with fine spatial (20-40 km) and temporal (0.13 s) resolution. Currently over 2000 well defined x-ray maps have been catalogued for the month of June, 1982. The XRIS images provide new details of various auroral features: pulsating aurora ($0.03<2<10$ s), daytime aurora, REP events, polar cap spikes and structured and diffuse auroral forms.

IAGA/IAMAP 5th Gen. Ass. p. 252 August 1985

Probing the Equatorial Plasma Density at L = 1.5 - 2.0 by Cyclotron Resonance Precipitation of Energetic *Electrons*

D.W. DATLOWE, W.L. IMHOF, and E.E. GAINES (All at: Lockheed Palo Alto Research Laboratory D91-20/B255, Palo Alto, Ca. 94304)

Cyclotron resonance precipitation of 70 - 500 keV electrons produces narrow spectral peaks at L values from 1.5 - 2.0. A significant feature of this phenomenon is the variation in energy of the peak with L, which can be used to measure the gradient of the plasma density near the magnetic equator. We report on a survey of over 200 events of this type observed by electron spectrometers on the S81-1 satellite. We compare the gradient inferred from our electron spectra with published models and find that the typical gradient is less steep than expected. These measurements also show the day-to-day variations in the inferred plasma density in the electron precipitation regions.

EOS Vol. 66 #46, p. 1039 November 12, 1985

Observations of Auroral Bremsstrahlung X-rays

W. L. IMHOF and H. D. VOSS (Lockheed Palo Alto Research Laboratory, Palo Alto, Ca. 94304)

Measurements of the bremsstrahlung x-rays produced in the atmosphere by precipitating electrons provide information on the electron fluxes and energy spectra. From satellites these measurements can lead to a unique separation of spatial and temporal variations. The technique, first demonstrated from the P72-1 satellite in 1972, has now provided coarse (from P78-1) and fine scale [$\sim$ 30 km $E > 4$ keV, from S81-1 (SEEP)] mappings of electron precipitation over wide areas under both daytime and nightime conditions. Electron precipitation patterns in the auroral zone as well as the polar cap from several low altitude polar orbiting satellites are presented including pulsating aurora, daytime aurora, inverted V and discrete arcs, polar cap spikes, and other structured and diffuse auroral forms. The expected results from future high altitude satellite programs which can provide mappings of the entire polar region are also discussed.

EOS Vol. 66 #46, p. 1047 November 12, 1985

The Spatial Extent of Lightning and Chorus Electron Precipitation Bursts in the Slot Region

W. L. IMHOF, H. D. VOSS, J. MOBILIA (Lockheed Palo Alto Research Laboratory, Palo Alto, Ca. 94304)

D. S. EVANS (National Oceanic and Atmospheric Administration, Boulder, Co. 80303)

Bursts of precipitating energetic electrons with risetimes less than one second are observed in the slot region; many of the nightside events appear to be associated with lightning whereas those on the dayside may be related primarily to VLF chorus. Based on seven months of data in 1982 acquired with the SEEP payload on the low altitude (170 - 280 km) S81-1 spacecraft a tabulation has been made of narrow bursts in the region L = 2-3. A total of 227 bursts were found; 103 in the daytime and 124 at night. At the time of each of these events data from the NOAA-6 spacecraft (at ~815 km altitude) were examined to find occurrences of bursts observed at the same times as the SEEP events. Events observed simultaneously from the two satellites will be presented along with the results of a study of their frequency of occurrence as a function of the difference in longitude and L value of the two satellites. The preliminary investigations indicate that individual lightning and chorus induced electron precipitation events rarely extend more than about 45° in longitude.

EOS Vol. 66 #46, p. 1039 November 12, 1985

Observations of Auroral Bremsstrahlung X-rays

W. L. IMHOF and H. D. VOSS (Lockheed Palo Alto Research Laboratory, Palo Alto, Ca. 94304)

Measurements of the bremsstrahlung x-rays produced in the atmosphere by precipitating electrons provide information on the electron fluxes and energy spectra. From satellites these measurements can lead to a unique separation of spatial and temporal variations. The technique, first demonstrated from the P72-1 satellite in 1972, has now provided coarse (from P78-1) and fine scale [~ 30 km E > 4 keV, from S81-1 (SEEP)] mappings of electron precipitation over wide areas under both daytime and nighttime conditions. Electron precipitation patterns in the auroral zone as well as the polar cap from several low altitude polar orbiting satellites are presented including pulsating aurora, daytime aurora, inverted V and discrete arcs, polar cap spikes, and other structured and diffuse auroral forms. The expected results from future high altitude satellite programs which can provide mappings of the entire polar region are also discussed.

EOS Vol. 66 #46, p.1047, November 12, 1985

Lightning Observations from the Seep/S81-1 Satellite

J. MOBILIA, H.D. VOSS, W.L. IMHOF (Lockheed Palo Alto Research Laboratory, Palo Alto, California 94304)
S.J. GOODMAN (NASA/Marshall Space Flight Center, Huntsville, Alabama 35812)

During the period from May to December 1982 over 1000 strong terrestrial lightning events with multi-flash bursts were observed with the cooled airglow photometer on-board the low altitude and 3-axis stabilized SEEP/S81-1 satellite. The N^+ excitation line (391.4 nm) is well known from ground based studies to be a component of lightning spectra and was monitored on SEEP with two filter bandwidths of 0.8 and 2.4 nm. The geographic distribution of the lightning flash events are found to be consistent with the location of the major thunderstorm centers. During a SEEP pass over the Oklahoma lightning detection network on 15 June 1982 a one-to-one correlation was observed between the satellite and groundbased measurements of multi-stroke cloud-to-ground flashes. Additional cloud-to-cloud flashes were observed with the SEEP photometer. Several optical lightning flash events have been correlated on a one-to-one basis with electron precipitation bursts from the earth's radiation belt consistent with the expected time delay for interactions near the equator.

EOS Vol. 66 #46, p. 1001 November 12, 1985

Thunderstorm Effects in Space Observed with the SEEP/S81-1 Satellite

H.D. VOSS, W.L. IMHOF and J. MOBILIA (Lockheed Palo Alto Research Laboratory, Palo Alto, California 94304)

Strong coupling is suggested between the terrestrial and space environment based on the low-altitude SEEP/S81-1 satellite data. The SEEP observations above thunderstorms include remote sensing of 391.4 and 630.0 nm wavelengths from lightning flashes and in situ measurements near 200 km altitude of medium scale travelling ionospheric disturbances (TIDs), lightning-induced electron precipitation (LEP), and electric field transients. Thunderstorm weather fronts have been identified from weather satellite maps as being located in the 391.4 nm flash regions and directly beneath the in situ SEEP measurements of TIDs, electric field spikes and LEP bursts. The TIDs have a horizontial wavelength of about 200 km and may be the result of a gravity wave produced from the thunderstorm activity. The transient electric field signatures have rise times faster than the instrument resolution of 64 msec. The energetic electron precipitation bursts ($100 < E < 500$ keV) have energy fluences as great as 10^{-3} ergs cm^{-2} and were frequently observed in the L-shell region between 2 and 3. This region was also associated with the efficient precipitation of energetic electrons from the radiation belts by the controlled injection of 17.8 kHz VLF signals from the NAA transmitter. The efficiency improved dramatically during times of thunderstorm activity.

EOS Vol. 66 #46, p. 1039 November 12, 1985

Pulsating Electron Precipitation at the Trapping Boundary

H.D. VOSS, W.L. IMHOF, G.T. DAVIDSON, and J. MOBILIA (Lockheed Palo Alto Research Laboratory, Palo Alto, California 94304)

Pulsating electron precipitation at the trapping boundary was frequently observed with the SEEP payload on the low-altitude S81-1 satellite (May- Dec, 1982). SEEP x-ray (4-40 keV) and photometer (391.4 nm) measurements remotely mapped energetic electron precipitation with a temporal resolution of 0.06 s. Onboard particle spectrometers indicated intense relativistic electron precipitation with energies extending beyond 1 MeV. The pulsations are identified by the quasi-periodic x ray and 391.4 nm flux variations ($\sim$ 5s period) that are much shorter than the temporal variations associated with the convolution of the instrument field-of-view with the emitting region. The trapping boundary in the auroral region as observed with the SEEP particle spectrometers is characterized by 1) a rapid increase in local mirroring flux from the low polar cap to high radiation belt intensities and 2) a strong energy versus L dependence for precipitating electrons $45<E<1000$ keV. X-ray images of the trapping boundary indicate an arc structure that is extended beyond the x ray field-of-view (600 km) in the direction of constant magnetic latitude. During substorm activity the trapping boundary is observed to move equatorward with associated strong pulsations. These measurements are consistent with previous results; however, the SEEP high sensitivity, low thresholds, and x ray mapping capability have important implications to the theory of particle trapping and precipitation.

EOS Vol. 67 #16, p. 345 April 22, 1986

Abstract for SCAR Upper Atmosphere Physics Working Group
Meeting 18 June 1986

X-RAY IMAGERY, OPTICAL AND ENERGETIC PARTICLE OBSERVATIONS OVER ANTARCTICA IN JUNE 1982

H.D. VOSS, W.L. IMHOF, AND J. MOBILIA
(Lockheed Palo Alto Research Laboratory, Palo Alto, CA, 94304)

X-ray images of the earth's aurora in the 4-40 keV range were acquired in June 1982 with the SEEP payload on the low-altitude polar orbiting S81-1 satellite. The x-ray imaging spectrometer (XRIS) remotely sensed bremsstrahlung x-rays from the atmosphere over a large area along the orbit cross- track (600 km) with fine spatial (20-40 km) and temporal (0.13 s) resolution. Currently over 2000 well defined x-ray maps have been catalogued for the month of June 1982. Simultaneous energetic particle ($2 < E < 1000$ keV), plasma density, and photometer (391.4 and 630.0 nm) measurements are compared with the x-ray images and provide new details of various auroral features: pulsating aurora, daytime aurora, trapping boundary arcs, polar cap spikes, inverted V events, and other structured and diffuse auroral forms.

SCAR Meeting, June 1986

Spectral Mapping of Precipitating Electrons with X-ray Images

D. W. DATLOWE, W. L. IMHOF, H. D. VOSS (Lockheed Palo Alto Research Laboratory, Palo Alto, California 94304)

We present, for the first time, a snapshot of the the spectral variation of > 5 keV electrons precipitating into the auroral zone as a function of magnetic local time. The measurements use the two-dimensional mapping characteristic of an X-ray imager to view the auroral oval for up to six hours of MLT in a single ~ 10 minute observation.

The measurements were made during June 1982 by the imaging proportional counter of the SEEP experiment on the low altitude polar orbiting satellite S81-1. The data consist of spatially resolved bremsstrahlung X-ray spectra in the energy range 4-40 keV. From the X-ray spectral maps we have inferred the spectra of the precipitating electrons and we have mapped the electron energy input to the atmosphere.

For selected auroral events we show the variation in electron spectral slope and the variation in precipitating flux with magnetic local time. In these events we have found that the spectral hardness increases toward midnight MLT.

EOS Vol. 67 #44, p. 1169-70 November 4, 1986

Electron Precipitation Patches at High Latitudes

W. L. IMHOF, H. D. VOSS, D. W. DATLOWE and J. MOBILIA (Lockheed Palo Alto Research Laboratory, Palo Alto, California 94304)

Isolated patches of electron precipitation at high latitudes have been investigated with bremsstrahlung x-ray images (>4 keV) and simultaneous airglow, particle and plasma data acquired with the SEEP payload on the S81-1 satellite. Many of these patches, which are typically ~200 km wide, were reported previously (Imhof et. al. JGR 90, 6515, 1985). We have now found that some patches can occur near each other. Within a patch, narrow spikes of electron precipitation were frequently observed by the SEEP electron spectrometers having thresholds at 2 to 45 keV. The temporal or spatial ambiguity of these spikes can often be resolved with the use of the bremsstrahlung x-ray observations. We have used the satellite data to investigate the following characteristics: 1) the intensities, 2) the shapes, 3) the frequency of spike occurrence, 4) the grouping of the patches, 5) the correlations to interplanetary B_z and various magnetospheric boundaries, and 6) the correlations with SEEP plasma probe measurements. The distribution of the patches in local time and invariant latitude is peaked in the evening sector similar to that of inverted V events. The patches occur on both open and closed magnetic field lines.

EOS Vol. 67 #44, p. 1158 November 4, 1986

Global Distribution of LEP Bursts

J. MOBILIA, H. D. VOSS, W. L. IMHOF (Lockheed Palo Alto Research Laboratory, Palo Alto, California 94304)

Over 200 lightning-induced electron precipitation (LEP) bursts have been identified with the SEEP particle spectrometers on the low altitude S81-1 satellite. The pulse shape of an LEP event (E>45 kev) is characterized by a rapid rise in electron flux (< 0.1 sec) followed by a decaying amplitude ($\tau \sim 1.0$ sec). The distribution of LEP events indicates a rather sharp low-latitude cutoff near L≈2.0 with a peak frequency of occurrence near L≈2.5. Also on SEEP was a quadrant photometer which was used to map the global distribution of lightning flashes at 391.4 and 630.0 nm. The geographic distribution of observed lightning flashes is consistent with the location of major thunderstorm centers. Comparison between the lightning and LEP global distributions suggests that an LEP event can be observed several thousand kilometers from the lightning source region. Satellite data have been used to investigate the following characteristics : 1) latitude/longitude differences, 2) conjugate effects, and 3) diurnal variations.

EOS Vol. 67 #44, p. 1168 November 4, 1986

Airglow Response to Energetic Electron Precipitation Compared with Satellite Observations

K.A. SPEAR, H.D. VOSS and W.L. IMHOF (Lockheed Palo Alto Research Laboratory, 3251 Hanover St., Palo Alto, CA 94304)

Theory and several recent observations suggest that energetic electron precipitation provides a significant source of ionization that can alter the composition of the upper atmosphere over relatively short timescales. Energetic electron precipitation is frequently observed near the trapping boundary by the low altitude Stimulated Emission of Energetic Particles (SEEP) payload on the S81-1 satellite. SEEP X ray images acquired during June of 1982 indicate that precipitation extends over the entire instrument field of view (≈700 km) during which time the SEEP and NOAA-6 satellite particle spectrometers show hard electron spectra (E_0 > 30 keV) with energies at times exceeding 1 MeV. Theories governing airglow production and depletion as a result of enhanced ionization are used to estimate fluxes of 391.4 nm (N_2^+), 215.0 nm (NO), and 1.27 microns (O_3). These estimates are then compared to 391.4 nm data from SEEP as well as the 215.0 nm and 1.27 micron emissions from the Solar Mesosphere Explorer (SME) satellite for selected northern hemisphere events.

EOS Vol. 67 #44, p.1140, November 4, 1986

Satellite Observations of Lightning-Induced Electric Fields

H.D. VOSS, W.L. Imhof, Y.T. Chiu, and J. Mobilia, (Lockheed Palo Alto Research Laboratory, Palo Alto, California 94304)

Strong electric field coupling is suggested between tropospheric lightning flashes and the space environment based on the low-altitude SEEP/S-81 satellite data. The electric field transients were observed as a current transient in the SEEP fixed-voltage Langmuir probe in association with the direct measurements of lightning flashes observed from the same satellite. The offset voltage transient of the Langmuir I-V characteristic is consistent with calculations of the three-axis stabilized satellite geometry in the presence of an external horizontal electric field of $\gtrsim$10 mV/m. The transient electric field signatures have rise-times shorter than the instrument resolution of 64 milliseconds and recovery times of the order of 1 second at 230 km. The SEEP observations above thunderstorms include remote sensing of 391.4 and 630.0 nm lightning flashes and frequent in situ measurements between 150 and 270 km altitude of medium scale traveling ionospheric disturbances (TID), lightning-induced electron precipitation (LEP) and lightning-induced electric field transients. Thunderstorm weather fronts have been identified from weather satellite maps as being located at the 391.4 nm flash regions. A preliminary map of the global distribution of horizontal electric field transients from June to December 1982 will be discussed. The observed strength of the lightning-induced electric field transients may be sufficient to form field-aligned density irregularities, drive ionospheric currents and excite plasma waves.

EOS Vol. 67 #44, p. 1166 November 4, 1986

Spectral Mapping of Precipitating Electrons with X-ray Images from a satellite

D. W. DATLOWE, W. L. IMHOF, H. D. VOSS (Lockheed Palo Alto Research Laboratory, Palo Alto, California 94304)

X-ray images made in the auroral zone have been used to create two dimensional maps of the patterns of precipitation of electrons above 5 keV. We present the first systematic survey of the auroral features found in a set of approximately 100 maps. Data from the X-ray imaging spectrometer on the S81-1 satellite are used to calculate the fluxes and energy spectra of precipitating electrons averaged over ~40 km FWHM square pixels. The field of view is 16 pixels wide, and one image is made for each pass of the satellite over the polar regions. The shapes of the observed X-ray features range from isolated patches and single arcs to complex multi-filament structures. Using the observed X-ray spectrum in each pixel we have derived maps of the intensity and characteristic spectral slope of the precipitating electrons. The characteristic energy of the electrons is often nearly uniform over many pixels, although order of magnitude intensity variations may be present on the same spatial scales.

EOS Vol. 68 #44, p.1435, November 3, 1987

Fast Time Variations in the Energy Spectra of Electron Precipitation Bursts From the Radiation Belts

W. L. IMHOF, H. D. VOSS, M. WALT, J. MOBILIA, D. W. DATLOWE and E. E. GAINES (Lockheed Palo Alto Research Laboratory, Palo Alto, California 94304)

Short duration electron precipitation bursts (>6 keV) with risetimes of less than 1 second and decay times of less than 3 seconds have been studied from the low altitude S81-1 satellite at $L > 2$. The time histories of the events are often comparable in the nighttime and daytime, but the spectral variations with time within a burst are typically quite different. Spectral changes have been observed on time scales of less than 0.1 second. If the precipitation is caused by resonant wave-particle interactions, the frequency variation of the waves will influence the time variation of the electron energies. Many nightside events clearly show a hardening with time which indicates resonant precipitation by waves having a falling frequency with time, a pattern characteristic of whistlers. On the other hand, this time evolution is not evident in most dayside events. The time variations of the energy spectra and other characteristics are consistent with the hypothesis that many of the nighttime precipitation events are caused by lightning and the daytime events by other classes of waves, particularly those associated with chorus. The temporal variations in the energy spectra and the rise and fall times of the events are presented as a function of local time and geographic position.

EOS Vol. 68 #44, p.1440, November 3, 1987

X-RAY IMAGING OF THE AURORAL ZONE BY THE S81-1 SATELLITE

Datlowe, D. W., Imhof, W. L., and Voss, H. D.,
Lockheed Palo Alto Research Laboratories, 3251
Hanover Street, Palo Alto Ca.,94304, USA

We report on the results of a systematic survey of X-ray images of the Auroral Zone acquired by the X-ray spectrometer on the low altitude polar orbiting satellite S81-1. X-ray images from this instrument map the precipitation of electrons with energies above a few keV. The measurements use the two-dimensional mapping characteristic of an X-ray imager to view the auroral oval for up to six hours of MLT in a single $\sim$ 10 minute observation. These images show single or multiple discreet arcs of typical width $\sim$ 100 km crossing the 500 km instrumental field of view. We have obtained the intensities and spectral characteristics of the precipitating electrons in many of these arcs from the observed X-ray spectra. The average energies of the energetic electrons change only slowly along the arcs, although substantial intensity variations are seen. Some of these arcs serve to map out the boundaries between the plasma sheet and the polar cap or the boundaries between the plasma sheet and belts of trapped particles. At the location of maximum precipitation the energetic electron energy input dominates the energy input by particles, but 391.4 nm photometer data taken by the same satellite show that between arcs other sources of ionization must be dominant. These spatial differences mean that X-ray and photometer data provide different information about the origin of particle precipitation in the auroral zone.

IUGG XIX Gen. Ass. Vancouver Canada 1987

XI. Reprints of Publications

IEEE Transactions on Nuclear Science, Vol. NS-29, No. 1, February 1982

A SPACECRAFT MULTICHANNEL ANALYZER FOR A MULTIDETECTOR SOLID STATE DETECTOR ARRAY

H. D. Voss, J. C. Bakke and S. N. Roselle
3251 Hanover Street, Building 255
Lockheed Palo Alto Research Laboratory
Palo Alto, California 94304

Abstract

A newly designed low power spacecraft multichannel analyzer (16 to 256 energy channels) has been developed with the capability of servicing a multidetector array of solid state particle detectors. Various system configurations are presented based on the requirements of a specific detector array concept. The multidetector-multichannel analyzer features controllable energy and time resolution, eleven bit data compression, compactness (13 x 20 cm PC card), and analog display outputs of formatted and accumulated data for CRT display and microprocessor interface. Also featured is the ability of the system to automatically accommodate detector noise level fluctuations (e.g. light, temperature, leakage, amplifier gain, etc.) among individual sensors. Additional parallel processing concepts permit accurate energy coincident logic, fault tolerant redundancy and multiple energetic particle mass analysis.

I. Introduction

Pulse height analyzers are widely used in all fields of nuclear radiation spectroscopy. Recent developments in solid state detector imaging and microelectronics have dictated the need for new concepts in pulse height analysis with the ability to parallel process data from large arrays of solid state detectors.

The fundamental assumption for such parallel processing is the requirement that the sampling rate be long relative to the analysis time. For such conditions, a high speed multiplexing arrangement is possible whereby multiple detectors can be serviced from a single analyzer with appropriate memory capacity. Significant instrument performance is realized along with substantial savings in weight, size, power and cost.

A completed design of a parallel analyzer is described for a six detector particle spectrometer. Unique features and limitations of this analyzer are presented using the various display modes of the microprocessor interface circuitry. Energy resolution is selectable from 16 to 256 binary stepped energy intervals depending on the time behavior, spectral energy resolution, and spacecraft telemetry readout rate. Options of the system include the possible use of 1) advanced coincident energy analysis for a multiple detector telescope to improve signal to noise ratio, 2) RAM look up tables based on the coincident logic of a telescope to define the type of energetic event and 3) fault tolerant design concepts since the multiplexed front end is ideally suited to backup an adjacent PHA if a failure occurs.

II. Types of Parallel Processing

Parallel processing is the ability of a single fast analyzer, to scan a number of variable pulse height sensor outputs and accumulate spectra according to energy, position, coincident logic identification and/or sensor location. In addition, parallel processing is applicable to fast coincident or anticoincident analysis of events from both telescopic arrays of detectors and/or individual sensor instruments. Figure 1 illustrates three basic analyzer methods for accumulating information from a telescopic array of solid state sensors. In these cases, the analysis of coincident pulse heights above certain thresholds is used to give unique information about the incident particle identity and total energy as illustrated in Figure 2.

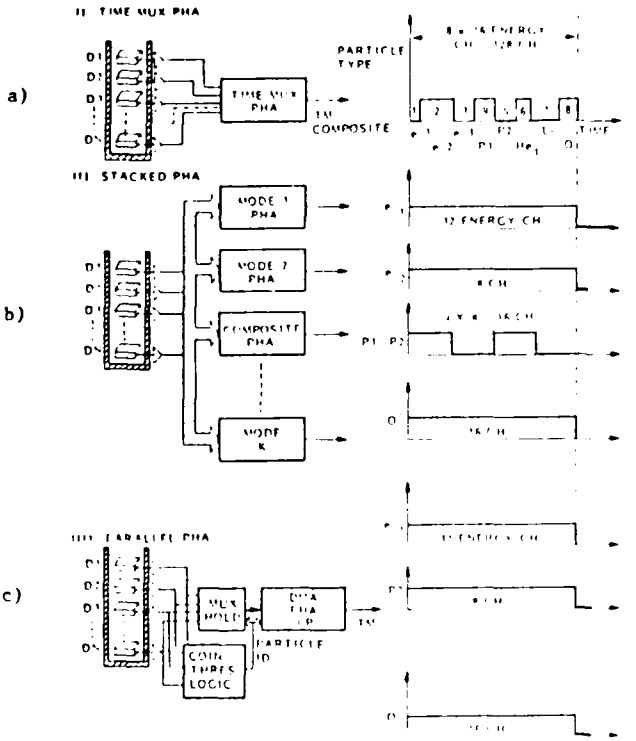

Figure 1. Three analyzer methods for accumulating information from a telescopic array of solid state sensors.

a. Time Multiplexed PHA

The time multiplexed PHA represented in Figure 1a is programmed to pulse height analyze one sensor at a time while the other sensors provide coincident threshold information for identifying valid events. Consequently, only one energetic particle type or energy range is analyzed at one time. After a programmed dwell time the analyzer is stepped to another sensor input and/or coincident logic configuration. For the illustrated case the analyzer steps sequentially through the analysis of low energy electrons (e1), medium energy electrons (e2), high energy electrons (e3), low energy protons (P1), high energy protons (P2), helium (He), lithium (Li) and oxygen (O) ions. The primary advantage of the system in Figure 1a is that one small and low power analyzer can time sample a number of energetic particle events (coincident logic configurations). The primary disadvantages are that large time gaps exists in the data and many valid counts are lost (i.e. 7/8 of the counts, per particle type, for the system of Figure 1a) since only one particle type is analyzed at one time (duty cycle).

0018-9499/82/0200-0173$00.75 © 1982 IEEE

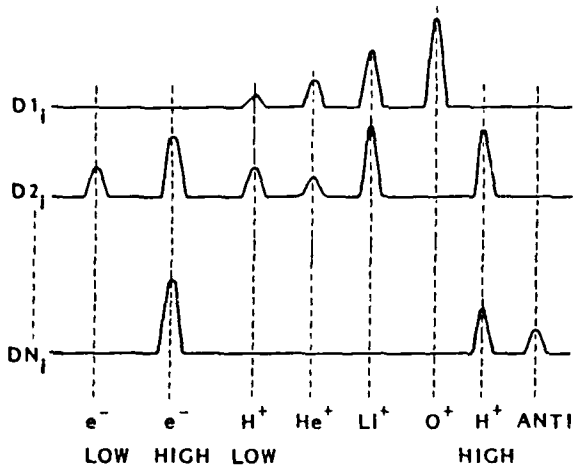

Figure 2. Analysis of coincident pulse heights above certain thresholds is used to give unique information about the incident particle identity and total energy.

b. Stacked PHA

The stacked PHA concept shown in Figure 1b eliminates the disadvantages of the time multiplexed PHA since several PHA's are used in parallel to improve the time-statistics and duty cycle. The various particle types and energy ranges are accumulated in parallel as shown. Other advantages of the system in Figure 1b include redundancy and tailoring of each analyzer to the type of particle measured (i.e. variable number of energy channels and accumulation time). The obvious disadvantages are increased weight, size, power and cost which usually limits this concept to a maximum of two PHA units for spacecraft applications.

c. Parallel PHA

A completely parallel system which minimizes the above logistical constraints is illustrated in Figure 1c. Here, each pulse height event is momentarily stored with a peak hold circuit for each detector. Depending on the validity of the time coincident and pulse height coincident logic thresholds the appropriate detector is selected by the multiplexer and analyzed. The resultant count is stored or accumulated at the specified memory location based on the pulse height and coincident-threshold logic decision. The basic assumption of such an analysis scheme is that the digital PHA analysis time (e.g. 1 μ sec using a high speed digitizer) is usually much faster than the rate at which we wish to sample and accumulate data or, in general, is limited by the analog electronics throughput rate (e.g. 10^5 Hz). For a 1 μ sec analysis time it follows that ten spectrometers could be pulse height analyzed every 10 μ sec at the maximum throughput rate of each spectrometer. For PHA applications which do not require that every pulse be analyzed at the maximum throughput rate of the front-end electronics (i.e. a sampling of input spectra is sufficient) then many more additional spectrometer inputs may be multiplexed into the parallel PHA for analysis.

In general, the Coincident timing logic and amplitude Threshold Logic (CTL) must exist as separate boxes (i.e., stacked) for each identification mode of interest. However, in most cases there is sharing of coincident and threshold logic signals for the various modes and thus less electronics. Furthermore, the fortuitous accompaniment of additional thresholds in the CTL, for all the designed modes, may be intelligently used to improve the particle identification algorithm. To insure that a saturating count rate of one particle type (e.g. low energy electron mode) does not preclude the analysis of other low count rate particle types, it is necessary to use a sequentially stepped priority interrupt for initiating PHA analysis.

For redundancy, it is usually best to implement two parallel PHA's with each servicing half the spectrometers at the maximum sampling rate. Since the multiplexed front end of a parallel PHA is ideally suited for incorporating additional spectrometers a single analyzer can, if need be, process all the spectrometers at half the sampling rate. Some of the advantages of a parallel process design are summarized as follows:

- o Dramatic reduction in size, weight, power and cost for the equivalent analysis capability of an alternate method
- o Ability to analyze multiple spectrometers (usually 4 to 128)
- o No time gaps (100% duty cycle) or significant statistical count rate loss in any of the spectrometers
- o Ideally suited for microprocessor interface or direct readout since accumulated and formatted in a single RAM
- o Saturation protection of high count rates in any channel
- o Allows for fault tolerant redundancy

The primary disadvantage of a parallel processor is that special attention must be given to cross talk in very high energy resolution systems using one A-D converter. Multiple A-D converters with digital multiplexing or a low impedance front-end eliminate this problem.

III. Sampling Techniques

a. First Serve Sampling (RS)

The standard technique for sampling pulse height spectra is based on the analysis of the first pulse which exceeds some threshold voltage, V_T, above the noise in the accumulation interval, t. This technique is simple to implement and preserves the original spectral form. This first-come, first-serve sampling procedure is illustrated in Figure 3 for the case labeled R. Although this technique is appealing for many applications and is mandatory for coincident logic detector systems, there are some significant limitations (particularly in spacecraft instrument) associated with first-serve sampling. These limitations include:

- o The requirement of many commandable thresholds, V_T, for each detector in order to insure the lowest energy thresholds
- o The loss of all data when a saturating high count rate environment of low energy particles is encountered above the threshold, V_T
- o The necessity of setting V_T to the maximum level of the noise expected over an extended period of time (e.g. orbit related noise due to temperature, light, etc.)
- o The significant reduction in the number of high pulse height events, where the number of counts are fewest to start with, since most spectrums are rapidly falling with increasing pulse height. First serve sampling greatly favors the plentiful low energy counts while masking the high energy counts
- o The requirement of a singles rate counter to correct for analyzer deadtime

- o The lack of continuous information about the noise spectral shape
- o The loss of energy analysis capability below the threshold V_T

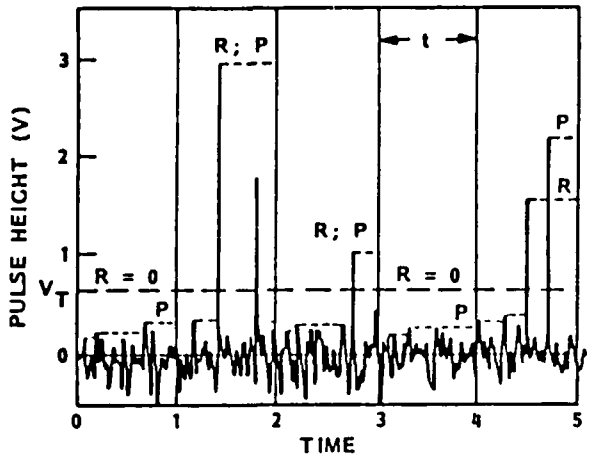

Figure 3. Example of peak sampling, P, and first-serve sampling, R, for energetic pulse events in the time interval t. Note that P sampling follows the noise level and records the maximum peak in interval t while R sampling records zeros in the absence of events above V_T and records the first peak in the interval t.

b. Peak Sampling (PS)

Most of the above problems can be eliminated by using a scanning technique which records only the maximum pulse peak in the time interval t (labeled P in Figure 3). This scanning technique may be preferred in single spectrometer application where only anticoincidence is encountered. This sampling technique is not applicable to coincident telescope systems. At time t = 0, 1, 2, ...N, the peak detect circuit is read and reset to zero. During anticoincidence it is reset. Although spectral deadtime corrections are necessary, as shown in the next section, they are not irreversible, and the true spectrum may be recovered assuming that certain restrictions are placed on the length of the sampling interval t. The incentives for this sampling technique include:

- o Elimination of the lower analysis threshold logic and thus no command overhead and operational simplicity are realized
- o No loss of data in the advent of a noise burst or a saturating high count rate of low energy particles
- o Realization of lowest possible energy thresholds
- o Good statistics for the highest energy counts which are usually fewest in number. The plentiful low energy counts do not mask the infrequent high energy counts
- o The continuous recording of the noise distribution provides information about the engineering status of the instrument and the integral low energy flux contribution to the noise level

In Figure 4 a pulse height spectrum is illustrated for the case of comparing the first-serve and peak detect sampling techniques. The point labeled 1 is the lowest energy (1.5 keV) which can be measured (signal-to-noise ratio of 1) with the peak sampling technique. The ability of the peak detect system to automatically accommodate detector noise level fluctuations is illustrated by the point labeled 2. For high count rate environments (count rate $\geq$ sampling rate) spectral deadtime corrections are required as shown in Figure 4 and the next section.

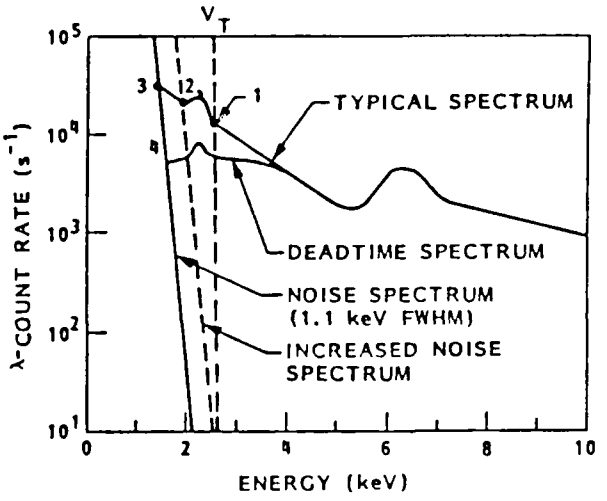

Figure 4. Comparison of pulse spectrum and threshold for peak sampling and first-serve sampling.

c. Spectral Deadtime Correction with Peak Sampling Technique

Although spectral deadtime corrections are required for the peak sampling technique, since counts of high energy have priority in the interval t, the original spectrum may be reconstructed. The basis for reconstruction is the random nature of the incident particle flux which permits the utilization of the Poisson probability distribution given by;

$$P_n(t) = \frac{(\lambda t)^n}{n!} \exp(-\lambda t) \qquad (1)$$

where $P_n(t)$ denotes the probability that n particles will be detected in a t-second interval and λ is the mean count rate. $P_o(t)$ is the probability that no counts occur in the interval t, hence, $1-P_o(t)$ is the probability that one or more events will occur. For a peak detect sampling technique the further restriction must be made that no particle with energy greater than an energy, E, will occur in the interval t. The probability, P, that a count of energy E will be observed in the interval t is given as;

$$P = [1 - P_o(\text{of count } E)][P_o(\text{of all counts} > E)] \qquad (2)$$

This may be solved for a general source spectrum, $F_S(E)$, to give the distorted peak sampling spectrum $F_D(E)$;

$$F_D(E) = \frac{1}{t}(1-\exp(-tF_S(E)))\exp\left(-t\int_E^{\infty} F_S(E)dE\right) \qquad (3)$$

Various numerical methods are available which iterate back from an arbitrary measured input spectrum, $F_D(E)$, to the source spectrum $F_S(E)$. The true

spectrum is derived readily from the measured spectrum by starting at the highest energy channel and working back to the lower energy channels. At each energy channel the corrected integral counts greater than E are used to calculate the deadtime for channel E. Using this procedure equation 3 may be solved for the true source spectrum as

$$F_S(E) = \frac{-1}{t} \ln(1 + tF_D(E) \exp(t \int_E^{\infty} F_S(E)dE)) \quad (4)$$

IV. Parallel Processor Design with Peak Sampling

A block diagram of a six-channel parallel processor is shown in Figure 5 and a photo of the processor in Figure 6. Variable pulse height signals from the six sensors are each routed for analysis to a peak detect circuit (OEI 5902) and to an analog multiplexer. Each peak detector circuit is allowed to track and hold the highest peak value of its input pulses over a time interval, t (e.g., 30 usec). The read and reset of each peak detect circuit is controlled by the master clock strobes in such a way that a continuous and sequential scan is made of each detector. During the read cycle of a particular detector, the output of the peak detector is compared with its input in the coincident logic circuit. If an input pulse is currently raising the peak detector output the sample and hold trigger is delayed until the input pulse peak value is reached. After the read strobe the peak detector output is reset to zero providing the concident logic finds no negative slope on the input signal.

Simultaneous with the reset command, the 256-channel analog-to-digital converter is activated and the resulting digital pulse height (8 bits) is placed on the address bus of a 24-kbit RAM. Also placed in the address bus of the RAM are the three bits which specify which detector is being processed. The content of this memory cell (12 bits) is read into the ALU or fast counter, incremented by one and then read back into the memory cell. The multiplexers are stepped to the next detector and the above process is repeated.

Since the accumulate function is well defined, the use of sequential strobes from a master timer is significantly faster than with a microprocessor. However, the microprocessor is well suited to formatting, compressing, and editing the accumulated RAM contents using direct memory access (DMA) or, in our case, by using two memory banks; one for accumulation while the other is used for readout. An address counter was used to sequentially step through the entire readout RAM. The RAM data compressor packs the 11-bit sum into an 8-bit byte for serial interface with the satellite telemetry.

The contents of the data bus and address bus can be interrogated during any of the strobed time steps using the two 12-bit latches and digital-to-analog converters as shown. For example, during the read-out strobe, the data bus D-A converter would produce a pulse height spectrum on an oscilloscope.

The variable resolution function of the analyzer was particularly effective as a research tool since the energy and time resolution was selectable. The numbers of energy channels selected were 16, 32, 64, 128, or 256 while the time required for a spectral scan would correspondingly be 64, 128, 256, 512, or 1024 msec. This variable resolution is essential for studying a wide range of phenomena when

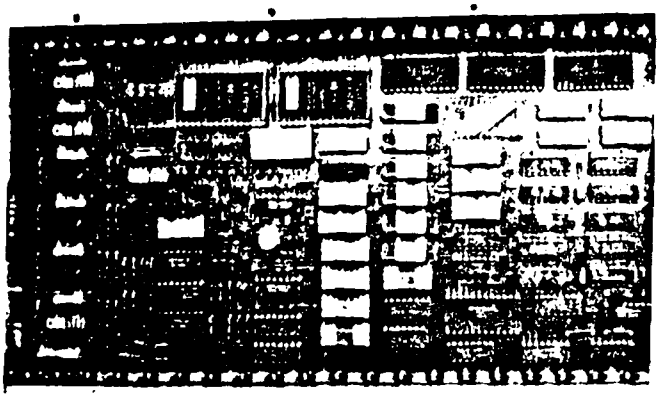

Figure 6. Photo of six spectrometer PHA.

the output data rate is limited to a fixed value. The variable resolution capability was simply implemented by latching high the lowest order bits of the pulse height address. Likewise, the address counter was preset with the latched high bits and incremented by one to obtain the correct readout increment.

An example of the multiplexed PHA output (low gain setting for spectrometer input 2) is shown in Figure 7 for an Am 241 source. The surface barrier detector used is 50 mm^2 by 1 mm thick and is operated at room temperature (6 keV FWHM). This figure, also illustrates the use of the peak sampling technique compared to a threshold voltage (first serve sampling), if used, of V_T.

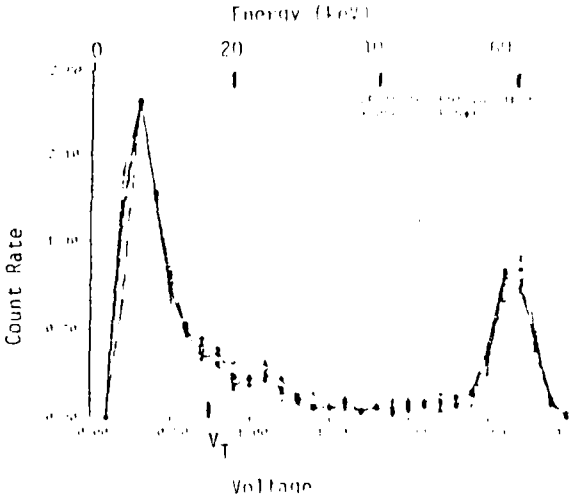

Figure 7. Output of spectrometer 2 on the multiplexed PHA using peak sampling.

V. Conclusion

Parallel PHA processing of a multidetector array of detectors is advantageous for most applications compared to time-multiplexed or stacked PHA methods, particularly in space instrumentation. The implementation of peak sampling techniques for spectrum analysis offers many advantages compared to first-serve sampling when coincident logic is not required. The design of a six spectrometer input PHA system indicates that small size can be realized without sacrificing analyzer performance.

VI. Acknowledgments

This work was sponsored by the Office of Naval Research through Contract N00014-79-C-0824. Analysis of a portion of these data was supported by the Lockheed Independent Research Program. The authors wish to acknowledge the fruitful discussions with Dr. J.B. Reagan, Dr. W.L. Imhof and Mr. D.A. Simpson. Also, acknowledgment of Dr. L.G. Smith from the University of Illinois whose assistance in implementing some of the above mentioned concepts is greatly appreciated.

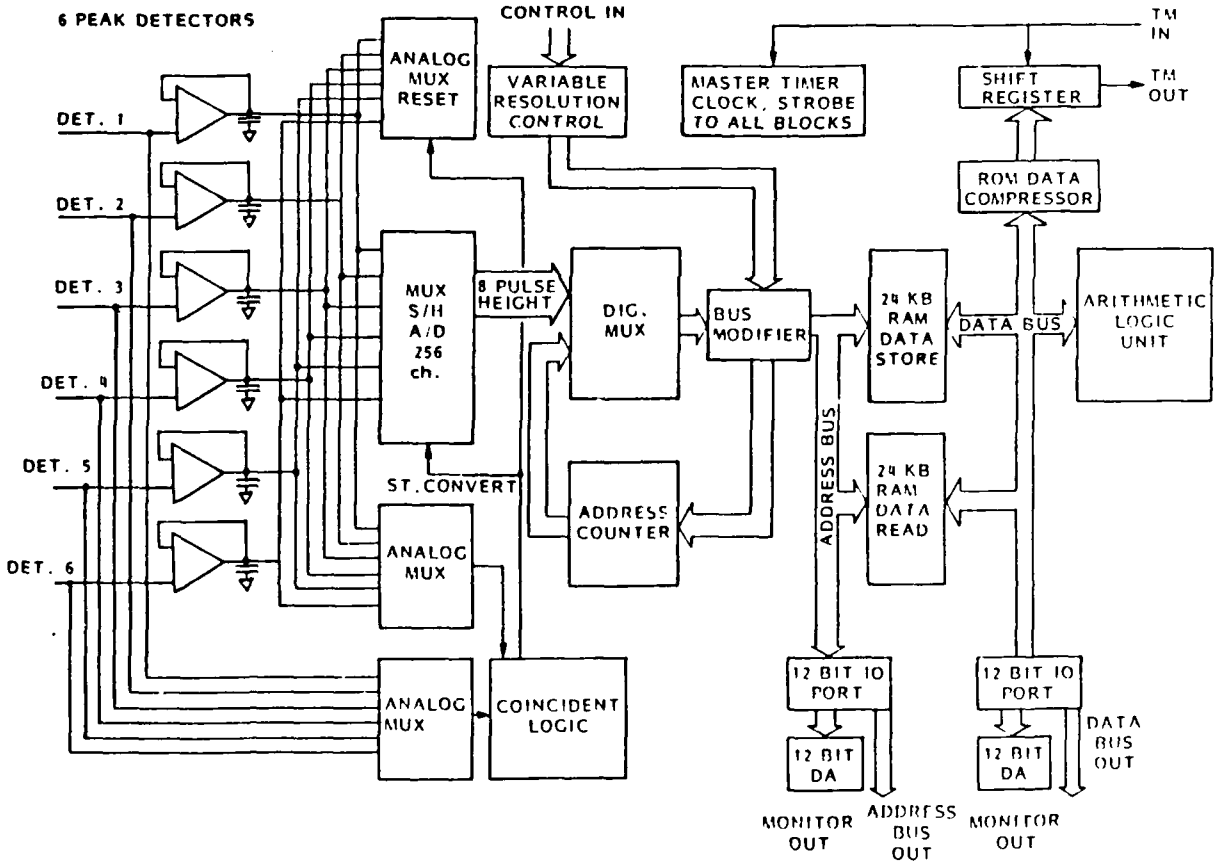

Figure 5. Block diagram of a six spectrometer, multiplexed, PHA.

IEEE Transactions on Nuclear Science, Vol. NS-29, No. 1, February 1982

LOW TEMPERATURE CHARACTERISTICS OF SOLID STATE DETECTORS FOR ENERGETIC X-RAY, ION AND ELECTRON SPECTROMETERS

H. D. Voss, J. B. Reagan, W. L. Imhof, D. O. Murray, D.A. Simpson, D. P. Cauffman and J. C. Bakke
3251 Hanover Street, Building 255
Lockheed Palo Alto Research Laboratory
Palo Alto, California 94304

Abstract

The low temperature characteristics of silicon surface barrier detectors have been investigated to obtain high resolution energetic particle and x-ray measurements for spacecraft applications. Relatively simple electrical and thermal coupling techniques were implemented such that large detector array concepts are feasible. For a 50 mm^2 by 1.5 mm depletion depth surface barrier detector cooled to -80°C the x-ray resolution is 800 eV FWHM using an AC coupled spacecraft instrument preamplifier. Detector system design and calibration results are presented for a spacecraft instrument using both passive radiators and thermoelectric coolers. Energy loss rates in the dead zone region are given for energetic electrons with gold and aluminum surface deposits on the detectors.

I. Introduction

Cooled silicon solid state detectors offer many new advantages for spacecraft applications since high energy resolution (1 keV FWHM) and low energy thresholds (2 keV) are achievable while maintaining continuous particle registration over the energy range 2 to >2,000 keV. Consequently, many new magnetospheric and ionospheric particle events will be studied for the first time. Additional advantages of a cooled solid state detector include:

- Large sensitive area (e.g. 10 cm^2) and resulting geometrical factors for recording low flux levels
- Fast charge collection resulting in short dead-times for high counting rate environments
- Small sensitive volume to minimize background radiation
- Linear pulse height-to-energy ratio
- High detection efficiency for energetic particles
- Relatively low bias voltage (< 500 volts)
- Good gain stability
- Sensitivity to energetic electrons, ions, neutrals and X-rays
- Operation not affected by typical magnetic or electric fields in the vicinity of the solid-state detector
- Rugged-compact detectors for easy application in space instrumentation

The disadvantages of a cooled detector are the susceptibility of some semiconductors to radiation damage, the requirement for cooling the solid state sensor and the mass defect associated with heavy ion measurement.

This paper presents, for the first time, calibration results from a spacecraft instrument using cooled surface barrier detectors for the measurement of energetic electron (E > 2 keV) and ion fluxes with high spectral resolution. Previous investigations[1,2,3] have shown that cooling of a surface barrier detector significantly reduces the system noise. However, application of this technology is only now being realized. Detector evaluation and characterization results are presented first based on theoretical analysis and experimental observations followed by results obtained from a completed spacecraft instrument.

II. Apparatus and Typical Results

A schematic of the cold-vacuum test chamber, which was used to study experimentally the characteristics of various detector configurations, is shown in Figure 1. Air roughing, liquid nitrogen absorption, and vac-ion pumps were used to eliminate chemical contamination within the chamber. A vacuum feed-through cold finger, coupled to the detector mount, controls the temperature of the test detector by dipping into a liquid nitrogen dewar. Microphonics were therefore eliminated by this technique since no coolant was circulated within the chamber. A resistive heater in the thermal path controls the temperature.

Commercially available surface barrier detectors were used with the only special requirement being that cryogenic epoxy was substituted for standard epoxy in the fabrication process. Both p- and n-type partially depleted and n-type totally depleted detectors were used with depletion depths of 1500 to 2000 microns and areas from 25 to 150 mm^2. The gold barrier surface deposit has either 25 or 40 $\mu g\ cm^{-2}$ evaporation and the aluminum contact 40 to 60 $\mu g\ cm^{-2}$.

Calibration of the detector and spacecraft amplifying system was performed using x-rays from Am 241, Cd 109, Fe 55 and Co 57 sources. Electron measurements were made with various conversion electron radioactive sources. Thermocouples were located on the detector mount and cold finger.

A typical Am 241 X-ray spectrum is shown in Figure 2 for a 50 mm^2 x 2 mm surface barrier detector. The complete spacecraft instrument amplifier, preamplifier (Section III) and detector mounting hardware (section V) were used to generate this spectrum. At a temperature of -80°C the X-ray resolution was 0.8 keV FWHM for the AC coupled electronics (2 μsec time constant and bias and feed-back resistors of 5000M ohm each). These results, obtained from a relatively straightforward solid state detector and front-end electronics design, allow for a new class of spaceborne low energy particle spectrometers.

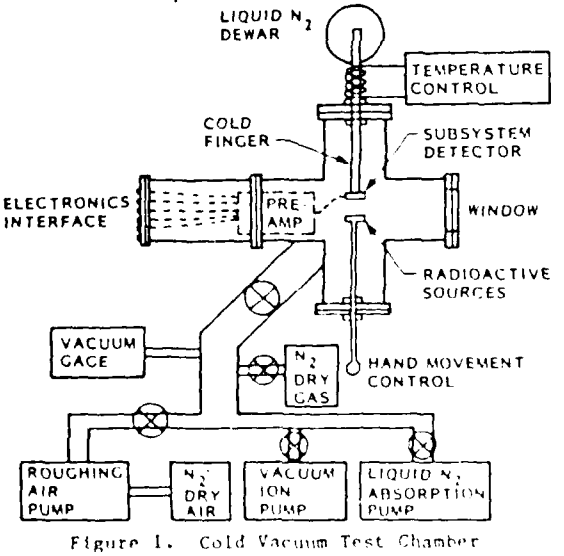

Figure 1. Cold Vacuum Test Chamber

0018-9499/82/0200-0164$00.75 © 1982 IEEE

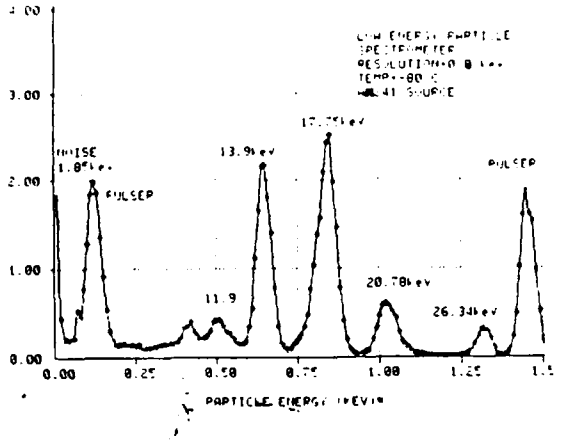

Figure 2. A typical high resolution Am241 spectrum obtained with a cooled surface barrier detector and the space instrument electronics.

III. Practical Considerations

The basic semiconductor equations are applied with the electrical circuit equations to derive the functional dependence of system noise (i.e. energy resolution) on such variables as detector temperature, bias voltage, resistivity and amplifier noise and time constant. The following analysis applies to both AC and DC coupled amplifier designs. However, we have used the AC coupled configuration for our spacecraft application. This was necessary since we required operation of the detector at equivalent room temperature leakage currents introduced from temperature fluctuations, radiation damage and low light level sensitivity.

Total noise of the AC coupled preamplifier with a 6pf input capacitor was 0.7 keV FWHM for a 3 microsecond shaping time constant. This total system noise is less than the energy loss of particles in the dead zone layer and therefore complex optical feedback and FET cooling requirements are unnecessary.

a. Noise Model Analysis

The circuit schematic and AC equivalent circuit of the detector and preamplifier front end are shown in Figure 3. The field effect transistors Q_1 and Q_2 are hand selected[4], and cascaded-coupled as shown for minimizing noise since a constant voltage is applied to the input FET. The equivalent circuit capacitance, C_T, is the sum of the detector and input circuit capacitance. The resistance, R_T, is the parallel combination of R_F and R_B. The current source, I_{TN}, is the sum of the detector leakage current (shot noise), I_{dN}, and resistor current noise, I_{RN}. The voltage noise source, V_{TN}, is the equivalent noise developed in the first amplifying device.

The three current sources can now be transformed into three series voltage sources by dividing them by ωC_T using Thevenin's theorem as shown in Figure 3c. The signal output, V_{SO}, is given by:

$$V_{SO} = \frac{qE}{C_f \epsilon} \qquad (1)$$

where q is the elementary charge, E the energy of an incident particle and ϵ the effective number of electron-hole carriers produced by an energetic particle (3.7 eV for electrons in silicon). The bandgap for silicon is 1.12 eV; however, only approximately 30% of the initial energetic particle energy is effectively used for carrier production while the rest is lost to Raman phonon emission and electron thermal losses to the lattice. For a 1 keV energetic electron within the depletion region the generated charge is 270 electron-hole carriers (4×10^{-17} coulombs). For the circuit of Figure 3 with C_f = 0.1pf the resulting output voltage, V_{SO}, is 0.4 mV.

When the three independent and uncorrelated voltage noise sources are connected in series the total power is the sum of the individual source powers. Consequently, the root-mean-square voltage sources must be added in quadrature such that the total RMS noise, E_{NO}, is given by

$$E_{NO}(RMS) = \frac{1}{C_f}\sqrt{\frac{I_{ND}^2}{\Delta f^2} + \frac{I_{NR}^2}{\Delta f^2} + C_T^2 V_{NT}^2} \qquad (2)$$

where from basic theory [5]

$$I_{ND}^2 = 2qI_d\Delta f$$

$$I_{NR}^2 = 4kT\Delta f/R_T \qquad (3)$$

$$V_{NT}^2 = 4kT\, R_{eq}\, \Delta f$$

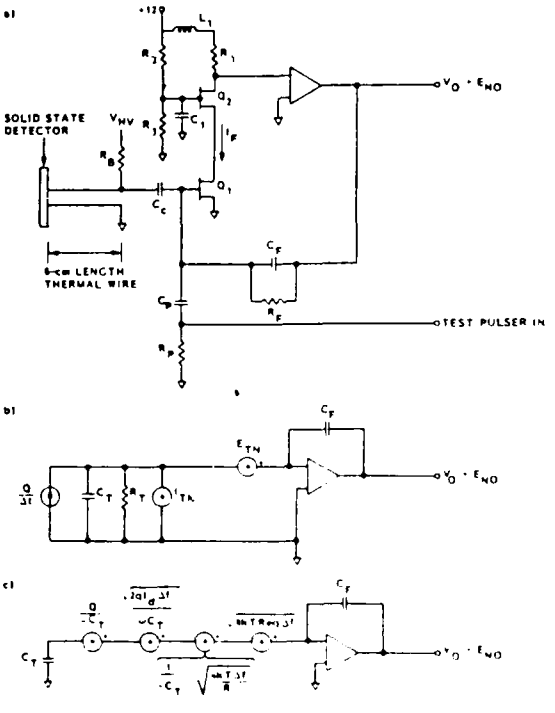

Figure 3. a) Circuit Schematic, b) Lumped Noise source and impedance, c) Transformed Noise sources.

and T is the temperature in Kelvin, Δf the bandwidth or reciprocal time constant, τ, of the amplifier and R_{eq} the equivalent Johnson noise source developed in the first amplifying device based on the majority of

carriers in the channel. Note that the amplifier noise is the only noise source which is affected by the input capacitance. The signal to noise ratio, S/N, is given by V_{SO}^2/E_{NO}^2. It is also convenient to express E_{NO} not only in terms of the true RMS noise voltage (i.e. σ or standard deviation for Gaussian noise) but also in terms of spectral line width; that is the full width at half maximum (FWHM) where

$$E_{NO}\ (FWHM) = 2(2\ \ln\ 2)^{0.5}\ E_{NO}\ (RMS) \qquad (4)$$

$$= 2.35\ E_{NO}\ (RMS)$$

Equations 2, 3 and 4 may be combined to give:

$$E_{NO}(FWHM) = \frac{2.35}{C_f}\sqrt{2qI_d\tau + \frac{4kT\tau}{R_T} + \frac{4kTR_{eq}C_T^2}{\tau}} \qquad (5)$$

b. Resistive Noise

To achieve a low noise design each noise term in equation 5 must be minimized. The preamplifier noise, R_{eq}, associated with a particular equivalent detector input capacitance, C_T, is chosen first. A hand selected low noise FET operating at room temperature with simple RC feedback will give noise resolutions of 0.8 keV FWHM for a capacitance, C_T, of 12 pF (i.e. R_{eq} is 200 Ω). At 6 pf input capacitance, E_{NO} is 0.5 keV FWHM. Lower noise is achieved by reducing the temperature of the input FET and by using optical feedback in place of the feedback resistor R_f. For large capacitance detectors the use of parallel input FET's and FET cooling may be necessary.[6,7]

The bias resistance, R_B, is usually chosen as 5000 M ohm for a cooled solid state detector since the leakage current, I_d, is low ($<10^{-10}$ Amps) and the introduced resistive noise is less than 0.5 keV. For spacecraft instruments the leakage current may increase due to radiation damage, low light intensity and degradation of the cooling system with time. By choosing a lower value of R_B the resistive noise will increase (e.g. 0.8 keV for 1000 M ohm), however, the detector will be sufficiently biased for good operation at room temperature (0.3 μA). The applied voltage, V_{HV}, versus noise characteristics at various temperatures are given in Figure 4 for two different detectors. The selection of an operating bias voltage is predicated on the maximum voltage the detector can tolerate and the worst case leakage current.

c. Leakage Current Noise

Equation 5 may be used to quantify the experimental measurements illustrated in Figure 4 by including the relationships for leakage current and detector capacitance as a function of temperature.

The detector capacitance varies with applied high voltage and thus depends on the leakage current and bias resistance, R_B. The capacitance behaves like a parallel plate capacitor about the depletion region and may be represented as:

$$C_d = \frac{\epsilon_R \epsilon_O S}{W} \qquad (7)$$

where

$$W = \frac{\epsilon_R (V_d + V_o)^{0.5}}{2\pi q N_a}$$

and W is the width of the depletion region (linear electric field variation assumed), ϵ_R is the relative dielectric constant, ϵ_o the permeability of free space, S the surface area of the depletion region, V_o the diode equilibrium voltage (0.7 volt for Si), N_a^o the net density of carriers in the lightly doped depletion region and V_d the voltage across the detector. The total capacitance may be experimentally derived from the lowest temperature characteristic curve of Figure 4 where the leakage current term becomes negligible. For this case:

$$C_T = \frac{A_1}{(V_a + V_o)^{0.5}} + A_2 \qquad (8)$$

where A_1 and A_2 are experimental constants. The noise term, $C_T V_{NT}$, of equation 2 is plotted in Figure 4a for C_T given by equation 8 when A_1 equals 144 pf and A_2 equals +2.4 pf.

The dependence of I_d on temperature is given by the product of the depletion volume (W*S) times the intrinsic carrier density[8], n_i;

$$I_d = Kn_i(V_d + V_o)^{0.5} \qquad (9)$$

where

$$n_i = 2.8*10^{16}\ T^{1.5}\ \exp\ (-6450/T)\ cm^{-3}$$

and K is a constant based on the room temperature leakage current of a fully biased detector. As illustrated in Figure 5, the leakage current noise ($2qI_d\tau$) versus temperature shows good agreement with experimental data.

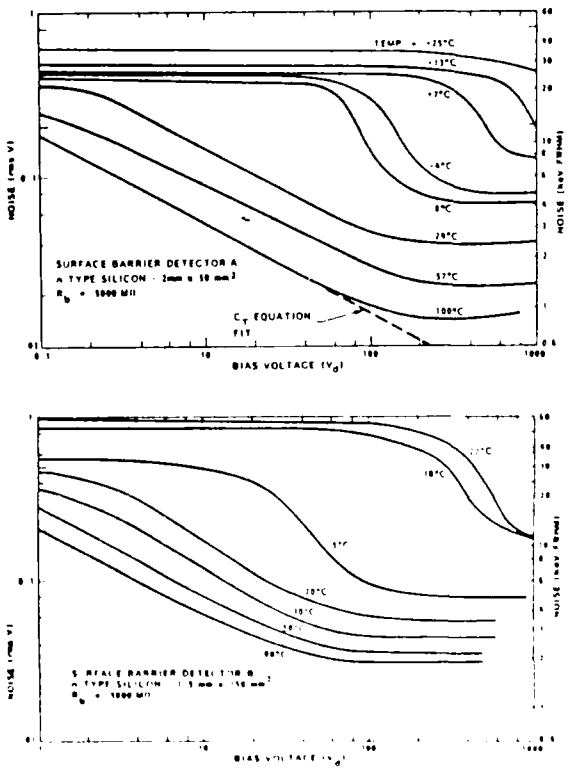

Figure 4. Detector A and B applied voltage, V_{HV}, versus noise characteristics at various temperatures.

The detector voltage, V_d, depends on the leakage current and thus voltage drop across the bias resistor ($V_d = V_{HV} - I_d R_B$) such that equation 9 becomes:

$$I_d = \frac{K^2 n_i^2}{2}\left[-R_B + \sqrt{R_B^2 + 4(V_{HV}+V_o)/(K^2 n_i^2)}\right] \quad (10)$$

d. Total Noise

The total noise of the system as a function of temperature, applied high voltage, bias resistance, leakage current and time constant is given by:

$$E_{NO}(FWHM) = \frac{2.35}{C_f}\left[2qI_d\tau + \frac{4kT_\tau}{BR_T} + \frac{4kTR_{eq}}{\tau} + \left[\frac{A_1}{V_o + V_{HV} - R_B I_d} + A_2\right]^2\right]^{0.5} \quad (11)$$

where I_d is given by equation 10 and B is a constant.

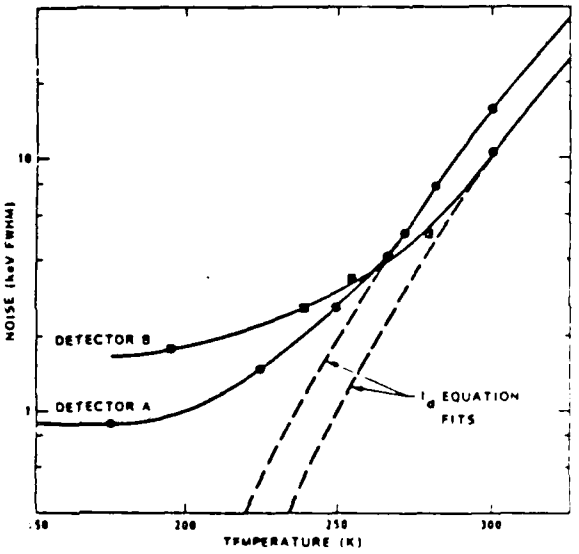

Figure 5. Noise versus temperature for two n type surface barrier detectors.

IV. Window Thickness

The entrance window thickness, x, or dead layer for energetic charged particles must be extremely thin since energy lost here does not contribute to generation of charge carriers in the depletion region. Fortunately this is the case for surface barrier detectors. Ewing[9] and Ray and Barnett[2] have found that the depletion region for low resistivity, n-type detectors extends completely to the gold contact (200Å or 40 $\mu g\ cm^{-2}$). Forcinal[10] has shown that for high resistivity detectors ($\rho > 10^4$ Ω-cm) the entrance window includes a thin dead zone of silicon which may be reduced or eliminated with increased detector bias voltage.

A particularly useful set of data given by Tung[11] on the range and range straggling of energetic electrons (E < 10 keV) in gold and aluminum foils is shown in Figure 6. The range straggling (dashed curves) is a measure of the statistical distribution of ranges about their mean value. For a typical 40 $\mu g\ cm^{-2}$ gold junction the mean range is 1.1 keV and the range straggling is 2.5 keV.

We have also experimented with a 25 $\mu g\ cm^{-2}$ gold surface barrier detector with good results. For this case, the window thickness is only 0.5 keV for electrons and the straggling range 1.2 keV. The significance of this straggling range at low energies is the reason for including an energy dependent transmission term.

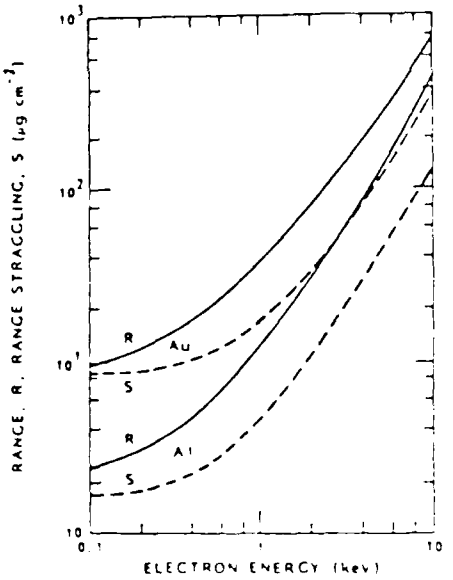

Figure 6. Range-energy curves in Gold and Aluminum for energetic electrons.[11]

V. A Spacecraft Low Energy Particle Spectrometer

A cross-sectional view of the particle spectrometer is shown in Figure 7. The silicon surface-barrier detector is held in place by a thin wall (0.010 inch) fiberglass cylinder. Two electrically insulated thermal cold fingers are attached to the detector housing and provide cooling from either a four stage thermoelectric cooler or by a copper manifold connected to a passive primary radiator (-80°C). The entire detector is shielded from background particles and X-rays with tungsten collimators and shielding as shown. The secondary radiator is covered with an optical solar reflective surface and cools the entire detector housing down to -40°C. The electrical signals from the solid state sensor pass through a 0.375 inch fiberglass tube used as a low capacitance coax for the manganin thermally resistive wire. The preamplifier (not shown) is operated at +20°C.

The cooled solid state particle spectrometer array is shown in Figure 8. Sensors LE1, LE2, and LE3 are used to map the particle angular distribution function. LE2, LE4, and LE5 are used to determine the electron and ion ratio and the identity of the primary ion.[12] The primary radiator is designed to cool the LE1, LE2, and LE3 sensors to -80°C. A detailed thermal-vacuum test has verified the thermal design and the low energy capability of the instrument.

AD-A108 724 STIMULATED EMISSION OF ENERGETIC PARTICLES (SEEP)(U) 2/3
LOCKHEED MISSILES AND SPACE CO INC PALO ALTO CA PALO
ALTO RESEARCH LAB W L INHOF ET AL. 30 NOV 87
UNCLASSIFIED LMSC/D068456 N00014-79-C-0024 F/G 4/1 NL

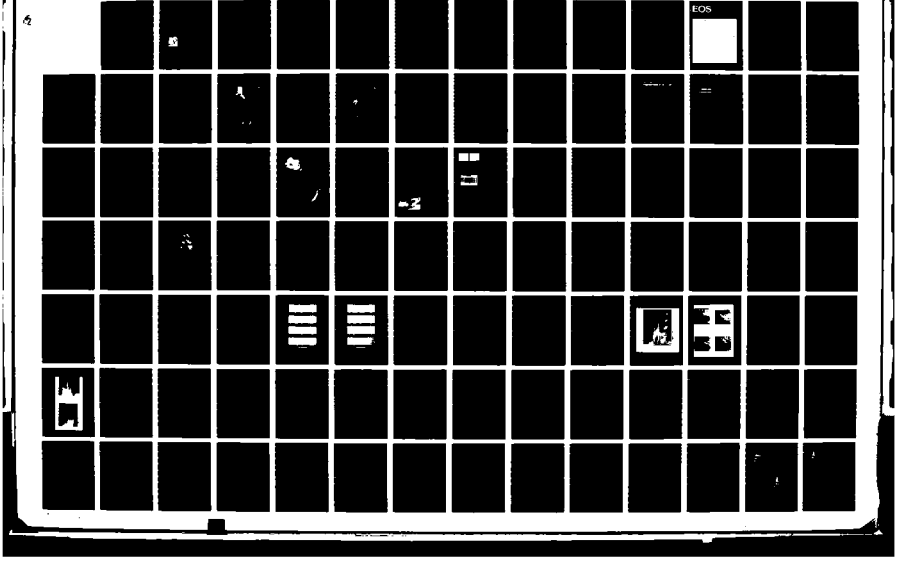

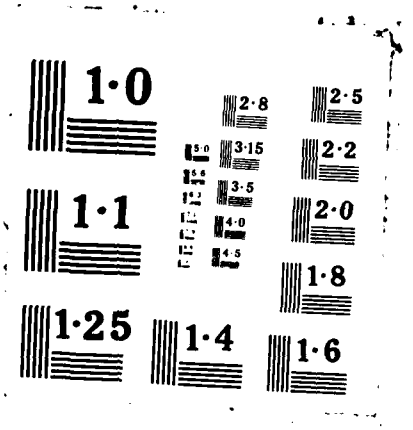
1·0
1·1
1·25
1·4
1·6
1·8
2·0
2·2
2·5
2·8
3·15
3·5
4·0
4·5
5·0

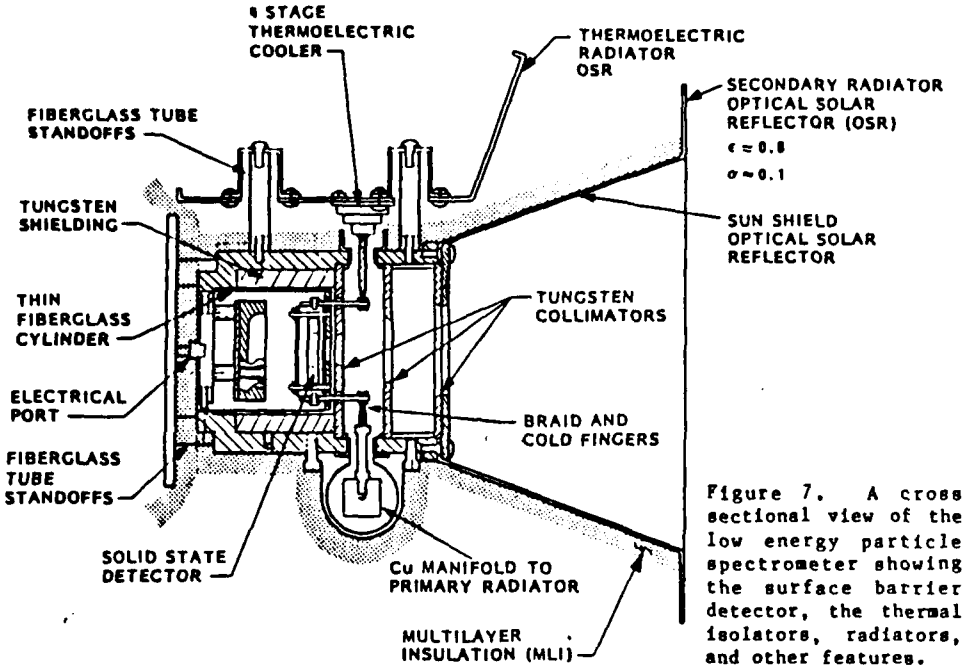

Figure 7. A cross sectional view of the low energy particle spectrometer showing the surface barrier detector, the thermal isolators, radiators, and other features.

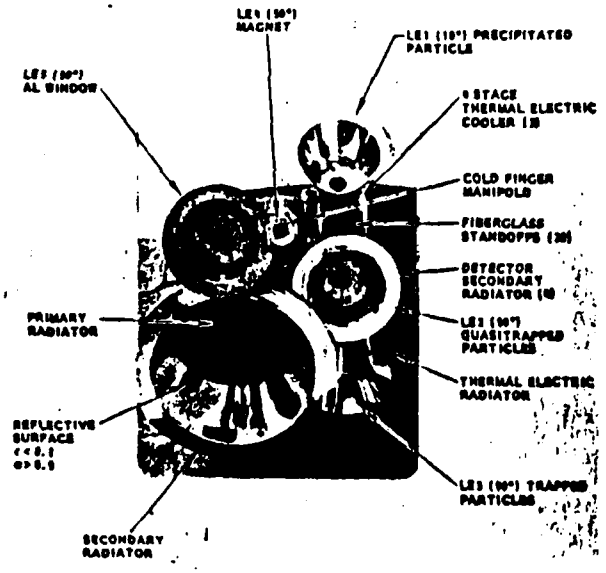

Figure 8. Photograph of the cooled solid state spectrometer experiment showing the five particle spectrometer heads and thermal radiators.

VI. Conclusion

When properly operated at low temperatures, silicon surface-barrier detectors can perform with high resolution (< 1 keV FWHM) and with low energy thresholds (2 keV) for energetic particle analysis using relatively straightforward design procedures. Laboratory and theoretical results indicate the dependence of system noise on temperature, bias voltage, time constant, and input impedence for detector optimization.

VIII. Acknowledgments

This work was sponsored by the Office of Naval Research through Contract N00014-79-C-0824. Analysis of a portion of these data was supported by the Lockheed Independent Research Program. The authors wish to acknowledge the fruitful discussions with Dr. G. H. Nakano, Mr. E. E. Gaines and Mr. S. J. Battel. Thanks are also due to Mr. S. Roselle, who assisted in the measurements made for this paper.

IX. References

1. E. Elad and M. Nakamura, Nucl. Instr. and Meth., 41, 161 (1966).
2. J. A. Ray and C. F. Barnett, IEEE Trans. Nucl. Sci., NS 16, 82 (1969).
3. E. Elad and R. Sareen, IEEE Trans. Nucl. Sci., NS 21, No. 1, 75 (1974).
4. Various selected FETS were used. The data presented in this paper was obtained using a TI SFB 8558 or Solitron SFD 3001.
5. C. D. Motchenbacher and F. C. Fitchen, Low-Noise Electronic Design, John Wiley and Sons, New York, 1973.
6. T. V. Blalock, IEEE Trans, Nucl. Sci., NS 13, No. 3, 457 (1966).
7. K. F. Smith and J. E. Cline, IEEE Trans. Nucl. Sci., NS 13, No. 3, 468 (1966).
8. F. S. Goulding, Semiconductor Detectors for Nuclear Spectrometers, p 27, UCRL-16231, Univ. of Calif., Lawrence Radiation Laboratory, Berkely, 1965.
9. R. J. Ewing, IRE Trans. Nucl. Sci., NS 9, no. 3, 207 (1962).
10. G. Forcinal, P. Siffert and A. Coche, IEEE. Trans. Nucl. Sci., NS-15, 475 (1968).
11. C.J. Tung, J.C. Ashley and R.H. Ritchie, IEEE. Trans. Nucl. Sci., NS-26, 4874 (1979).
12. H.D. Voss, IEEE. Trans. Nucl. Sci., this publication, (1981).

GEOPHYSICAL RESEARCH LETTERS, VOL. 10, NO. 4, PAGES 361-364, APRIL 1983

DIRECT OBSERVATION OF RADIATION BELT ELECTRONS PRECIPITATED BY THE CONTROLLED INJECTION OF VLF SIGNALS FROM A GROUND-BASED TRANSMITTER

W. L. Imhof, J. B. Reagan, H. D. Voss, E. E. Gaines,
D. W. Datlowe, and J. Mobilia
Lockheed Palo Alto Research Laboratory, Palo Alto, CA 94304

R. A. Helliwell, U. S. Inan, and J. Katsufrakis
STAR Laboratory, Stanford University, Stanford, CA 94305

R. G. Joiner
Office of Naval Research, Arlington, VA 22217

Abstract. Radiation belt electrons precipitated by controlled injection of VLF signals from a ground based transmitter have been directly observed for the first time. These observations were part of the SEEP (Stimulated Emission of Energetic Particles) experiment conducted during May - December 1982. Key elements of SEEP were the controlled modulation of VLF transmitters and a sensitive low altitude satellite payload to detect the precipitation. An outstanding example of time-correlated wave and particle data occurred from 8680 to 8740 seconds U.T. on 17 August 1982 when the satellite passed near the VLF transmitter at Cutler, Maine (NAA) as it was being modulated with a repeated ON (3-s)/OFF (2-s) pattern. During each of twelve consecutive pulses from the transmitter the electron counting rate increased significantly after start of the ON period and reached a maximum about 2 seconds later. The measured energy spectra revealed that approximately 15 to 50 percent of the enhanced electron flux was concentrated near the resonant energies for first order cyclotron interactions occurring close to the magnetic equator with the nearly monochromatic waves emitted from the transmitter.

Introduction

Our purpose is to present first observations of direct bounce loss cone precipitation of radiation belt electrons by controlled injection of VLF signals from a ground based transmitter. This result was recently achieved in an active wave-particle experiment called SEEP (Stimulated Emission of Energetic Particles). Past observations have shown that electrons can be precipitated from the radiation belts by ground-based VLF transmitters, but the evidence was predominantly based on observations of electrons in the drift loss cone. Narrow resonant peaks in the energy spectra (Imhof et al., 1974, 1981; Vampola and Kuck, 1978; Koons et al., 1981) and coordinated wave-particle observations (Imhof et al., 1981) have provided evidence for the effects of transmitters. In addition, natural whistlers and emissions have been observed to produce secondary ionospheric effects (x-rays, enhanced D-region ionization and photometric radiation) that have been attributed to VLF wave-induced electron precipitation in the direct bounce loss-cone (Rosenberg et al., 1971; Helliwell et al., 1973; Helliwell et al., 1980; Carpenter and LaBelle, 1982). Theoretical models of the gyroresonant wave-particle interaction in the magnetosphere have been used to predict the levels, energy spectra and temporal variations of particle fluxes that would be precipitated by monochromatic VLF signals at the VLF transmitter frequencies (Inan et al., 1982; Inan, 1981). These models have been useful in carrying out the experiments reported here.

The SEEP experiment was conducted from May until December 1982. Electron counting rate time profiles measured during a coordinated satellite-transmitter operation are presented and compared with the programmed modulation patterns of the VLF transmitter and the observed energy spectra are interpreted in terms of energy selective precipitation mechanisms occurring in the near equatorial regions.

Description of the Active Experiment and the Satellite Instrumentation

During the course of this experiment the U. S. Navy VLF transmitters at Annapolis, Maryland (NSS), at Cutler, Maine (NAA) and at Jim Creek, Washington (NLK) operating at frequencies of 21.4 kHz, 17.8 kHz, and 24.8 kHz, respectively, and the Stanford University research VLF transmitter at Siple Station, Antarctica operating in the 4 - 6 kHz range were modulated for ten-minute periods during overpasses of the S81-1 spacecraft. At the time of the data presented here, only one transmitter (NAA: 44.65°N, 67.28°W, L = 3.2) was modulated with a SEEP format. The ON-OFF modulations were performed in one of ten selectable formats chosen to provide a variety of periodic, pseudo-periodic and random patterns with ON times ranging from 0.3 seconds to 8 seconds. One commonly used format which also applies to the data presented here consisted of an ON (3-s)/OFF (2-s) pattern repeated for the entire duration of the modulation period, normally 10 minutes.

The SEEP payload on the three-axis stabilized S81-1 spacecraft measured precipitated particles directly with an array of silicon solid state detectors, and indirectly through an imaging x-ray proportional counter to map bremsstrahlung x-rays (> 3 keV) and an airglow photometer to measure optical emissions. The electron spectrometers were oriented at various angles to the

Copyright 1983 by the American Geophysical Union.

Paper number 3L0320.
0094-8276/83/003L-0320$3.00

Table 1 Electron Spectrometers

Central Zenith Angle	Central Pitch Angle	Acceptance Half Angle	Geometric Factor (cm^2 ster)
0^o	34^o	30^o	2.47
10^o	32^o	20^o	0.49
50^o	46^o	20^o	0.17
90^o	78^o	20^o	0.17

local vertical and covered an energy range of 2-1000 keV. Several were cooled to -120^oC to improve the sensor response characteristics (Voss et al., 1982). Pulse height analyses were performed on the sensor signals to provide the energy spectra. Some key parameters of the electron spectrometers used in the present analysis at 8710 seconds U. T. on August 17, 1982 are summarized in Table 1.

Observations

A good example of electron flux modulations in correlation with the transmitter ON-OFF signals occurred on 17 August 1982 at 8680 to 8740 seconds U.T. when the SEEP payload was passing near the NAA transmitter as it was being modulated with a 3-s ON/2-s OFF pattern. In Figure 1 the electron fluxes measured at various zenith angles are plotted as a function of time. A modulation period of 5 ± 0.1 seconds is clearly seen for 12 consecutive cycles. For reference, the measured ON times of the transmitter at NAA are indicated. From the Stanford recordings at Palmer Station, Antarctica, it was verified that the transmitter modulation began within 6 milliseconds of the exact start of a UT minute.

The measurements were made at a satellite altitude of ~220 km, and at the positions indicated in the abscissa. Due to the South Atlantic Anomaly, the mirror points conjugate to the satellite are below sea level so any electrons measured could not travel from one mirror point to the other (with bounce times of 0.1-0.5s at L=2.3) without interacting with the atmosphere. Ducted waves can travel this distance in less than one second, but unducted waves may take several seconds to reach their reflection points in the opposite hemisphere depending upon their trajectories. From the geometry of the magnetic field line it can be shown that the individual electrons observed by the SEEP payload in the northern hemisphere must have experienced a pitch angle scattering of at least 1^o during a single bounce period.

Superposed epoch analyses were clearly not needed to show the strong 5-second modulation, but they were performed to obtain an average shape of the precipitating electron intensities with respect to the transmitter signal. Counts were combined from eight consecutive 5-second intervals and the results are shown in Figure 2 for two counter outputs. A time of 0 seconds refers to the start of the transmitter ON period. The possibility that micropulsations could account for the SEEP spectrometer observations is discounted because micropulsations are generally only psuedo-periodic and are seen mainly at higher latitudes ($L \geq 5$) (e.g., Barcus et al., 1966). Also, natural electron microbursts as seen on satellites occur predominantly on higher L shells and at later local times than that of the case in question (e.g., Oliven et al., 1968). Association of the present observation with the NAA transmitter is further supported by the precise 5-second periodicity and the time correlations with the programmed modulation of the transmitter.

Model calculations (Inan et al., 1982) of the time response curve were performed assuming field aligned propagation of the wave and computing the scattering into the loss cone of particles from an assumed trapped distribution by a 3-second long monochromatic signal. The nonlinear equations of motion were integrated in an inhomogeneous medium also accounting for the wave and particle travel times. Using typical transmitter signal intensities applicable to this case it was found that a significant number of individual particles can be scattered in pitch angle by greater than 1^o in a single encounter with the wave and this constitutes the fluxes represented by the dashed line in Figure 2. The onset time and the full-width-at-half maximum duration of the prediction are in good agreement with the data, although the calculated response reaches a maximum sooner than that observed. Additional delay in the calculated function and less steepness in the leading and trailing observed ramps may result from the effects of non-field aligned propagation and from wave triggering and amplification. More

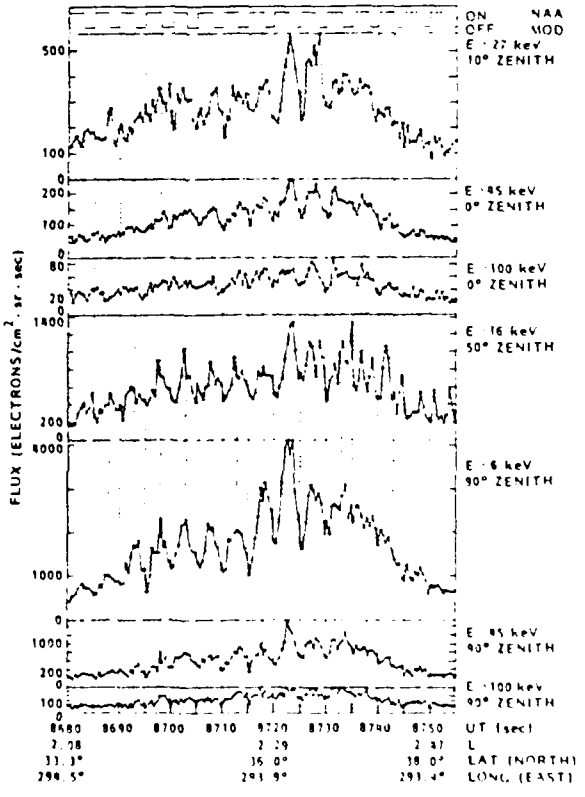

Figure 1. Electron fluxes on August 17, 1982 plotted as a function of time. Also shown are the ON and OFF times of the NAA transmitter.

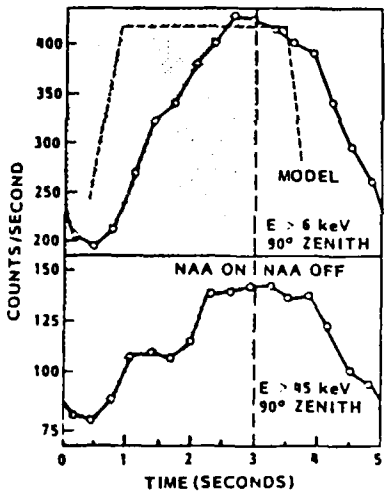

Figure 2. Superposed epoch counts/second versus time profiles from eight consecutive 5.0-second intervals during the period 8690 sec to 8730 sec U.T. on 17 August 1982. Also shown is the normalized time response curve computed using a theoretical model (Inan et al., 1982).

detailed analysis of the precipitation pulse shape and comparisons with theory will be reported later.

Differential energy spectra of the precipitating electrons as measured with the spectrometer oriented at 90° zenith angle are shown in Figure 3. These are raw counts from the pulse height analyzer, uncorrected for deadtime. Each of the spectra in the upper section is taken from a 1.984 second time interval beginning 1.7 seconds after start of the transmitter ON pulse. In the lower sections the spectra are taken from 1.280 second intervals beginning 4.2 seconds after start of each transmitter ON pulse. The latter spectra correspond approximately to the minima in electron counting rate and are summed from a shorter time period to minimize any contributions from the enhanced flux regions. Prominent peaks appear in the spectra taken during the times of enhanced electron precipitation, but there is little evidence of their presence during times of minimum intensity. The central energies of the peaks in the spectra are labelled and it is clear that the peak energies decrease with increasing L value. From the absolute fluxes it has been estimated that the rate of deposition of energy into the atmosphere was of the order of 10^{-4} ergs/cm^2 sec.

Let us now compare the central energies of the peaks shown in Figure 3 with the energies calculated for first order cyclotron resonance near the equator with 17.8 kHz waves traveling parallel to the earth's magnetic field lines. Figure 4 shows curves representing the calculated resonant energies for assumed cold plasma density models of 3000 $(L/2)^{-4}$ cm^{-3} and half that value along with the measured central energies of the peaks. Plasma density models in this region of space are scarce but those assumed in Figure 4 are consistent with other values quoted and have been used in past investigations of cyclotron resonance interactions in the upper edge of the inner radiation belt (Imhof et al., 1974). The measured peak energies are consistent with those expected for cyclotron resonance with waves traveling parallel to the earth's magnetic field lines. On the other hand, with a 60° wave normal angle the resonant electron energies for the same plasma density

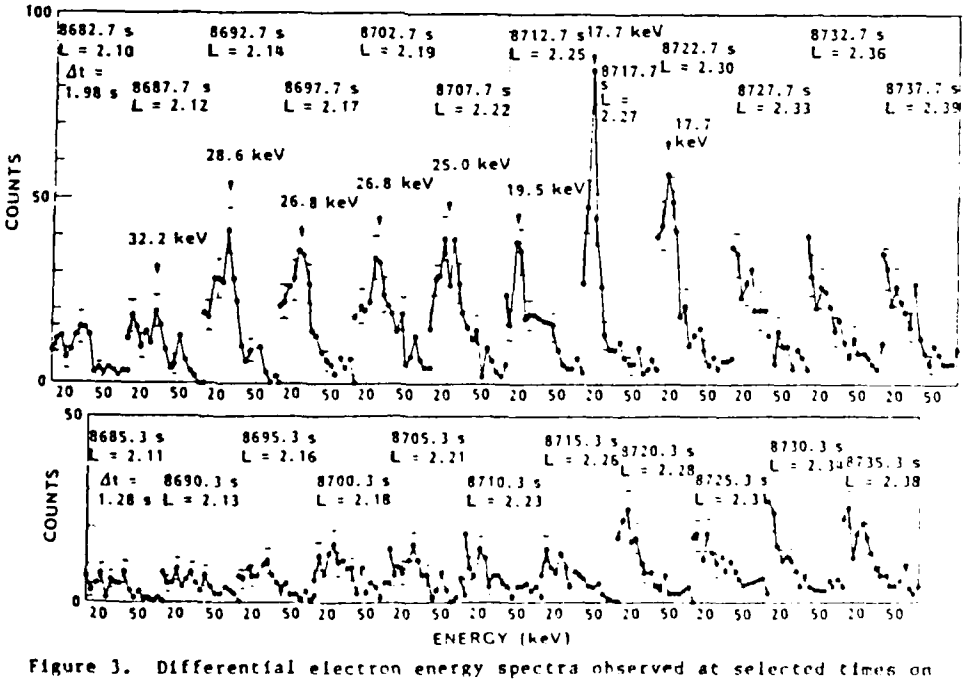

Figure 3. Differential electron energy spectra observed at selected times on August 17, 1982 in the form of raw counts uncorrected for deadtime.

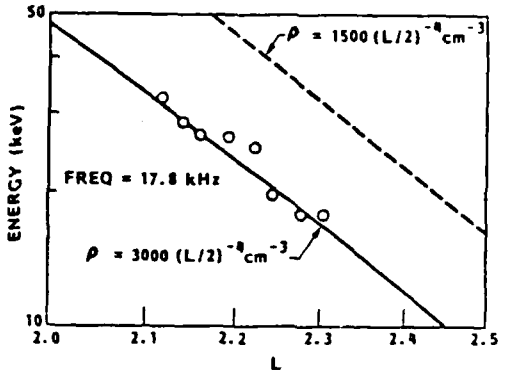

Figure 4. Open circles give measured energies of the peaks; curves represent calculated resonant energies.

would be approximately 1.3-1.5 times larger or equivalently the plasma densities corresponding to the observed resonant energies would be larger by a similar factor. Of particular importance is the finding that approximately 15-50 percent of the enhanced electron flux during the spikes is concentrated close to the resonant energies for near equatorial interactions. The enhanced precipitation at energies off the peaks is probably due to wave-particle interactions occurring off the equator and/or to interactions with waves traveling in various directions with respect to the field line.

Events similar to August 17 were not found to be common, but others with 5-second periods and similar phasings with respect to the transmitters have been found and more details of these events will be published elsewhere. In summary, the first direct observations in the bounce loss cone have been found for the precipitation of radiation belt electrons by controlled signals from a ground-based VLF transmitter. A large data base has been acquired and the surveys are still in preliminary stages.

Acknowledgments. The LPARL portion of the SEEP experiment was sponsored by the Office of Naval Research (contract N00014-79-C-0824). Launch and orbital support were provided by the Air Force Space Test Program Office. Appreciation is extended to the payload system engineer, Mr. S. J. Battel, to Dr. D. P. Cauffman for his program management of the satellite payload development, and to J. C. Bakke for his role in developing the instrumentation. We acknowledge the efforts of Messrs. W. E. Francis, B. A. Mooyman-Beck, J. W. Holley, Jr. and Dr. P. Filbert in data analysis.

The Stanford University effort in SEEP was supported by ONR grant N00014-82-K-0489 and by the Division of Polar Programs of the National Science Foundation under contract DPP80-22282 for the Siple Station program and contracts DPP80-22540 and DPP79-24600 for the Roberval and Palmer Station experiment programs.

References

Barcus, J.R., R. R. Brown, and T. J. Rosenberg, Spatial and temporal character of fast variations in auroral-zone X-rays, J. Geophys. Res. 71, 125, 1966.

Carpenter, D. L., and J. W. LaBelle, A study of whistlers correlated with bursts of electron precipitation near L = 2, J. Geophys Res., 87, 4427, 1982.

Helliwell, R. A., J. P. Katsufrakis, and M. L. Trimpi, Whistler-induced amplitude perturbation in VLF propagation, J. Geophys. Res., 78, 4679, 1973.

Helliwell, R. A., S. B. Mende, J. H. Doolittle, W. C. Armstrong and D. L. Carpenter, Correlations between 4278 optical emissions and VLF wave events observed at L ~ 4 in the Antarctic, J. Geophys. Res., 85, 3376, 1980.

Imhof, W. L., R. R. Anderson, J. B. Reagan, and E. E. Gaines,The significance of VLF transmitters in the precipitation of inner belt electrons, J. Geophys. Res., 86, 11225, 1981.

Imhof, W. L., E. E. Gaines, and J. B. Reagan, Evidence for the resonance precipitation of energetic electrons from the slot region of the radiation belts, J. Geophys. Res., 79, 3141, 1974.

Inan, U. S., A preliminary study of particle precipitation induced by VLF transmitter signals, Technical Report No. E477-1, Radioscience Laboratory, Stanford Electronics Laboratories, Stanford University, Stanford, California 94305, August 1981.

Inan, U. S., T. F. Bell, and H. C. Chang, Particle precipitation induced by short-duration VLF waves in the magnetosphere, J. Geophys. Res., 87, 6243, 1982.

Koons, H. C., B. C. Edgar, and A. L. Vampola, Precipitation of inner zone electrons by whistler mode waves from the VLF transmitters UMS and NWC, J. Geophys. Res., 86, 640, 1981.

Oliven, M. N., D. Venkatesan, and K. G. McCracken, Microburst phenomena 2. Auroral-zone electrons, J. Geophys. Res., 73, 2345, 1968.

Rosenberg, T. J., R. A. Helliwell, and J. P. Katsufrakis, Electron precipitation associated with discrete very-low-freqency emissions, J. Geophys. Res., 76, 8445, 1971.

Vampola, A. L. and G. A. Kuck, Induced precipitation of inner zone electrons, 1, Observations, J. Geophys. Res., 83, 2543, 1978.

Voss, H. D., J. B. Reagan, W. L. Imhof, D. O. Murray, D. A. Simpson, D. P. Cauffman and J. C. Bakke, Low temperature characteristics of solid state detectors for energetic x-ray, ion and electron spectrometers, IEEE Transactions on Nuclear Science, Vol. NS-29, 164, 1982.

(Received January 5, 1983;
accepted February 1, 1983.)

GEOPHYSICAL RESEARCH LETTERS, VOL. 10, NO. 8, PAGES 615-618, AUGUST 1983

THE MODULATED PRECIPITATION OF RADIATION BELT ELECTRONS BY CONTROLLED SIGNALS FROM VLF TRANSMITTERS

W. L. Imhof, J. B. Reagan, H. D. Voss, E. E. Gaines
D. W. Datlowe, and J. Mobilia

Lockheed Palo Alto Research Laboratory, Palo Alto, CA 94304

R. A. Helliwell, U. S. Inan, and J. Katsufrakis

STAR Laboratory, Stanford University, Stanford, CA 94305

R. G. Joiner

Office of Naval Research, Arlington, VA 22217

Abstract. The first direct observations of the precipitation of radiation belt electrons by the controlled injection of VLF signals from a ground based transmitter were recently reported from data acquired in the SEEP (Stimulated Emission of Energetic Particles) experiment. That outstanding example of time-correlated wave and electron data has now been enhanced by the finding of four additional modulated events out of 65 satellite passes when one of the U. S. Navy VLF transmitters at Cutler, Maine (NAA) or at Annapolis, Maryland (NSS) was being modulated in a 3s ON/2s OFF format. During each of these events the fluxes of precipitating electrons were observed repeatedly to display a characteristic time behavior with respect to the transmitter modulation: a relatively slow rate of increase after start of the ON period leading to a maximum about 2 seconds later. Details of this consistent pattern and the statistics of occurrence of modulation events are presented along with comparisons of the absolute fluxes of precipitating electrons observed during normal transmitter operation with those recorded when one of the transmitters was modulated.

Introduction

Several investigations in the past have addressed the precipitation of radiation belt electrons by VLF signals from a ground based transmitter (Imhof et al., 1974, 1981, 1983; Vampola and Kuck, 1978; Koons et al., 1981; Goldberg et al., 1983). The first direct observations of bounce loss cone precipitation of radiation belt electrons by controlled injection of VLF signals from a ground based transmitter were recently reported by Imhof et al. (1983). In that study, preliminary details were published on an outstanding example of time-correlated wave and electron data on August 17, 1982 when the VLF transmitter at Cutler, Maine (NAA) was being modulated with a repeated 3s ON/2s OFF pattern. To establish the frequency of occurrence of such events and to study the precipitating flux versus time profiles more data have now been surveyed.

Copyright 1983 by the American Geophysical Union.

Paper number 3L0875.
0094-8276/83/003L-0875$03.00

Description of the Experiment

The satellite payload in the SEEP (Stimulated Emission of Energetic Particles) experiment contained an array of cooled silicon solid state detectors to measure electrons and ions directly with high sensitivity and fine energy resolution (Voss et al., 1982). The electron spectrometer of present interest was mounted at 90° zenith angle and at 90° to the orbit plane on the three-axis stabilized S81-1 spacecraft which was in a high inclination orbit and for the data presented here at an altitude of ~ 220 km. The spectrometer had a threshold energy of 6 keV, an acceptance angle of $\pm 20^{\circ}$ and a geometric factor of 0.17 cm^2 ster.

An important part of the SEEP experiment involved the programmed modulation of U. S. Navy transmitters and the Stanford University research VLF transmitter at Siple Station, Antarctica. Of present interest are the two U. S. Navy transmitters at Cutler, Maine (NAA; 292.72°E, 44.65°N) and at Annapolis, Maryland (NSS; 283.55°E, 38.98°N) operating at frequencies of 17.8 kHz and 21.4 kHz, and nominal radiated powers of 1000 kw and 265 kw, respectively. Throughout the SEEP experiment, conducted during May-December 1982, the transmitters were modulated for 10 minute periods during overpasses of the SEEP payload in one of 10 formats. Only the 3s ON/2s OFF format is pertinent to the data considered here.

Observations

Surveys of the SEEP electron data have been conducted in the longitude interval 274°E to 310°E over the L shell range from 2.0 to 2.75 and only for nighttime passes (near 2230 local time). Higher L shells were precluded in this initial analysis to minimize naturally occurring fluctuations in the electron fluxes. Initially, a tabulation was made of all fluctuations in counting rate of the electron spectrometer at 90° which met the following criteria: 1) the counting rate increased by a factor of at least 1.5 during the fluctuation, and 2) the time duration of the flux increase fell in the range 1 - 3 seconds. Events were then selected in which four or more such fluctuations occurred with a time spacing of one period. It was required that at least one of the four fluctuations met both of the above criteria but the

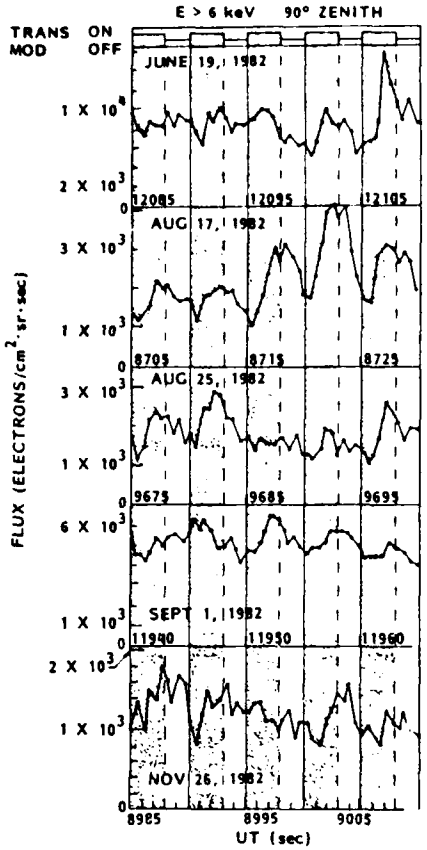

Fig. 1. Electron fluxes measured on five different satellite passes. ON and OFF times of the pertinent transmitter.

counting rate increase could be smaller for the adjoining fluctuations. Using this procedure for finding events, 5 were found from the 65 passes of the satellite when one of the transmitters was being modulated in a 3s ON/2s OFF format. No such events were found in the 175 passes when neither transmitter was being modulated in this format. Within the selected L-shell range, no events meeting these criteria but with periods significantly different from 5 seconds were found.

The electron flux profiles and transmitter ON and OFF times during each of the selected events are shown in Figure 1 for the electron spectrometer at 90° zenith angle. The particles measured by this detector were all near 90° pitch angle and therefore locally mirroring, but in every one of the cases the conjugate point was below sea level so the electrons must have been precipitated into the atmosphere during the bounce period in which they were observed. Corresponding counting rate increases often occurred in other electron spectrometers oriented at different pitch angles, but only data from the 90° detector are considered here.

In order to compare more accurately the time profiles for each of the events, superposed epoch analyses have been performed and these are shown in Figure 2. All of the time profiles display a similar pattern in which the fluxes increase rather slowly after start of the ON period and reach a maximum about 2 seconds later. These temporal features should provide important guidelines for understanding the coherent wave induced precipitation phenomenon in detail and for studying the interactions of VLF waves with trapped electrons (e.g., Helliwell, 1967; Inan et al., 1982). The consistent 5-second period and the phasing with respect to the transmitter ON/OFF times for each of the events strongly support the conclusion that all are related to the transmitter modulation. The absence of any such events when neither transmitter was being modulated in the special format further justifies this conclusion. Within the events large flux differences often exist between successive 5-second periods. Based on these data alone it is not clear whether the differences are associated with spatial or temporal variations in either the wave or particle characteristics.

During a modulation of the NSS transmitter on July 6, 1982 as part of the overall SEEP program, Goldberg et al. (1983) reported a 5-second modulation period in the bremsstrahlung x-rays measured from a rocket. In contrast with the 1 - 2 second delay between transmitter turn-on and electron precipitation reported in the five cases of the present paper Goldberg et al. found no such delay in their one event. The reason for the difference in the two sets of experi-

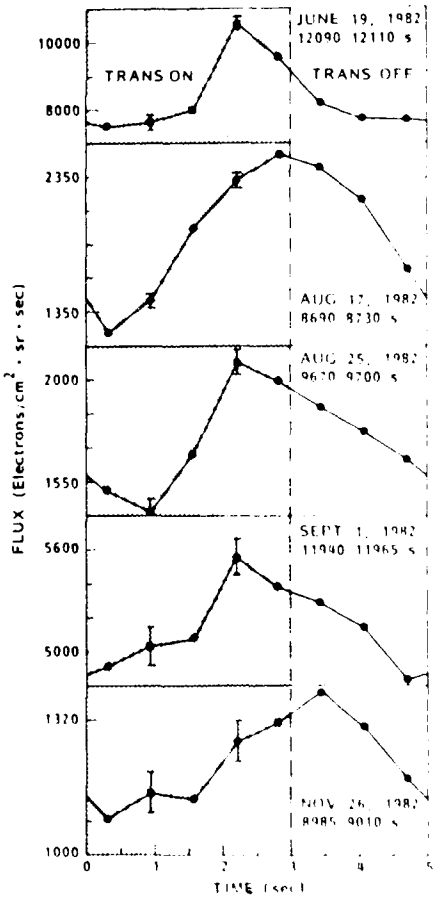

Fig. 2. Superposed epoch flux > 6 keV profiles for consecutive 5.0-second periods.

Table 1 Summary of Events

Date(1982)	Modulating Transmitter	Long. of Observ.	L-Shell Range of Flux Mod.
June 19	NAA	279.1°E	2.63-2.79
Aug. 17	NAA	294.0°E	2.13-2.34
Aug. 25	NAA	289.9°E	2.21-2.38
Sept. 1	NSS	280.0°E	2.46-2.63
Nov. 26	NAA	291.5°E	2.21-2.35

mental results may be due to differences in local time, Goldberg's being near dawn whereas the measurements presented here were all performed about two hours before local midnight, or possibly due to the limited signal to noise ratio of the rocket data.

In past studies of particle precipitation by nearly monochromatic waves generated at ground-based VLF transmitters, narrow L-dependent peaks have been observed in the energy spectra of electrons in the drift loss cone (e.g., Imhof et al., 1981; Koons et al., 1981). Similar peaks were observed in the electrons precipitated by the modulated NAA transmitter during the event of August 17, 1982 (Imhof et al., 1983). We have now found L-dependent peaks during the event of August 25, 1982, but with lower resonant energies suggesting higher cold plasma densities at that time. Pronounced peaks were not observed in the other events. Those on June 19 and Sept. 1, 1982 were at higher L shells where the equatorial cyclotron resonance energies were near the detector threshold. In the Nov. 26, 1982 event the signal to background was relatively weak for spectral analyses.

The longitudes and L-shell intervals of the events are listed in Table 1. Three of the four Cutler events and the one associated with Annapolis occurred at longitudes very near that of the transmitter. The NSS event took place at an L value very close to that of the transmitter, which is located at L = 2.6, whereas all of the NAA events were at significantly lower L values than Cutler (L = 3.2) and three of them were considerably below the upper end of the L-shell range used in the survey. This result may be due partly to the higher energies for near equatorial cyclotron resonance on lower L shells with more favorable observing conditions.

The frequency of occurrence of electron flux modulated events meeting the selection criteria is summarized in Table 2. The limited sample of data indicates that over the L-shell range 2.0 to 2.75 and with the selection criteria used modulations in the electron fluxes occurred in 5 out of 65 cases when one of the transmitters was being operated in the 3s ON/2 s OFF format. For the NAA transmitter alone 4 events were observed out of 26 cases. Consideration of the dependence of the event occurrence upon the choice of transmitter being modulated and upon the longitude of observation as well as other parameters is beyond the scope of this paper.

Even if modulations in the fluxes of precipitating electrons do not appear, the transmitters might still play a significant role in the precipitation. For example, the spread in propagation times could exceed the OFF times and hence inhibit the detection of the modulations (Inan and Helliwell, 1982). To further address the role of transmitters we compare the fluxes measured during normal operations with those observed when the transmitters were operated in the 3s ON/2s OFF format. Normal operation consists of a constant amplitude signal with the frequency shifted as often as once every 25 ms. During the SEEP format a continuous wave with

Table 2 Electron Modulation Events

Status of Transmitter Cutler	Annapolis	Number of Cases	Electron Modulation Events
Normal	Normal	175	0
3s ON/2s OFF	Normal	26	4
Normal	3s ON/2s OFF	39	1

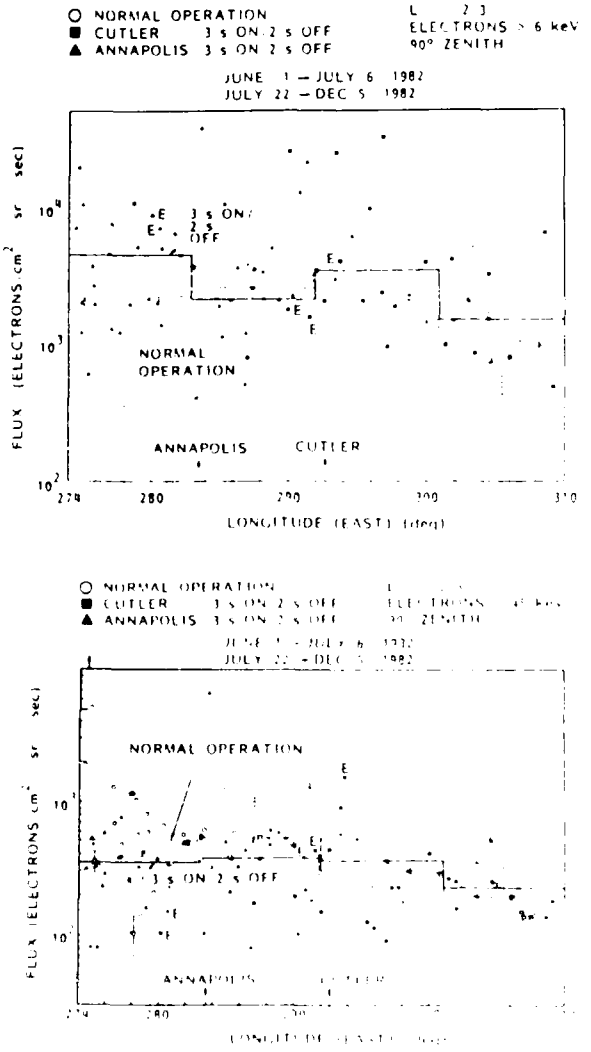

Fig. 3. Electron flux versus longitude. Locations of the transmitters at Annapolis and Cutler are indicated. The letter E indicates fluxes measured on a pass when an event was observed.

fixed frequency and amplitude is turned ON for 3 seconds and OFF for 2 seconds. The frequency spectrum of the transmitted signal is typically wider during normal operation. The reduced coherence of the wider bandwidth signal has been found to inhibit temporal growth and triggering during VLF wave injection experiments from Siple (Raghuram et al., 1977). The results of the present investigation are presented in Figure 3 where the observed electron fluxes >6 keV and > 45 keV are plotted as a function of longitude with separate symbols for the normal operation of both transmitters and for the special modulations of either transmitter. The time period surrounding a major geomagnetic storm on July 14, 1982, when the fluxes of precipitating electrons were significantly higher, has been excluded. Otherwise no selection of events was made on the basis of geomagnetic conditions. Median flux levels over 9^0 longitude bins are shown. For electrons > 6 keV and all longitudes combined, the median flux values for normal operation and for the special modulation of either transmitter are 1.8×10^3 and 2.7×10^3 electrons/cm^2 ster sec, respectively. For electrons > 45 keV, the fluxes are 3.3×10^2 and 3.2×10^2, respectively. The data do not indicate a significant increase in the average precipitation rate when the transmitters are operated at fixed frequency with a 60% duty cycle as compared to the normal broader frequency operation at 100% duty cycle. Smaller flux changes with mode of transmitter operation may be found when detailed account is taken of the flux variations with longitude and time.

In summary, data have been presented from five events in which modulations were observed in the fluxes of precipitating electrons that were in phase with the controlled modulations of one of the U. S. Navy transmitters at Cutler, Maine or at Annapolis, Maryland. Although only 5 cases were found with the selection criteria used here, others may be discovered after more detailed analyses.

Acknowledgments. The LPARL portion of the SEEP experiment was sponsored by the Office of Naval Research (contract N00014-79-C-0824). Launch and orbital support were provided by the Air Force Space Test Program Office. Appreciation is extended to the payload system engineer, Mr. S.J. Battel, to Dr. D.P. Cauffman for his program management of the satellite payload development, and to J. C. Bakke for his role in developing the instrumentation. We acknowledge the efforts of Messrs. W.E. Francis, B.A. Mooyman-Beck, J.W. Holley,Jr., and Dr. P. Filbert in data analysis.

The Stanford University effort in SEEP was supported by ONR grant N00014-82-K-0489 and by the Division of Polar Programs of the National Science Foundation under contract DPP80-22282 for the Siple Station program and contracts DPP80-22540 and DPP79-24600 for the Roberval and Palmer Station experiment programs.

References

Goldberg, R. A., S. A. Curtis, J. R. Barcus, C. L. Siefring and M. C. Kelley, Controlled stimulation of magnetospheric electrons by radio waves: experimental model for lightning effects, Science, 219, 1324, 1983.

Helliwell, R. A., A theory of discrete VLF emissions from the magnetosphere, J. Geophys. Res., 72, 4773, 1967.

Imhof, W. L., R. R. Anderson, J. B. Reagan, and E. E. Gaines, The significance of VLF transmitters in the precipitation of inner belt electrons, J. Geophys. Res., 86, 11225, 1981.

Imhof, W. L., E. E. Gaines, and J. B. Reagan, Evidence for the resonance precipitation of energetic electrons from the slot region of the radiation belts, J. Geophys. Res., 79, 3141, 1974.

Imhof, W. L., J. B. Reagan, H. D. Voss, E. E. Gaines, D. W. Datlowe, J. Mobilia, R. A. Helliwell, U.S. Inan, J. Katsufrakis, and R. G. Joiner, Direct observation of radiation belt electrons precipitated by the controlled injection of VLF signals from a ground-based transmitter, Geophys.Res.Lett., 10, 361,1983.

Inan, U. S., T. F. Bell, and H. C. Chang, Particle precipitation induced by short-duration VLF waves in the magnetosphere, J. Geophys. Res., 87, 6243, 1982.

Inan, U. S., and R. A. Helliwell, DE-1 observations of VLF transmitter signals and wave-particle interactions in the magnetosphere, Geophys. Res. Lett., 9, 917, 1982.

Koons, H. C., B. C. Edgar, and A. L. Vampola, Precipitation of inner zone electrons by whistler mode waves from the VLF transmitters UMS and NWC, J. Geophys. Res., 86, 640, 1981.

Raghuram, R., T. F. Bell, R. A. Helliwell, and J. P. Katsufrakis, Echo-induced suppression of coherent VLF transmitter signals in the magnetosphere, J.Geophys.Res., 82, 2787,1977.

Vampola, A. L. and G. A. Kuck, Induced precipitation of inner zone electrons, 1, observations, J. Geophys. Res., 83, 2543, 1978.

Voss, H. D., J. B. Reagan, W. L. Imhof, D. O. Murray, D.A. Simpson, D.P. Cauffman, and J.C. Bakke, Low temperature characteristics of solid state detectors for energetic x-ray, ion and electron spectrometers, IEEE Transactions on Nuclear Science, Vol. NS-29, 164, 1982.

(Received March 11, 1983;
accepted May 23, 1983.)

EOS

Transactions, American Geophysical Union
Vol. 64 No. 48 November 29, 1983

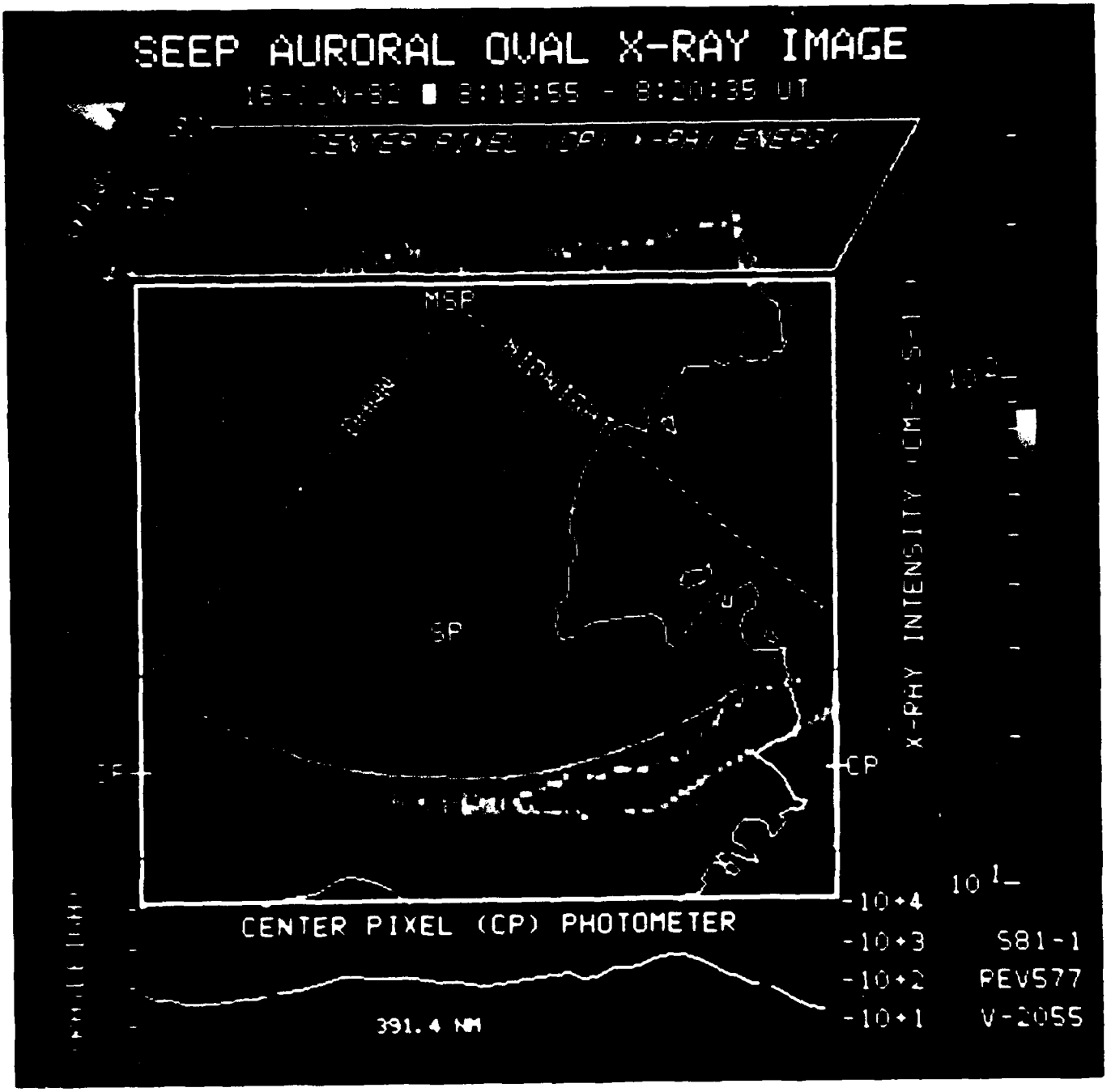

Cover. X ray image of the earth's southern auroral oval obtained with the Lockheed X ray imaging spectrometer in the Stimulated Emission of Energetic Particles (SEEP) satellite payload. Superimposed on the map of Antarctica is the spatial distribution of auroral X ray luminosity that is produced by kilovolt electron precipitation. Conspicuous is the auroral oval with intense luminosity near midnight and structured energetic precipitation near dawn. The upper panel displays the energy spectra of X rays observed in the center pixels of the image, while the lower panel shows the simultaneous visible auroral emissions measured by the SEEP photometer. The X ray image is the subject of a paper to be presented at the 1983 AGU Fall Meeting: H. D. Voss et al., SEEP X ray imagery of the earth's aurora (*Eos*, November 8, 1983, p. 792). (Photo courtesy of H. D. Voss, Lockheed Missiles and Space Company, Palo Alto, CA 94304.)

Copyright 1983 by the American Geophysical Union
0096-3941/83/0048-0953$01.00

JOURNAL OF GEOPHYSICAL RESEARCH, VOL. 89, NO. A12, PAGES 10,837–10,846, DECEMBER 1, 1984

A Coordinated Satellite and Ground-Based Study of an Intense Electron Precipitation Spike Over the Southern Polar Cap

W. L. IMHOF,[1] T. J. ROSENBERG,[2] L. J. LANZEROTTI,[3]
J. B. REAGAN,[1] H. D. VOSS,[1] D. W. DATLOWE,[1]
J. R. KILNER,[1] E. E. GAINES,[1] J. MOBILIA,[1]
AND R. G. JOINER[4]

An electron precipitation event has been investigated with bremsstrahlung X ray mapping data taken from two satellites and with ground-based riometer and magnetometer data. The event occurred near 2300 UT on June 27, 1982, in the vicinity of South Pole Station, which was in the dusk-midnight local time sector. The main precipitation was associated with a poleward-moving westward electrojet and produced the largest riometer absorption (exceeding 10 dB at 30 MHz) recorded during 1982 at that station. The feature examined in detail here is an intense spike of ~10 s duration and limited spatial extent that occurred as a short-lived eastward ionospheric current developed equatorward of the westward electrojet. At the time of the spike, two sensors on the P78-1 satellite essentially simultaneously measured X rays from the region viewed by the ground-based instruments. Movement of the spike precipitation region toward the pole was indicated by the measurements. From ratios of the riometer absorption at different frequencies it is concluded that the spike precipitation region is consistent with a strip of width ~25 km and length greater than 100 km. The total flux of the precipitating electrons in the spike was $\sim 4 \times 10^{23}$ el s ($\sim 2 \times 10^{16}$ ergs/s) with an e-fold energy of ~40 keV. The fluxes and energy spectra of X rays emitted from a large area, as measured by the spacecraft, were about the same before and after the spike. However, following the spike there was a pronounced decrease in riometer absorption, which suggests a movement of the main precipitation region away from the south pole at that time.

INTRODUCTION

The precipitation of electrons > 20 keV into the atmosphere at high latitudes is an important aspect of the earth's ionospheric environment. Detailed data on the phenomena are still limited in scope in many respects, and particularly, more detailed mappings of the energetic electron intensities and energy spectra as a function of time and space are needed. The spatial and temporal variations of structured precipitation are not well understood, especially as they might relate to energetic electrons from the magnetotail being injected into the atmosphere.

Of special interest are the so-called "spike events," in which impulsive electron precipitation produces a sudden increase in the absorption of cosmic radio noise followed by a rapid return to a less disturbed level. Data obtained with narrow-beam riometer systems in the auroral zone suggest that spike events cover a smaller area than the general radio noise absorption [*Nielsen and Axford*, 1977; *Hargreaves et al.*, 1979]. In the typical absorption spike the precipitation occurs in a latitudinally narrow region (≤ 50 km) located at the poleward border of a poleward moving and intensifying westward electrojet during the expansion phase of a substorm [*Nielsen and Greenwald*, 1978; *Nielsen*, 1980]. Evidence has been reported by *Biordal et al.* [1971] for a narrow precipitation region in the north-south direction but with a large extension in the east-west direction during impulsive electron precipitation events in the midnight sector near the onset of a negative bay.

Direct measurements from satellites of energetic electron spikes on latitudes below, at, or above the local trapping boundary have been reported on numerous occasions [e.g., *McDiarmid and Burrows*, 1965; *Brown and Stone*, 1972]. In addition, electron "islands" have been reported in the geomagnetic tail [e.g., *Anderson*, 1965; *Meng*, 1971; *Keath et al.*, 1976; *Roelof et al.*, 1976], and these may be related to the spikes observed at low satellite altitudes. *Nielsen et al.* [1982] have reported measurements of the energy spectrum (≤ 100 keV) of field-aligned electron fluxes at synchronous altitude at the time of an absorption spike which occurred in the region of the magnetic flux tube mapped through the satellite. However, because spikes often appear very dynamic in nature, the spatial temporal aspects of the phenomena are difficult to unravel from single-satellite particle measurements.

From a properly positioned and instrumented satellite the temporal and spatial variations of electron precipitation can be separated by measuring the bremsstrahlung X ray production. Energy spectral information can also be obtained from the bremsstrahlung measurements in a manner nearly independent of effects of the atmosphere and location geometry. Such measurements can potentially provide an answer to the important question as to whether the spike events are associated with electrons having energies of ~100 keV or greater. Satellite-measured bremsstrahlung X ray data are of particular value when combined with ground-based measurements, such as those taken with riometers and magnetometers, since the latter provide a different time-space perspective. To date, no investigations have been reported with detailed data as outlined above. Some bremsstrahlung X ray studies have been made of impulsive electron precipitation events at high latitudes [*Imhof et al.*, 1978], but these measurements were capable only of very coarse spatial coverage. Many riometer absorption spikes have been recorded at high latitudes, including the south pole [*Hargreaves et al.*, 1979], but to date there has been no opportunity for correlation with bremsstrahlung X ray measurements from high altitudes. Presented here are coordinated X ray and riometer data acquired during an electron precipitation event that occurred on June 27, 1982, in the

[1] Lockheed Palo Alto Research Laboratory, California
[2] University of Maryland, Institute for Physical Science and Technology, College Park
[3] AT&T Bell Laboratories, Murray Hill, New Jersey
[4] Office of Naval Research, Arlington, Virginia

Copyright 1984 by the American Geophysical Union

Paper number 4A9085
0148-0227/84/004A-9085$05.00

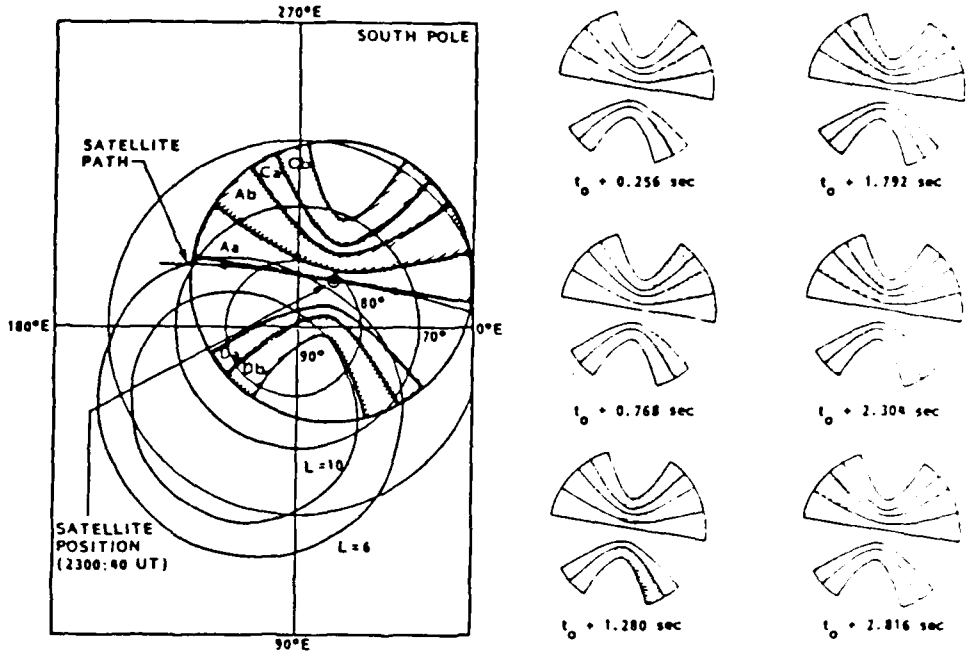

Fig. 1. Schematic presentation of the areas viewed by each of the six cadmium tellunde spectrometers (Aa, Ab, Ca, Cb, Da, and Db) performing at the time of the measurements presented here. In the left-hand section are illustrated the locations of the zones covered when the satellite was at the indicated position during the south polar cap crossing of interest. In the right-hand section the hatched regions indicate the areas observed by each of the sensors at six different times during a single spin of the satellite.

vicinity of South Pole Station. During this event the precipitating electron fluxes were extremely high, and a spike of very short duration occurred at the time of the X-ray measurements.

Description of Instrumentation

Satellite X Rays

The bremsstrahlung X ray mappings presented here were obtained with an array of cadmium telluride spectrometers on board the P78-1 spacecraft and with a large-area imaging proportional counter in the stimulated emission of energetic particles (SEEP) payload onboard the S81-1 satellite. The P78-1 spacecraft was launched into a sun-synchronous, noon-midnight, nearly circular polar orbit at ~600 km altitude on February 24, 1979, and is still providing good data after 5 years in orbit. The satellite spins with a period of ~5.5 s about an axis perpendicular to the orbit plane and pointed eastward at the ascending node. Thus the array of eight cadmium telluride X ray detectors, oriented at selected view angles with respect to the spacecraft spin axis, provides fine-scale mappings of the sources of X rays >21 keV. The instrumentation is described in more detail elsewhere [*Imhof et al.*, 1980], but for the convenience of the reader the viewing geometry is considered here. The areas of the atmosphere viewed by each of the six spectrometers operational at the time of present interest are illustrated schematically in Figure 1 during the pass when the X ray spike was observed. During the satellite pass the geographic south pole was observed with the two detectors labeled Da and Db. At any given instant a spectrometer can view at most only a portion of its full zone. Approximately 3 s are required for the field of view to sweep completely across the swath as illustrated in the right-hand section of Figure 1. In this simplified drawing, penumbra effects are neglected along with any absorption of the X rays in the atmosphere. It is possible to unfold information on the spatial distributions of the bremsstrahlung X ray sources from the counting rates observed at each of the different orientations of the satellite during its spinning motion and at various positions during the forward movement.

For the X ray proportional counter imaging spectrometer in the SEEP payload a wide-angle field of view (±45°) was divided into 16 pixels in the direction perpendicular to the satellite trajectory. The counter responded to X rays over the energy range from 4 to 40 keV. The instrumentation was mounted on the three-axis stabilized S81-1 satellite in polar orbit at an altitude of about 270 km for the data presented here. The instrumentation will be described in papers by W. Calvert et al. and H. D. Voss et al. (private communication, 1984).

South Pole Station

The facilities for upper atmosphere physics research at the geographic south pole were recently expanded to emphasize coordinated studies of the polar cusp and auroral oval [*Detrick et al.*, 1982]. In this paper we consider only the riometer and magnetometer measurements. Cosmic radio noise is measured with riometers and broad-beam antennas operating at 20.5, 30, and 51.4 MHz. The circular (±30°) antenna patterns are centered on the zenith and provide fields of view of 100-km diameter at the *D* region heights (80-90 km), where most of the enhanced ionization caused by energetic electron precipitation occurs. Ionospheric absorption relative to a quiet-day signal level, computed by the method described by *Krishnaswamy and Detrick* [1983], is obtained from the digitally sampled (at 1 Hz) riometer data. Surface variations of the

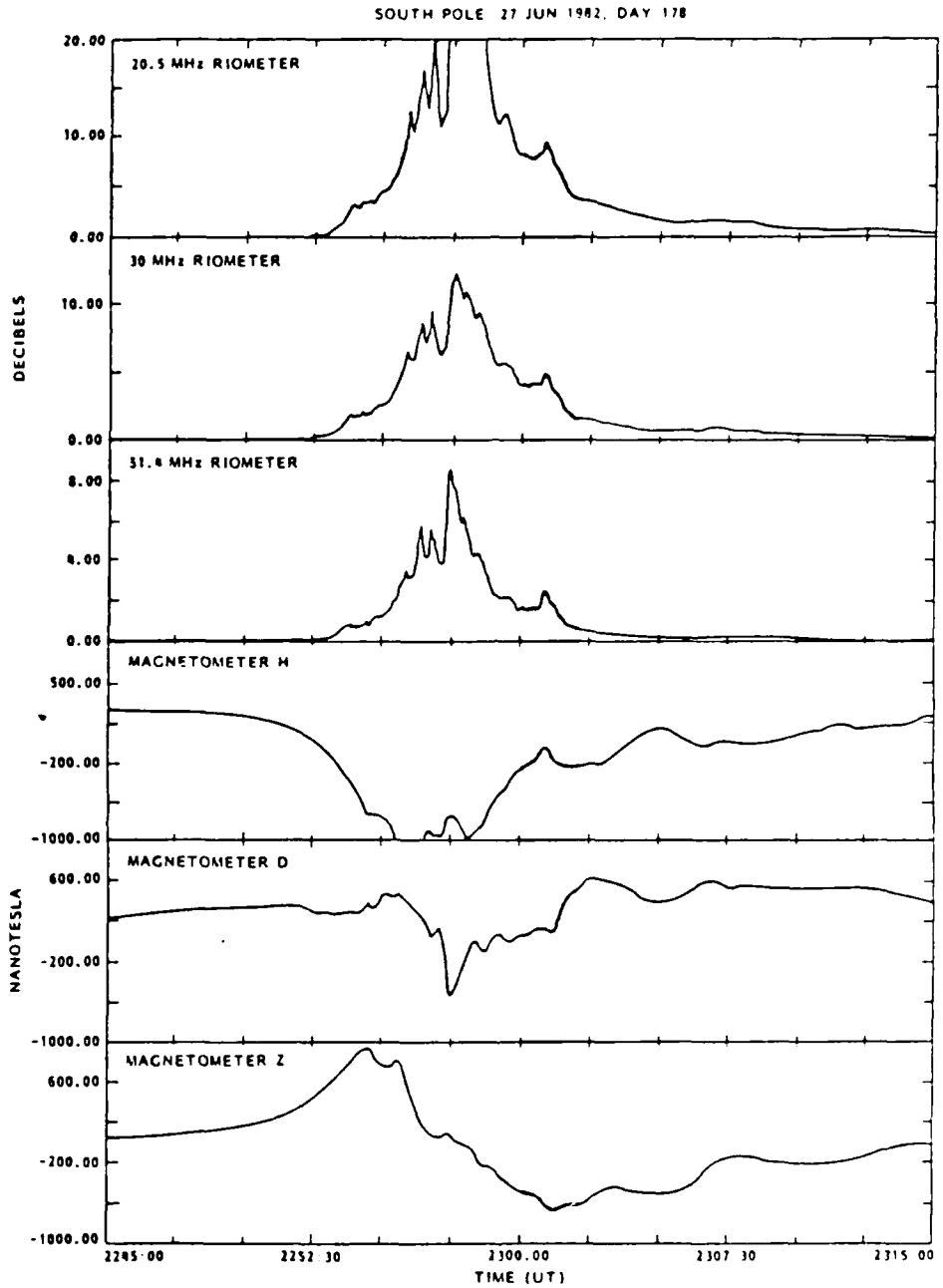

Fig. 2. The riometer absorption recorded at three frequencies at South Pole Station is shown in the top three sections. The three components of the magnetometer response are shown in the bottom three sections. The narrow absorption spike considered in this paper is within the shaded strip which spans the time interval covered in Figures 5 and 7.

geomagnetic field, also sampled at 1 Hz, are measured with a three-axis flux gate magnetometer having temperature compensation. The three components of the field were measured in the magnetic north-south (H), east-west (D), and vertical (Z: positive increase upward) directions.

Experimental Results

General Features of the Event

The largest auroral absorption event recorded during 1982 at South Pole Station ($L \approx 13$) occurred near 2300 UT on June 27 when the station was in the dusk-midnight local time sector (1930 MLT). The absorption profiles for this event are shown in Figure 2. Absorption began at 2253 UT, reached maximum intensity at 2258 UT, and recovered rapidly; however, weak residual activity could still be detected as late as 2400 UT. The peak absorption exceeded 10 dB at 30 MHz. At the peak the 20.5-MHz riometer signal was so weak that available calibrations of the riometer response are inadequate to determine the actual absorption at this frequency. An absorption spike (~1 dB increment at each frequency) of short duration at about 2301 UT is highlighted in Figure 2 with a

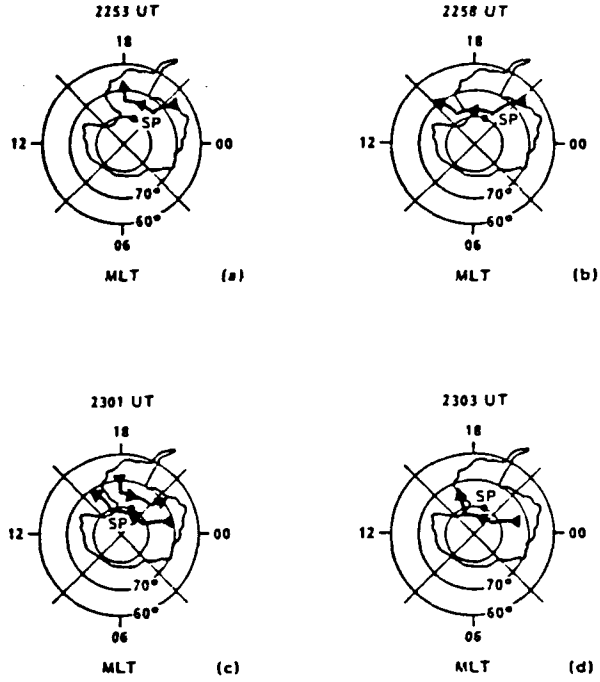

Fig. 3. Schematic illustrations of the ionospheric and field-aligned current systems with respect to South Pole (SP) Station at four different times during the overall event. A westward electrojet moves poleward over the station, reaching its maximum excursion at Figure 3*d*. A short-lived eastward current (Figure 3*c*) develops equatorward of the westward electrojet at the time of the precipitation spike.

shaded strip spanning the time period of data presented later in Figures 5 and 7. This spike was well covered with the P78-1 X ray measurements and is the main subject of the present paper. Note, however, that this spike is not a typical example of the absorption spikes previously reported and referenced above. The spike did not occur at the onset of the event and (see below) was associated with an eastward electrojet.

Fluxgate magnetometer measurements (Figure 2) at South Pole Station indicate that the energetic electron precipitation responsible for the overall absorption event was associated with a poleward moving substorm surge. The surge current began to be clearly detected at South Pole Station at ~2245 UT as the *H* component of the local field began to decrease and the *Z* component began a sharp increase. This signature indicates a westward current equatorward of the station. The maximum depression in the north-south component occurred at ~2255 UT and saturated the instrument. As the current surge moved overhead from the equator toward the (geomagnetic) pole ($\Delta Z \sim 0$ at ~2258 UT), a sharp decrease was observed in the *D* component value, corresponding to an enhanced westward field direction. The *Z* component reached its maximum negative excursion at ~2301 UT, at the time of the small positive spike in the *H* component. In the absence of this spike the magnetic traces suggest that the *Z* component would have reached a maximum negative value at ~2303 UT, probably corresponding to the maximum poleward excursion of the westward electrojet.

The location of South Pole Station relative to the ionospheric and field-aligned current systems at three different times during the overall event is shown in a schematic fashion in Figures 3*a*, 3*b*, and 3*d*. The actual longitudinal extents of the current systems are unknown because of the limitations in observation sites. These depictions are based upon the substorm current wedge concept of *McPherron et al.* [1973]. At the time of the overhead passage of the westward current, South Pole Station appears, from the *D* component variations, to have momentarily been quite close to (a little west and poleward of) an intense downward field-aligned current (Figure 3*b*). If the maximum excursion in the horizontal component field is taken as ~1800 nT, then the intensity of the westward electrojet which moved across the station (assumed at 100 km altitude) was $\sim 9 \times 10^5$ A.

At the time of the absorption spike near 2301 UT the P78-1 satellite was in the southern hemisphere, and enhanced fluxes of X rays emitted from the vicinity of the geographic south pole were observed in two of the CdTe spectrometers. From the central values and the observed widths of the peaks in the angular distributions it was possible to obtain mappings of the X ray sources. Since the satellite was in the outer edge of the radiation belts during much of the pass, some bremsstrahlung X rays were produced in the vehicle; these relatively low backgrounds were subtracted on the basis of the observed angular distributions. An X ray mapping, expresses in terms of counts per second, obtained at times before and after the spike at ~2301 UT, is shown in Figure 4*a*. (The X ray emission during the spike is treated separately in Figure 6 and discussed later.) Each of the small squares in Figure 4*a* represents an area ~113 × ~113 km. Six different shadings are used to indicate the counting rates of 21- to 68-keV X rays corrected for source area and distance to source with an arbitrary normalization. Since the source regions were observed from low altitudes with a wide field of view, the corrections cannot be performed with high precision. The maps indicate the general regions of X ray emission but do not resolve fine-scale structure in the intensity profiles. For the measurements shown in Figure 4, certain areas of the atmosphere were viewed for longer time periods than others, so the statistical sampling for obtaining the averages is not uniform. The squares marked with an N indicate regions that were not sampled during the time interval. Overall, the mappings clearly indicate that the X rays were emitted predominantly from a large region encompassing the geographic south pole.

Approximately 40 min after termination of the P78-1 satellite pass over the southern polar cap, finer-scale X ray mappings at lower energies (4–40 keV) were obtained with the X ray imager in the SEEP payload on the S81-1 satellite. The observed X ray emissions are indicated in Figure 4*b* in a map covering exactly the same region of space as in Figure 4*a*. This map reveals a localized region of strong X ray emission that is ~400 km magnetically east of the geographic south pole; however, the field of view of the X ray imager is rather limited, and it does not include the south pole itself where a residual riometer absorption (≤0.3 dB) was still present (not shown here).

At about the time when the SEEP X ray mappings were performed in the southern polar cap the X ray emissions over the north polar region were mapped from the P78-1 spacecraft. In contrast to the earlier measurements over the south polar cap, no major regions of enhanced X ray emission were observed poleward of the trapping boundary. Although the conjugate position to the geographic south pole was not within the field of view of the X ray spectrometer on this pass over the north, conjugate regions to areas of X ray emission previously seen in the southern polar cap were within the viewing range of the X ray spectrometer. However, no signifi-

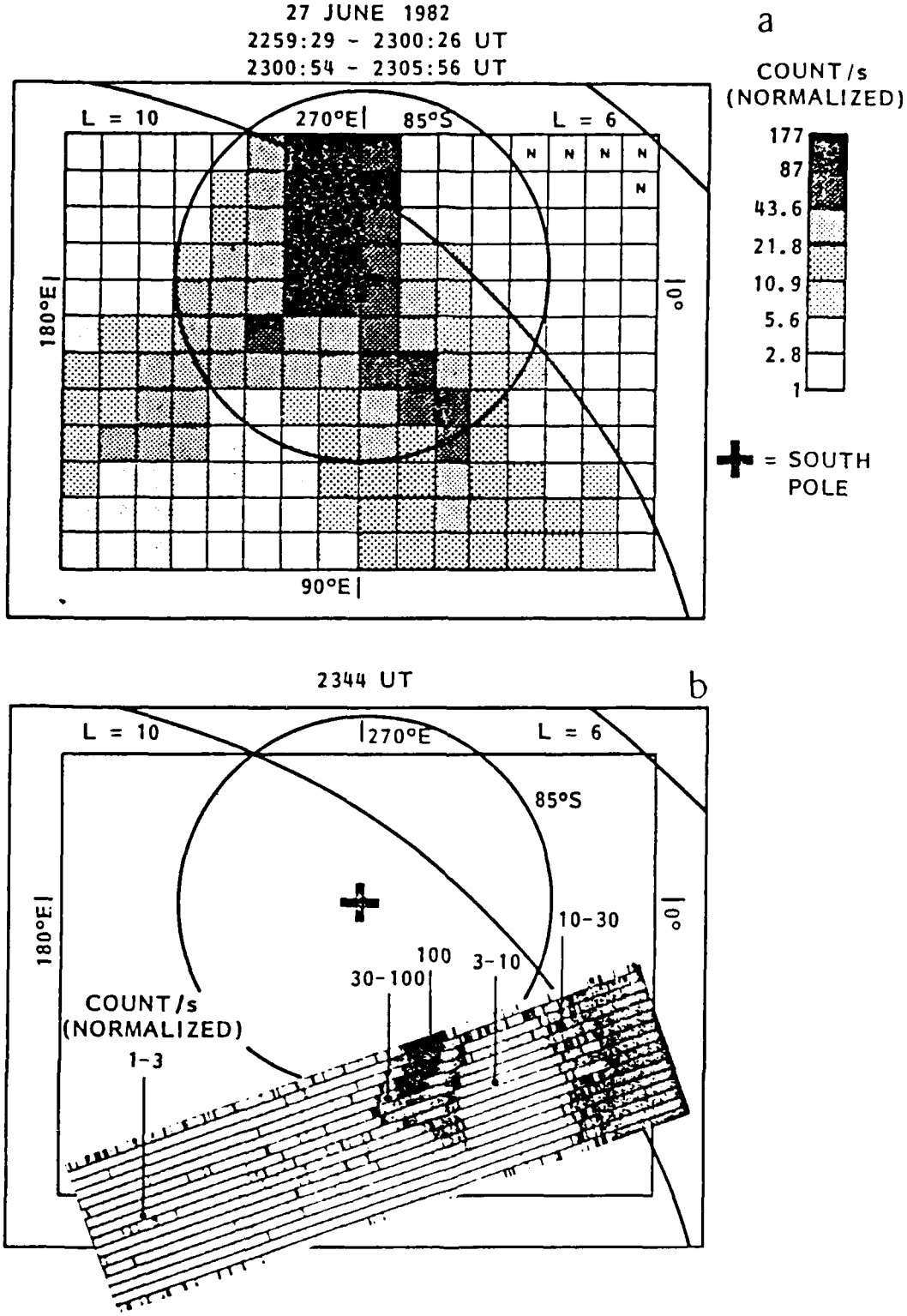

Fig. 4. (*a*) The bremsstrahlung X ray counting rate map recorded during a pass of the P78-1 satellite over the south polar region. A geographic latitude of 85° is shown as a circle. (*b*) A map of the X ray counting rates observed ~40 min later with the X ray imager on the S81-1 satellite. The map in Figure 4*b* covers exactly the same region of space as the one in Figure 4*a*, although the region of X ray observations is more confined.

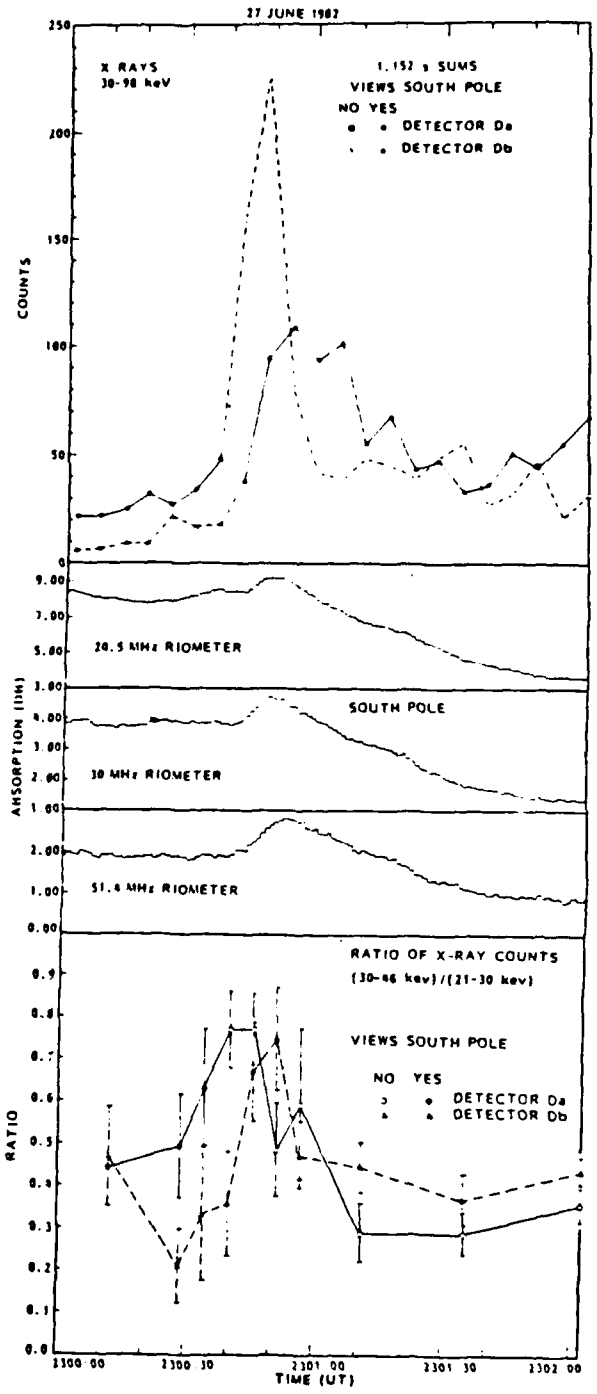

Fig. 5. (top) X ray counts recorded per 1.152 s in each of the detectors Da and Db (bottom) Ratios of counts in channel 2 (30–46 keV) to those recorded in channel 1 (21–30 keV) in each of the spectrometers Da and Db. (middle) The riometer absorptions recorded at the south pole at three different riometer frequencies.

cant fluxes of X rays were observed to be emitted from these regions.

The X ray intensity versus time profiles for the spike are compared in Figure 5 with the cosmic noise absorption measured at South Pole Station. A threshold energy of 30 keV has been selected for the X ray fluxes to enhance the prominence of the ~10-s duration spike. The ratio of X ray counts in channel 2 (30–46 keV) to those recorded in channel 1 (21–30 keV) is plotted in the bottom section of Figure 5 to provide a measure of the spectral changes with time. As for the X ray flux plots, the solid symbols indicate when each detector viewed the south pole. Clearly, the X ray energy spectra and therefore the inferred precipitating electron energy spectra were harder (larger number of higher-energy X rays) during the enhanced precipitation spike than before or after.

After ~2301 UT the riometer absorption decreased rapidly (Figure 5), while the X ray fluxes emitted from a large area at the south polar region remained relatively constant, as did the shape of the X ray energy spectrum. This behavior requires that after occurrence of the spike the region of precipitation moved away from South Pole Station. Possible confirmation of such a movement comes from the SEEP X ray measurements at a much later time (~2344 UT) when an enhanced region of X ray emission at lower energies was observed over a small area about 400 km from the south pole.

The spatial-temporal features of the X ray emission around the time of the spike at 2300:40 UT are illustrated schematically in Figure 6 with a time sequence series of maps. The raw counting rates in each of the detectors that viewed the south pole are shown in Figure 6 along with schematic indications of the areas from which the X rays were emitted. It is unlikely that the apparent spatial variation in the X ray measurements is associated with satellite motion since during that interval its position changed by only 30–40 km, a distance smaller than the spatial resolution of the X ray mapper. These data therefore indicate a spatial movement of the precipitation region from the area covered by detector Da to that covered by Db. Since the riometer spike at South Pole Station occurred at approximately the same time as the X ray spike in detector Db which encompassed the south pole, one concludes that the motion of the spike was generally toward the latter position. Such a finding is consistent with the situation discussed by *Hargreaves et al.* [1979], in which a spike event in cosmic noise absorption moves rapidly in a direction at right angles to the elongation.

Electron Energy Spectrum and Precipitation Rate

The observed X ray intensities and energy spectra for the spike at 2300:40 UT were compared with theoretical calculations by *Walt et al.* [1979] of X ray bremsstrahlung expected for incident electron fluxes having exponential spectral shapes and for various atmospheric escape angles. This comparison indicates that the spike event was produced by an electron spectrum having an e-fold energy of ~40 keV with an estimated uncertainty of ±7 keV. This is considerably harder than the spectrum of field-aligned electron fluxes reported at geosynchronous orbit by *Nielsen et al.* [1982] during an absorption spike. The Nielsen et al. electron spectrum could be characterized by an e-folding energy of ~11 keV in the 10–100 keV range.

From the best fits to the *Walt et al.* [1979] theoretical curves and the measured X ray fluxes in detector Da it is further estimated that the total rate of precipitation of electrons (>0 keV) during the spike within the field of view of detector Da was $\sim 2 \times 10^{23}$ el s with an uncertainty of $\pm 1 \times 10^{23}$ el s. Detector Da was used for this comparison since the south pole location was close to the spatial borderline between detectors Da and Db and the spike was more intense and the time duration better defined in Da.

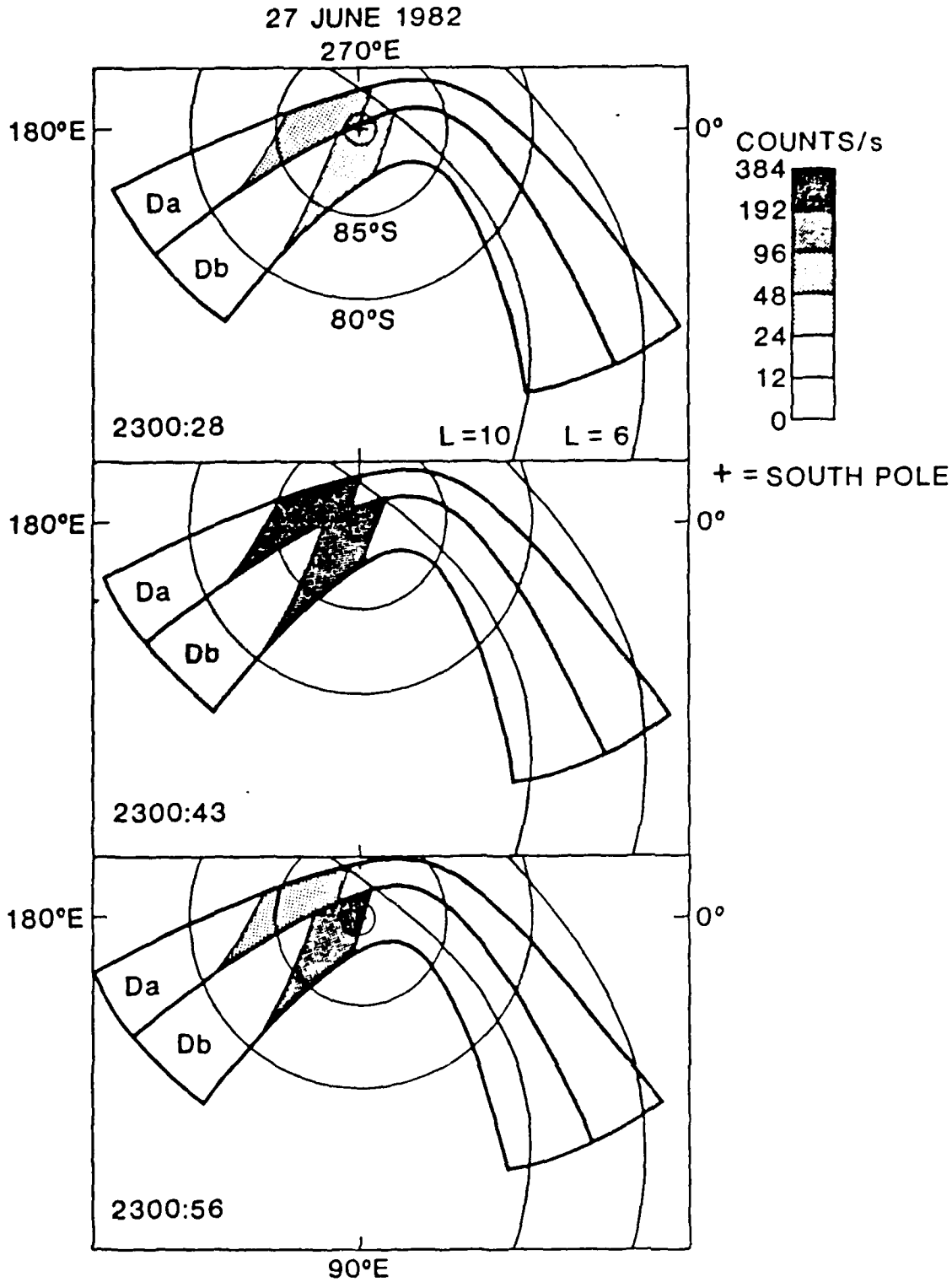

Fig. 6. Schematic presentation of the areas viewed by detectors Da and Db and their respective counting rates at selected times around the narrow spike event at ~2300:40 UT

An estimate of the total precipitation rate in the spike can also be obtained from the magnetometer response, which is compared in Figure 7 with the riometer data. The precipitation spike was accompanied by an ~150-nT positive impulse in the H component field. The D component remained essentially unchanged while the Z component decreased by ~75 nT. The increase in the H component and the additional decrease in the Z component can be attributed to the devel-

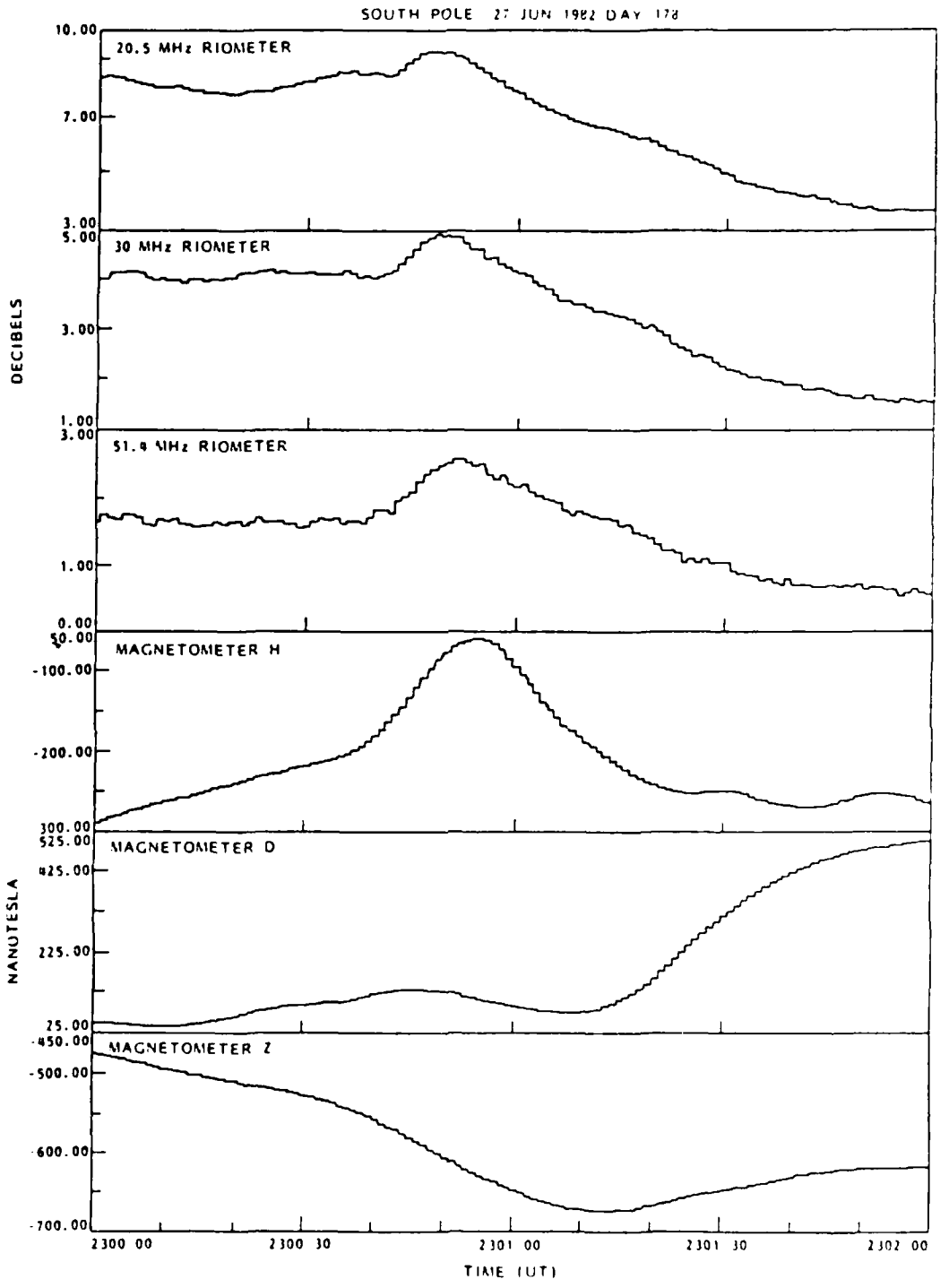

Fig. 7. The south pole riometer absorptions and magnetometer responses at 1-s resolution around the time of the spike

opment of a short-lived eastward current system equatorward of South Pole Station (Figure 3c). If it is assumed that the eastward current system is ~150 km from South Pole Station, then the intensity of the current would be $\sim 1.1 \times 10^5$ A. This corresponds to $\sim 6.8 \times 10^{23}$ el s or $\sim 4 \times 10^{16}$ ergs s, a somewhat larger value than that deduced from the X ray data taken during the spike.

The geometry depicted in Figure 3c is similar to current patterns discussed in connection with high-latitude electrojets in the postnoon sector by *Rostoker et al* [1979]. See, in particular, their Figure 7, where an eastward auroral electrojet is shown to lie equatorward of the higher-latitude westward electrojet. Energetic (~1.3 to ~150 keV) precipitating electrons were reported to occur within the poleward portion of the

region of eastward flow [*Rostoker et al.*, 1979]. Of course, from a single station the interpretation in terms of an eastward electrojet is not unique. However, this interpretation for the short-lived event appears more reasonable than speculating that the far poleward westward electrojet suddenly intensified and moved farther poleward momentarily. If the westward electrojet at the time of the spike was ~200 km distant, then an intensification and poleward movement would produce a larger relative change in Z than in H (by about a factor of 2), while the opposite behavior is actually observed ($\Delta Z \sim 100$ nT, $\Delta H \sim 200$ nT; Figure 7).

Spatial Scale of Spike Precipitation Region

The prespike absorption at 30 and 51.4 MHz was at essentially constant levels of 4.1 and 1.7 dB, respectively. Enhanced ionization associated with the spike produced an additional ~0.9 dB absorption at each frequency. The ratio between the absorption at 30 and at 51.4 MHz immediately prior to the spike was ~2.4, whereas an absorption ratio ≈1 characterized the spike precipitation alone. This frequency dependence of the absorption can be used to infer information about the spatial scale size of the precipitation region and the electron energy spectrum.

The frequency dependence of absorption (A_0) at the zenith can be characterized by the relation $A_0 \sim f^{-n}$, where f is the riometer radio frequency and n is the spectral index [*Lerfald et al.*, 1964]. In theory, n is in the range 0–2, the value for any given event being dependent on the predominant altitude at which the main ionization is produced. Typically, auroral absorption occurs in the upper D region, for which $n = 2$, giving a ratio of 2.94 between the absorption at 30 MHz and that at 51.4 MHz. However, it can be shown that absorption will be independent of frequency ($n = 0$; absorption ratio = 1.0) if the precipitation-enhanced ionization is predominantly at low altitude (≤ 60 km).

Because unrealistically high electron energies (1–10 MeV) are required to obtain absorption ratios which depart significantly from f^{-2} in substorm events, the more likely interpretation of such circumstances is that suggested by *Nielsen and Axford* [1977] and *Hargreaves et al.* [1979]. They showed that smaller ratios could occur if narrow, intense precipitation structures only partially fill the field of view of a broad-beam riometer. Thus we assume that the absorption spike at 2301 UT (absorption ratio ≈ 1) is caused by a narrow structure within the more widespread (absorption ratio ≈ 2.4) precipitation that is part of the recovery of the main absorption event. In the following analysis we adopt the "Gaussian strip" geometry of *Nielsen and Axford* [1977] as used in the calculations by *Hargreaves et al.* [1979].

For this geometry the absorbing region has the form $A = A_0 \exp(-x^2/2x_0^2)$, where x_0 is a characteristic width of the strip expressed as a fraction of the assumed height of the absorbing layer. From Figure 3 of *Hargreaves et al.* [1979] note that a low absorption ratio (< 1.5), coupled with ~1 dB broad-beam absorption at 51.4 MHz (as in the spike at 2301 UT), requires a narrow strip ($x_0 < 0.1$) and a high zenithal absorption ($A_0 > 10$ dB at 51.4 MHz) through the strip. With $x_0 = 0.1$, and assuming 90 km for the height of the absorbing layer, a strip width (i.e., the distance between $e^{-1} A_0$ points of the region) of ~25 km is obtained.

Total Electron Flux

The riometer absorption measurements indicate that the spike precipitation region can be approximated by a strip of width ~25 km and length greater than 100 km. On the other hand, the viewing geometry of the Da detector on P78-1 indicates a maximum source width of ~250 km in one direction. Therefore for purposes of computation we take the area of the region of X ray emissions to be 25 × 250 km or 6.25×10^{13} cm^2. If the precipitation rate of 2×10^{23} el s obtained from the X ray measurements is uniform over this area, then the precipitating flux of electrons (>0 keV) is $\sim 3 \times 10^9$ el cm^{-2} s^{-1}, corresponding to an isotropic distribution for $\sim 1 \times 10^9$ el cm^{-2} sr^{-1} s^{-1}.

We can also estimate the total electron flux from the calculated zenithal absorption through the strip (10 dB) and knowledge of the input electron spectrum. The spike electron spectrum, determined from the X ray data, is characterized by an e-folding energy of 40 keV. For this spectrum, and using the TANGLE program [*Vondrak and Baron*, 1976] to compute modified electron density profiles and resulting absorption, we obtain a total electron flux (>0 keV) of $\sim 1 \times 10^9$ el cm^{-2} sr^{-1} s^{-1}, in agreement with the value obtained from the X ray data.

SUMMARY

An electron precipitation event within the southern polar cap has been measured with the satellite bremsstrahlung X ray technique in conjunction with ground-based riometer and magnetometer observations. The particular feature examined in detail was an intense precipitation spike of ~10 s duration. Quantitative estimates of the spatial extent, electron energy spectrum, flux, and precipitation rate associated with the spike were derived in a reasonably self-consistent way from the three different measurement techniques. The following characteristics were noted:

1. The spike was likely associated with an eastward ionospheric current that developed equatorward of the main substorm westward electrojet.

2. Poleward motion of the spike and main precipitation regions as well as both current systems can be inferred from the measurements.

3. The spatial extent of the spike, as determined from multifrequency riometer data, is consistent with a strip of width ~25 km and length greater than 100 km.

4. An e-fold energy of ~40 keV characterized the spike precipitation, a harder spectrum than was applicable to the precipitation prior to and following the spike.

5. The total rate of precipitation of electrons (>40 keV) in the spike was determined to be $\sim 2 \times 10^{23}$ s^{-1} (from the X ray data) and $\sim 6.8 \times 10^{23}$ s^{-1} (from the magnetic field variations). The discrepancy may be related to underestimating the electron flux below ~20 keV when extrapolating the X ray-derived spectrum to zero energy.

6. The electron flux (>0 keV) in the spike, derived from the X ray and riometer data, is (assuming isotropy) $\sim 1 \times 10^9$ cm^{-2} s^{-1} sr^{-1}.

Several features of this spike are atypical of the spike events reported previously. These include the spike's occurrence following the main precipitation event rather than at the onset, its association with an eastward electrojet, and possibly the hardness of the electron spectrum. Further study is required to determine if these features represent fundamental differences in the precipitation processes among classes of spike events.

The coordinated data discussed here illustrate how a combination of bremsstrahlung X ray imaging and ground-based measurements can be used to study the dynamics of electron precipitation events. Further advances can be expected from

improvements in instrumentation to provide finer-scale X ray and absorption mappings.

Acknowledgments. Development of the P78-1 satellite X ray spectrometers was supported by the Defense Advanced Research Projects Agency through the Office of Naval Research (contract N00014-78-C-0070). The Office of Naval Research (contract N00014-79-C-0824) sponsored the SEEP experiment on the S81-1 spacecraft. Much of the X ray data analysis presented here was sponsored by a grant from the Division of Polar Programs in the National Science Foundation (DPP-8209967). Support of the riometer measurements at South Pole Station was provided by National Science Foundation grants DPP-7925014 and DPP-8304844 from the Division of Polar Programs. Logistic support for the magnetometer measurements was provided by the Division of Polar Programs of the National Science Foundation.

The Editor thanks E. Nielsen and another referee for their assistance in evaluating this paper.

REFERENCES

Anderson, K. A., Energetic electron fluxes in the tail of the geomagnetic field, *J. Geophys. Res.*, *70*, 4741, 1965.

Bjordal, J., H. Trefall, S. Ullaland, A. Bewersdorff, J. Kangas, P. Tanskanen, G. Kremser, K. H. Saeger, and H. Specht, On the morphology of auroral-zone X-ray events, I, Dynamics of midnight events, *J. Atmos. Terr. Phys.*, *33*, 605, 1971.

Brown, J. W., and E. C. Stone, High-energy electron spikes at high latitudes, *J. Geophys. Res.*, *77*, 3384, 1972.

Detrick, D. L. Lutz, T. J. Rosenberg, D. L. Carpenter, W. Gail, J. Katsufrakis, R. L. Arnoldy, L. J. Cahill, Jr., L. J. Lanzerotti, F. T. Berkey, J. R. Doupnik, R. H. Eather, and S. B. Mende, Ground-based studies of the magnetospheric cusp and auroral oval from South Pole Station, Antarctica, *Eos Trans. AGU*, *63*, 408, 1982.

Hargreaves, J. K., H. J. A. Chivers, and E. Nielsen, Properties of spike events in auroral radio absorption, *J. Geophys. Res.*, *84*, 4245, 1979.

Imhof, W. L., G. H. Nakano, and J. B. Reagan, Satellite observations of impulsive bremsstrahlung X ray events associated with substorms, *J. Geophys. Res.*, *83*, 4237, 1978.

Imhof, W. L., J. R. Kilner, G. H. Nakano, and J. B. Reagan, Satellite X ray mappings of sporadic auroral zone electron precipitation events in the local dusk sector, *J. Geophys. Res.*, *85*, 3347, 1980.

Keath, E. P., E. C. Roelof, C. O. Bostrom, and D. J. Williams, Fluxes of $\geq$50-keV protons and $\geq$30-keV electrons at $\sim$35 R_E, 2, Morphology and flow patterns in the magnetotail, *J. Geophys. Res.*, *81*, 2315, 1976.

Krishnaswamy, S., and D. L. Detrick, A computer program to determine quiet day curves using the inflection point method, *IPST Tech. Note BN-1008*, Univ. of Md., College Park, 1983.

Lerfald, G. M., C. G. Little, and K. Parthasarathy, *D* region electron density profiles during auroras, *J. Geophys. Res.*, *69*, 2857, 1964.

McDiarmid, I. B., and J. R. Burrows, Electron fluxes at 1000 kilometers associated with the tail of the magnetosphere, *J. Geophys. Res.*, *70*, 3031, 1965.

McPherron, R. L., C. T. Russell, and M. P. Aubry, Satellite studies of magnetospheric substorms on August 15, 1968, 9, Phenomenological model for substorms, *J. Geophys. Res.*, *78*, 3131, 1973.

Meng, C. I., Energetic electrons in the magnetotail at 60 R_E, *J. Geophys. Res.*, *76*, 862, 1971.

Nielsen, E., Dynamics and spatial scale of auroral absorption spikes associated with the substorm expansion phase, *J. Geophys. Res.*, *85*, 2092, 1980.

Nielsen, E., and W. I. Axford, Small-scale auroral absorption events associated with substorms, *Nature*, *267*, 502, 1977.

Nielsen, E., and R. A. Greenwald, Variations in ionospheric currents and electric fields in association with absorption spikes during the substorm expansion phase, *J. Geophys. Res.*, *83*, 5645, 1978.

Nielsen, E., A. Korth, G. Kremser, and F. Mariani, The electron pitch angle distribution at geosynchronous orbit associated with absorption spikes during the substorm expansion phase, *J. Geophys. Res.*, *87*, 887, 1982.

Roelof, E. C., E. P. Keath, C. O. Bostrom, and D. J. Williams, Fluxes of $\geq$50-keV protons and $\geq$30-keV electrons at $\sim$35 R_E, 1, Velocity anisotropies and plasma flow in the magnetotail, *J. Geophys. Res.*, *81*, 2304, 1976.

Rostoker, G., J. D. Winningham, K. Kawasaki, J. R. Burrows, and T. J. Hughes, Energetic particle precipitation into the high-latitude ionosphere and the auroral electrojets, 2, Eastward electrojet and field-aligned current flow at the dusk meridian, *J. Geophys. Res.*, *84*, 2006, 1979.

Vondrak, R. R., and M. J. Baron, Radar measurements of the latitudinal variation of auroral ionization, *Radio Sci.*, *11*, 939, 1976.

Walt, M., L. L. Newkirk, and W. E. Francis, Bremsstrahlung produced by precipitating electrons, *J. Geophys. Res.*, *84*, 967, 1979.

D. W. Datlowe, E. E. Gaines, W. L. Imhof, J. R. Kilner, J. McBride, J. B. Reagan, and H. D. Voss, Lockheed Palo Alto Research Laboratory, Missiles and Space Department 91-20, Bldg. 255, 3251 Hanover Street, Palo Alto, CA 94304

R. G. Joiner, Office of Naval Research, 800 North Quincy Street, Arlington, VA 22217

L. J. Lanzerotti, AT&T Bell Laboratories, 600 Mountain Avenue, Murray Hill, NJ 07974

T. J. Rosenberg, University of Maryland, Institute for Physical Science and Technology, College Park, MD 20742

(Received April 16, 1984
revised July 23, 1984
accepted July 25, 1984)

7. Mazets, E. P., Golenetskii, S. V., Ilinskii, V. N., Aptekar', R. L. & Guryan, Yu. A. *Nature* 282, 587–589 (1979).
8. Ramaty, R., Lingenfelter, R. E. & Bussard, R. W. *Astrophys. Space Sci.* 75, 193–203 (1981).
9. Ramaty, R. *et al. Nature* 287, 122–124 (1980).
10. Woosley, S. E. *Am. Inst. Phys. Conf. Proc.* 77, 273–292 (1982).
11. Colgate, S. & Petschek, A. *Astrophys. J.* 248, 771–782 (1981).
12. Lamb, F. K. *Am. Inst. Phys. Conf. Proc.* 115, 179–214 (1984).
13. Helfand, D. J. & Long, K. S. *Nature* 282, 589–591 (1979).
14. Pedersen, H. *et al. Nature* 312, 46–48 (1984).

Lightning-induced electron precipitation

H. D. Voss*, W. L. Imhof*, M. Walt*, J. Mobilia*, E. E. Gaines*, J. B. Reagan*, U. S. Inan†, R. A. Helliwell†, D. L. Carpenter†, J. P. Katsufrakis† & H. C. Chang†

* Lockheed Palo Alto Research Laboratory, Palo Alto, California 94303, USA
† STAR Laboratory, Stanford University, California 94305, USA

The broadband very low frequency (VLF, 0.3–30 kHz) radiation from lightning propagates in the Earth–ionosphere cavity as impulsive signals (spherics) and in the dispersive plasma regions of the ionosphere and magnetosphere it propagates as tones of descending or rising frequency (whistlers)[1]. VLF radio waves propagating in the magnetospheric plasma scatter energetic electrons by whistler-mode wave–particle interactions (cyclotron resonance) into the atmosphere[2–6]. These electrons, through collisions with the atmospheric constituents, cause localized ionization, conductivity enhancement, visual and ultraviolet light emissions, and bremsstrahlung X rays. We have reported previously on the precipitation of energetic electrons from the radiation belts by the controlled injection from the ground of VLF radio waves[7,8]. Here we report the first satellite measurements of electron precipitation by lightning. The measured energy deposition of these conspicuous lightning-induced electron precipitation (LEP) bursts ($\sim 10^{-3}$ erg cm^{-2}) is sufficient to deplete the Earth's radiation belts and to alter subionospheric radiowave propagation ($\lesssim$1 MHz). A one-to-one correlation is found between ground-based measurements of VLF spherics and whistlers at Palmer, Antarctica, and low-altitude satellite (S81-1) measurements of precipitating energetic electrons.

Detailed measurements of the pulse shape, spectrum, and pitch angle distribution of LEP events have not previously been obtained nor have direct satellite or ground-based measurements of LEP events been obtained within the plasmasphere where most VLF whistler activity occurs[9]. The plasmasphere (average magnetic invariant latitude $\lesssim 60°$) is characterized by cold plasma densities of 10^2–10^4 electrons cm^{-3} and is the region of the magnetosphere which contains the bulk of the radiation belts. The only *in situ* measurement of lightning-induced electron precipitation that we are aware of was reported by Rycroft[10] using rocket data. He observed a single electron burst event having the proper time relationship to an associated whistler and explained the observation as a gyro resonant interaction between $\sim$100 keV electrons and a $\frac{1}{2}$-hop whistler taking place in the magnetospheric equatorial plane. Our *in situ* satellite observations confirm this initial rocket measurement by establishing a one-to-one correlation with a series of strong electron burst events and clarify the details of the precipitating electron temporal behaviour. Electron precipitation due to whistler-triggered emissions outside of the plasmasphere has been observed with balloon-borne X-ray detectors[6] and ground-based photometers[11,12]. Indirect evidence of LEP events within the plasmasphere has been derived from amplitude and phase perturbations in VLF signals propagating in the Earth–ionosphere waveguide[13,14].

High sensitivity measurements and fine-resolution energy spectra ($2 < E < 1{,}000$ keV) of the prominent LEP bursts were obtained with a cooled solid-state spectrometer array[15] included as part of the stimulated emissions of energetic particles (SEEP) experiment on the three-axis stabilized, low-altitude ($\sim$230 km) S81-1 satellite. The trapped energetic (TE) electron spectrometer ($\pm 20°$ field of view) was aligned perpendicularly to the orbit plane and during these observations was at an angle of 89° to the local magnetic field line. The TE detector had a geometrical factor of 0.17 cm^2 sr and was cooled (-120 °C) to achieve a system noise resolution of 1.2 keV FWHM. An identical detector was positioned to observe electrons with central pitch angles (α) of 52°. The medium energy (ME), precipitating electron spectrometer ($\pm 30°$ field of view) was aligned to the zenith direction and during these observations was at an angle of 25° to the local magnetic field line. The ME geometrical factor was 2.47 cm^2 sr.

Seven LEP events recorded on 9 September 1982 with the SEEP experiment TE particle spectrometer are shown in Fig. 1 (A–G) with the simultaneous VLF spectra received at Palmer, Antarctica ($L \approx 2.3$). These LEP event signatures are interpreted as follows. The whistler wave in passing through the magnetosphere from north to south alters the pitch angles of energetic trapped electrons which are moving northward and can, therefore, resonate with the VLF wave. This interaction reduces the pitch angles of some of the electrons, lowers their mirror points below the satellite altitude, and produces the first electron pulse of the event. Some of these electrons are then magnetically reflected and some are scattered by the atmosphere, resulting in an electron bunch moving to the Southern Hemisphere where the lower mirroring altitude (due to the South Atlantic anomaly) causes the electrons to encounter the atmosphere. Some electrons are backscattered by the atmosphere and return to the Northern Hemisphere where they are observed as the second pulse in the event. Subsequent reflections and backscattering in the Northern and Southern Hemispheres produce the train of pulses of diminishing intensity which makes up the individual events shown in Figs 1 and 2. These measurements were made 3 days after the strong magnetic storm ($D_{st} = -297$) of 6 September 1982. Magnetic storms of this intensity are known to inject electrons which diffuse into the slot region ($2 < L < 3$) of the radiation belt several days after the storm onset[16,17].

In the strong LEP events A, D, and E, electron fluxes are observed to increase rapidly in strength, about 100 times background, in $<$200 ms. The envelopes of the individual pulses then decay relatively slowly to background levels over several seconds. Event G is a factor of 10 above background and event F about three times background. Events B and C are relatively weak on the integral energy display of Fig. 1 but are more prominent in the differential energy spectrum ($120 < E < 140$ keV). The reason why the multiflash LEP event E does not show echo pulses may be due to the superposition of four closely spaced LEP bursts. The flux measured with the ME detector ($\alpha \approx 25°$) is a factor of $\sim$10 less than the flux measured with the TE detector ($\alpha \approx 89°$) indicating an anisotropic pitch angle distribution peaked near 90° at the satellite altitude. VLF spectra of lightning generated spherics and whistlers were detected in the conjugate hemisphere at Palmer Station, Antarctica, (65° S, 64° W) and are shown in Fig. 1*a*. The uniform transition in VLF wave intensity at $\sim$1.9 kHz indicates a well defined Earth–ionosphere waveguide cutoff frequency. The scaled spherics and whistlers are shown beneath the VLF spectrogram. The dashed portion of a scaled whistler curve is extrapolated based on the observed solid portion and the known properties of more completely defined events such as *F*. The conjugate of the SEEP satellite (60° S, 98° W) is 34° to the west of Palmer and thus the VLF spectrogram intensity at Palmer is not simply related to the magnetospheric whistler intensity nor to the flux of precipitating electrons.

Whistler-dispersion techniques[1] are used to identify the spherics that precede the delayed whistler signal on the VLF spectrogram. Event E has four similar whistler traces within a 1-s period and is consistent with multiflash lightning. Event C also has two lightning flashes associated with it. An important observation is that the spherics precede the peak of each LEP event by the expected time interval ($\sim$0.4 s) for all seven cases.

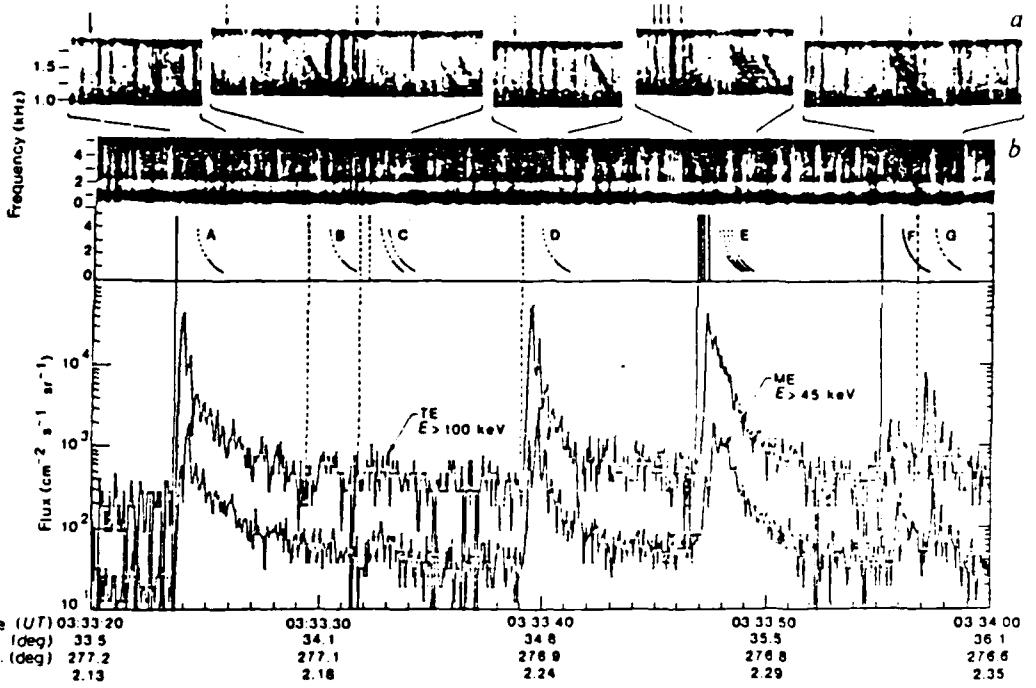

Fig. 1 Energetic electron measurements obtained with the S81-1 satellite are correlated one-to-one with concurrent ground-based VLF whistlers at Palmer Station, Antarctica (65° S, 64° W, $L = 2.3$). Panels *a* and *b* show the VLF spectrograms and the scaled whistlers and spherics. The uppermost insets show the Palmer VLF data with an expanded time scale for the seven LEP events. The strong energetic electron bursts labelled A, D and E have peak fluxes that are 100 times background levels. The sampling interval for the energetic particle measurements is 64 ms. The solid lines and arrows represent spherics that were directly identified on these (and other) records, while the dashed lines represent time estimates based on evidence of essentially identical dispersion properties in all events.

Further evidence for the triggering of precipitation by lightning is given by the LEP pulse shapes and spectra. In the pulse shapes of LEP events A, D, F and G, repetitive pulses of constant period and decaying amplitude that follow the LEP peak are conspicuous. Figure 2 shows LEP events F and G on an expanded scale with the associated whistler signals and the subionospherically propagating signals from the transmitter NAA as received at Palmer. The detailed characteristics of the LEP events shown in Fig. 2 include: (1) the rapid rise of electron flux; (2) the subsequent and relatively slow decay of the flux; (3) the in-phase and repetitive pulses on the TE and ME detector (labelled 1-3 for event F and 1-5 for event G); (4) the greater intensity of the near 90° pitch angle flux (TE) compared with the near 0° pitch angle flux (ME); and (5) the weak or completely absent first pulse on the ME spectrometer (indicating a high ratio of drift-loss-cone to direct bounce-loss-cone flux) compared with the subsequent pulses (labelled 2-5 for event G).

A pulse period of 0.32s is associated with pulses 1-7 of event A. This period agrees with the bounce time of relativistic electrons (~150 keV) echoing between conjugate hemispheres at $L = 2.1$. For 175-keV electrons, the relativistic velocity is $0.67c$ and for 125 keV electrons $0.60\,c$, where c is the velocity of light. As the velocity approaches c the bounce period becomes less sensitive to electron energy variations. For the above energy difference, about five bounce periods (pulses) can occur before the 175-keV electrons are 180° out of phase with the 125-keV electrons. The pulse period of LEP event G at $L = 2.3$ is 0.38 s. This longer period relative to LEP event A agrees with the longer path length of relativistic electrons echoing between conjugate hemispheres at $L = 2.3$ instead of $L = 2.1$.

Examination of the electron energy spectra of LEP events A-G indicates a prominent but broad peak in electron energy between 80 and 200 keV that decreases in energy with increasing L. From comparison of the travel time characteristics of the 9 September 1982, whistlers with similar but more completely defined events recorded on another day at Palmer when whistler-associated precipitation was observed[18], the equatorial electron density at $L = 2.1$ is estimated to have been 3,200 electrons cm^{-3}. Assuming ducted propagation the VLF wave frequency would be ~4 kHz based on an equatorial gyroresonant interaction with 150 keV electrons. This frequency is in the upper region of the more broadly defined whistlers, such as event F.

Figure 2*a* shows a small perturbation in the signal received at Palmer from NAA (propagating in the Earth-ionosphere waveguide) which is coincident with the strong whistler and weak LEP burst F. The raw data show the 17.8-kHz signal intensity using a 300-Hz bandwidth filter. Also shown are the smoothed curves of the raw data (dashed lines) outside of the rapid transition interval (±0.5 s) that were obtained using a 2.4 s averaging filter. The amplitude of the NAA transmitter signal received at Palmer exhibits a fast decrease (< 1.5 s) followed by a slow recovery (~10 s). Such a signal perturbation or 'Trimpi' event is associated with lightning-induced electron precipitation which modifies the ionosphere at the ~80 km reflection altitude[13,14]. Considered in isolation, this event is weak because of atmospheric noise at the NAA frequency. However, it is similar in form to a series of stronger events that occurred within several minutes preceding and following the period of satellite data. The strong whistler event F and associated Trimpi event recorded at Palmer are consistent with a relatively strong LEP burst occurring near Palmer. For the other six relatively weak whistler signals no Trimpi events were detected although strong electron precipitation is evident in the SEEP detectors for events A, D, E and G. The simultaneous electron precipitation at the SEEP satellite and near Palmer (Trimpi) which are separated in longitude by 2,000 km, for event F, suggest that a single lightning flash can precipitate electrons at two widely separated locations.

The electron precipitation energy fluxes are estimated to be about 10^2-10^5 times the wave energy flux at the equatorial plane, indicating that only a little VLF signal energy is required to perturb the relativistic electrons near the edge of the loss cone enough to cause precipitation[1]. The energy fluxes reported here are consistent with suggestions that whistlers may cause a

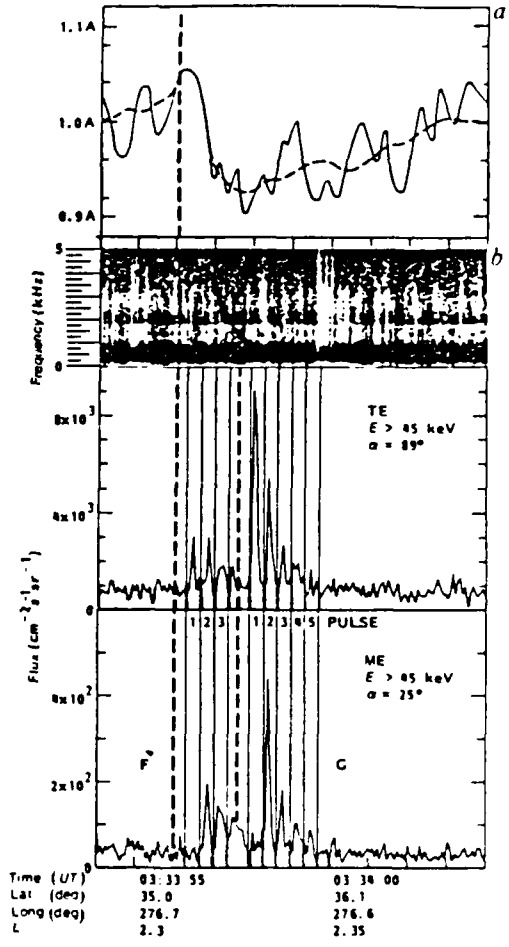

Fig. 2 Expanded view of lightning-induced electron precipitation (LEP) events F and G. The repetitive pulses of constant period labelled 1 to 5 are consistent with the echo period for electrons mirroring between conjugate hemispheres. The vertical dashed line indicates the calculated time of the lightning flash. Panels *a* and *b* show the simultaneous whistler spectrogram and the amplitude of signals received at Palmer from NAA.

significant loss of radiation belt electrons[3-5,19,20,22]. Assuming that the slot regions of the radiation belts are initially filled after a magnetic storm with an omnidirectional flux of 10^4 electrons $cm^{-2}\,s^{-1}$ for $E > 100$ keV at $L = 2.3$, a single LEP burst (such as event D) can empty ~0.001% of the belt in the region covered by the burst magnetic field lines.

The observations of LEP events provide direct evidence of an important coupling mechanism between terrestrial lightning and relativistic radiation belt electron precipitation. Further study should clarify details of the wave-particle interaction since wide ranges of VLF signal strength and frequencies are present. The global mapping of LEP events can also provide an insight into the penetration of wave energy through the ionosphere and its propagation in the magnetosphere. The role of LEP events in the overall loss rates of trapped electrons is uncertain, because the frequency of occurrence of these events and their relative importance in comparison, for example, with plasmaspheric hiss[21] is not well known. However, a substantial amount of electrons can be removed in a single event, and additional electron losses can be expected to result from an enhancement of the effective pitch angle diffusion coefficient by whistler waves.

The Lockheed Palo Alto Research Laboratory portion of the SEEP experiment was sponsored by the Office of Naval Research (contract N00014-79-C-0824). Launch and orbital support were provided by the Air Force Space Test Program Office. Much of the data analysis was performed under the Lockheed Independent Research Program. We thank Dr D. P. Cauffman for program management of the satellite payload; the payload system engineer, Mr S. J. Battel; and Dr D. W. Datlowe for help in processing the data. The Stanford University effort in SEEP was supported by ONR grant N00014-82-K-0489 and by the Division of Polar Program of the NSF under grant DPP82-17820 for the Palmer Station VLF program.

Received 21 June; accepted 3 October 1984.

1. Helliwell, R. A. *Whistlers and Related Ionospheric Phenomena* (Stanford University Press, California 1965)
2. Kennel, C. F. & Petschek, H. E. *J. geophys. Res.* **71**, 1–28 (1966)
3. Inan, U. S., Bell, T. F. & Helliwell, R. A. *J. geophys. Res.* **83**, 3235–3253 (1978)
4. Chang, H. C., Inan, U. S. & Bell, T. F. *J. geophys. Res.* **88**, 7015–7023 (1983)
5. Inan, U. S., Bell, T. F. & Chang, H. C. *J. geophys. Res.* **87**, A243–A264 (1982)
6. Rosenberg, T. J., Helliwell, R. A. & Katsufrakis, K. P. *J. geophys. Res.* **76**, 8445–8452 (1971)
7. Imhof, W. L. *et al. Geophys. Res. Lett.* **10**, 615–618 (1983)
8. Imhof, W. L. *et al. Geophys. Res. Lett.* **10**, 361–364 (1983)
9. Carpenter, D. L. *Radio Sci.* **3**, 719–724 (1968)
10. Rycroft, M. J. *Planet. Space Sci.* **21**, 239–251 (1973)
11. Helliwell, R. A., Mende, S. B., Doolittle, J. H., Armstrong, W. C., Carpenter, W. L. *J. geophys. Res.* **85**, 3376–3386 (1980)
12. Doolittle, J. H. & Carpenter, D. L. *Geophys. Res. Lett.* **10**, 611–614 (1983)
13. Helliwell, R. A., Katsufrakis, J. P. & Trimpi, M. L. *J. geophys. Res.* **78**, 4679–4688 (1973)
14. Carpenter, D. L. & La Belle, J. W. *J. geophys. Res.* **87**, 4427–4434 (1982)
15. Voss, H. D. *et al. IEEE Trans. nucl. Sci.* **NS-29**, 164–168 (1982)
16. Lyons, L. R. & Williams, D. J. *J. geophys. Res.* **80**, 3985–3994 (1975)
17. Voss, H. D., Imhof, W. L., Mobilia, J., Gaines, E. E. & Reagan, J. B. *Space Res.* (in the press)
18. Carpenter, D. L., Inan, U. S., Trimpi, M. L., Helliwell, R. A. & Katsufrakis, J. P. *J. geophys. Res.* **89** (in the press)
19. Dungey, J. W. *Planet. Space Sci.* **11**, 591–595 (1963)
20. Cornwall, J. M. *J. geophys. Res.* **69**, 1251–1259 (1964)
21. Lyons, L. R. & Thorne, R. M. *J. geophys. Res.* **78**, 2142–2149 (1973)
22. Kelley, M. C. *et al. J. geophys. Res.* (in the press)

A new radiation source for the infrared region

J. Yarwood*, T. Shuttleworth†, J. B. Hasted‡ & T. Nanba‡

* Department of Chemistry, University of Durham, Durham DH1 3LE, UK
† Department of Physics, Birkbeck College, Malet Street, London WC1E 7HY, UK
‡ Department of Physics, Tohoku University, Sendai, Japan

Spectroscopy in the far-infrared and millimetre-microwave regions has always been hampered by the lack of intense broad-band sources. After several predictions[1-4] suggesting the possibility of obtaining improved infrared fluxes from an electron source, the Daresbury (SERC) synchrotron storage ring (SRS) has now been shown to produce an intense and very bright source of infrared photons. The infrared port (IR-13(1)) at Daresbury will provide scientists interested in the microscopic structure and dynamics of materials with a radiation source having several unique properties. As well as these properties, we describe here the work that has been done, since January 1984, in characterizing the infrared beam and suggest some wide-ranging potential experimental applications.

Because the photon beam is composed of electromagnetic radiation emitted by a highly relativistic electron beam[5], the radiation is highly collimated in the forward direction and is strongly linearly-polarized in the orbit plane. Furthermore, it provides a well-defined train of pulses of radiation[6] of ~200 ps in width with a period of either 320 ns (for a single electron bunch) or 2 ns (for 160 electron bunches). The pulse width and shape are entirely independent of frequency, and the inherent photon noise level is expected to be very low compared with that of black-body sources. The beam lifetime is 8–10 h at 2 GeV electron energy. Although the SRS is more intense (in terms of photons emitted per second) than a black body emitter only in the far-infrared region (below ~50 cm^{-1}), its other advantages—especially its brightness (watts per unit area-solid angle) and its precise time structure—are manifest throughout the infrared

A SATELLITE IMAGER FOR ATMOSPHERIC X-RAYS

W. Calvert+, H. D. Voss, and T. C. Sanders

Lockheed Palo Alto Research Laboratory
3251 Hanover St., Building 255
Palo Alto, California 94304

ABSTRACT

A high-sensitivity X-Ray Imaging Spectrometer (XRIS) was developed for measurements of atmospheric bremsstrahlung X-rays. The XRIS instrument flown on a 3-axis stabilized polar orbiting satellite (S81-1) employed a one-dimensional pinhole camera to acquire a 2-dimensional X-ray image as the satellite passed over an auroral scene. Using a position sensitive gas proportional counter, with an active area of 1200 cm^2 divided into sixteen cross-track pixels, the instrument had a geometric factor of about 0.4 cm^2-steradian per pixel (6 cm^2-sr total) for X-rays of 4 to 40 keV. At an orbital altitude of 250 km, it provided a spatial resolution of 30 km and the temporal resolution was one-eighth of a second. Designed primarily to detect artificial electron precipitation at lower latitudes, the instrument also produced the first satellite X-ray images of the aurora during May and June, 1982. Special features of the instrument included a quadrupole broom magnet to reject energetic electrons, a multilayer plastic-on-tantalum shielding to suppress the bremsstrahlung X-rays generated from electrons which impact the instrument surface, and a new technique for position sensing within the detector, using signal division in a resistor array.

INTRODUCTION

The X-Ray Imaging Spectrometer (XRIS) on the S81-1 satellite produced the first high-sensitivity satellite images of the X-ray aurora during May and June, 1982. Such images are useful in auroral studies since they pertain to higher energies of the precipitating electrons than do conventional optical images (i.e. a few keV rather than a few eV). Moreover, those images readily show the daytime auroral structure that would otherwise be difficult to observe by optical techniques because of scattered sunlight.

Previous to the XRIS, the satellite imaging observations of the x-ray aurora were limited to rather high energies ($E \geq 20$ keV) using an eight pixel x-ray sensor on the P78-1 spinning satellite [1]. Two rocket flights employing single detector with a rather large geometric factor (2 cm^2 sr; $E > 5$ keV) produced x-ray images of the aurora using the rocket spin motion to scan the scene [2]. Relatively high energy ($E \geq 20$ keV) x-ray images of the aurora have also been obtained from balloon-borne instrumentation [3]. Although most of the satellite-borne x-ray astronomy instruments would be capable of making highly sensitive and detailed auroral x-ray images those satellites are usually limited to very low latitudes and altitudes to minimize the energetic particle and x-ray backgrounds [4], and generally view only in the upward direction. On a DMSP-F2 satellite (830 km altitude) a single x-ray detector has shown the importance of covering the low energy auroral x-rays [5]. A recent DMSP satellite (F6) included a single x-ray detector on a scan platform to produce a raster-scan x-ray auroral image [6]. The DMSP images complement the S81-1 images since XRIS is at a lower altitude, had higher temporal and spatial resolution, and also had substantially higher sensitivity.

The high sensitivity of XRIS (6 cm^2 sr) was accomplished with a 1200 cm^2 area position sensitive proportional counter at the image plane of a pinhole camera collimator. Techniques were employed for reducing interferring radiation: passive shielding, a unique broom magnet, and active anticoincidence rejection. The XRIS instrument weighed 35.5 kg and required 12 watts of power. The purpose here is to describe the XRIS instrument design, including the rationale behind its configuration.

The XRIS instrument was part of the Stimulated Emissions of Energetic Particle (SEEP) experiment. The principal objective of SEEP was to detect the artificial precipitation of magnetospheric electrons by ground-based radio transmitters. In addition to XRIS, the SEEP payload on the S81-1 satellite included a high-sensitivity cooled solid state particle spectrometer array [7], a plasma probe and an optical photometer. The need for high-sensitivity in both the x-ray and particle instruments stemmed from the rather weak predicted fluxes of energetic particles and bremsstrahlung x-rays at mid-latitudes. To date no x-rays have been found which correlated with the transmitter-induced artificial precipitation. However, direct electron measurements by SEEP have clearly demonstrated the correlation between transmitter modulation and electron precipitation [8]. The XRIS has been valuable in measuring auroral X-rays, even though it was not optimized for that purpose.

DESCRIPTION

Instrument

The XRIS instrument employed a pinhole camera which formed a one-dimensional crosstrack image as the satellite moved over the auroral scene. Its total field of view was about 90° by 7°, facing forward and tipped downward at an angle of 35° below the local horizon. Its long dimension was perpendicular to the direction of satellite motion. It thus yielded a strip image of the upcoming X-rays about 500 km wide at a distance 200 km ahead of the spacecraft (assuming a source altitude of 90 km). The angle of view was chosen both to increase the scene width and to provide a time separation between the actual X-ray image and the false signals of energetic particles striking the instrument. The primary XRIS Instrument characteristics are shown in Table 1.

Figure 1 shows a photograph of the XRIS instrument. The pinhole entrance aperture was in the form of a slit, 2 cm by 15 cm, flanked by a quadrupole broom magnet to reject interfering energetic electrons. Behind the entrance aperture and broom magnets was a collimator cone, with two sets of parallel plates to defined the narrow acceptance angle for the instrument. Behind the cone was a Xenon filled pressure vessel containing the proportional counter. On one side a gas fill valve and a getter were located. Most of the instrumental electronics, were contained in a separate box behind the instrument, except for the high-voltage power supply and the pulse preamplifiers.

+ Now at the Dept of Physics & Astronomy, The University of Iowa, Iowa City, Iowa 52240.

0018-9499/85/0002-0112$01.00 © 1985 IEEE

TABLE 1 XRIS Characteristics

Detector:	Proportional Counter
Active Area (cm^2)	1200
Anode Wire Size (mm)	0.025
Cathode Wire Size (mm)	0.100
Wire Type	Gold Plated Tungsten
Wire Spacing (mm)	6.35
Energy Range (keV)	4-40
Angular Resolution	$7^o \times 7^o$ (E<10 keV)
	$7^o \times 14^d$, (E>20 keV)
Spatial Resolution (km)	30 x 60
Temporal Resolution (sec)	0.125
Sensitivity factor (Φt, cm^{-2} sr^{-1})	3.4

Optics

A section view of the instrument, in a plane parallel to the internal collimator plates and hence perpendicular to the long dimension of the entrance slit, is shown in Figure 2. The scene is divided into sixteen pixels, left to right, by electronically segmenting the proportional counter. In the space enviornment a vacuum extends through the entrance slit all the way back to a beryllium window, which is supported against the gas pressure of the detector by the collimator assembly. The collimator, made of aluminum, provided the 7^o narrow field of view for X-ray photon energies below about 10 keV. A second collimator, made of tantalum and mounted in front of the aluminum collimator, similarly defined a 14^o field of view at higher photon energies, where greater sensitivity is needed.

Image Acquisition

The pulses from each of the sixteen detector segments, which indicated the arrival of an individual X-ray photons, were sorted into eight amplitude levels, to measure the photon energy, and accumulated in a 16 x 8 memory. The 128 photon tallies were transferred to the telemetry system eight times a second, for onboard recording and subsequent relay to the ground. The eighth-second temporal resolution that this provided corresponds to only about one kilometer of orbital motion and hence to a small fraction of the projected pixel size on the ground. Therefore, the temporal resolution did not significantly compromise the spatial resolution. Auroral pulsations yielded a prominent striping of the images whenever such temporal modulation was present. The pulses from the two center pixels were also pulse-height analyzed into 24 levels and transferred to the telemetry sixteen times a second to provide improved energy and time resolution at the center of the scene.

Detector

As shown in Figure 2, the proportional counter consists of five electrode planes, each one consisting of thin parallel tungsten wires aligned perpendicular to the plane of the figure. The detector segmentation consisted of isolating the pulse signals from different wires, by a new technique described below. The purpose of the multiple electrode planes was to provide two separate detection layers, in order to distinguish the signal of an X-ray photon, which originates in one of the layers, from that of an ionizing particle (e.g. a cosmic ray) which would be detected in both layers. The dual proportional counter serves as both the primary and anticoincidence detectors: using the front and rear layers, respectively. A cathode bias, of a few hundred volts with respect to the chamber walls, was provided to create a drift potential region that extended the effective detection layer forward to the beryllium window, and that of the anti layer to the rear of the chamber.

The active gas for the proportional counter was Xenon and methane, the methane quenching gas was chosen because a selective getter was found (ST171 SAES) which would remove other impurities. The gas pressure inside the chamber (18 PSI) was slightly above atmospheric pressure simply to keep a positive pressure on the beryllium window during all of the pre-launch operations.

The electrode frames (not shown) were made from selected fiberglass epoxy printed-circuit board, of those specific manufacturer's lots which proved to be least prone to outgassing. Along the sides of the electrode frames, and opposing the stress of the tungsten wires, were carbon-epoxy thermal compensating segments to allow for the significantly different thermal expansion coefficients of the tungsten wires and the fiberglass. The entire frame structure was mounted from the rear of the chamber on floating standoffs so the frames could expand and contract independently.

The gold-coated tungsten wires (25 μ for the anodes, and 100 μ for the cathodes) were first wrapped on a threaded frame, anchored to the fiberglass frame with epoxy, and then soldered to printed-circuit pads. Although this mounting scheme proved satisfactory, and avoided the need for installing each of the wires independently, it was hard to achieve uniform tension. In particular, it was necessary to pre-stress the frames inward until after the epoxy had set and the excess wire was cut away, using a special spring jig, so that the released frames would then bear the load of the stretched wires evenly. The wire tension in the completed frames was checked by exciting visible acoustical oscillations with an audio amplifier and speaker. It was found that excessively taut wires could be stretched by lightly stroking with a pencil eraser, whereas a few of the slack wires had to be restrung individually.

Enclosure

To minimize weight almost all of the load-bearing structures were made of aluminum. The alternative of using structural tantalum to serve double duty as shielding was considered, but it was discarded because of the added weight required to satisfy some of the structural demands. The gas enclosure for XRIS was rectangular, although less weight might have been needed with a cylindrical chamber. The side and front walls of the pressure chamber shown in Figure 2 were milled from solid aluminum, with a labyrinth of pockets to reduce weight. The back wall was made of honeycomb aluminum, permanently epoxied to the side walls. This and the front wall were bolted together, with the beryllium window sandwiched in between and sealed with a O-ring. The entire instrument in front of the beryllium window was encased in a tantalum shield and covered with plastic. A plastic of low atomic number was chosen for its low X-ray yield for energetic electrons, and the tantalum was chosen to absorb any X-rays which were produced. Care was taken to lap each of the tantalum pieces and cap every fastener hole with tantalum and plastic, so there would be no straight path into the instrument with less than 2 gm/cm^2 of shielding. The black plastic coating, which was impregnated with carbon and applied as layers of tape, also provided the thermal control by having the right spectral absorption and emission properties.

DESIGN CONSIDERATIONS

The choice of a simple pinhole camera was based on program constraints and a careful consideration of the available alternatives for acquiring an X-ray image. In particular, the coded aperture technique which has proven successful in X-ray astronomy was

examined and rejected because of the filled auroral scenes that XRIS would encounter. Moreover, the choice of only sixteen pixels was found to be optimum for the proper matching of resolution and sensitivity.

Constraints

Much of the XRIS design was dictated by the flight opportunity: The available orbit was sun-synchronous (10:30 am and 10:30 pm local time) and nearly circular at an altitude of about 250 km. Although this low altitude gave excellent resolution and sensitivity to search for manmade precipitation without large background contamination from the radiation belts, it required a wide field of view to obtain suitable images. The S81-1 spacecraft was 3-axis stabilized and oriented with respect to the earth. The fixed orientation gave the XRIS instrument 100% duty cycle for viewing the atmospheric X-rays. The weight restriction on XRIS was critical for the design, since that dictated the ultimate sensitivity and resolution which were achieved.

Imaging Technique

Only a few techniques are available for X-ray imaging, since X-rays cannot be focused by lenses. These consist of either grazing-incidence reflection, or those techniques which depend upon detecting a geometric shadow, like the collimator, the pinhole camera, and the coded aperture. Grazing incidence, unfortunately, only works for the lowest energies of interest, and then only with a prohibitively narrow field of view. The low orbit of SEEP, and hence the need for a wide field of view, automatically precluded its use, leaving only the various shadow techniques.

All of the shadow techniques are similar, in that they rely upon forming the shadow of an entrance aperture upon a detector placed some distance away. With a collimator, the active segment of the detector is determined by the collimator structure, and this permits increasing the instrument sensitivity by using a large detector and many individual collimator plates adjacent to one another (e.g. either in a planar or an "egg crate" configuration). With a pinhole camera, the active segment of the detector is defined by some other means, such as using an array of individual detectors, or as with XRIS, using some type of position-sensitive detector. In either case, the angular acceptance of the instrument is determined strictly by the geometry of photons entering through an aperture and reaching the active segment of the detector. For a colinear aperture and detector of equal width, the angular response is triangular and it reaches zero at twice the width. For a rectangular pixel, the equal response contours are roughly diamond shaped, with that of half-maximum approximately formed by connecting the midpoints of the geometric shadow of the aperture. Except for inverting the image, an array of collimators, each pointed in a slightly different direction, is equivalent to a pinhole camera having the same aperture and detector area. As will be discussed below, a coded aperture uses multiple pinholes to produce overlapping images in the detector plane, suitable for a correlation analysis, but the angular acceptance is still determined by the same shadow geometry.

A mechanically scanning sensor like that used on DMSP might perhaps have been simpler for XRIS, since it would have eliminated the need for a position-sensitive detector. However, since XRIS was to be flown on a stabilized platform, the rotation required to scan the scene would have to have been implemented artificially.

The One-Dimensional Format

In forming an image of a stable scene, a moving collimator and a pinhole camera are exactly equivalent, except that the collimator examines one pixel at a time while the pinhole camera examines all of the pixels simultaneously. For the same total detector area, they both yield the same number of counts in the same total time. The same concept applies to a conventional two-dimensional pinhole camera and its one-dimensional equivalent, which, like XRIS, forms its image by sweeping across the scene. Whereas the former examines all the scene pixels simultaneously, the latter examines one row at a time. But again, for the same total detector area, it acquires the same number of counts for each pixel in the same total time. The main point, then, of different imaging configurations, is how long they dwell on a given pixel, compared to the temporal resolution which is required. The collimator dwells the shortest time on a given pixel, and hence it would be suitable for studying only the most rapid signal variations, quicker than 250 milliseconds for the XRIS parameters. For a square image of 16 x 16 pixels, the total time for the two-dimensional equivalent of XRIS would be 64 seconds, and that would have permitted examining temporal variations as long as 64 seconds. The one-dimensional scheme actually implemented for XRIS permits examining an intermediate time scale, between roughly 250 msec and 4 seconds, and it was chosen for that reason, since the modulation that it was designed to detect occupied that range.

The selection of a one-dimensional camera also simplified the instrument design and data handling. In the instrument, it was sufficient to sense position in only one dimension, and that allowed allocating groups of anode wires to a given pixel, rather than having to cross-wrap the wire arrays or to adopt some other technique for determining where the photon arrived along a given anode wire. Dealing with only one-dimensional positioning also simplified the processing electronics and reduced the memory required to accumulate the X-Ray photon counts. Finally, in the data handling, the one-dimensional configuration made it unnecessary to correct for the satellite motion during the observation of a given scene pixel, as it moved across the different pixels of the detector array.

Coded Aperture

A very serious competitor for the imaging technique used on XRIS was the coded aperture, invented by Mertz and Young [9]. In this technique, a shadow plate in front of the detector is divided into N cells, K of which are open to transmit X-rays. Each point of the source creates a shadow image on the detector, and many such point sources create overlapping shadows which can be separated mathematically by cross-correlation with the known pattern of the shadow plate. Although this technique has proven excellent for measurements of a few point sources, where it acts somewhat like K separate pinhole cameras, the advantage diminishes rapidly for a scene like the aurora, which have distributed sources. The reason for the degradation of the reconstructed image is that each point of the source contributes noise for every point. For only a few point sources, the noise is at a tolerable level, being roughly the square root of the peak signal in every other pixel (assuming an optimum shadow pattern). However, when the number of filled pixels in the scene becomes comparable to the square root of the total count from one pixel, the noise from all the other pixels will become comparable to the signal of the one pixel. In other words, the presence of many filled pixels will destroy the signal-to-noise ratio for all the others. This problem would have been serious for XRIS, which was so close to the scene that one auroral arc would sometimes fill all the pixels. Although the coded aperture technique is not much worse than a pinhole

camera (within a factor of two), it would have involved massive calculations and high counting rates to reconstruct each image. Therefore, the coded aperture, despite its popularity in other applications, was discarded as a viable technique for XRIS.

Resolution and Sensitivity

A fundamental factor in the design of space X-ray instruments is the tradeoff between the sensitivity and the spatial or temporal resolution. A quite obvious, but sometimes overlooked factor is that the count rate of a photon detector increases as the fourth power of the spatial resolution, since it is proportional to the product of the collecting area and the solid angle, and both of those are proportional to the square of the spatial resolution. This applies equally to a collimator, a pinhole camera, and the more-complex coded aperture. As a result, it is necessary to choose the spatial resolution for the weakest flux which has to be measured. Adding the counts from adjacent pixels to detect weaker signals does not achieve the same goal, since that yields only half the sensitivity which would have been possible, each time the effective spatial resolution is doubled.

The criterion for selecting the spatial resolution of XRIS was the signal-to-noise ration (SNR) which could be achieved in a count-rate limited observation. That ratio, considering only the statistical fluctuations, equals the square root of the number photons counted in the measurement. It can be shown, for a pinhole camera with n square pixels and a total detector area A, that the SNR for a single pixel should be

$$SNR = [\Phi A t / n]^{1/2} d / D \qquad (1)$$

where Φ is the photon flux (in units of cm^{-2} sr^{-1} sec^{-1}), t is the observing period, d is the spatial resolution, and D is the distance from the scene to the instrument. For XRIS, the total scene width (W = nd) was limited by its low orbital altitude, and this dictated using the largest practical transverse field of view. That, in turn, was dictated by the oblique arrival of photons at the edge pixels of the planar photon detector (see Figure 2), and it was chosen to be 90°. This gave W = 2D and, for a SNR of 2, which was considered the threshold for a useful measurement:

$$n^3 = A t \Phi \qquad (2)$$

using equation (1). Thus, under these circumstances, the maximum number of pixels was determined by the product of the flux density, the total detector area, and the observing period. Moreover, because of the cube in equation (2), it increases rather slowly with that product. From the allocated weight for XRIS, it was determined that A = 1200 cm^2 was the largest practical detector area. Thus, for detecting manmade precipitation with a modulation period of 0.5 sec and an expected flux density of 10 cm^{-2} sr^{-1} sec^{-1}, the maximum number of pixels was eighteen, and the corresponding spatial resolution (for W = 500 km) was about 30 km. For the strongest aurora, with $\Phi = 10^4$ cm^{-2} sr^{-1} sec^{-1} above 4 keV, the spatial resolution for the same observing period might have been much better, with almost 200 pixels across the scene.

Equation (2) indicates that the product Φt for XRIS was about 3 cm^{-2} sr^{-1}. This means that XRIS could measure (with SNR = 2) a flux density of 3 cm^{-2} sr^{-1} sec^{-1} in one second, or 0.3 cm^{-2} sr^{-1} sec^{-1} in ten second, or 3,000 cm^{-2} sr^{-1} sec^{-1} in one millisecond. This quantity was found a bit more useful than the per-pixel geometric factor (which equals Ad^2/nD^2) in typifying an imager, since it tells immediately how long it takes to make a measurement.

It is worth noting that XRIS is not at all poorly designed for the aurora, in spite of it being optimized for a different purpose. Although XRIS might have had a somewhat better spatial resolution, that would have substantially increased the Φt product (e.g. to 3,000 cm^{-2} sr^{-1} for d = 3 km) and that would have substantially increased the time it takes to measure a given flux. This is particularly serious for measurements of the X-ray energy spectrum, which falls off rapidly with increasing energy. For instance, in a moderate aurora, with $\Phi = 10^3$ cm^{-2} sr^{-1} sec^{-1} (above 4 keV), the flux density above 20 keV might be as low as 30 cm^{-2} sr^{-1} sec^{-1}, and a reliable measurement of the spectrum at such energies would have thus required almost two minutes at the higher resolution, rather than the tenth of a second that XRIS actually required. This, in fact, would have prevented the measurement of spectra in all but the most intense auroral arcs, since XRIS passed over such features in a few seconds. XRIS constituted a unique opportunity of measuring the energy spectrum of relatively weak aurora, and similarly, of detecting X-ray aurora which would have otherwise been missed by an instrument with finer resolution.

Detector

The choice of a proportional counter, over the more advanced solid state devices to detect X-rays, was based primarily on cost considerations. The proportional counter has potential problems including: breakage of the fine wire electrodes during launch, contamination or leakage of the active gas, electrode poisoning, and high voltage breakdown.

As is well known, the proportional counter detects each energetic electron which is ejected when an X-ray photon is absorbed, by drawing the secondary electrons it produces (at roughly 25 eV per secondary) toward a thin wire anode where the electric field is strong enough to produce a cascade [10]. The charge of that cascade, collected on the anode, is released when the resulting cascade ions subsequently migrate toward the cathode, and that produces a current pulse in the external circuit between the anode and cathode, which is proportional to the initial ejected electron energy. A heavy monatomic gas like Xenon is needed, for its large X-ray cross section and for its lack of disassociation or vibration as an alternative to electron ejection. Excepting the radioactive Krypton and Radon, there was little latitude in choosing the active gas for XRIS, since the next best candidate was Argon, with cross sections at the pertinent X-ray energies about an order of magnitude smaller. This yielded output pulses (controlled by the Xenon ion mobility) which were slower than desired and that established the maximum counting rate for the instrument.

Position Readout

A new technique was invented for XRIS, to solve the problem of electronically segmenting the proportional counter. A variety of other possibilities might have been used for this purpose, all with certain advantages and disadvantages. The simplest uses individual amplifiers for each anode, and an array of logic circuits to encode which amplifier received the pulse. Probably the most difficult to implement would have been that of using resistive anode wires and measuring the position along the anode by the different rise times of the pulses at its opposite ends; the difficulty being a need to work with thin carbon-filament anodes and a need for circuits with very precise timing. Perhaps the best-developed scheme is one in which the anode (and/or cathode) pulses are coupled to a delay line inside the chamber, and thereby become encoded by the delay of the pulses coming out the ends of that delay

line. Its only disadvantage for the XRIS was the need for placing the delay lines inside the chamber, where they would become potential sources of gas contaminants.

Instead of encoding with the pulse delay or rise time, as in the delay line and resistive wire techniques, the encoding in the XRIS was accomplished by dividing the total pulse current into two signals with a resistor array like that shown schematically in Figure 3. Each of the anodes was thus connected to two low-impedance rails inside the chamber (A and B), by a pair of resistors (R_1 and R_2), each having different values for each of the anodes. The resistance ratio then determined how the pulse currents were divided (into I_1 and I_2) between the two rails. The two signals were then added and subtracted outside the chamber, after being amplified and stretched by the preamplifiers. It is then possible to retrieve both the pulse amplitude ($\Sigma = A + B$) and a signal ($\Delta = A - B$) from which the pulse position can be determined, according to the relation:

$$\frac{\Delta}{\Sigma} = \frac{R_2 - R_1}{R_2 + R_1} \qquad (3)$$

This calculation was performed with logarithmic amplifiers, and the resistor values were adjusted (according to equation 3) so that the result would be proportional to the anode position. In other words, the two signals A and B brought out of the proportional counter indicated the pulse amplitude by their sum and the position by their ratio.

Resistors were easy to install and did not outgas like the wrapped delay lines. The analysis electronics turned out to be somewhat simpler than the fast-pulse timing that the delay lines required. A practical limitation of the scheme is imposed by the shunt resistance of all the resistor pairs, compared to the dynamic input impedance of the preamplifiers, since that tends to short together the A and B signals. Although a careful choice of resistors can always compensate for this effect, a practical constraint on the precision and matching of the preamplifiers is imposed when the number of anodes becomes large. In XRIS, however, where only sixteen pixels were involved, no difficulty was encountered, even using off-the-shelf integrated circuit preamps, and stock 1% resistors.

Broom Magnet

In order to protect against energetic electrons coming through the pinhole aperture, a broom magnet was installed on XRIS to sweep those electrons aside. A new magnet was designed for this purpose, having the distant field of a quadrupole in order to minimize interference with the host vehicle and the other SEEP instruments, as well as also having a means to tailor the local field for maximum effectiveness. The magnetic material, instead of being at the pole faces, was placed at the top, bottom and sides of the aperture in Figure 1, with all four elements in opposing directions. The pole faces, then, were made of soft magnetic material to direct the flux lines in opposite directions across the top and bottom halves of the pinhole slit. The electrons at both halves of the pinhole are thus both deflected toward the center of the instrument and behind an aluminum brace which serves simultaneously to cover the null point of the magnetic field and to hold the magnets in place. Behind this brace is an electron trap made of plastic coated tantalum, which consisted of progressively smaller plates mounted on a central spine, with each one shadowing the detector from the electron impact area left uncovered by its predecessor.

Shielding

For shielding against extraneous electrons, a mass of dense material is required, having the highest possible atomic number, since that gives higher X-ray absorption cross sections. Excluding radioactive materials like uranium and expensive materials like gold and platinum, lead and tantalum are best choices, with the latter being structurally superior. The shielding of XRIS was of tantalum, with about 2 gm/cm^2 of material in all directions. This mass thickness for the shielding was decided upon by equating the background expected from electrons through the pinhole to that for the same electrons striking the external surfaces, using our best estimate for the spectrum of precipitating magnetospheric electrons. With this criterion, the instrument dimensions were scaled to match the imposed weight restrictions. The result was an instrument with about one third of its weight devoted to shielding. The shielding thickness derived from this exercise was sufficient for a 1/e attenuation at all photon energies below 100 keV, and an attenuation factor of better than 10^{-8} below about 15 keV. For such a large shielding factor at the lower energies, it was essential to plug even tiny gaps in the shielding.

The shielding is most effective, of course, for lower X-ray energies, and this dictated using a material on the surface, outside the tantalum, with a low atomic number, since that reduces the yield at high energies. A special plastic was chosen, with no heavy constituents, and applied over the tantalum in layers, to a thickness of about one millimeter.

Window

Considerable effort was devoted to finding a better window material before it was concluded that only beryllium would be sufficiently leak tight and transparent to X-rays for a closed-gas system. The next best candidate, incidentally, was cross-grain multilayer plastic, of the sort used for potato chip packaging. The window was made thicker than it might have been, according to the stress calculations, and its 0.76 mm thickness established the 4 keV low energy threshold of XRIS.

PERFORMANCE

After about one month of operation, the useful life of XRIS was terminated by an electronic failure leaving an instrument which could only measure a peculiar combination of lateral position and X-ray energy. However, during its month of life, XRIS produced some three thousand excellent X-ray images of five minutes duration (each covering about 2400 x 500 km), totaling about 250 hours of useful observations. With its great sensitivity, XRIS detected auroral X-rays on virtually all of its auroral zone crossings, four times every orbit. It has already revealed multiple arcs, pulsations, the poleward expansion of the aurora during magnetospheric substorms, and isolated polar spikes of X-rays, which turned out to be quite localized spots rather than arcs. It has also provided valuable information on the Earth's Albedo for X-rays between 4 and 40 keV, during a dozen or so dayside passes during intense solar X-ray flares.

The auroral observations of XRIS will be reported separately and only one example (Figure 4) will be presented here. To form such images, all the energy channels for each pixel were summed and plotted as a vertical line with a varying color value or shading, using a color Rantek display unit. Adjacent lines in these images correspond to adjacent eighth second measurements. Because of the low altitude, it was not necessary to correct for earth curvature, since it introduces at most a 20 km distortion at the edge of

the scene. The spatial displacement of the measurement (about 200 km in front of the satellite) is often significant, but it has not been applied to this figure.

The darkest shading in Figure 3 corresponds to a flux density of about 10^3 cm^{-2} sr^{-1} sec^{-1}, varying down to about 10 or less. In order to compensate for the slant transmission of the beryllium window and the otherwise varying efficiencies of the different pixels, it was necessary to apply an empirical correction separately for each pixel. This was accomplished by starting with the theoretical slant transmission of the window and adjusting the individual correction factors until the most uniform images were obtained under a variety of circumstances. Although this produces the most pleasing images, the correction is energy dependent, and this can introduce perceptable distortions, depending on the X-ray spectrum. This correction, also being applied to the background signals, produces a center-peaked enhancement for the interferring signals and that has proven useful in distinguishing them from real X-ray patterns.

Figure 4 shows a multiple-arc aurora in the southern hemisphere with respect to the geographic and magnetic south poles shown respectively by the small cross and circle. It shows an increase of about 30:1 between dawn and midnight, and a width of about 100 km. This aurora pertains to moderately quiet times and it is typical of those seen by XRIS, except for it being one of the rare cases when the satellite track followed the auroral form for a very long time. In most of the data the orbit cuts more obliquely across the polar cap and yields only two brief intercepts of the aurora.

SUMMARY

The XRIS instrument has been described, with an emphasis on the rationale behind its design. It was shown that the simple pinhole camera was chosen over a coded aperture, principally because the coded aperture gives only a marginal advantage whenever the scene is more or less filled with sources. The choice of a one dimensional configuration was dictated by the need to explore certain time scales, and it was shown why this choice did not affect the overall image quality. A criterion was presented, based on the count-limited signal to noise ratio, for selecting the spatial resolution of such instruments, and it was shown why combining adjacent pixels is not equivalent to choosing a different resolution.

Two unique features of the instrument were described, those being the detector readout scheme and the broom magnet design. The readout scheme, for determining the position of photon events in a proportional counter, involves dividing the pulse between two signals, such that the sum yeilds the original pulse amplitude and the difference indicates the position. The advantage of this technique is that it minimizes the number of signals which must be brought out of the detector and it requires only simple analog electronics to retrieve both amplitude and position. The broom magnet was a quadrupole to minimize external interference, with the pole faces made of soft iron so the field could be easily optimized.

Other aspects of the design, which were less unique but no less important to its success, included the need for gas purity (which was accomplished with a selective getter), the choice of window material, and the design of shielding. The last consisted of tantalum coated with a special plastic providing both a low X-ray yield from energetic electrons and the correct absorption and radiation properties for thermal control.

The instrument functioned for over one month, without measurable degradation, before an electronic failure caused a loss of position information. XRIS produced several thousand auroral images of unique sensitivity and temporal resolution.

ACKNOWLEDGMENTS

This project was supported by the Office of Naval Research (Contract N00014-79-C-0824). Launch and orbital support were provided by the Air Force Space Test Program Office. Heartfelt thanks are due Dr. Johan Stadsnes, who was then visiting Lockheed from Bergen, Norway and generously gave us the benefit of his considerable experience with similar instruments. Special thanks are also due Mr. Art Knapp who was crucial in the fabrication of the proportional counter. Thanks are also extended to Professor Victor Perez-Mendez for much helpful advice and for allowing us to use his machine for wrapping the wire frames. The project was managed by J. B. Reagan, D. P. Cauffman, and W. L. Imhof, to whom thanks are extended. Appreciation is also given to the following Lockheed engineers; J. C. Bakke, J. P. Harrison, S. V. Roger, S. Battel, R. Bostedt, and L. Pagendarm.

REFERENCES

1. W. L. Imhof, J. R. Kilner, G. H. Nakano, and J. B. Reagan, J. Geophys Res., 85, 3347 (1980).

2. J. R. Barcus, R. A. Goldberg, and L. H. Gesell, J. Atmos. Terr. Phys., 43, 1003 (1981).

3. B. H. Mauk, J. Chin, and G. Parks, J. Geophys. Res., 86, 6827 (1981).

4. L. E. Peterson, Annual Review of Astronomy and Astrophysics, 13, 423 (1975).

5. P. F. Mizera, J. G. Luhmann, W. A. Kolasinski, and J. B. Blake, J. Geophys. Res., 83, 5573 (1978).

6. P. F. Mizera, D. J. Gorney, and J. L. Roeder, EOS, 64, 793 (1983).

7. H. D. Voss, J. B. Reagan, W. L. Imhof, D. O. Murray, D. A. Simpson, D. P. Cauffman, and J. C. Bakke, IEEE Tran. Nuc. Sci NS-29, 164 (1982).

8. W. L. Imhof, J. B. Reagan, H. D. Voss, E. E. Gaines, D. W. Datlowe, J. Mobilia, R. A. Helliwell, U. S. Inan, J. Katsufrakis, and R. G. Joiner, Geophys. Res. Lett., 10, 8, 615 (1983).

9. L. Mertz, and N. O. Young, Proc. Intl. Conf. Optical Instrumentation, 305, Chapman and Hall, London (1961).

10. F. Sauli, Principles of Operation of Multiwire Proportional and Drift Chambers, CERN Lectures 1975-76, CERN 77-09 (3 May 1977).

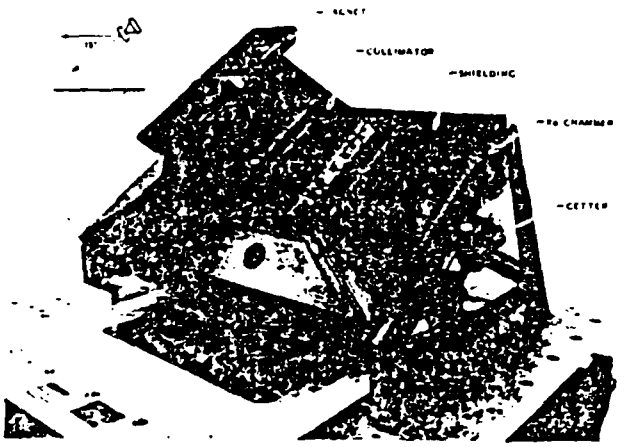

Figure 1. The XRIS X-ray imaging spectrometer flown on SEEP, with an inset showing how it was mounted looking forward and down to accumulate an X-ray image as the satellite overflew the scene.

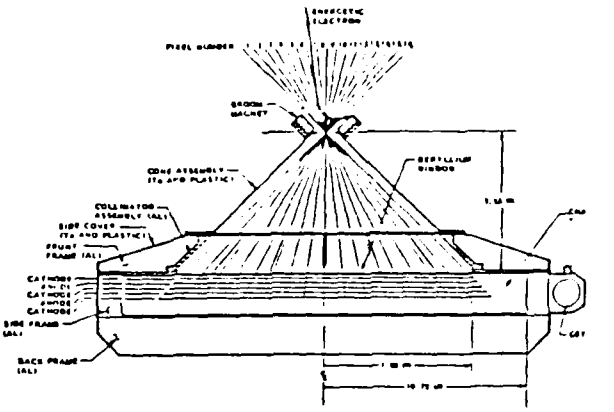

Figure 2. A schematic plan view of XRIS, showing the sixteen cross-track pixels of the position-sensitive proportional counter at the rear of the instrument. Not shown are the multiple collimator plates parallel to the plane of this figure which define the vertical width of the pixels.

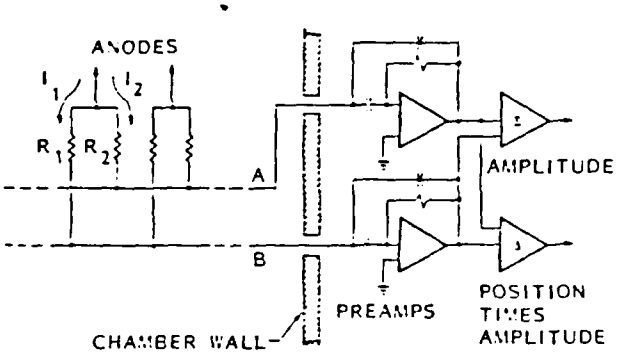

Figure 3. The readout scheme used in XRIS to determine the pulse amplitude and position with only two feedthrus for each detector plane. The pulse currents were divided by the resistor pairs R_1 and R_2 into I_+ and I_-, so that their sum and difference could be used to electronically calculate both parameters.

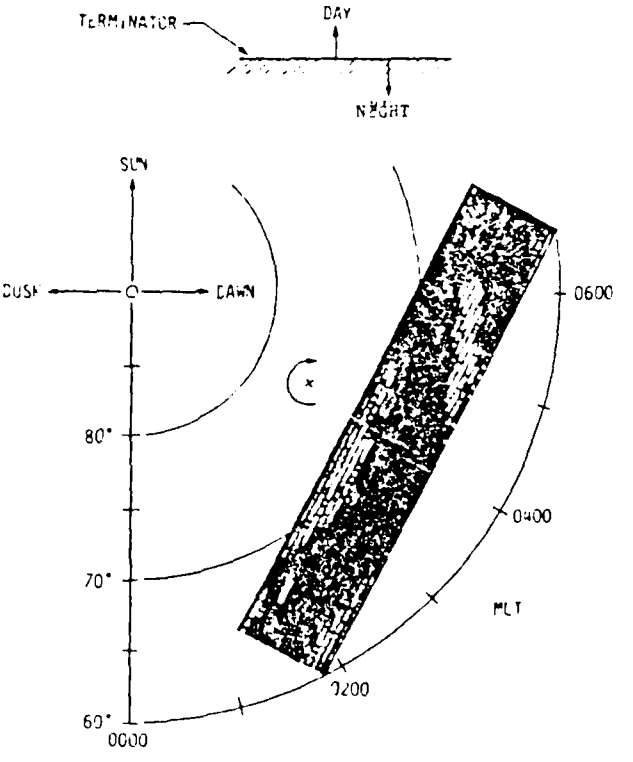

Figure 4. An XRIS image of the aurora.

IEEE Transactions on Nuclear Science, Vol. NS-32, No. 1, February 1985

THE GROUND SUPPORT COMPUTER AND IN-ORBIT SURVEY DATA ANALYSIS PROGRAM FOR THE SEEP EXPERIMENT

H. D. Voss, J. Mobilia, D. W. Datlowe, and S. N. Roselle

Lockheed Palo Alto Research Laboratory
3251 Hanover St., Building 255
Palo Alto, California 94304

ABSTRACT

The ground support computer equipment (GSE) and production survey plot and analysis software are described for the Stimulated Emissions of Energetic Particles (SEEP) experiment on the S81-1 satellite. A general purpose satellite data acquisition circuit was developed based on a Z-80 portable microcomputer. By simply changing instrument control software and electrical connectors, automatic testing and control of the various SEEP instruments was accomplished. A new feature incorporated into the SEEP data analysis phase was the development of a correlative data base for all of the SEEP instruments. A CPU efficient survey plot program (with ephemeris) was developed to display the approximate 3100 hours of data, with a time resolution of 0.5 sec, from the ten instrument sensors. The details of the general purpose multigraph algorithms and plot formats are presented. For the first time new associations are being investigated of simultaneous particle, X-ray, optical and plasma density satellite measurements.

INTRODUCTION

From May to December 1982, the Stimulated Emissions of Energetic Particles (SEEP) payload was operated on board the S81-1 satellite. The primary objective of the SEEP payload was to measure the effects of VLF transmitter induced precipitation of energetic particles [1]. With recent computer processing and technology advances many new and cost effective techniques were available for use in the SEEP program. In particular, the pre-launch Ground Support computer Equipment (GSE) and the in-orbit Production Survey (PS) data analyis software, are described here. The SEEP payload consisted of an array of energetic particle spectrometers (E > 2 keV), an airglow photometer, a Langmuir probe, and an imaging X-ray spectrometer (XRIS).

During the pre-launch phases a portable microcomputer (Heath H-89) was used as the ground support computer. Interface circuitry was designed to allow automatic testing and control of the various SEEP instruments (excluding the X-ray spectrometer) by simply changing computer software and an electrical connector.

In the SEEP data analysis phase a correlative data base was developed for all of the instruments. This allowed new associations to be investigated between the unique instrumentation on SEEP. Some of the significant results of the correlative data base, to date, have included the association of plasma waves (Travelling Ionospheric Disturbance) with the efficient precipitation of energetic electrons by VLF transmitters [2, 3], the first one-to-one correlation of lightning-induced electron precipitation events [4] and the first coordinated X-ray, airglow and energetic particle measurements of numerous auroral features. Examples and computer algorithms of the general purpose multigraph plots are presented.

PORTABLE COMPUTER GSE

The ground support computer equipment consisted of a portable 8-bit microcomputer system (Heath H-89 purchased in 1979) that was supplemented with the Satellite Acquisition and Command (SAC) interface. A system diagram of the portable GSE is illustrated in Figure 1. Specialized software was written for each instrument to control the general purpose and programmable SAC interface.

Hardware

The general purpose H-89 portable computer was configured with 64k of dynamic RAM, an 80 X 24 character CRT, two 100 Kbyte 5 1/4" floppy disk drives, and a three port serial I/O board. All components including the SAC interface were enclosed in the H-89 cabinet (Figure 2). The portability of the general purpose GSE system allowed for ease of movement to various testing sites. The fact that full documentation and schematics came with the microcomputer was a major advantage in the design of the custom SAC interface.

The GSE allowed for both real-time displays and data storage on floppy disk. Display devices included a CRT, a dot-matrix printer, an oscilliscope, and a chart recorder. Off-the-shelf communications software converted the H-89 to an intelligent terminal so that stored data could be transfered either by direct serial line (9600 Baud) or MODEM (1200 Baud) to a VAX 780 computer.

The SAC interface system block diagram is shown in Figure 3. It consisted of one 15 x 22 cm wire wrapped plug-in board. Although the SAC interface board plugged into the master board within the H-89, several major signals were additionally jumpered directly from the Z-80 8-bit processor, as needed, for efficient SAC operation. The multi-purpose SAC I/O board included the following features:

- 24 parallel output lines
- 16 parallel input lines
- 24-bit serial input port
- 4 ea 8-bit DACs
- 2 ea 12-bit DACs
- 1 ea 8-input analog data acquisition system (MN 7100)

Since the SEEP instruments and portable GSE operated on 5 volts the low power SAC board (CMOS and LS circuits) was powered by the H-89. Multiple 8-bit transparent latches (4508) provided parallel output directly off of the Z-80 primary data bus. Multiple 8-bit tri-state latches (LS 373) were used for strobing instrument data input onto the bus. Datel 8-bit (DAC-08BP) and Beckman 12-bit (872) DACs were used for analog output while a hybrid analog data acquisition system (MN 7100) provided 8 analog input signals to a 2 usec sample-and-hold and 8 bit ADC. A pair of 1-of-16 line decoders (LS154) provided up to 16 write and 16 read internal control strobes including fast strobes for external use. The decoder and

0018-9499/85/0002-0168$01.00 1985 IEEE

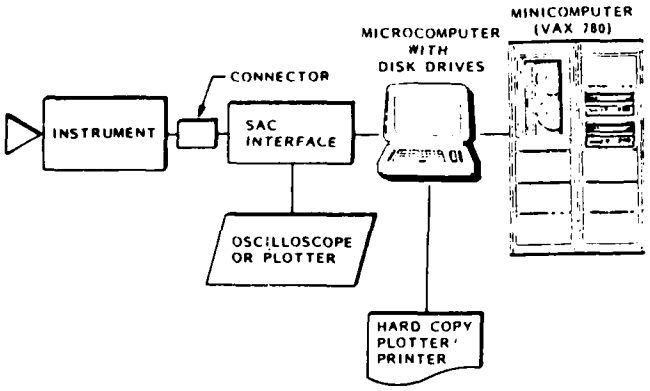

Figure 1. Schematic of GSE system with interface to VAX 780 computer

thus the entire I/O board was accessed directly by I/O addressing of the Z-80 microprocesser below port 120. Recently, most of the components included on the SAC interface have been integrated onto a single microchip gate array, including analog and digital functions.

Five independent instrument systems on the payload were tested, one at a time by changing software and replacing a patch cable (a 50 pin IDC connector on one end that was crosswired to an instrument specific D type connector). The instrument's unique patch connector was required because of the nonstandard telemetry and command signals.

Software and Display Formats

The software for the H-89 control of the SAC interface was written in Microsoft BASIC and assembly code. Languages other than BASIC would have been better suited technically (i.e. C, Turbo Pascal, Forth), however, BASIC availability, familiarity at the time, simplicity and adequacy for doing the job made it a logical choice. Z-80 machine language modules were called from BASIC in cases where speed and efficiency were essential (such as serial clocking of telemetry and I/O transfers). Various display formats were readily programmed for output to one of the display devices. For example, a pulse-height spectrum could be routed to either the video screen or line printer. Furthermore, the DAC output feature allowed the use of an oscilloscope or chart recorder for PHA spectrum displays. This was accomplished by a simple machine code program that transferred a block of data from RAM to the DAC repetitively. Spectra could be displayed in real time with the desired regions expanded as needed by simply changing the oscilloscope scale (Figure 4).

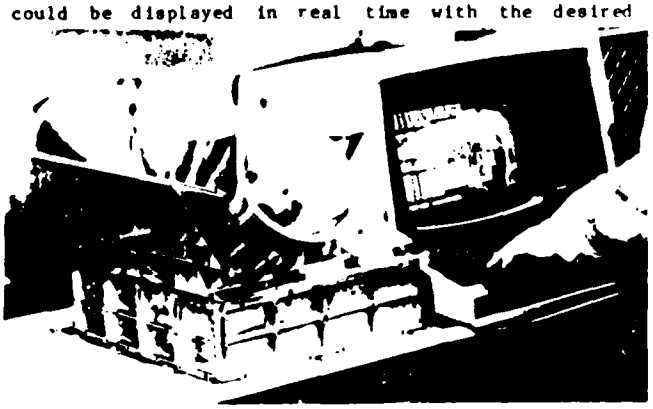

Figure 2. Photograph of the SEEP experiment GSE testing the energetic electron particle spectrometer array

PCM Interface

The SAC interface also allowed for a quick look at all of the SEEP instruments during payload level testing. The GSE was hooked up directly to pulse-code modulation (PCM) decommutation equipment during system checkout. The SEEP payload had a 32K bit telemetry rate. However, play-back from analog magnetic tapes could be at other speeds. The H-89 was programmed in assembly code to sync up to the frame counter in the data stream and strip off any data pertinent to specific instruments. The data were then displayed in various formats. A typical screen of demultiplexed analog and bilevel PCM data for all of the SEEP instruments is displayed in Figure 5.

SEEP PRODUCTION SURVEY PLOTS

Following the successful development and calibration of the SEEP instruments, the S81-1 satellite was launched into a low altitude polar orbit. The payload provided high quality data during the lifetime of the mission.

Approximately 3100 hours of data were acquired by the on-board tape recorders and downlinked to earth stations. The SEEP data were provided in the form of PCM analog tapes. Decommutation on a VAX 750 computer of all the SEEP data resulted in 2100 digital tapes (1600 bpi). Following decommutation a digital survey

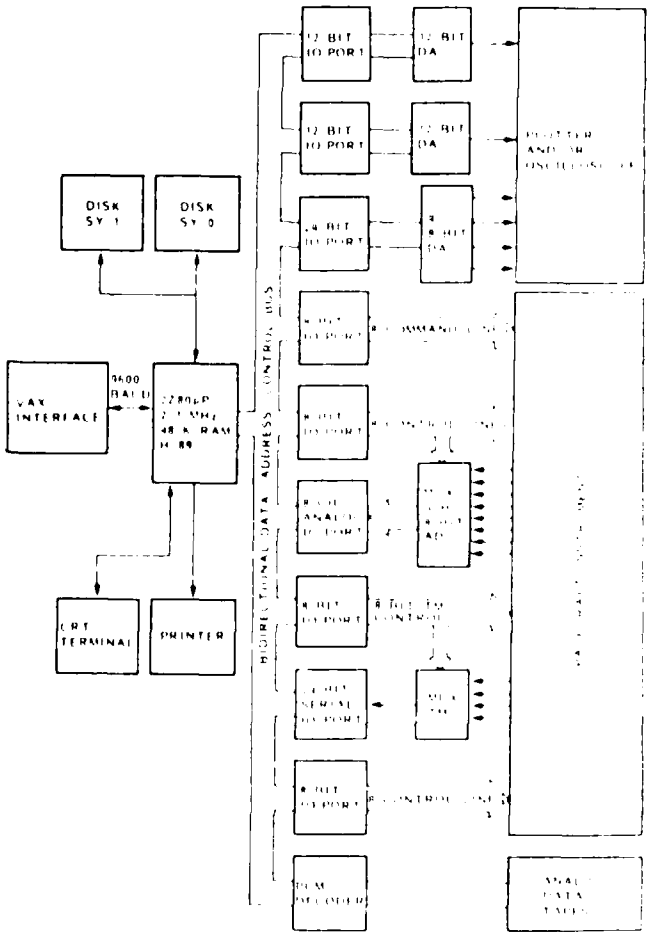

Figure 3. H-89 system and satellite acquisition and control (SAC) interface board.

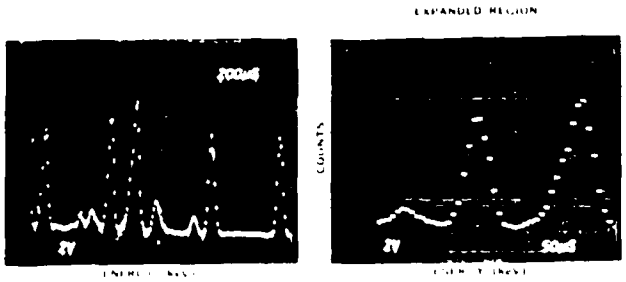

Figure 4. SAC oscilloscope display of Am-241 spectra

tape was made. The survey tape included time averaging and key data selection of the SEEP satellite 32K bit data stream. Ephemeris and magnetic field data were also included. The data compression produced 370 survey tapes. Each record on the survey tape contained a header (ephemeris and bookkeeping information), eight seconds worth of scaler information for all instruments, and pulse-height information for all applicable instruments over eight seconds. The software to process the survey tape data was written in Fortran 77 with assembly language (Macro) utility modules for I/O processing. Figure 6 illustrates the various plot formats which could be generated by the production survey analysis software.

Figure 5. Photograph of the PCM analogs and bilevels during payload testing taken from CRT screen.

SEEP Survey Plot Program

The production survey analysis software algorithm is given in Figure 7. The plotting modules were written on a VAX 780 computer using a device and machine independent plot package, DI3000, from Precision Visuals, Inc. DI3000 allowed the use of several different graphic devices including a Versatec printer/plotter, AED color terminal, Tektronics 4025 terminal, and a VT 100 Retrographics terminal. These were utilized by simply changing the device number called in the code. This freedom was useful in the software development stage and for special processing. Each survey tape was processed on a VAX 780 computer with a Versatec plotter (V-80F) to produce the Production Survey (PS) plots. The software stripped off the pertinent instrument parameters and stored them in a three dimensional array. The array dimensions were 34 by 60 by 16, where 34 was the number of sensor parameters plotted, 60 the number of tape records per plot page, and 16 was the number of sensor parameter points per record. The order of accessing the array was important for efficient processing. Sixty records, therefore, gave 960 points per page which was commensurate with the resolution of the plotter (200 points per inch or 1900 points per page). Originally the number was choosen to be compatible with a Versatec model 1100 which had a resolution of 100 points per inch. The higher resolution Versatec plotter allowed for better readablity while still utilizing the plotter's capablity. By simply making changes in the software input parameter file or by calling different plotting routines the production data analysis program would produce several different formats (i.e. Figure 6). Only approximately 70 manhours were necessary to produce the production plot software using Fortran on a VAX 780 computer.

Placing all of the key instrument parameters on a single plot with the same time scale allows one to acquire a correlative data set of particle, X-ray, plasma, and airglow measurements. Advantages gained from this include the speed of surveying, finding cause-and-effect interrelationships, and developing a low cost production archive. Because plasma interactions in the magnetosphere and ionosphere affect the atmosphere it is difficult to piece together interelationships unless both in situ and remote sensors are capable of simultaneously measuring multiple geophysical parameters in the near earth-space environment. Each satellite mission adds pieces but many times, because of incomplete satellite instrumentation or the difficulty of many investigators to comprehensively intercompare their instrument data, valuable information is lost. In the SEEP mission the instrument scientists were fortunately located in the same laboratory and were able to resolve this basic problem.

Survey Multigraph Plots

The multigraph production survey format of Figure 8 was chosen for quick look plots. This standard plot format consisted of ten graphs for displaying each of the ten SEEP sensors. The various energy thresholds for the particle and X-ray spectrometers, wavelengths for the airglow photometer, and current for the plasma probe were plotted within the designated graph. By changing an input file the sensor graph positions could be readily changed or replaced or certain sensor channels could be designated for smoothing (i.e. low count rate channels).

Besides plotting instrument data, ephemeris information was included: Time (UT), Latitude (LAT), Longitude (LONG), L shell (LSH), Altitude/Conjugate Altitude (ALTC), and the calculated pitch angle for detectors pointing at 0^{o}, 10^{o}, 50^{o} and 90^{o} from zenith (1059). Status and bookkeeping information were listed on the bottom of the plot. Time ticks were

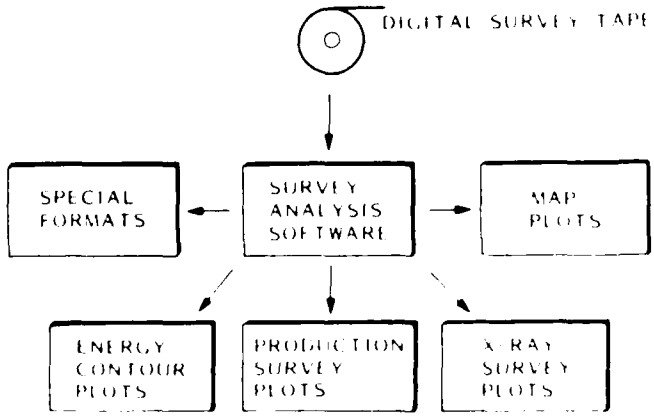

Figure 6. Five black and white plot formats were used for the SEEP experiment survey.

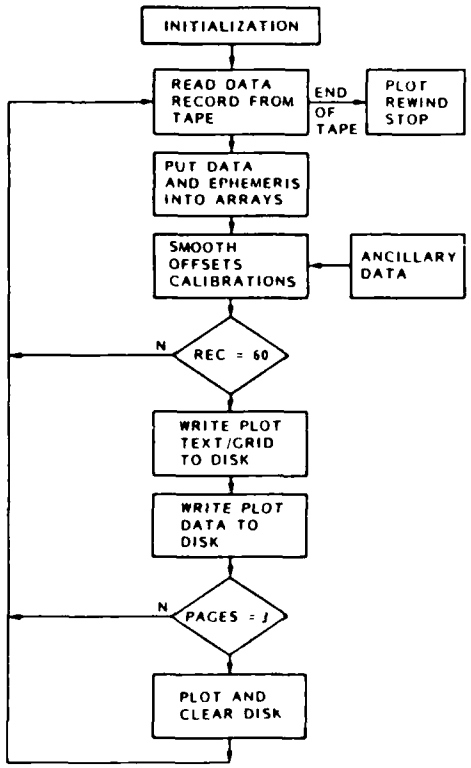

Figure 7. Algorithm of SEEP survey plot software

placed every frame (8 seconds) while ephemeris information was plotted every 32 seconds. All of the vertical scales were logarithmic with each tic mark indicating a decade.

The graphs in Figure 8 start with 1 at the top and 10 at the bottom. Graph 1 shows the four airglow photometer (AP) channel intensities. The SEEP photometer measured emission lines at 630.0 nm and 391.4 nm. There were two filter bandwidths of 391.4 nm (0.8 nm and 2.4 nm) and also a background channel. The data of Figure 8 were at a relatively quiet time period except for a few scattered spikes which in this case were associated with weak lightning flashes. The measurement of optical lightning flashes and energetic electron precipitation had not been observed until it was correlated by use of these plots [4]. Graph 2 shows the Langmuir probe (APP) current. The 200 km long plasma oscillations observed near 8611 seconds are identified as a Travelling Ionospheric Disturbance (TID). Also observed with the current probe were transient drop outs with slow recovery times (~ 3 sec) in the vicinity of thunderstorms. These were identified with an electric field induced current associated with the lightning discharge. The relationships between TIDs, plasma irregularities, electric field spikes, and particle precipitation were some of the most intriguing finds, to date, based on the survey plots.

The X-ray imaging spectrometer (XS) count rates were placed in Graph 3. For the period under consideration in Figure 8 the X-ray flux was below threshold for latitudes less than 46°. In the auroral zone encountered at latitudes greater than 46°, both weak bremsstrahlung X-rays and particle background contamination were observed. Bremsstrahlung X-ray detection is important as a remote sensing technique of energetic electron precipitation and is helpful in determining energy disposition into the ionosphere.

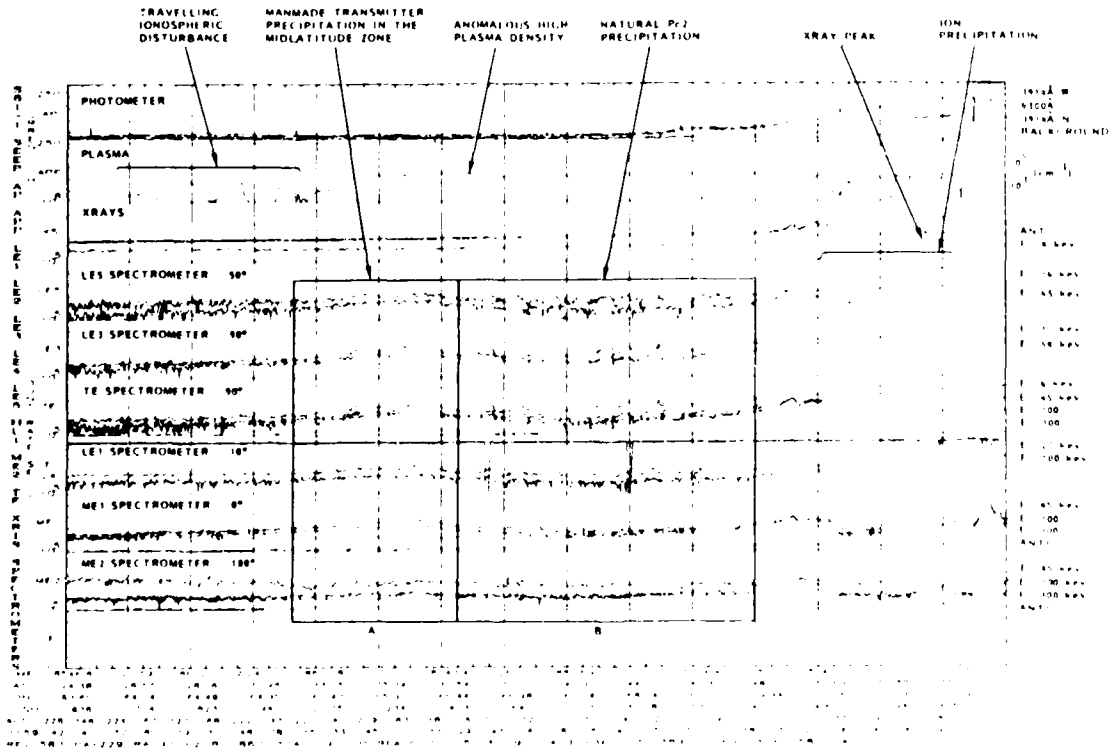

Figure 8. Production survey plot for 17 August 1982 showing 9 instrument sensors.

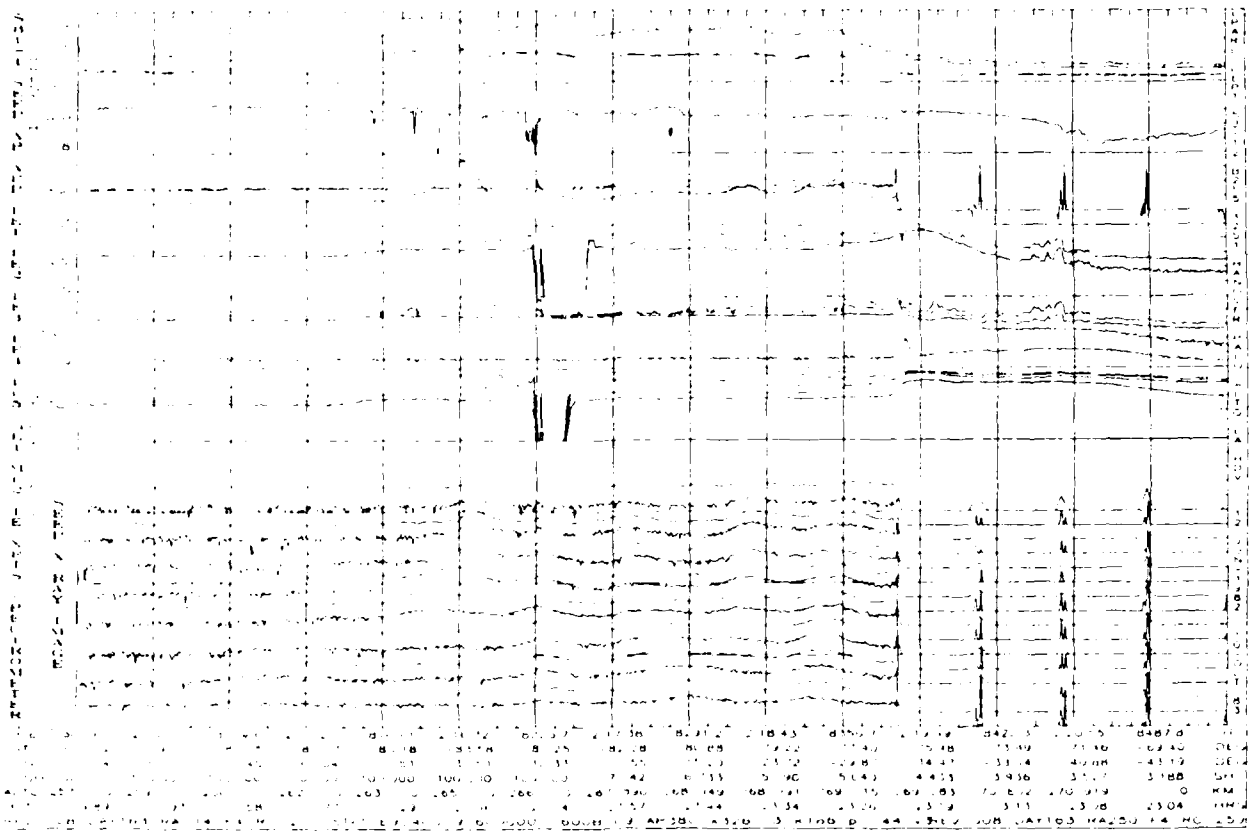

Figure 9. Sample of X-ray imager survey plot which shows multiple arcs in the auroral region. The XRIS high voltage was off after 02:19 UT.

Graphs 4 - 9 contain the array of energetic particle spectrometers; LE is for low energy particles, TE for trapped energetic particles, and ME for medium energy particles. These are at fixed angles on the 3-axis stablized satellite as indicated. The TE spectrometer has four integral energy thresholds plotted in Graph 6 with the highest energy (E > 300 keV) smoothed. The threshold plots on Graph 4-9 are unique because they are integral counts and thus do not cross one another. In Graph 10 various non-standard sensor thresholds are normally plotted.

In the boxed region A the first direct observations of particle precipitaion caused by a VLF transmitter [1] are displayed. The Navy transmitter at Cutler, Maine (NAA) was modulated with a 5 second period in a predetermined pattern during this overpass of the SEEP satellite. In box B, the natural oscillations in the measured particle population (called Pc2 precipitation) are observed. As can be seen, the amount of information and fine structure observed in 480 seconds in Figure 8 is considerable. The ability to quickly survey such interrelated events for reoccuring phenomena is of fundamental importance.

All of the 370 digital survey tapes were run through the production survey plot program, creating a complete data base for the 3100 hours of the SEEP mission. This resulted in 44 notebook binders which contained hardcopy Versatec survey plots, each 8 1/2 x 11 inches. Because of the complexity of the data acquisition and limited temporary storage capability, the data were not chronologically ordered. To overcome this a list containing the time interval data coverage along with the corresponding tape was generated.

X-Ray Image Survey Plot

The flexibility in the software (Figure 6) allowed for the easy changing of formats without extensive new coding. To study the X-ray imager data all pertinent tapes (i.e. ~ 1 month period of X-ray imaging data) were processed by a slightly different version of PS software. Some particle spectrometer information was replaced by the 16 individual position channels of the XRIS while the remaining information was rearranged by simply changing the input file parameters (Figure 9). The resulting effect is a

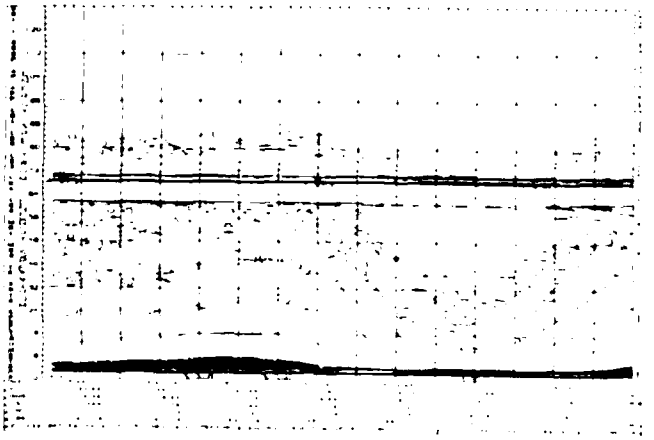

Figure 10. Example of an energy spectrogram survey plot. The equatorial ion zone minimum is at the 11p equator (14 July 1982).

3-dimensional perspective plot. In the auroral feature displayed multiple structure is present. This format is very useful to investigations of auroral features, such as arcs and patches, that are found at high latitudes. The comparison of the X-ray image with the associated particle information is a very important new feature. The ephemeris information was altered by replacing pitch angle with the Magnetic Local Time (MLT).

Spectrogram Survey Plots

A third format of the production survey plot program is shown in Figure 10. The equatorial ion precipitation zone [5] is depicted in terms of an energy-time contour plot near the dip equator (10:04:01 UT). Energy channels 0-64 on the y-axis represent the TE particle spectrometer while channels 65-120 represent the ME particle spectrometer.

Orbit and Map Survey Plots

To locate where data were acquired another plot option was implemented. It included program modules that called a modified version of the NCAR Supmap subroutine. Figure 11 shows the SEEP payload ground trace superimposed on a cylindrical equidistant earth projection. The enclosed shapes on this plot represent transformed circles around selected coordinates. The associated equation for the circle in cylindrical equidistant coordinates was arrived at by finding the intersection of a plane with a circle and solving the resulting second order equation. These circles represent the regions on the earth where the SEEP payload was commanded to record data. The orbit trace was acquired from the header records on the survey tape. Another variation of this program allowed data to be plotted along the orbit. Figure 12 illustrates an expanded view over North America of AP data that were acquired along the orbit path. The wideband 391.4 nm airglow photometer emission line is displayed during the 14 July 1982 magnetic storm and indicates the strong energetic particle precipitation at mid and low latitudes. Other map projections could be readily called (i.e. orthographic, Lambert, stereographic, etc.).

Special Formats

Besides the four standard formats, special formats were also developed. Color plot formats were designed showing energy versus time with color

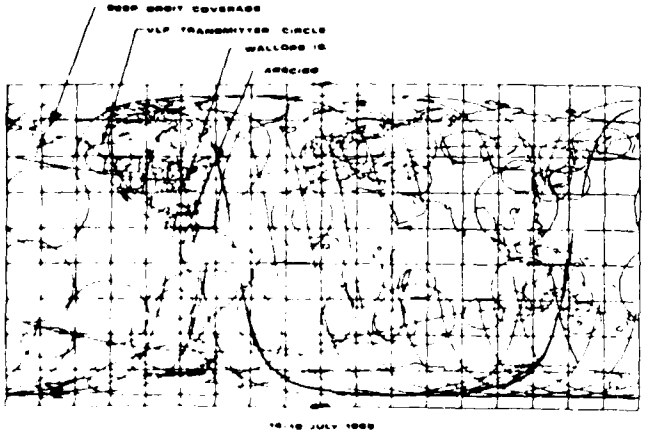

Figure 11. SEEP orbital tracks are plotted on a cylindrical equidistant projection of he earth.

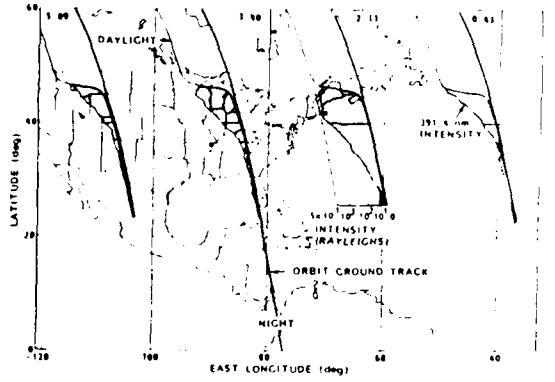

Figure 12. Expanded plot of SEEP payload orbital tracks with 391.4 nm photometer data plotted along the path. The transition at 43° occurs at the terminator.

indicating the intensity (spectrograms). An X-ray image format was developed to show the aurora superimposed on a polar map [6].

SUMMARY

With modern advances in technology and computer design, space instrument testing was greatly simplified with improved performance. The general purpose SAC interface could be adapted to many other control applications. The compactness of this system allows for flexibilty and portability. Recently, a completed SAC interface board, combining analog and digital I/O was developed on a single chip microcircuit for both flight and ground based applications. The production survey plot software design for the SEEP instruments also allowed for flexibility. The cost of the software development (~ 70 manhours) produced a comprehensive correlative data base. The development of a correlative data base covering the entire six month SEEP mission provided a basis for many new and correlated observations.

ACKNOWLEDGEMENTS

This work was sponsored by the Office of Naval Research through contract N00014-79-C-0824. A portion of the data analysis was supported by the Lockheed Independent Research Program. The authors would like to thank the following who consulted in various phases of the program: Drs. W. L. Imhof, D. P. Cauffman, J. B. Reagan, and Mr. E. E. Gaines.

REFERENCES

1. W. L. Imhof, J. B. Reagan, H. D. Voss, E. E. Gaines, D. W. Datlowe, J. Mobilia, R. A. Helliwell, U. S. Inan, J. Katsufrakis, and R. G. Joiner, Geophys. Res. Lett., 10, 361 (1983).
2. J. Mobilia, H. D. Voss, W. L. Imhof, J. B. Reagan, and K. L. Miller, EOS, Trans. Am. Geophys. Union, 64, 289 (1983).
3. H. D. Voss, W. L. Imhof, J. B. Reagan, K. L. Miller, and J. Mobilia , EOS, Trans. Am. Geophys. Union, 65, 267 (1984).
4. H. D. Voss, W. L. Imhof, M. Walt, J. Mobilia, E. E. Gaines, J. B. Reagan, U. S. Inan, R. A. Helliwell, D. L. Carpenter, J. P. Katsufrakis, and H. C. Chang, NATURE, in press (1984).
5. H. D. Voss, W. L. Imhof, J. Mobilia, E. E. Gaines, and J. B. Reagan, COSPAR XXV, July (1984).
6. H. D. Voss, W. L. Imhof, J. B. Reagan, R. R. Vondrak, M. Walt, J. Mobilia, D. W. Datlowe, D. P. Cauffman, W. Calvert, R. G. Joiner, EOS, Trans. Am. Geophys. Union, 64, 953, (EOS Cover) and 792 (1983).

. Vol.5, No.4, pp.175-178, 1985
Printed in Great Britain. All rights reserved.

0273-1177/85 $0.00 + .50
Copyright © COSPAR

ENERGETIC PARTICLES IN THE NIGHT-TIME MIDDLE- AND LOW-LATITUDE IONOSPHERE

H. D. Voss, W. L. Imhof, J. Mobilia,
E. E. Gaines and J. B. Reagan

Lockheed Palo Alto Research Laboratory, 3251 Hanover Street, Palo Alto, CA 94304, U.S.A.

ABSTRACT

Data are presented on the zones of energetic particle precipitation at middle and low latitudes observed during and after magnetic storm injection events. Satellite measurements of the equatorial zone ion flux ($\sim 10^3 - 10^4$ cm^{-2} s^{-1} sr^{-1} for E > 45 keV at 240 km) are consistent with the development of a temporary low altitude ion radiation belt at the magnetic equator. In the midlatitude ion zone the flux ($\sim 10^3 - 10^5$ ions cm^{-2} s^{-1} sr^{-1} for E > 45 keV at 220 km) is directly related to magnetic activity while the midlatitude electron zone flux has a delayed response ($\sim$ 4 days).

INTRODUCTION

Paucity of data has so far prevented the accurate and comprehensive global mapping of precipitating energetic electrons and ions at middle and low latitudes (L $\lesssim$ 3). However, it is known that the particle intensities during and immediately following magnetic storms are sufficient to cause primary nighttime ionization and significantly modify radiowave propagation in the earth's ionospheric waveguide /1/. Additionally, these precipitating particles provide an important boundary condition for modeling the decay rates associated with the earth's ring current and radiation belt.

Previously Voss and Smith /1/ have made an effort to resolve the many seemingly contradictory low and midlatitude electron and ion flux measurements using available data from rocket, satellite and ground based experiments. Based on this preliminary study various global zones of precipitating energetic particles were identified: the midlatitude electron zone, the midlatitude ion zone, the low latitude zone and the equatorial zone. The review article contains an extensive list of references to subauroral particle precipitation. Here we present some new satellite results on the spatial and temporal characteristics of the midlatitude ion and electron zones (2 < L < 3) and the equatorial zone ($\pm$ 20° geomagnetic latitude).

INSTRUMENTATION

From May to December 1982, the Stimulated Emission of Energetic Particles (SEEP) payload on the S81-1 satellite made high sensitivity measurements of precipitating energetic electron and ion fluxes. The S81-1 satellite was a low altitude (lower F-Region), three axis stabilized vehicle in a polar orbit. The payload instrumentation included a fine energy resolution (1 keV FWHM) and high sensitivity cooled solid state spectrometer array, a 16 pixel wide x-ray imaging proportional counter, a quadrant photometer and a plasma density probe. The Trapped Energy (TE) spectrometer ($\pm$20° field of view) was aligned perpendicular to the orbit plane and had a geometrical factor of 0.17 cm^2 sr. It was sensitive to both electrons and ions. The medium energy (ME) precipitating electron spectrometer ($\pm$ 30° field of view) was aligned to the zenith direction and had a geometrical factor of 2.4 cm^2 sr. A thick window on ME prevented ions with E < 550 keV from impinging on the solid state sensor.

RESULTS AND DISCUSSION

In Figure 1 a latitude profile is shown of the TE particle spectrometer flux for 00:06 - 00:18 and 03:11 - 03:19 UT on 15 July 1982. Two second averages are plotted. The time periods were selected because they occurred well into the recovery phase of the strong magnetic storm ($D_{st} \simeq -325$) of 13 July 1982 and a coordinated rocket launch was made with a University of Illinois, Nike-Orion rocket 31015, near L = 2.5. To present fluxes over the full latitute range it was necessary to use data acquired on two different satellite passes. The overlap at low latitudes is shown and illustrates the temporal and spatial stability of the equatorial zone on opposite sides of the South Atlantic anomaly. The conjugate altitudes of locations in the geomagnetic north are significantly lower in the south; therefore, the observed particles in the north are precipitating in the bounce loss cone.

electron generated bremsstrahlung x-ray luminosity (E > 4 keV). The observed burst of electrons shown in Figure 1 has the detailed characteristics of lightning-induced electron precipitation (LEP) events /11/ and represents electrons that are removed from the slot region of the radiation belt.

The temporal variation of energetic particle precipitation (E > 45 keV) in the midlatitude zone at L = 2.3 is shown in Figure 3. These data were obtained over a 100 day period in 1982 with the SEEP TE and ME detectors in the north for longitudes between 260° and 320°E. A median value of flux was calculated for a 5 second interval centered at L = 2.3. The magnetic activity index, D_{st}, is also shown in the lower panel for comparison with the particle data. The four major magnetic storms are marked with vertical lines and the smaller magnetic storms with upward pointing arrows. The TE detector is sensitive to both electrons and ions while the ME detector responds principally to electrons. A strong correlation is evident between D_{st} and the measured flux incident on the TE detector during the times of magnetic storms as indicated by the downward pointing arrows. This midlatitude flux frequently observed during stormtime conditions is consistent with midlatitude energetic ion precipitation as shown in Figure 1. The energy flux at 200 km was previously found /10/ to vary with magnetic activity as given by $E_T = 2 \times 10^{-5} \exp(0.48\ I)$ ergs cm^{-2} s^{-1} where $I = Kp + \ln D_{st}$ and $D_{st} \neq 0$. During periods when major magnetic storms were not occuring, the responses of the various detectors indicate that the midlatitude flux is primarily electrons.

The electron precipitation observed with the ME detector is not directly correlated with magnetic activity except for the case of the large magnetic storm of 13 July 1982 where auroral fluxes (i.e. EAB) penetrate down to L = 2.3 (Figure 2). In general, the precipitating energetic electron flux at L = 2.3 indicates a rather slow buildup in electron intensity following a major storm; of the order of four days for the well-defined magnetic storms commencing on days 195 and 249. After the electron flux reaches its delayed maximum it is observed to decay back to prestorm levels on the order of 15 days. This slowly decaying component of electron flux is also evident on the TE detector; however, it is somewhat masked by the presence of the stormtime ion flux indicated by downward arrows in Figure 3.

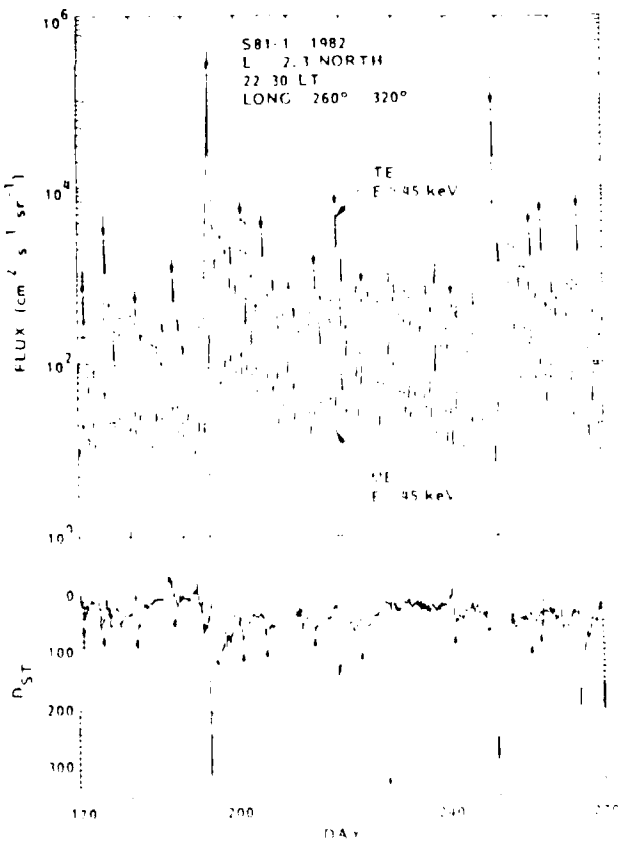

Figure 3. Variations of midlatitude zone (L=2.3) particle precipitation with magnetic activity. The TE detector responds to electrons (E > 550 keV).

Major magnetic storms are known to inject electrons which diffuse into the slot region (2 < L < 3) of the radiation belt several days after the storm onset /12-14/. Because of the delayed response of midlatitude electron precipitation (as shown in Figure 3) the past magnetic activity dominates over the current magnetic activity for predicting electron precipitation at L = 2.3. The 20 day long response function of the electrons has no doubt contributed significantly to the discrepancies in the correlation of flux associated with the precipitation of midlatitude electrons with magnetic indices /14/. An example of the latitude and energy variation in the midlatitude electron zone is shown in Figure 4 for 17 August 1982 when the average electron flux is relatively high following a moderate magnetic storm. This pass was selected because it includes the strongest observed case, to date, of manmade precipitation of energetic electrons by the controlled injection of ground based signals from a VLF transmitter (NAA at 17.8 kHz) /15/. The manmade precipitation is predominantly at lower

Equatorial Zone

The prominent equatorial zone is observed between geomagnetic latitudes of $\pm$ 20° and is stable and repeatable in form during each equatorial pass. The particles of the equatorial zone are identified as energetic helium and/or hydrogen ions based on: 1) the ion transmission characteristics of different thicknesses of gold and aluminum surface deposits on the solid state detectors /2,5/, 2) the angular distribution of the particles over a constant pitch angle near 90 degrees due to an east-west effect /2/ and 3) previous studies /1-7/. The charge exchange lifetime of energetic hydrogen and helium ions in the equatorial ionosphere is short and therefore the low latitude ion radiation belt is short lived /3/. This is consistent with the conspicuous double maximum in flux observed in the equatorial zone as shown in Figure 1 (i.e. maxima displaced $\pm$ 10° in latitude about the geomagnetic equator). At the observed equatorial flux minimum, between the peaks, the S81-1 satellite is at the magnetic equator and beneath the temporary ion belt.

The temporal variation of ions in the equatorial zone for 13-14 July 1982 is shown in the top panel of Figure 2. In the center panel the L shell variation of the plasma trough location and the equatorward auroral boundary (EAB) location are shown and indicate the relative compression of the magnetosphere and the displacement of the auroral zone to middle latitudes. The EAB is similar to the optical auroral Q index and represents the equatorward edge of the auroral zone as indicated by strong particle precipitation. The magnetic indices Kp and D_{st} are shown in the lower panel. Near 01:00 hours UT on 14 July 1982 the storm reaches a maximum (D_{st} = -325) and the equatorial zone ion flux is observed to simultaneously increase by a factor of about 500 over pre-storm levels. The energetic equatorial ions, however, remain high (~ 10^3 cm^{-2} s^{-1}) after the storm and confirm the development of a low latitude (L ~ 1.14) ion radiation belt during the storm main phase that decays relatively slowly in time producing equatorial zone ionization /1-6/. The similarity of the day and night intensity and slow temporal variation of energetic particles in the equatorial zone indicate the global extent of ion precipitation.

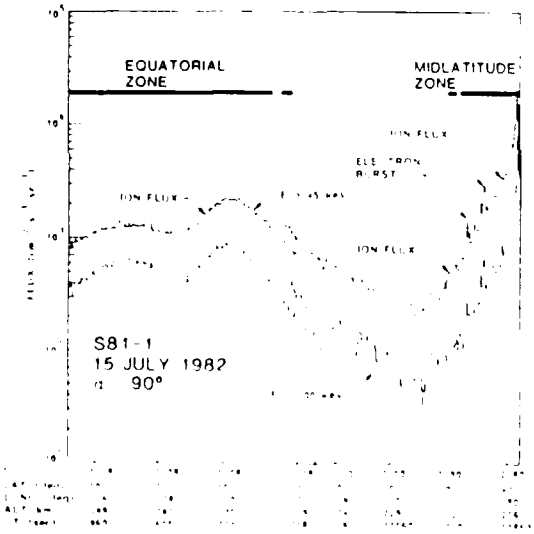

Figure 1. Low altitude satellite observations of precipitating energetic electrons and ions in the midlatitude and equatorial zones.

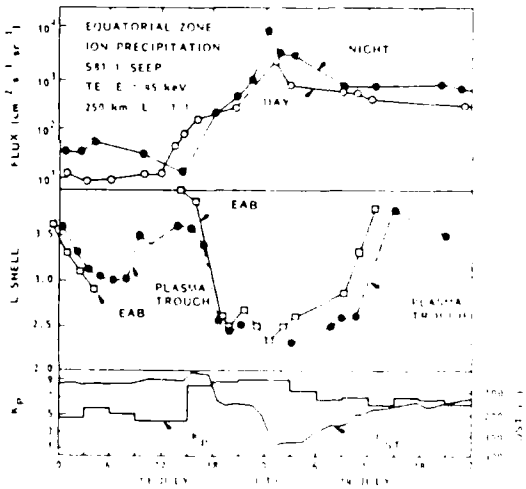

Figure 2. Variation of equatorial zone ion precipitation during the magnetic storm of 13-14 July 1982. The location of the plasma trough and equatorward auroral boundary (EAB) are also shown.

Midlatitude Zone

Also evident in the data of Figure 1 is the presence of strong particle precipitation in the midlatitude zone. The dominant particles, in this case, are identified as quasitrapped ions that are occasionally supplemented by an intense burst of energetic electrons. The ion flux is observed to increase monotonically with increasing latitude and is suggestive of a radial diffusion mechanism, which is stable (temporally and spatially), that transports ring current ions to lower L shells. The intensities, energy spectra and quasitrapped angular distribution are consistent with previous studies of the midlatitude ion zone (1, 8-10). Evidence for ion precipitation during the main phase and early recovery phase was also obtained from the remote sensors on SEEP which show significant 391.4 nm emission and no

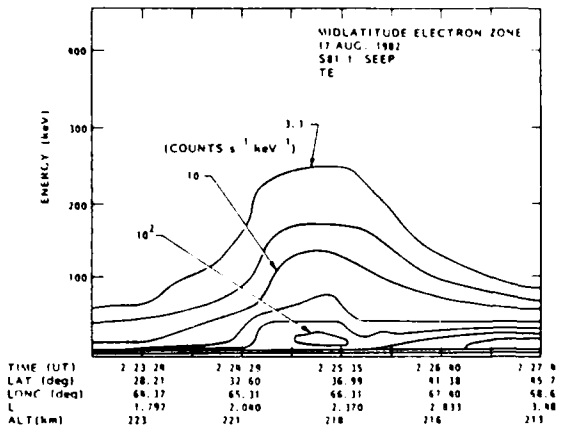

Figure 4. Energy spectrogram of the midlatitude electron zone.

energies (~ 20 keV at L ~ 2.3) relative to the much higher characteristic energies associated with the midlatitude electron zone (~ E^{-1} in keV). The midlatitude electron zone is a persistent feature in the L region between 2 and 3 after magnetic storms and intensifies in the drift loss cone near the region of lowest magnetic field. The features of the electron zone at this time include the hard spectra, the flux maximum, the zone width (~ 10^{o} latitude), and the soft low energy flux poleward of the zone peak. The high energy electrons present in the midlatitude zone suggest that low frequency waves (< 6 kHz) and/or off equatorial interactions play an important role in scattering radiation belt electrons into the drift loss cone /11/.

ACKNOWLEDGEMENTS

The SEEP experiment was sponsored by the Office of Naval Research (contract N00014-79-C-0824). Launch and orbital support were provided by the Air Force Space Test Program Office. Much of the data analysis was performed under the Lockheed Independent Research Program.

REFERENCES

1. Voss, H. D., and L. G. Smith, J. Atmos. Terr. Phys., 42, 227 (1980)

2. Voss, H. D., and L. G. Smith, Space Research, 131 (1980)

3. Tinsley, B. A., JATP, 43, 617 (1981)

4. Moritz, J., J. Geophys. Res., 38, 701 (1972)

5. Smith, L. G., and B. Goushmand, 7th ISEA, Hong Kong, in press (1984)

6. Meier, R. R., and C. S. Weller, J. Geophys. Res., 80, 2813 (1975)

7. Mizera, P. F., and J. B. Blake, J. Geophys. Res., 78, 1058 (1973)

8. Voss, H. D., L. G. Smith, and F. M. Braswell, Space Research, 149 (1980)

9. Cornwall, J. M., F. V. Coroniti, and R. M. Thorne, J. Geophys. Res., 76, 4428 (1971)

10. Voss, H. D., and L. G. Smith, Geophys. Res. Lett., 6, 93 (1979)

11. Voss, H. D., W. L. Imhof, J. Mobilia, E. E. Gaines, M. Walt, U. S. Inan, R. A. Helliwell, D. L. Carpenter, J. P. Katsufrakis, and H. C. Chang, Nature, in press (1984)

12. Lyons, L. R., and D. J. Williams, J. Geophys. Res., 80, 3985 (1975)

13. Larsen, T. R., W. L. Imhof, and J. B. Reagan, J. Geophys. Res., 81, 3444 (1976)

14. Reagan, J. B., Dynamical and Chemical Coupling of the Neutral and Ionized Atmosphere, D. Reidel Publishing Co., Holland, 146 (1977)

15. Imhof, W. L., J. B. Reagan, H. D. Voss, E. E. Gaines, D. W. Datlowe, J. Mobilia, R. A. Helliwell, U. S. Inan, J. Katsufrakis, and R. G. Joiner, Geophys. Res. Lett., 10, 8, 615 (1983)

Printed in the United States of America.

LOCALIZED ELECTRON PRECIPITATION EVENTS AT HIGH LATITUDES STUDIED WITH X-RAY IMAGERY FROM A SATELLITE

W. L. Imhof, H. D. Voss, J. B. Reagan, D. W. Datlowe and J. Mobilia

Lockheed Palo Alto Research Laboratory, 3251 Hanover Street, Palo Alto, CA 94304, U.S.A.

INTRODUCTION

At very high latitudes, existing data and theoretical models suggest there may be isolated patches of energetic electron precipitation into the atmosphere. Islands of energetic electrons have frequently been observed in the geomagnetic tail /1,2,3/. Also, theoretical studies have advanced the idea of localized plasma entry through the magnetopause involving clouds or plasmoids /4/. With direct particle measurements, Hoffman and Evans /5/ observed a "burst region" poleward of the auroral oval that was characterized by a very soft spectrum and large structures in the precipitation patterns. The sporadic and structured precipitation of soft electrons over the polar caps has been observed by Winningham and Heikkla, /6/. Higher energy spikes have been observed at high latitudes by McDiarmid and Burrows /7/ for > 40 keV electrons and by Brown and Stone /8/ for $\geq$ 425 keV electrons. However, the structured precipitation of electrons at high latitudes is not well understood due to the two-dimensional character, the confined extent and the temporal variations. For energetic electrons even less is known due to limitations in the available data.

Many of the existing spatial-temporal ambiguities associated with the structured precipitation of energetic electrons at high latitudes can be unraveled by observing the bremsstrahlung x-ray footprints in the atmosphere, preferably with fine spatial resolution over an extended period of time and with spectrum coverage extending to relatively high energies. Here we present some fine spatial resolution mappings of small isolated patches of bremsstrahlung x-rays observed at high latitudes.

BRIEF DESCRIPTION OF INSTRUMENTATION

The x-ray mapping spectrometer was part of the SEEP (Stimulated Emission of Energetic Particles) payload on the S81-1 spacecraft. The basic design of the spectrometer is to be described in a publication of Calvert et al. (private communication) and the calibration and performance by Voss et al. (private communication). The instrument consisted of a large area position-sensitive proportional counter filled with xenon gas and sensitive over the energy range 4 to 40 keV. The spectrometer was oriented in a forward and downward (35° below horizontal) direction viewing the atmosphere with a $\pm 45^{\circ}$ field-of-view to the left and right. The field of view was divided into 16 pixels in the direction perpendicular to the trajectory of the low altitude (170 - 280 km) polar orbiting satellite. The spatial and temporal resolutions were ~ 30 km and 0.13 second, respectively. Energy spectra of the x-rays were measured over 24 channels for the center two pixels and over 8 channels for each of the remaining pixels.

OBSERVATIONS

Examples of the bremsstrahlung x-ray mappings obtained with the SEEP payload have been shown previously /9,10/. Here, the x-ray data were surveyed for the occurrences of small isolated patches of bremsstrahlung x-ray emission over the polar caps. For this purpose the following criteria were established: 1) the maximum x-ray flux from the central region of the patch must exceed 2×10^{2} /cm^{2} ster sec 2) the spot must be completely surrounded by an intensity close to the background level 3) the full width-at-half-maximum in any direction should not exceed 300 km. A total of 29 isolated patches were noted. Examples of the x-ray spots are shown in Figure 1. Each section of the figure represents the mapping observed during a different pass of the spacecraft. The invariant latitudes and magnetic local times (MLT) are at the positions of the satellite. The center x-ray pixels view the same position 20 - 50 seconds earlier; the exact time difference depends upon the altitude of the satellite and the altitude of x-ray production, which is energy dependent. These maps represent total x-ray counting rates over the energy range 4 - 40 keV. One should note the variations in intensity, area, and shape of the patches. Two of the illustrated passes (June 16 and June 26) also contain an elongated patch or narrow arc spanning the field-of-view which does not meet the criteria for selection of small patches.

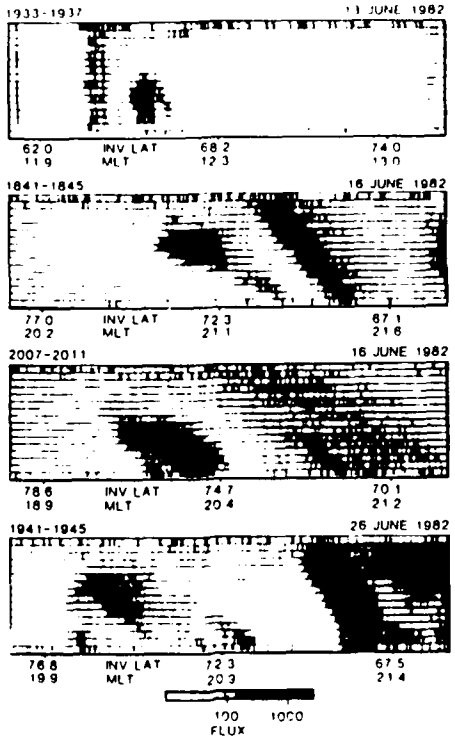

Figure 1. Mappings of the x-ray intensities (4 - 40) keV. The invariant latitudes and the magnetic local times refer to the positions of the satellite. Fluxes are in units of photons/cm^2 ster sec.

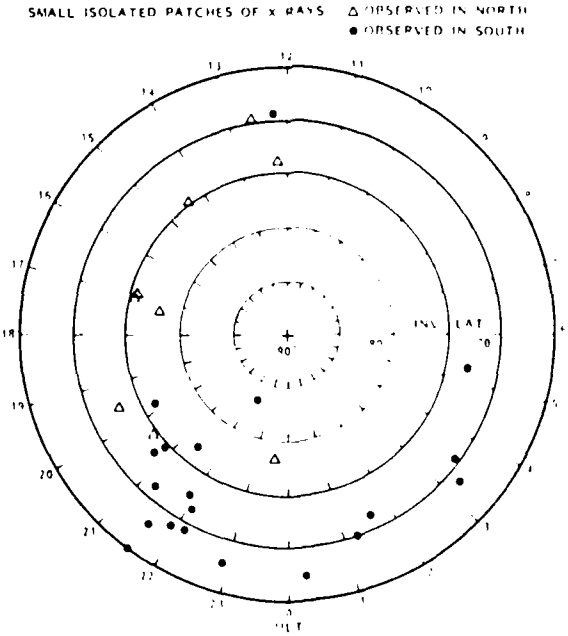

Figure 2. Position in invariant latitude and magnetic local time of the isolated patches.

The positions in invariant latitude and magnetic local time of the isolated spots of x-ray emission are summarized in Figure 2. Clearly, the bulk of the patches span the magnetic local time interval from noon to midnight, with very few spots observed in the morning hours. The x-ray patches occurred over a rather broad range of invariant latitudes from 65^0

to 83°, with a median latitude of 72.5°. The night to day preference spanned all latitudes but at low latitudes the events occurred primarily at times just before midnight.

In order to study the occurrence frequency of small x-ray patches as a function of magnetic local time, the observations at invariant latitudes above 70° were subdivided into selected MLT intervals and these are plotted in Figure 3. As in Figure 2 the data indicate a preference for spot observation between noon and midnight, with patches rarely appearing in the morning hours. A more quantitative assessment of the local time dependence has been made by correcting for the non-uniform sampling of MLT intervals. The number of spot observations in each of several selected MLT intervals was divided by the number of observations in those intervals and the results are shown in Figure 3.

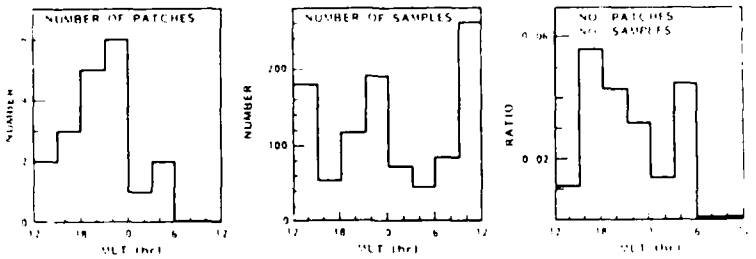

Figure 3. The number of x-ray patches versus MLT for invariant latitudes > 70°. Also shown are the number of sample passes at invariant latitude ≥ 73° and the number of patches divided by the number of samples.

Two representative energy spectra of the x-rays emitted from isolated x-ray patches are presented in Figure 4. In these examples the spectra were taken in the center two pixels where 24 channel energy resolution was available. The spectra have been corrected for detection efficiency and for transmission of the x-rays through the 0.76 mm thick beryllium plate at the entrance. The total intensities of the x-rays emitted from the patches span a broad range, and the e-fold energies of the x-rays were generally within 1-6 keV, with corresponding electron e-fold energies of ~ (2-12) keV.

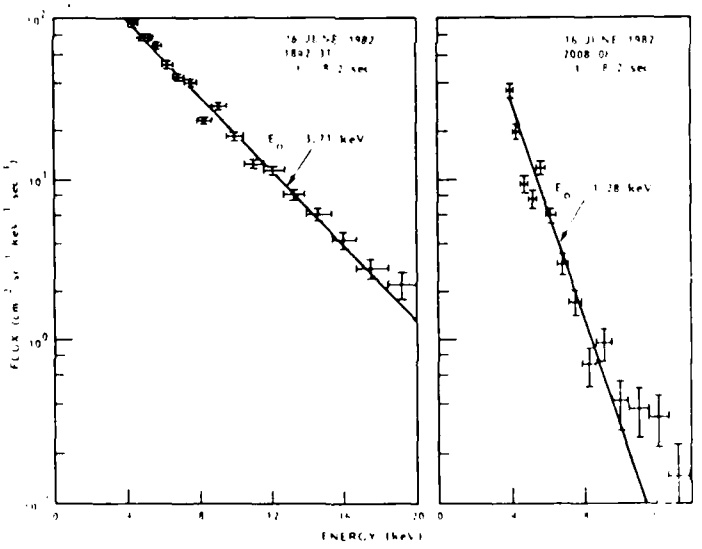

Figure 4. Examples of the energy spectra for the x-rays emitted from the center two pixels in the heart of representative isolated x-ray patches.

DISCUSSION

Since the majority of x-ray patches occurred from dusk until dawn except for those observed in the early afternoon, many of them may be related to the geomagnetic tail. Their isolated nature suggests a similarity to the islands, but more evidence is required before a definitive association can be made.

The mid-afternoon patches considered here might represent the impulsive entry of localized plasma clouds /4/. However, the present x-ray spots correspond to much higher energy

electrons than the bulk of those generally associated with plasma clouds or with the localized "polar showers" observed over the polar caps by Winningham and Heikkila /6/. The present observations may possibly indicate that the localized plasma clouds extend up to energies of a few keV.

On infrequent occasions isolated narrow patches were observed that were too long to qualify as a small patch. Some of these long and narrow patches were observed at invariant latitudes as high as 75^{o}, and were therefore poleward of the auroral oval. In that regard they might be called polar cap arcs but the elongated patches were typically not sun-aligned as are polar cap arcs. Also due to the limited spatial coverage of the SEEP x-ray observations they may not be very long and may merely be modified forms of x-ray patches.

More analysis is underway to consider possible correlations of the x-ray patches with geomagnetic conditions and various phenomena such as x-ray microbursts, and a more comprehensive paper will be published later.

SUMMARY

Small isolated patches of bremsstrahlung x-rays with typical dimensions of 100 - 300 km have been observed over the polar caps with the following characteristics:

- o The x-ray patches were most often observed in the dusk-to-midnight sector, but some were observed at all magnetic local times except the early morning.
- o Small patches of x-rays were observed at invariant latitudes of 65^{o} - 83^{o}.
- o The x-ray energy spectra displayed e-fold energies of (1-6) keV.

REFERENCES

1. K. A. Anderson, Energetic electron fluxes in the tail of the geomagnetic field, J. Geophys. Res., 70, 4741, 1965.

2. C. I. Meng, Energetic electrons in the magnetotail at 60 R_E, J. Geophys. Res. 76, 862, 1971.

3. E. C. Roelof, E. P. Keath, C. O. Bostrom, and D. J. Williams, Fluxes of $\geq$ 50 keV protons and $\geq$30 keV electrons at ~35 R_E. 1. Velocity anisotropies and plasma flow in the magnetotail, J. Geophys. Res., 81, 2304, 1976.

4. W. J. Heikkila, Impulsive plasma transport through the magnetopause, Geophys. Res. Lett., 9, 159, 1982.

5. R. A. Hoffman and D. S. Evans, Field-aligned electron bursts at high latitudes observed by OGO-4, J. Geophys. Res., 73, 6201, 1968,

6. J. D. Winningham and W. J. Heikkila, Polar cap auroral electron fluxes observed with ISIS 1, J. Geophys. Res., 79, 949, 1974.

7. I. B. McDiarmid and J.R. Burrows, Electron fluxes at 1000 kilometers associated with the tail of the magnetosphere, J. Geophys. Res., 70, 3031, 1965.

8. J. W. Brown and E.C. Stone, High-energy electron spikes at high latitudes, J. Geophys. Res., 77, 3384, 1972.

9. H. D. Voss, W. L. Imhof, J. B. Reagan, R. R. Vondrak, M. Walt, J. Mobilia, D. W. Datlowe, D. P. Cauffman, W. Calvert, and R. G. Joiner, SEEP X-ray Imagery of the earth's aurora, EOS Trans. Am. Geophys. Union, 64, 792, 1983A

10. H. D. Voss, et al., EOS Cover, Nov. 29, 1983B.

ACKNOWLEDGMENTS

The experiment was sponsored by the Office of Naval Research (Contract N00014-79-C-0824). Launch and orbital support were provided by the Air Force Space Test Program Office. Appreciation is extended to the ONR program manager, R. G. Joiner, to the payload system engineer, Mr. S. J. Battel, to Dr. D. P. Cauffman for his program management of the satellite payload development, and to Dr. W. Calvert, Mr. T. C. Sanders, and Mr. J. C. Bakke for their major contributions to the design and development of the x-ray imager.

Radio Science, Volume 20, Number 3, Pages 511-518, May-June 1985

Results from the SEEP active space plasma experiment: Effects on the ionosphere

W. L. Imhof, E. E. Gaines, H. D. Voss, J. B. Reagan, D. W. Datlowe, and J. Mobilia

Lockheed Palo Alto Research Laboratory, California

R. A. Helliwell, U. S. Inan, and J. Katsufrakis

STAR Laboratory, Stanford University, California

R. G. Joiner

Office of Naval Research, Arlington, Virginia

(Received August 14, 1984; revised October 15, 1984; accepted October 29, 1984.)

An active satellite-ground coordinated space plasma experiment was conducted from May to December, 1982, in which electrons were precipitated from the radiation belts into the ionosphere by the controlled injection of VLF signals from ground-based transmitters. The results confirm the hypothesis that electrons can be precipitated from the radiation belts by ground-based VLF transmitters, and they provide information relating to the effects of such precipitation on the ionosphere. The ionization produced in the atmosphere of the northern hemisphere at $L = 2.3$ by the modulated signals from ground-based VLF transmitters was shown to be as great as one ion pair/cm^3 s at 80 km altitude. The ionization at comparable positions produced by naturally occurring electron precipitation varies greatly, and can be as low as 0.1 ion pair/cm^3 s, but is also sometimes larger than 100 ion pairs cm^3 s at times of lightning flashes.

INTRODUCTION

An active experiment, stimulated emission of energetic particles (SEEP), was conducted during May–December 1982. In this experiment the U.S. Navy operational VLF transmitters at Cutler, Maine (NAA); Annapolis, Maryland (NSS); and Jim Creek, Washington (NLK) and the Stanford University research VLF transmitter at Siple Station, Antarctica, were operated in special controlled formats at times of overpasses of the low-altitude polar-orbiting satellite S81-1. The spacecraft payload measured both direct electron precipitation >2 keV and bremsstrahlung X rays >4 keV from the atmosphere. The experiment concept is illustrated schematically in Figure 1. The locations of the VLF transmitters are indicated along with a representation of the satellite paths during three successive passes. In addition, the modulated VLF waves and their regions of interaction with the trapped electrons are also shown.

Copyright 1985 by the American Geophysical Union

Paper number 4S1333
0048-6604/85/004S-1333$08.00

The SEEP experiment payload on the three-axis stabilized polar-orbiting S81-1 spacecraft contained an array of cooled silicon solid state detectors to measure electrons and ions directly with high sensitivity and fine energy resolution [*Voss et al.*, 1982]. The data presented here were taken with electron spectrometers mounted at 90° zenith angle and at 90° to the orbit plane (TE detector), at 0° zenith angle (ME1) and at 180° zenith angle (ME2). The TE spectrometer had an electron threshold energy of 6 keV, an acceptance angle of ±20° and a geometric factor of 0.17 cm^2 sr. It is sensitive to both electrons and ions, but on the basis of the responses of other detectors in the payload, all of the precipitation events presented here are taken to be associated with electrons. Each of the ME1 and ME2 spectrometers had an electron threshold energy of 45 keV, an acceptance angle of ±30° and a geometric factor of 2.47 cm^2 sr. A thick window on ME1 and ME2 prevented ions with energies below 0.5 MeV from impinging on the silicon detector, and therefore in all of the data shown the counts were predominantly due to electrons. The measurements were performed at satellite altitudes of ~220 km.

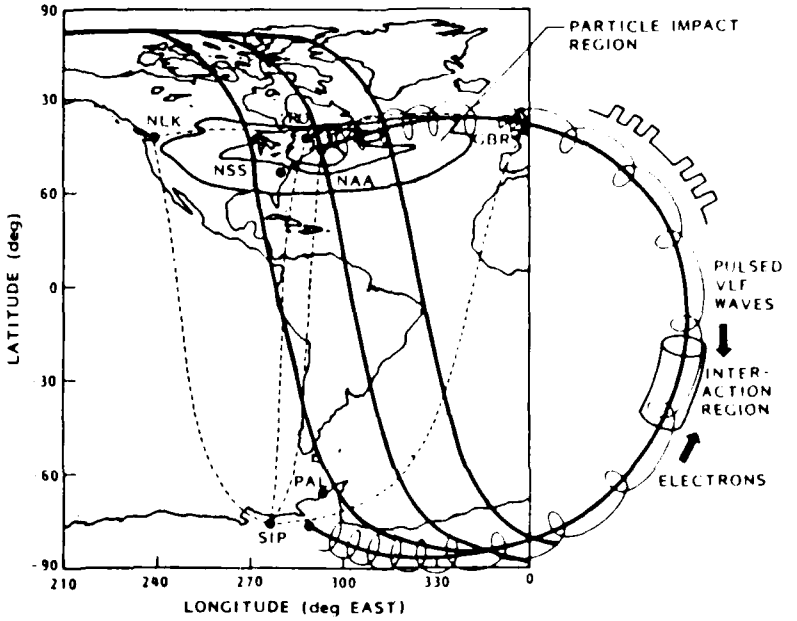

Fig. 1. Schematic illustration of the SEEP experiment concept. The locations of the pertinent VLF transmitters are indicated along with a representation of the satellite paths during three successive passes. Also shown are the modulated VLF waves and the region of wave-particle interactions.

With this payload the first observations were made of direct bounce loss cone precipitation of radiation belt electrons by the controlled injection of VLF signals from a ground based transmitter [*Imhof et al.*, 1983*a*]. Although past observations had shown that electrons can be precipitated from the radiation belts by ground-based VLF transmitters, the evidence was based predominantly on observations of electrons in the drift loss cone. Narrow resonant peaks in the energy spectra [*Imhof et al.*, 1974, 1981; *Vampola and Kuck*, 1978; *Koons et al.*, 1981] and coordinated wave-particle observations [*Imhof et al.*, 1981] had provided evidence for the effects of transmitters. In spite of the SEEP findings, relatively little is known about the importance of transmitters in relation to other loss processes for radiation belt particles. It is realized, however, that electrons are regularly precipitated from the radiation belts and that these electrons can cause measurable ionization at midlatitudes.

The purpose of this paper is to assess the effects on the ionosphere of electrons precipitated by the transmitters NAA and NSS during the observed SEEP events and to compare these with the effects of electron precipitation induced by natural causes.

OBSERVATIONS OF ELECTRONS PRECIPITATED BY VLF TRANSMITTERS

A good example of electron flux modulations in correlation with the transmitter on-off signals occurred on August 17, 1982 at 8680–8740 seconds UT when the SEEP payload was passing near the NAA transmitter as it was being modulated with a 3-s on and 2-s off pattern. In Figure 2 the electron fluxes measured at various zenith angles are plotted as a function of time. A modulation period of 5 ± 0.1 s is clearly seen for 12 consecutive cycles. For reference, the measured on times of the transmitter at NAA are indicated. The risetime of the electron flux and the observed delay in decay time of ~ 1.5 s are now understood [*Inan et al.*, 1985] in terms of the pitch angle dependence of the particle distribution near the edge of the loss cone and by the multiple interaction of the particles with the waves due to significant atmospheric backscatter.

Differential energy spectra of the precipitating electrons taken during the times of enhanced electron precipitation showed prominent peaks but there was little evidence of their presence during times of minimum intensity. It was shown that the measured peak energies and their variations with L are consistent

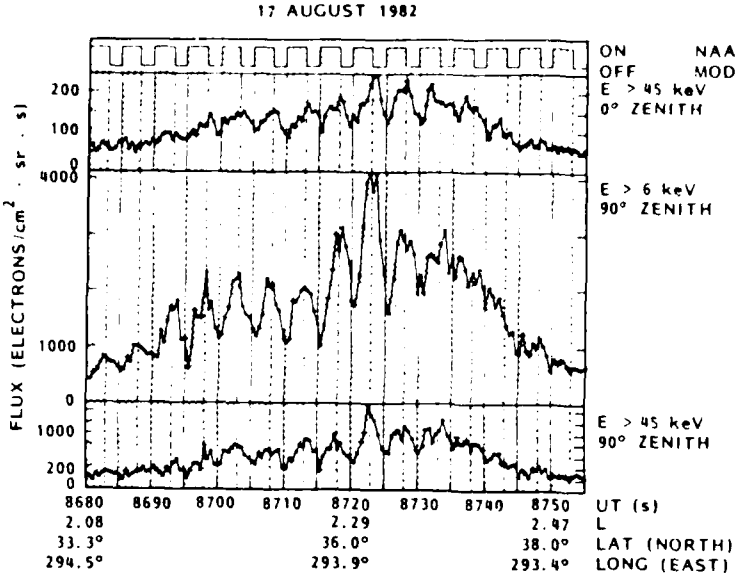

Fig. 2. Electron fluxes on August 17, 1982, plotted as a function of time. Also shown are the on and off times of the NAA transmitter.

with those expected for cyclotron resonance with waves of the transmitter frequency travelling parallel to the earth's magnetic field lines [*Imhof et al.*, 1983*a*].

From surveys of the SEEP data five electron modulation events were found from the 65 passes of the satellite when one of the transmitters was being modulated in a special 3-s on and 2-s off format. No such events were found in the 175 passes when neither the NAA nor NSS transmitter was being modulated in one of the special SEEP formats. All of the time profiles for the events displayed a similar pattern in which the fluxes increased rather slowly after start of the on period and reached a maximum about 2 s later. The temporal profile and the absolute count rates of the observed fluxes were found to be in good agreement with the predictions of an extended test particle model of the wave-particle interaction in the magnetosphere [*Inan et al.*, 1985].

Although modulated electron precipitation events associated with the controlled injection of VLF signals from a ground-based transmitter were not observed frequently, transmitters may still play a strong role in the precipitation of electrons from the radiation belts. Narrow peaks in the energy spectra of electrons precipitating from the inner radiation belt in the drift loss cone have been shown to result from cyclotron resonance interactions with waves from ground-based transmitters [*Imhof et al.*, 1981]. Even in the bounce loss cone the transmitters might have contributed significantly to the observed fluxes in the absence of a detectable modulation. To assess the role of transmitters it is important, therefore, to compare the absolute fluxes of electrons measured during normal operations with those observed when the transmitters were either off or operated in a special manner such as in the SEEP 3-s on and 2-s off format. Unfortunately, a significant amount of data were not acquired with both the NAA and NSS transmitters off. Normal operation consisted of a constant amplitude signal with the frequency shifted as often as once every 25 ms. In the SEEP format the frequency was fixed during the on time of 3 s. The wider bandwidth signal during normal operations may possibly have inhibited temporal growth of the waves, as found in earlier Siple experiments [*Raghuram et al.*, 1977].

The possible effects of transmitter operation on the fluxes of precipitating electrons are illustrated in Figure 3 where the median electron fluxes >6 keV observed during a 5.6-s period centered at $L = 2.3$ are plotted as a function of longitude. Separate symbols are used for the normal operation of both transmitters and for the special modulation of either transmitter in the 3-s on and 2-s off format. During the normal mode pass on August 11, 1982, a narrow spike of precipitating electrons with the clear characteristics of those induced by lightning [*Voss et al.*,

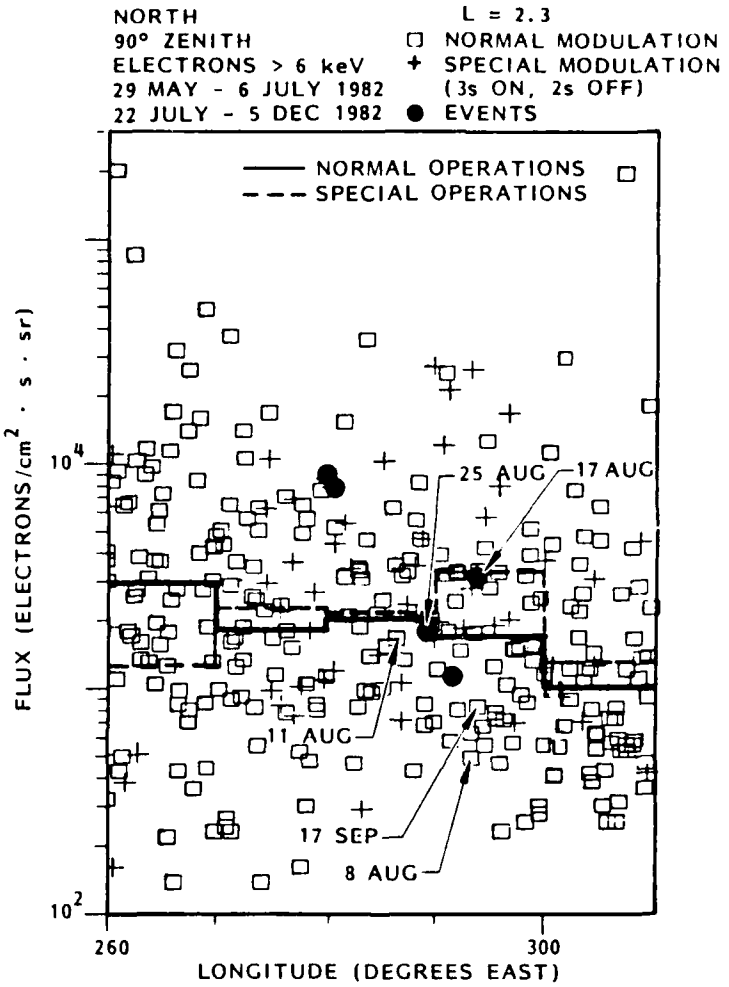

Fig. 3. The median electron flux measured during a 5.6-s period centered at $L = 2.3$ plotted versus longitude. Solid circles indicate fluxes measured on a pass when an event was observed. Median flux levels for normal operation and for modulation in a special format (3-s on/2-s off) are shown in 10° longitude bins.

1984*b*] was observed at an L value close to 2.3 and that event is treated later in this paper with a shorter summation time interval. To minimize the flux variations associated with magnetic activity the time period July 7–21, 1982, has been excluded from the plot. At the times covered in the figure the electron fluxes in this longitude interval increased by as much as an order of magnitude subsequent to the magnetic storms with a peaking at a time delay of about 4 days [*Voss et al.*, 1984*a*]. The pronounced transmitter modulation event on August 17, 1982, occurred during one of these enhanced electron periods. The median flux levels shown for 10° longitude bins do not seem to indicate a significant change in the average precipitation rate when the transmitters were operated at fixed frequency with a 60% duty cycle as compared to the normal broader frequency operation at 100% duty cycle. Although evidence for a strong effect of the transmitters was not found by this technique (see also *Imhof et al.* [1983*b*]), it should be emphasized that the ideal experiment was not conducted in which one could compare the fluxes of precipitating electrons observed when both NAA and NSS transmitters were off and when both were on.

EFFECTS OF PRECIPITATED ELECTRONS ON THE IONOSPHERE

We now consider the ionization in the atmosphere that would be associated with the pronounced transmitter modulation events of August 17 and August 25, 1982, and compare the ionization profiles with other representative cases of electron precipitation

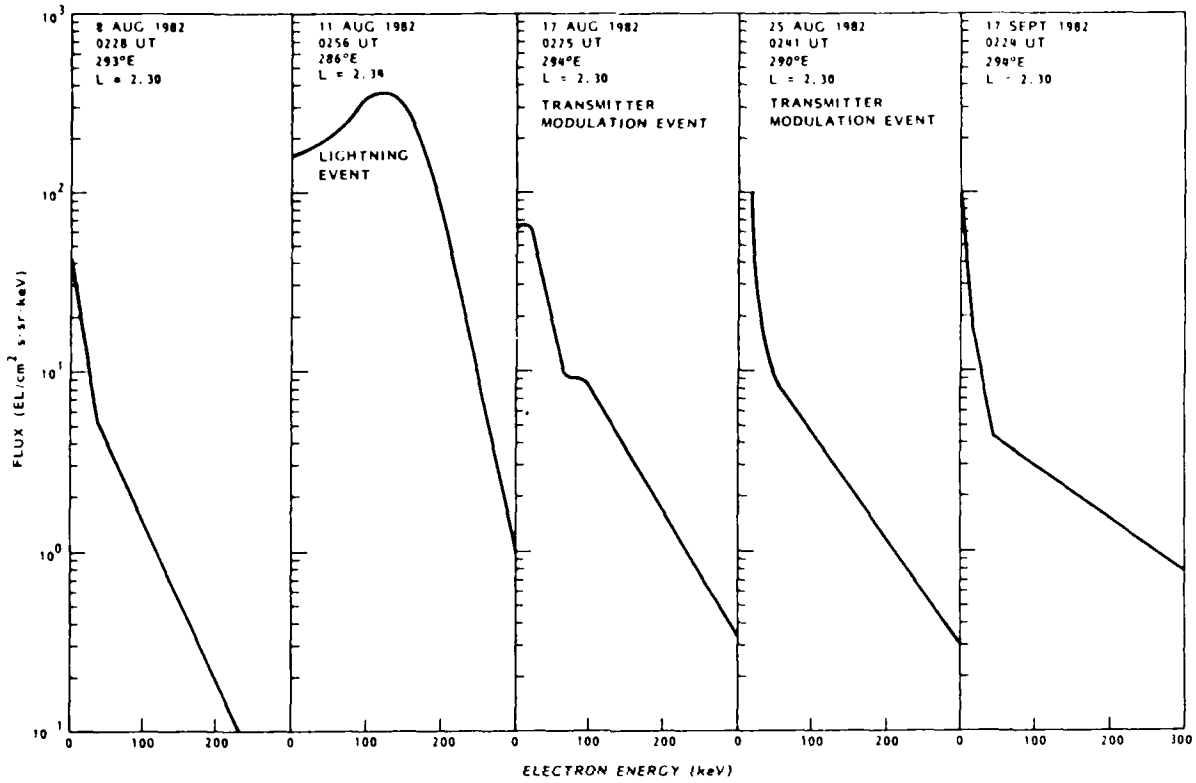

Fig. 4. Energy spectra of electrons measured in the northern hemisphere during each of several satellite passes. The curves are best fits to the measured data points. For the August 11, 1982, event the spectrum was summed over a time period of 0.70 s. For all of the other spectra the summation interval was 8.19 s.

Based on both the energy spectrum and the pitch angle distribution of the precipitating electrons the ionization profile can be calculated by using the AURORA computer program [*Walt et al.*, 1968]. Energy spectra of the electrons in the northern hemisphere were measured with fine energy resolution, and the spectra at $L = 2.3$ and longitudes of 286°E to 294°E during these transmitter modulation events and at other selected times are shown in Figure 4. The applicable time interval is 8.19 s except for the lightning associated spectrum on August 11, 1982, for which the summation time is 0.70 s. These spectra represent electrons observed with the detector at a central pitch angle of 90°-96°. All of the observed electrons have mirror points below sea level in the southern hemisphere; i.e., the electrons were all precipitating within one bounce, except for backscattering. Only those with pitch angles less than ~78° precipitated in the northern hemisphere, but for purposes of calculating energy deposition profiles we shall assume the spectra of electrons precipitating in the north are the same as shown in Figure 4.

The pitch angle distributions were measured directly at positions above the atmosphere with the array of collimated electron spectrometers in the SEEP payload. However, measurements were made at only a few pitch angles with relatively broad angular resolution. A histogram representation of the fluxes observed in those detectors during the August 17, 1982, measurement is shown in Figure 5. A Gaussian fit (B) to the northern hemisphere measurements is also shown in the figure, normalized to unity at 90°. In addition, a narrower Gaussian pitch angle distribution (C) is plotted based on the measurements in the northern hemisphere for some of the other events. It should be realized that both the absolute fluxes and the shapes of the pitch angle distributions can vary considerably from one satellite pass to another. Although the transmitters were routinely operated at the same power level, the intensities of the waves after passage through the ionosphere are known to vary considerably due to changes in ionospheric conditions [*Heyborne*, 1966].

We have calculated energy deposition profiles at

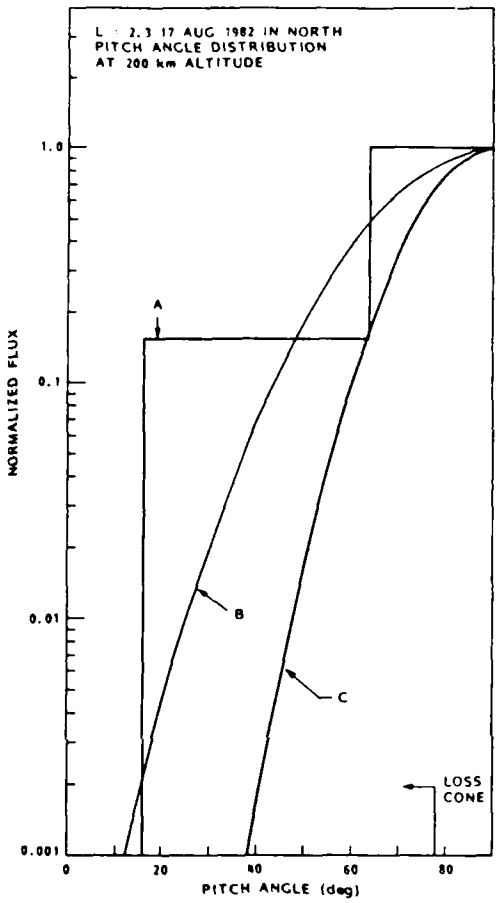

Fig. 5. Pitch angle distributions at $L = 2.3$ in the northern hemisphere for electrons >45 keV. Curves A and B are histogram and Gaussian representations, respectively, of the distribution measured during the transmitter modulation event on August 17, 1982. Curve C is a narrower Gaussian distribution based on the TE measurements at a variety of longitudes. The pitch angle distributions are normalized to 1.0 at 90°.

$L = 2.3$ using the AURORA program for the pitch angle distributions shown in Figure 5 each normalized to the same flux at 90° pitch angle and for the observed spectral shape. The results are shown in Figure 6. As one can see, the differences between the histogram (A) and the corresponding Gaussian pitch angle distribution (B) for the August 17, 1982, event are only of the order of 25% and therefore the details of the pitch angle distribution measured during this event are not critical in regard to the calculated energy deposition profile. The deposition profile for the August 17, 1982, event was also calculated assuming the narrower pitch angle distribution (C) shown in Figure 5. For this narrower distribution, not actually measured during the event, the energy deposition profile would be reduced by a factor of 2–3. The energy deposition profiles A and B in Figure 6 are equivalent to an energy input of $\sim 10^{-4}$ ergs/cm^2 s and a corresponding riometer absorption of ~ 0.06 dB at 30 MHz [*Reagan et al.*, 1983].

Energy deposition profiles corresponding to the various energy spectra in Figure 4 and for the appropriate histogram pitch angle distributions are presented in Figure 7. The applicable histogram pitch angle distribution is based on the observed responses in detectors TE and ME1 during the satellite pass of interest, and the ratios of these responses are provided in Table 1. In all of these cases the counting rates in detector ME2 were much lower than in ME1. The modulated signals from the NAA transmitter during the August 17, 1982, event produced an ionization rate of ~ 1 ion pair/cm^3 s at 80 km altitude. Both the shapes and the absolute intensities of the ionization

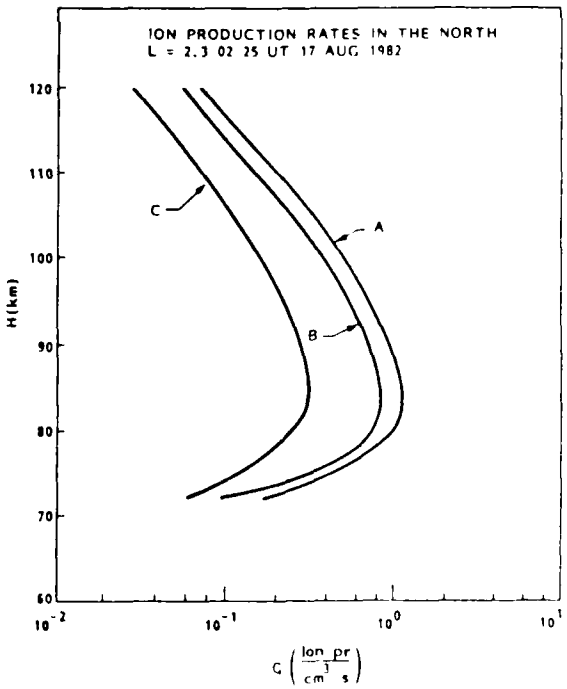

Fig. 6. Energy deposition profiles calculated with the Aurora program for the energy spectrum and pitch angle distributions shown in Figures 4 and 5, respectively. Curve A is for the histogram pitch angle distribution and curve B for the Gaussian pitch angle distribution. For the August 17, 1982, event, curve C corresponds to the narrower Gaussian pitch angle distribution.

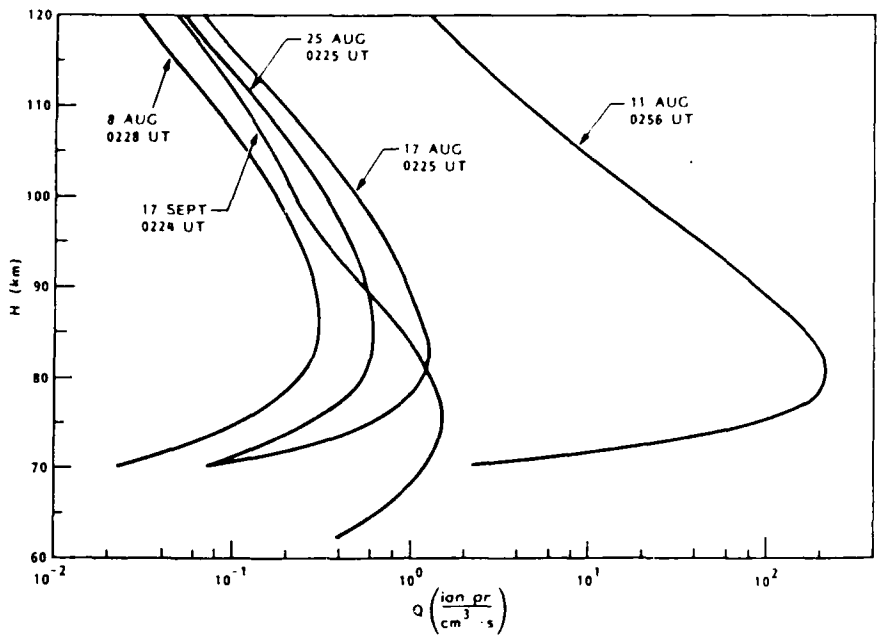

Fig. 7. Energy deposition profiles calculated for the energy spectra in Figure 4 and for the appropriate histogram pitch angle distribution based on the simultaneous counting rates measured in detectors TE and ME1.

profiles at $L = 2.3$ vary over a wide dynamic range, but may be as low as 0.1 ion pair/cm^3 s at (260°–310°) E in the northern hemisphere. Some of the precipitation events were fairly steady as observed from the satellite over broad time and latitude intervals. At other times, such as during the modulated transmitter events or lightning associated precipitation, significant variations were observed on a short time scale. These fluctuations can be particularly large for the precipitation produced by lightning. The latter type event on August 11, 1982 was summed over the peak response period of 0.70 s, but all of the other profiles were averaged over 8.19 s. For this and other lightning flashes the ionization rates at ~80 km altitude can be of the order of 100 ion pairs/cm^3 s or greater. Since the average electron precipitation is comparable to that observed during the August 17 event, it is not known at present how much of the ionization normally occurring in the northern hemisphere at $L = 2.3$ in this longitude region is associated with transmitters and how much results from other processes.

TABLE 1. MEIKTE Flux Ratios

Date	UT	Ratio
Aug. 8, 1982	0228	0.241
Aug. 11, 1982	0256	0.808
Aug. 17, 1982	0225	0.155
Aug. 25, 1982	0241	0.149
Sept. 17, 1982	0224	0.243

Analysis of the data acquired on many satellite passes through the regions of space considered here shows that a measurable ionization from precipitating electrons is generally produced at altitudes of 70–120 km. Some portion of this ionization in the northern hemisphere is generally present as a result of backscatter in the southern hemisphere of electrons in the drift loss cone. One of the two transmitters NAA and NSS was usually operating and so it has not been possible in this experiment to establish conclusively what the contribution of these transmitters is to the electron precipitation normally occurring. These ambiguities could be resolved with use of a much more powerful transmitter operating at a lower frequency, on a different L shell and or one placed above the ionosphere on a satellite such that the waves from the transmitter are much stronger in the near equatorial regions and the associated ionization effects considerably greater. It may then be possible to affect the ionosphere significantly through the controlled precipitation of electrons from the radiation belts.

SUMMARY

The modulated signals from a ground-based VLF transmitter have been shown to produce ionization rates at altitudes of ~80 km in the midlatitude ($L = 2.3$) northern hemisphere as high as 1 ion pair/cm^3 s. The naturally occurring ionization rates in this latitude region show large variations, are longitude dependent, and at (260°–310°) E in the northern hemisphere may be as low as 0.1 ion pair/cm^3 s. At these same locations the ionization at ~80 km associated with lightning flashes is sometimes in excess of 100 ion pairs/cm^3 s, but for each flash the time duration of the intense precipitation is of the order of only 1 s.

Acknowledgments. The LPARL portion of the SEEP experiment was sponsored by the Office of Naval Research (contract N00014-79-C-0824). Launch and orbital support were provided by the USAF Space Test Program Office. Appreciation is extended to the payload system engineer, S. J. Battel, to D. P. Cauffman for his program management of the satellite payload development, and to J. C. Bakke for his role in developing the instrumentation. We acknowledge the efforts of W. E. Francis, B. A. Mooyman-Beck, J. W. Holley, Jr., and P. Filbert in data analysis. The Stanford University effort in SEEP was supported by ONR grant N00014-82-K-0489 and by the Division of Polar Programs of the National Science Foundation under grants for the Siple Station, Roberval and Palmer Station experiment programs.

REFERENCES

Heyborne, R. L., Observations of whistler-mode signals in the OGO satellites from VLF ground station transmitters, *Tech. Rep. 3415-3418-1*, Stanford Univ., Stanford, Calif., 1966.

Imhof, W. L., E. E. Gaines, and J. B. Reagan, Evidence for the resonance precipitation of energetic electrons from the slot region of the radiation belts, *J. Geophys. Res.*, *79*, 3141, 1974.

Imhof, W. L., R. R. Anderson, J. B. Reagan, and E. E. Gaines, The significance of VLF transmitters in the precipitation of inner belt electrons, *J. Geophys. Res.*, *86*, 11,225, 1981.

Imhof, W. L., J. B. Reagan, H. D. Voss, E. E. Gaines, D. W. Datlowe, J. Mobilia, R. A. Helliwell, U. S. Inan, J. Katsufrakis, and R. G. Joiner, Direct observation of radiation belt electrons precipitated by the controlled injection of VLF signals from a ground-based transmitter, *Geophys. Res. Lett.*, *10*, 361, 1983*a*.

Imhof, W. L., J. B. Reagan, H. D. Voss, E. E. Gaines, D. W. Datlowe, J. Mobilia, R. A. Helliwell, U. S. Inan, J. Katsufrakis, and R. G. Joiner, The modulated precipitation of radiation belt electrons by controlled signals from VLF transmitters, *Geophys. Res. Lett.*, *10*, 615, 1983*b*.

Inan, U. S., H. C. Chang, R. A. Helliwell, W. L. Imhof, J. B. Reagan, and M. Walt, Precipitation of radiation belt electrons by man-made waves: A comparison between theory and measurement, *J. Geophys. Res.*, *90*, 359, 1985.

Koons, H. C., B. C. Edgar, and A. L. Vampola, Precipitation of inner zone electrons by whistler mode waves from the VLF transmitters UMS and NWC, *J. Geophys. Res.*, *86*, 640, 1981.

Raghuram, R., T. F. Bell, R. A. Helliwell, and J. P. Katsufrakis, Echo-induced suppression of coherent VLF transmitter signals in the magnetosphere, *J. Geophys. Res.*, *82*, 2787, 1977.

Reagan, J. B., W. L. Imhof, H. D. Voss, E. E. Gaines, R. A. Helliwell, U. S. Inan, J. Katsufrakis, and R. G. Joiner, Effects of transmitter-induced precipitation on the ionosphere, *Eos Trans. AGU*, *64*, 302, 1983.

Vampola, A. L., and G. A. Kuck, Induced precipitation of inner zone electrons, 1, Observations, *J. Geophys. Res.*, *83*, 2543, 1978.

Voss, H. D., J. B. Reagan, W. L. Imhof, D. O. Murray, D. A. Simpson, D. P. Cauffman, and J. C. Bakke, Low temperature characteristics of solid state detectors for energetic x-ray, ion and electron spectrometers, *IEEE Trans. Nucl. Sci.*, *NS-29*, 164, 1982.

Voss, H. D., W. L. Imhof, J. Mobilia, E. E. Gaines, and J. B. Reagan, Energetic particles in the nighttime middle and low latitude ionosphere, *Space Res.*, *25*, in press, 1984*a*.

Voss, H. D., W. L. Imhof, J. Mobilia, E. E. Gaines, M. Walt, U. S. Inan, R. A. Helliwell, D. L. Carpenter, J. P. Katsufrakis, and H. C. Chang, Lightning induced electron precipitation, *Nature*, *312*, 740, 1984*b*.

Walt, W., W. M. McDonald, and W. E. Francis, Penetration of auroral electrons into the atmosphere, in *Physics of the Magnetosphere*, edited by R. L. Carovillano, J. F. McClay, and H. R. Radoski, p. 534, D. Reidel, Hingham, Mass., 1968.

D. W. Datlowe, E. E. Gaines, W. L. Imhof, J. Mobilia, J. B. Reagan, and H. D. Voss, Lockheed Palo Alto Research Laboratory, Palo Alto, CA 94304.

R. A. Helliwell, U. S. Inan, and J. Katsufrakis, STAR Laboratory, Stanford University, Stanford, CA 94305.

R. G. Joiner, Office of Naval Research, Arlington, VA 22217.

JOURNAL OF GEOPHYSICAL RESEARCH, VOL. 90, NO. A7, PAGES 6515-6524, JULY 1, 1985

Bremsstrahlung X Ray Images of Isolated Electron Patches at High Latitudes

W. L. IMHOF, H. D. VOSS, D. W. DATLOWE, AND J. MOBILIA

Lockheed Palo Alto Research Laboratory, California

Small isolated patches of energetic electron precipitation have been observed at high latitudes with a bremsstrahlung X ray imager in the Stimulated Emission of Energetic Particles (SEEP) payload on the polar-orbiting S81-1 satellite. Twenty-nine patches of X rays (>4 keV) with typical widths of ~200 km were observed in June 1982 at invariant latitudes between 65° and 83° with a median latitude of 72.5°. The majority of X ray patches occurred from dusk until dawn, but a few were present in the early afternoon hours. The observed energy spectra were relatively soft (e fold energies about 1.6 keV) and independent of invariant latitude, magnetic local time, or geomagnetic activity. The occurrence frequency of the patches was somewhat greater at times of high geomagnetic activity. The patches were usually oblong by factors up to 3.7, with a median value of 1.75. No strongly preferred alignment was found. Comparisons of the direct electron measurements and the X ray observations from the same satellite have shown that in some cases the small isolated patches of electron precipitation at high latitudes may undergo significant changes in position on time scales of the order of a few seconds.

INTRODUCTION

At high invariant latitudes, existing data and theoretical models suggest there may be isolated patches of electron precipitation into the atmosphere. With direct particle measurements, *Hoffman and Evans* [1968] observed bursts of low-energy electrons poleward of the auroral oval. The polar rain, discovered by *Winningham and Heikkila* [1974] and more recently studied by *Gussenhoven et al.* [1984], can be interrupted by bursts of electrons [*Winningham and Heikkila*, 1974; *Hardy*, 1984]. This sporadic and structured precipitation of soft electrons over the polar caps has been named "polar showers" by *Winningham and Heikkila* [1974]. Also, theoretical studies have advanced the idea of localized plasma entry through the magnetopause involving clouds or plasmoids [*Lemaire*, 1977; *Heikkila*, 1982]. The signatures of plasmoids in the magnetotail have been investigated by *Hones et al.* [1984]. Auroral patches at relatively low latitudes in the trough region equatorward of the diffuse auroral boundary have been reported by *Moshupi et al.* [1979], with precipitating electrons above these auroral forms extending up to 210 keV [*Wallis et al.*, 1979]. Precipitating particle spikes have been observed at high latitudes by *McDiarmid and Burrows* [1965] for >40-keV electrons and by *Brown and Stone* [1972] for ≥425-keV electrons. Isolated patches or islands of energetic electrons were observed in the geomagnetic tail by *Anderson* [1965]. Subsequently, energetic electron bursts in the magnetotail were investigated by others [e.g., *Meng*, 1971; *Meng and Anderson*, 1971; *Keath et al.*, 1976; *Roelof et al.*, 1976]; these may relate to the isolated patches of energetic electron precipitation. Despite these varied observations and theories the structured precipitation of electrons at high latitudes is not well understood, because of the temporal and spatial variations.

The spatial and temporal ambiguities associated with measurements of the structured precipitation of energetic electrons at high latitudes can be improved by observing the bremsstrahlung X ray footprints, preferably with fine two-dimensional spatial resolution over an extended period of time and with complete spectral coverage. Here we present bremsstrahlung X ray images and electron measurements of small isolated patches observed at high latitudes. This paper provides more detailed analysis of data presented in a preliminary form at COSPAR [*Imhof et al.*, 1984].

Copyright 1985 by the American Geophysical Union

Paper number 5A8497
0148-0227/85/005A-8497$05.00

BRIEF DESCRIPTION OF INSTRUMENTATION

The X ray imaging spectrometer was part of the Stimulated Emission of Energetic Particles (SEEP) payload on the S81-1 spacecraft. The satellite was three-axis stabilized in a sun-synchronous 1030 LT and 2230 LT polar orbit at low altitude (170-280 km). The basic design of the spectrometer is described by *Calvert et al.* [1985]. The instrument consisted of a position-sensitive proportional counter using a pinhole camera technique to form a one-dimensional 16-pixel image. The counter was filled with xenon gas, sensitive over the energy range 4 to 40 keV, and had an effective area of 590 cm^2 (40.5 cm × 14.5 cm). The X ray field of view was maintained by the 2 × 15 cm entrance aperture to provide an overall geometric factor of ~6 cm^2 sr (~0.4 cm^2 sr per pixel). Backgrounds associated with penetrating energetic particles were reduced by requiring an anticoincidence with the back plane. The spectrometer was oriented in a forward and downward (35° below horizontal) direction with a field of view of 7° along track by 90° cross track. The field of view was divided into 16 cross-track pixels. The spatial and temporal resolutions were ~30 km and 0.13 s, respectively. Energy spectra of the X rays were measured over 24 channels for the center two pixels (8 and 9) and over eight channels for each of the remaining pixels. X ray mappings were acquired on a worldwide basis over the period May 26 to July 2, 1982.

The SEEP payload also contained an array of silicon solid-state electron spectrometers oriented at various angles to the local vertical and covering an energy range of 2-1000 keV. The central zenith angles for the electron spectrometers were 0°, 10°, 50°, 90°, and 180°. The corresponding pitch angles were dependent upon the location of the spacecraft, but the coverage generally extended from the region of trapping well into the local bounce loss cone. The acceptance half angles and geometric factors are listed in Table 1. The energy spectra were measured with 16 to 256 channels. Several were cooled to ~-120°C to improve the sensor response characteristics [*Voss et al.*, 1982]. The spectrometer that provided the data presented here was oriented at a zenith angle of 90° and had a geometric factor of 0.17 cm^2 sr.

TABLE 1. Electron Spectrometers in SEEP Payload

Central Zenith Angle	Acceptance Half Angle	Geometric Factor (cm^2 sr)
0°	30°	2.47
10°	20°	0.49
50°	20°	0.17
90°	20°	0.17
180°	30°	2.47

OBSERVATIONS

Examples of the bremsstrahlung X ray mappings obtained with the SEEP payload have been shown previously [*Calvert et al.*, 1985; *Voss et al.*, 1983*a*, *b*]. In the present investigation the X ray data were surveyed for the occurrences of small isolated patches of bremsstrahlung X ray emission at high latitudes. For this purpose the following criteria were established: (1) the maximum X ray flux from the central region of the patch must exceed 200 cm^{-2} sr^{-1} s^{-1}, (2) the patch must be completely surrounded by an intensity close to the background level, and (3) the patch full width at half maximum in any direction should not exceed 300 km. A total of 29 isolated patches were noted out of 1022 high-latitude crossings. Examples of the X ray patches are shown in Plates 1*a* and 1*b*. Each section of the plates represents the mapping observed during a different pass of the spacecraft. The invariant latitudes and magnetic local times (MLT) are at the positions of the satellite. The upgoing X rays were always observed from an area ahead of the satellite, and one of the remote sensing pixels viewed the X ray emitting region 17–43 s earlier than the in situ particle measurements; the exact time difference depends upon the magnetic field geometry and the altitude difference between the satellite and the X ray production region. The maps of Plate 1 represent total X ray counting rates for energies of >4 keV except during June 18–23, 1982, when the gain was set lower and the energies were >6 keV. Eleven of the 29 isolated patches were observed during the low-gain period, indicating that the somewhat higher threshold energy did not significantly impact the selection criteria. The patches were generally so pronounced above the background that few if any were probably lost because of the higher threshold energy; thus inclusion of the June 18–23 data should not have altered significantly the frequency dependence upon local time or upon other parameters such as geomagnetic activity. Two of the illustrated passes (June 16 and June 26) also contain an elongated patch or narrow arc spanning the field of view which does not meet the criteria for selection of small patches.

The measured X ray fluxes and energy spectra were compared with those calculated by *Miller and Vondrak* [1985] for various auroral forms. These comparisons revealed several X ray patches with spectral shapes over the energy range ~(4–10) keV that were comparable to certain of the auroral forms, and in those cases the calculated energy deposition rates of Miller and Vondrak were assumed. It was then concluded that for many of the 29 X ray patches presented here

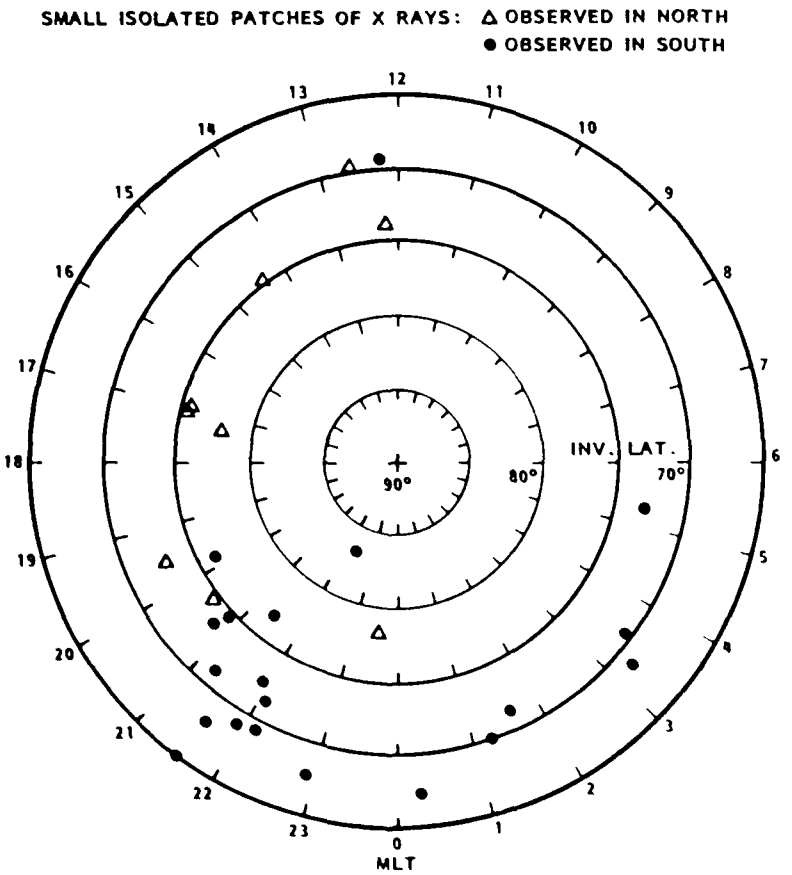

Fig. 1. Positions in invariant latitude and magnetic local time of the isolated patches of X ray emission.

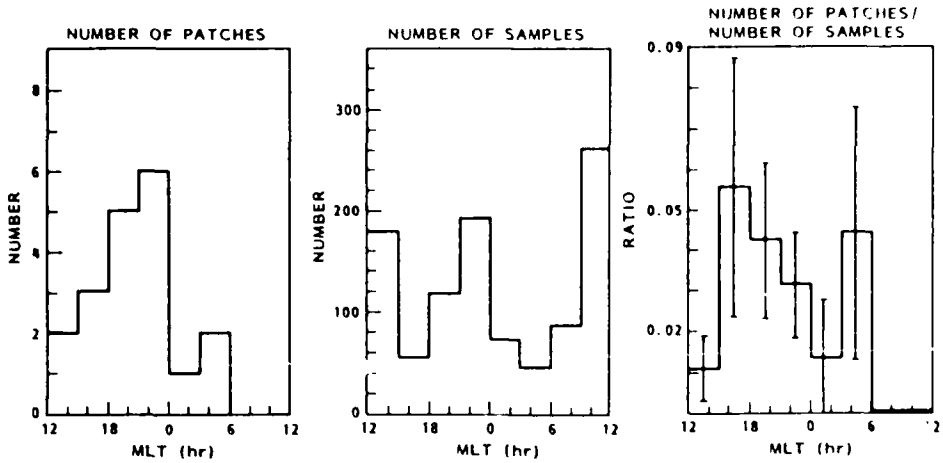

Fig. 2. The number of isolated X ray patches observed in each of eight 3-hour intervals in MLT plotted for events at invariant latitudes of $\geq 70°$. Also shown are the number of sample passes in each of those MLT intervals while crossing an invariant latitude of 72° and the number of event X ray spots divided by the number of samples. Error bars indicate the statistical uncertainties.

the energy inputs to the atmosphere were in the range 0.1–10 ergs $cm^{-2} s^{-1}$ with several being near 1 erg $cm^{-2} s^{-1}$.

The invariant latitude and magnetic local time (MLT) of the isolated patches are summarized in Figure 1. Clearly, the bulk of the patches span the magnetic local time interval from dusk to dawn, with a few in the early afternoon hours. The X ray patches occurred over a rather broad range of invariant latitudes from 65° to 83°, with a median latitude of 72.5°. The dusk to dawn preference spanned all latitudes, but at the lower latitudes the events occurred primarily at times just before midnight. The latter effect may partly reflect the lack of variation in MLT coverage at low latitudes.

In order to study the occurrence frequency of small X ray patches as a function of MLT, the observations were subdivided into 3-hour MLT intervals. The occurrence frequency is plotted in Figure 2 for those occurring at invariant latitudes above 70°. As in Figure 1 the data of Figure 2 indicate the occurrence of spots over a broad range of magnetic local times, with patches rarely appearing in the morning hours. A more quantitative assessment of the local time dependence has been made by correcting for the nonuniform sampling of MLT intervals. The number of patches observed in each of several selected MLT intervals was divided by the number of observations in those intervals while crossing an invariant latitude of 72°, and these ratios are presented in Figure 2. The average value of this ratio is 0.029. Statistical uncertainties are indicated in the plot.

The occurrence frequency of small isolated X ray patches is clearly dependent upon local time, but within the statistical uncertainties there may be no significant difference from dusk until dawn. The patches were found to occur less often at certain geographic longitudes, but that is equivalent to the MLT variation shown in Figure 2 when account is taken of the satellite orbit. Since other parameters may also play an important role in the occurrence frequency, the MLT values of the various X ray spots are plotted in Figure 3 as a function of day in June 1982. Within the limited statistical sample the MLT distribution does not appear to vary significantly during the time period covered, including June 18–23, when the spectrometer was operated with a lower gain. It appears, however, that small X ray patches occurred more often at certain times than others.

The scarcity of X ray events between 0600 and 1200 MLT is consistent with the findings of *Brown and Stone* [1972] for the precipitation of ≥ 425-keV electrons. On the basis of observations of sudden enhancements of energetic electrons in the magnetotail, *Meng* [1971] found that for higher-flux levels the

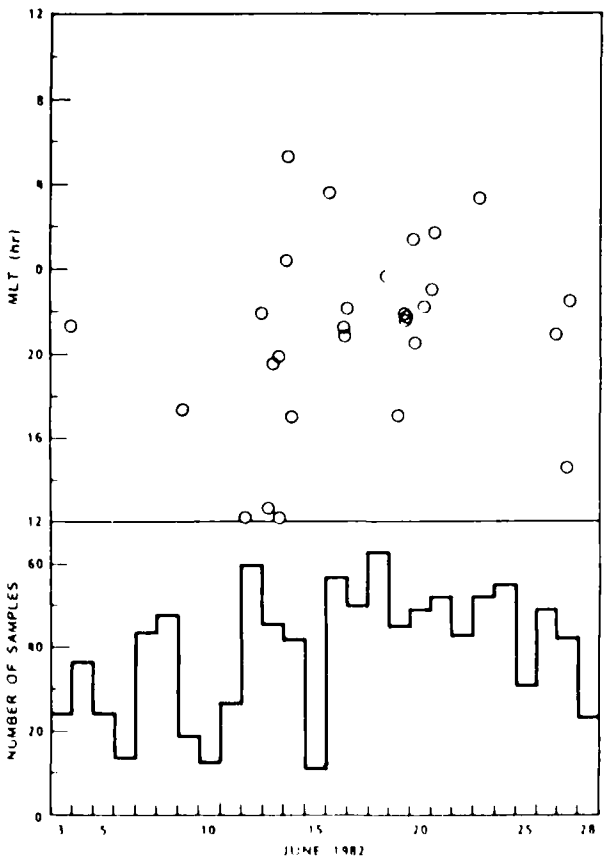

Fig. 3. The MLT values of the observed small isolated X ray patches plotted as a function of time in June 1982. Also plotted in the bottom section are the number of sample passes crossing an invariant latitude of 72°.

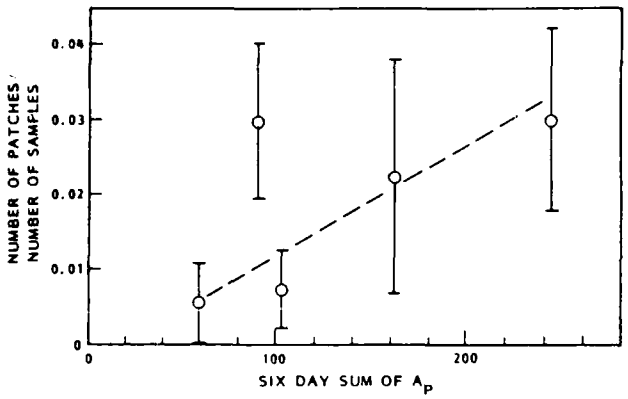

Fig. 4. The number of X ray patches at an invariant latitude of $>70^\circ$ divided by the number of satellite crossings with X ray data acquisition plotted as a function of 6-day sums of the *Ap* index.

occurrence frequency is much greater on the dawnside. However, when the energetic electron flux threshold was selected just above the background level, the occurrence frequency of energetic electrons in the magnetotail was about the same from the duskside to the dawnside. In the present patch data the fluxes were relatively low, and therefore comparisons with Meng should involve his low-flux threshold data. Under these conditions both sets of measurements are consistent with no significant variations in occurrence frequency from dusk until dawn.

The dependence of X ray patch occurrence upon geomagnetic activity level has been investigated. For this purpose the total time period of data acquisition in June 1982 was considered. A 6-day summation interval was selected to provide a compromise between an adequate statistical sampling for each point and a reasonable number of points. For each of these intervals a calculation was made of the number of X ray patches observed at an invariant latitude of $>70^\circ$ divided by the number of satellite crossings when X ray data were acquired, and the resultant points are plotted in Figure 4 as a function of the 6-day sum of *Ap*. Patches were observed during both quiet and disturbed geomagnetic conditions, but they tended to occur more often at times of high *Ap*. Any dependences on *Dst*, which are not shown, were less evident.

For quantitative studies of the distribution in size and direction of the X ray patches, contour plots were generated, and an example is shown in Figure 5. Corrections have been made for the projected dimensions, but in consideration of the low altitude of the satellite a flat earth has been assumed. This example illustrates the contour maps obtained both for an X ray patch that meets the foregoing criteria and for an elongated region of emission that was too long to be considered a small isolated patch. From such contour maps it was found that the patches considered here typically have dimensions of the order of 100–300 km. These sizes are consistent with the direct particle measurements of *McCoy* [1969] which indicate typical widths of 0.25° to 2° in invariant latitude. Similarly, *Brown and Stone* [1972] found that the characteristic widths of the spikes are a few tenths of a degree in latitude. *McDiarmid and Burrows* [1965] reported that 70% of the events have latitude widths of $<2^\circ$.

Isolated narrow regions of X ray emission were observed that were too long to qualify in this study as a small patch. Some of these long and narrow regions were observed at invariant latitudes as high as 75° and were therefore poleward of the auroral oval. In that regard they might be called polar cap arcs [e.g., *Gussenhoven*, 1982; *Hardy et al.*, 1982], but the elongated areas were typically not sun aligned as are polar cap arcs, although there was some tendency for elongation in this direction. Also, because of the limited spatial coverage of the SEEP X ray observations they may not be very long and may merely be modified forms of X ray patches.

For those X ray spots that qualify as patches under the

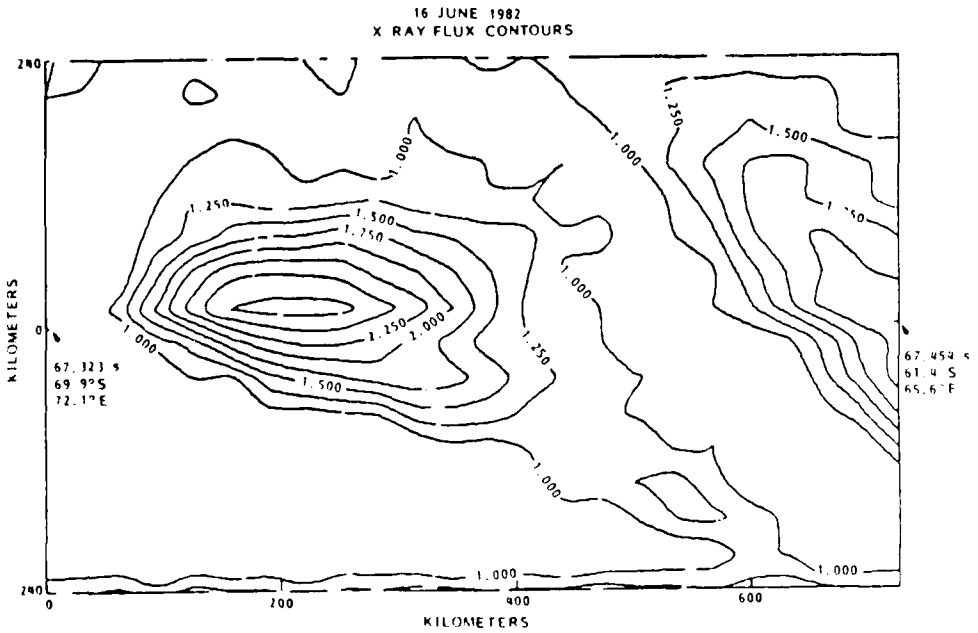

Fig. 5. Examples of the contour plots for an isolated small X ray patch and for an elongated patch. Corrections have been made for the projected dimensions with a flat earth approximation. The contours are labeled by the logarithm to the base 10 of the counts per second.

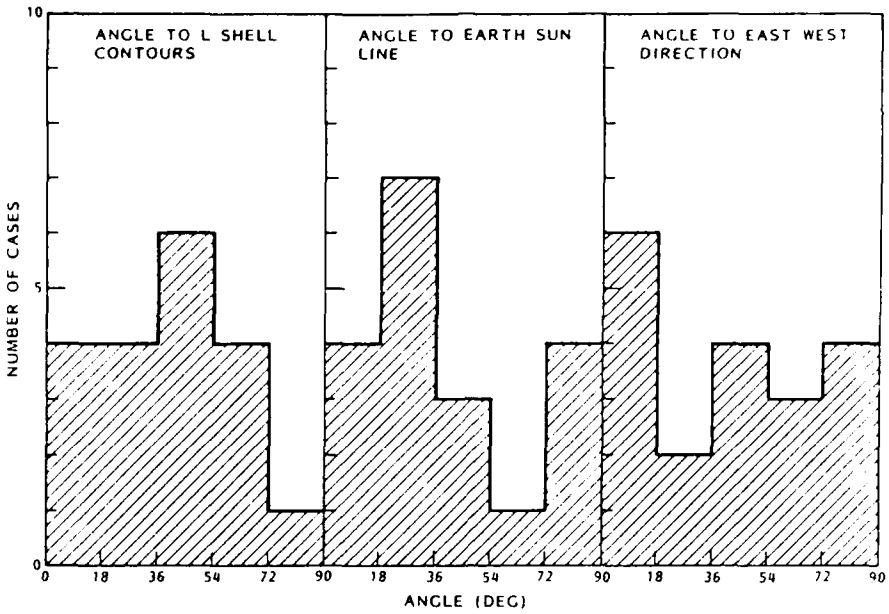

Fig. 6. Distributions in orientation for X ray patches in which the direction of greatest elongation to the length perpendicular to that direction was 1.5 or greater.

present criteria, a study was made of the deviations from being circular. The ratios of the length in the direction of greatest elongation to the length perpendicular to that direction were found to range between 1.1 and 3.7, with a median value of 1.75. For those cases where the latter ratio was 1.5 or greater, the direction of the longest dimension was considered with respect to the orientation of the nearby L shell contours, the earth-sun line, and the east-west direction. There was no strongly favored orientation, as illustrated in Figure 6.

Both the spectral shapes and the intensities of the X rays emitted from the patches spanned a broad range. Preliminary analyses were performed for the spectra from 4 keV to 8–18 keV. The best fit e fold energies associated with the center pixels were found to range from 1 keV to 6 keV with no clear dependence upon invariant latitude, local time, or geomagnetic activity.

Electron spectrometers oriented at various angles to the zenith and measuring electrons from 2 keV to 1000 keV were also included in the satellite payload, thus enabling one to compare the intensities and energy spectra of the X rays with the corresponding parameters for the precipitating electrons. Since the X rays were viewed ahead of the satellite, at high latitudes the intercomparisons must be made for X rays measured at earlier times than the electrons. The comparisons can, of course, only be performed for pixels near the center, and therefore such studies must be limited to satellite passes in which significant fluxes of X rays were observed in one of these pixels. Representative examples of the electron and X ray counting rate profiles for four separate satellite passes, all on June 16, are shown in Figure 7. In the plot are shown the counting rates of the X rays observed in three X ray pixels and the counting rates of electrons of >6 keV observed in the detector at 90° zenith angle. The appropriate X ray pixel was chosen on the basis of the inclination and declination of the magnetic field lines and is plotted as a solid curve. X ray pixels adjacent to the selected one are also shown as dashed curves to provide some indication of the variations in time profile associated with the choice of pixel number. The pixels are numbered 1–16, with 1 being the bottom row in the presentations of Plate 1. The outputs of the other electron detectors at various angles were examined, but in many of the cases studied, this did not lead to significantly different positions of the electron patches. In two of the passes shown in Figure 7, the electron counting rate increased so rapidly with time near the heart of the spike that the output was blocked and the curve is therefore discontinued. The edges of the profiles were generally sharper for electrons than X rays, perhaps because the electrons were measured only at the position of the satellite whereas the X ray observations spanned a zone of ~ 30 km width perpendicular to the satellite path. The electron and X ray plots have been shifted with respect to each other by times corresponding to the expected differences between the two based on the directions of the magnetic field lines and the geometries of the X ray viewing. It was assumed that the X ray production occurred at an altitude of 90 km. For production altitudes of 100 km and 80 km the corresponding changes in time of observation were $+2$ s. For the third and fourth passes in Figure 7 the time profiles of the X rays and electrons are in good agreement with each other, indicating a time stability of the precipitation patch where any implied velocities are no greater than ~ 2 km s. The correspondence between the X ray and electron patches in the first two passes is not as good, but within the experimental uncertainties the data do not indicate a significant movement.

From the 29 patches reported here, on 21 satellite passes a significant flux of X rays was observed to be emanating from pixels near the base of the satellite path. The X ray flux versus time profiles on these passes were compared with the direct electron measurements in the various spectrometers to look for significant time discrepancies, and the conclusions are summarized in Table 2. For reference, all four examples in Figure 7 are in category 2. This investigation has indicated that the electron precipitation patches seem to undergo significant changes on a time scale of a few seconds in three of the

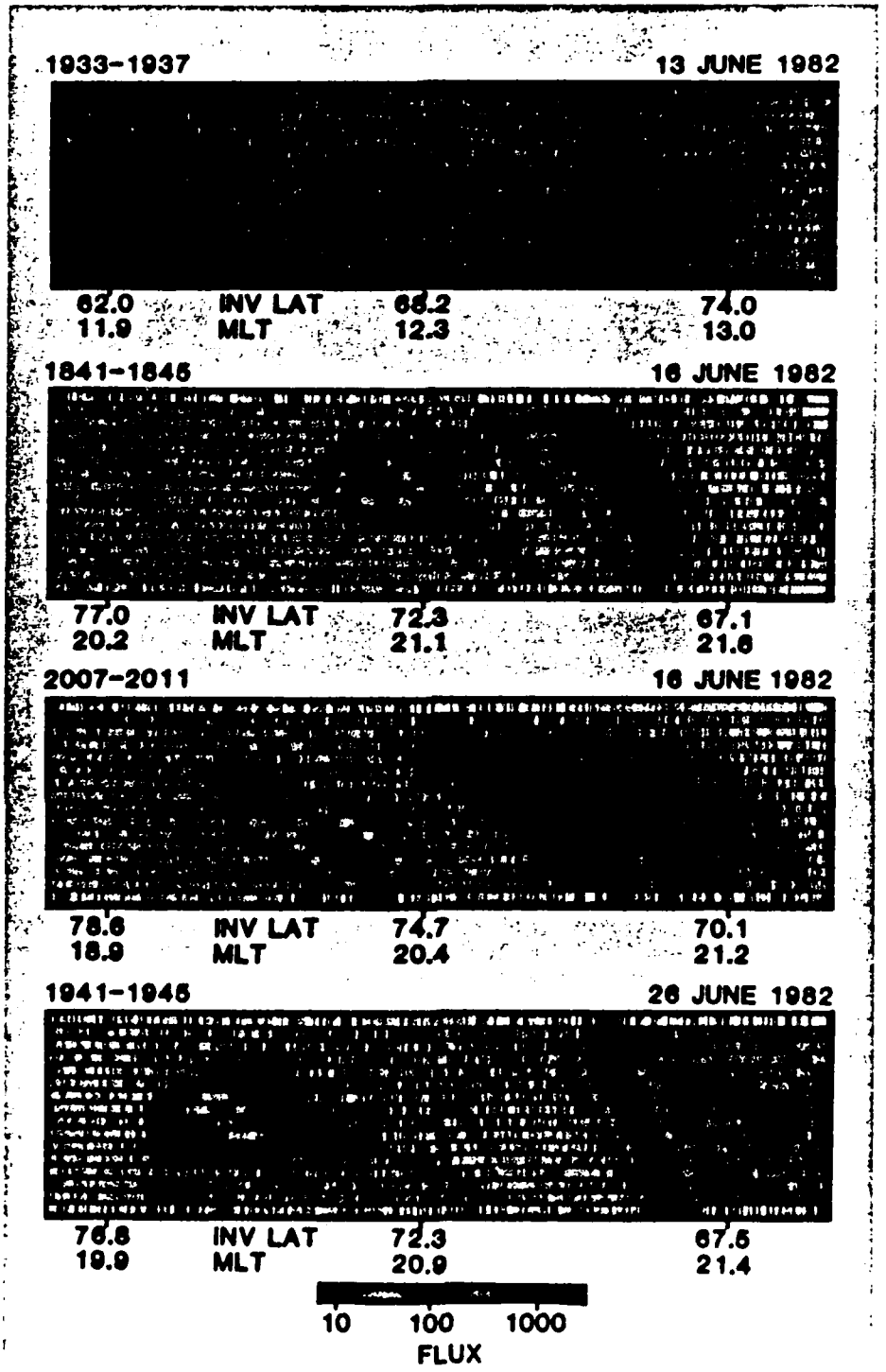

Plate 1*a*

Plate 1. Mappings of the X ray intensities (4–40 keV) observed at high latitudes. The invariant latitudes and the magnetic local times refer to the positions of the satellite. The center pixels view the same position 17–43 s earlier. The fluxes are in units of $cm^{-2}\ sr^{-1}\ s^{-1}$.

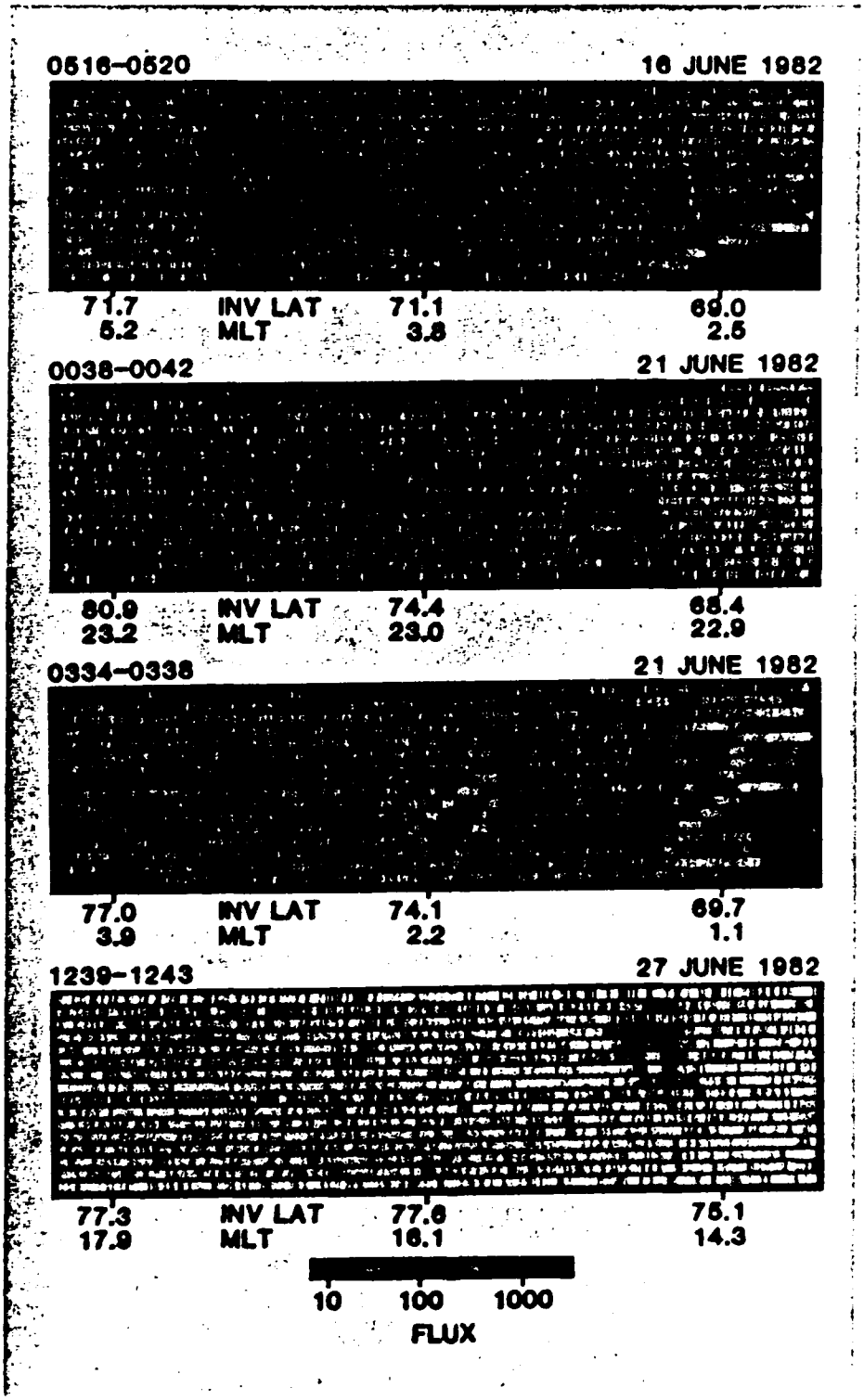
0516-0520
16 JUNE 1982
71.7
5.2
INV LAT
MLT
71.1
3.8
69.0
2.5
0038-0042
21 JUNE 1982
80.9
23.2
INV LAT
MLT
74.4
23.0
68.4
22.9
0334-0338
21 JUNE 1982
77.0
3.9
INV LAT
MLT
74.1
2.2
69.7
1.1
1239-1243
27 JUNE 1982
77.3
17.9
INV LAT
MLT
77.6
16.1
75.1
14.3
10
100
1000
FLUX

Plate 1b

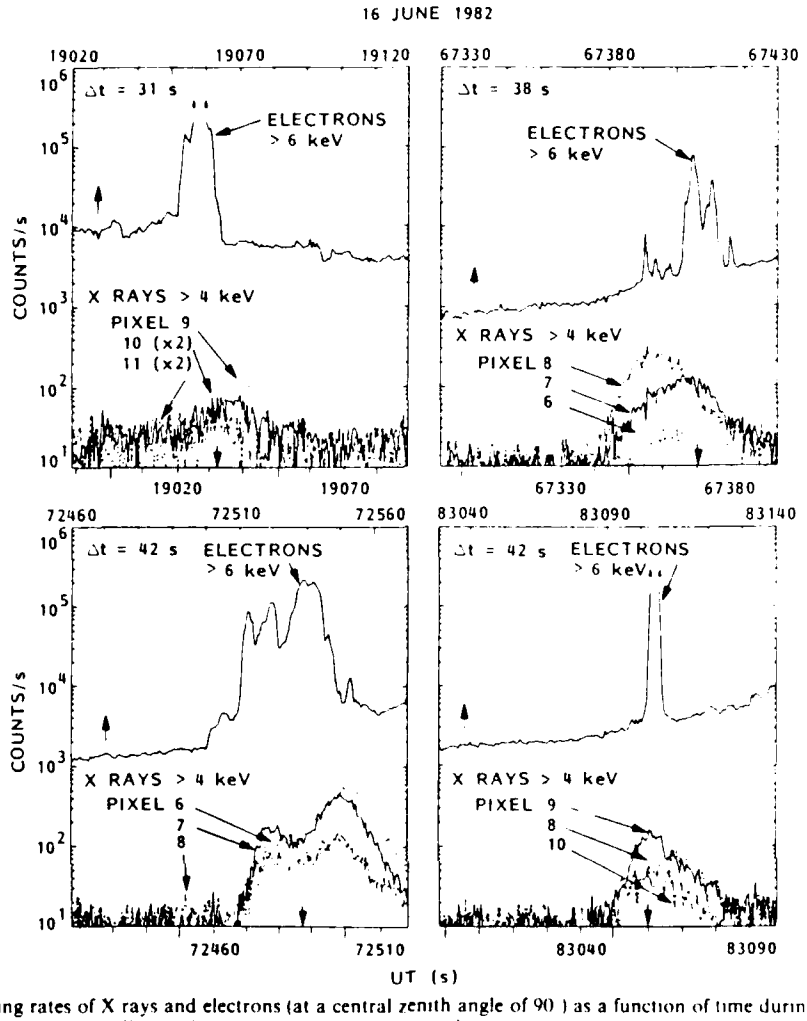

Fig. 7. Counting rates of X rays and electrons (at a central zenith angle of 90°) as a function of time during four passes of the S81-1 satellite. Arrows indicate which time scale (on the top or bottom) is appropriate. The electron and X ray plots have been shifted with respect to each other by times corresponding to the expected differences between the two based on the directions of the magnetic field lines and the geometries of the X ray viewing. These times are indicated.

cases. It is possible that the three cases with inferred velocities of 2–7 km/s were associated with the westward traveling surge during substorms. One of these events, at 1911 UT on June 19, occurred 61 min after the onset of a substorm according to the Boulder Geomagnetic Substorm Log. However, the X ray patch was observed at a longitude about 170° west of the localized substorm position, and therefore the association with a westward traveling surge is not so evident. One of the other events with inferred movement, at 0942 UT on June 14, occurred 112 min after a substorm. On the day of the third event, which occurred at 2136 UT on June 18, there was no distinct substorm activity. With this limited statistical sample one can only suggest the possible association with westward traveling surges. For a more quantitative appraisal the pitch angle distributions of the electrons and the intensities and energy spectra of both X rays and electrons should be considered in detail. However, the spatial and temporal patterns of the precipitation might best be studied with high-altitude observations of the bremsstrahlung X rays over a wide field of view.

For understanding the source mechanisms it is important to consider whether the isolated X ray patches occur simultaneously in both conjugate regions. The question of conjugacy was investigated by considering data acquired with the electron spectrometers on the NOAA 6 and NOAA 7 satellites, which were also in polar orbits, but at higher altitudes (~830 km) and therefore with longer orbital periods (D. Evans, personal communication, 1984). Although these satellites were in different local time planes from the S81-1 spacecraft, at high

TABLE 2. Comparisons of X Ray and Electron Flux Versus Time Profiles

Category	Number of Cases	Observation
1	8	X ray enhancements only at positions where the responsible electrons could not be measured from the satellite
2	10	Well-defined spikes in X ray and electron flux profiles at times consistent with each other or with implied velocities of ~2 km/s or less
3	3	Well defined spikes in X ray and electron flux profiles at times that suggest movement of the precipitation patches with velocities of 2–7 km/s
4	8	Corresponding X ray and electron patches not evident or with time widths that appear to be inconsistent with each other

latitudes, measurements were sometimes made in conjugate hemispheres at nearly the same local time, invariant latitude, and universal time. On five of the 29 X ray spot observations the NOAA 6 or NOAA 7 spacecraft was within a few minutes of the conjugate region. The closest case of nearly simultaneous SEEP electron and X ray data with conjugate NOAA electron measurements was at 2000 to 2008 UT on June 16. The time difference was about 8 min. In that case, enhanced electron fluxes were observed from NOAA 6 in the vicinity conjugate to the X ray patch, but a detailed correspondence between the measurements in conjugate hemispheres was not observed. This situation may reflect either a true lack of conjugacy or merely that the electron precipitation pattern changed significantly during the 8 min between observations. The latter interpretation seems to be consistent with the conclusions drawn from Table 2.

SUMMARY

We have just presented several important characteristics of small isolated patches of electron precipitation observed at high latitudes with X ray imagery. Certain features, such as the dimensions and the local time dependence, are reasonably well defined, but clearly a larger data base would permit a more definitive assessment of other important characteristics such as those associated with the occurrence of conjugacy and the dependence upon magnetic activity. The overall local time characteristics of the localized precipitation events reported here are in good agreement with those reported by *Brown and Stone* [1972] for their type 2 electron spikes. For spikes of this type that were observed at the trapping boundary, Brown and Stone found a tendency to occur conjugately. In the case of the small X ray patches reported here the frequency of occurrence of conjugacy is not known, because of the relatively small size of the data base and the associated lack of simultaneous measurements with particle detectors on other spacecraft.

The electrons responsible for the X ray patches must be of energies above 4 keV and are therefore higher in energy than those primarily associated with the localized polar showers observed by *Winningham and Heikkila* [1974]. The latter electrons typically have energies near 1 keV. Likewise, electrons in the plasma clouds or plasmoids suggested by *Lemaire* [1977] and *Heikkila* [1982] have predominantly energies below those corresponding to the X ray patches. However, some of the patches may be associated with localized plasma clouds that extend up to energies of a few keV.

Small auroral patches and detached arcs at 3914 Å and 5577Å and at latitudes slightly poleward of the plasmapause and equatorward of the present X ray patches have been reported by *Moshupi et al.* [1979]. Above these optical forms the precipitation of particles at energies up to 210 keV was observed by *Wallis et al.* [1979], and it was found that the precipitating electrons carry sufficient energy flux to account for the optical forms. The polar cap arcs were much more extended in space than the regions of electron precipitation considered here and corresponded principally to lower-energy electrons. Furthermore, both the patches and arcs of *Moshupi et al.* [1979] were at lower latitudes than the X ray patches presented here. The Moshupi et al. images were an evening phemonenon with a different magnetic time dependence than those considered here. However, there could be some association between the two types of phenomena.

Comparisons of the direct electron measurements and the X ray observations from the same satellite have shown that the small isolated patches of electron precipitation at high latitudes may undergo significant changes in position on time scales of the order of a few seconds. This dynamic nature of some of the precipitation patches can clearly complicate more quantitative attempts both to study conjugacy and to compare the calculated X ray spectra and intensities with measurements. Recently, *Mizera et al.* [1984] observed strong polar cap structures in X rays between 2 and 78 keV in the northern hemisphere that were not observed by the NOAA 6 and NOAA 7 satellites while crossing the south pole. The authors concluded that either the plasma was very short lived or the polar cap entry of plasma occurred only on northern polar cap field lines. However, the structures presented by *Mizera et al.* [1984] were basically on a much larger spatial scale than the small patches under consideration here.

An investigation has been made of the possible general association of the X ray patches and auroral substorms. It was found that out of the 29 X ray patches observed, five occurred within 61 min of the time of onset of a substorm as listed in the Boulder Geomagnetic Substorm Log. One additional patch occurred 112 min after onset of the substorm. When the *AE* index is available, more correlations might be found, but at present we can only suggest this possibility.

Clearly, more data are needed to achieve a good quantitative understanding of the source mechanism(s) associated with the small X ray patches. The X ray imagery should be performed over a much wider field of view with fine spatial resolution. Also needed is a large body of data for comparison with other geophysical parameters.

In summary, small isolated patches of bremsstrahlung X rays with typical widths of ~200 km have been observed at high latitudes with the following characteristics:

1. The occurrence frequency for satellite paths crossing an invariant latitude of 72° was 2.9% averaged over all MLT.
2. The X ray patches were most often found in the dusk-to-dawn sector, but some were observed at all magnetic local times except the late morning.
3. The locations were at invariant latitudes ranging from 65° to 83°, with a median value of 72.5°.
4. Representative electron precipitation fluxes were of the order of 1 erg cm^{-2} s^{-1}.
5. The median elongations of 1.75 were in no strongly preferred direction.
6. Coordinated electron and X ray measurements indicated that on time scales of 17–43 s the small precipitation patches sometimes underwent significant changes in position or area.
7. The X ray energy spectra typically displayed e fold energies in the range 1–6 keV, with no clear dependence on invariant latitude, MLT, or geomagnetic activity.

Acknowledgments. The experiment was sponsored by the Office of Naval Research (contract N00014-79-C-0824). Appreciation is extended to W. Calvert and T. C. Sanders for their major contributions to the design and development of the X ray imager, to E. E. Gaines for his major role in development of the particle spectrometers, to the ONR program manager, R. G. Joiner, to the payload system engineer, S. J. Battel, to J. B. Reagan and D. P. Cauffman for their program management of the satellite payload development, and to J. C. Bakke for his significant role in the prelaunch operations of the X ray spectrometer.

The Editor thanks C.-I. Meng and another referee for their assistance in evaluating this paper.

REFERENCES

Anderson, K. A., Energetic electron fluxes in the tail of the geomagnetic field, *J. Geophys. Res.*, *70*, 4741, 1965.

Brown, J. W., and E. C. Stone, High-energy electron spikes at high latitudes, *J. Geophys. Res.*, *77*, 3384, 1972.

Calvert, W., H. D. Voss, and T. C. Sanders, A satellite imager for atmospheric X-rays, *IEEE Trans. Nucl. Sci.*, *NS-32*, 112, 1985.

Gussenhoven, M. S., Extremely high latitude auroras, *J. Geophys. Res.*, *87*, 2401, 1982.

Gussenhoven, M. S., D. A. Hardy, N. Heinemann, and R. K. Burkhardt, Morphology of the polar rain, *J. Geophys. Res.*, *89*, 9785, 1984.

Hardy, D. A., Intense fluxes of low-energy electrons at geomagnetic latitudes above 85°, *J. Geophys. Res.*, *89*, 3883, 1984.

Hardy, D. A., W. J. Burke, and M. S. Gussenhoven, DMSP optical and electron measurements in the vicinity of polar cap arcs, *J. Geophys. Res.*, *87*, 2413, 1982.

Heikkila, W. J., Impulsive plasma transport through the magnetopause, *Geophys. Res. Lett.*, *9*, 159, 1982.

Hoffman, R. A., and D. S. Evans, Field-aligned electron bursts at high latitudes observed by OGO 4, *J. Geophys. Res.*, *73*, 6201, 1968.

Hones, E. W., Jr., D. N. Baker, S. J. Bame, W. C. Feldman, J. T. Gosling, D. J. McComas, R. D. Zwickl, J. A. Slavin, E. J. Smith, and B. T. Tsurutani, Structure of the magnetotail at 220 R_e and its response to geomagentic activity, *Geophys. Res. Lett.*, *11*, 5, 1984.

Imhof, W. L., H. D. Voss, J. B. Reagan, D. W. Datlowe, and J. Mobilia, Localized electron precipitation events at high latitudes studied with X-ray imagery from a satellite, paper presented at COSPAR XXV, Graz, Austria, July, 1984.

Keath, E. P., E. C. Roelof, C. O. Bostrom, and D. J. Williams, Fluxes of $\geq$50-keV protons and $\geq$30-keV electrons at $\sim$35 R_E, 2, Morphology and flow patterns in the magnetotail, *J. Geophys. Res.*, *81*, 2315, 1976.

Lemaire, J., Impulsive penetration of filamentary plasma elements into the magnetospheres of the earth and Jupiter, *Planet. Space Sci.*, *26*, 887, 1977.

McCoy, J. E., High-latitude ionization spikes observed by the POGO ion chamber experiment, *J. Geophys. Res.*, *74*, 2309, 1969.

McDiarmid, I. B., and J. R. Burrows, Electron fluxes at 1000 kilometers associated with the tail of the magnetosphere, *J. Geophys. Res.*, *70*, 3031, 1965.

Meng, C.-I., Energetic electrons in the magnetotail at 60 R_E, *J. Geophys. Res.*, *76*, 862, 1971.

Meng, C.-I., and K. A. Anderson, Energetic electrons in the plasma sheet out to 40 R_E, *J. Geophys. Res.*, *76*, 873, 1971.

Miller, K. L., and R. R. Vondrak, A high-latitude phenomenological model of auroral precipitation and ionospheric effects, *Radio Sci.*, *20*, 431, 1985.

Mizera, P. F., D. J. Gorney, and J. L. Roeder, Auroral X-ray images from DMSP-F6, *Geophys. Res. Lett.*, *11*, 255, 1984.

Moshupi, M. C., C. D. Anger, J. S. Murphree, D. D. Wallis, J. H. Whitteker, and L. H. Brace, Characteristics of trough region auroral patches and detached arcs observed by ISIS 2, *J. Geophys. Res.*, *84*, 1333, 1979.

Roelof, E. C., E. P. Keath, C. O. Bostrom, and D. J. Williams, Fluxes of $\geq$50-keV protons and $\geq$30-keV electrons at $\sim$35 R_E, 1, Velocity anisotropies and plasma flow in the magnetotail, *J. Geophys. Res.*, *81*, 2304, 1976.

Voss, H. D., J. B. Reagan, W. L. Imhof, D. O. Murray, D. A. Simpson, D. P. Cauffman, and J. C. Bakke, Low temperature characteristics of solid state detectors for energetic X-ray, ion and electron spectrometers, *IEEE Trans. Nucl. Sci.*, *NS-29*, 164, 1982.

Voss, H. D., W. L. Imhof, J. B. Reagan, R. R. Vondrak, M. Walt, J. Mobilia, D. W. Datlowe, D. P. Cauffman, W. Calvert, and R. G. Joiner, SEEP X-ray imagery of the earth's aurora, *Eos Trans. AGU*, *64*, 792, 1983*a*.

Voss, H. D., et al., *Eos Trans. AGU*, *64*, cover, 955, 1983*b*.

Wallis, D. D., J. R. Burrows, M. C. Moshupi, C. D. Anger, and J. S. Murphree, Observations of particles precipitating into detached arcs and patches equatorward of the auroral oval, *J. Geophys. Res.*, *84*, 1347, 1979.

Winningham, J. D., and W. J. Heikkila, Polar cap auroral electron fluxes observed with ISIS 1, *J. Geophys. Res.*, *79*, 949, 1974.

D. W. Datlowe, W. L. Imhof, J. Mobilia, and H. D. Voss, Lockheed Palo Alto Research Laboratory, 3251 Hanover Street, Palo Alto, CA 94304.

(Received January 22, 1985;
revised March 21, 1985;
accepted March 21, 1985.)

JOURNAL OF GEOPHYSICAL RESEARCH, VOL. 90, NO. A9, PAGES 8333-8342, SEPTEMBER 1, 1985

Multiple Peaks in the Spectrum of Inner Belt Electrons

D. W. DATTLOWE, W. L. IMHOF, E. E. GAINES, AND H. D. VOSS

Lockheed Palo Alto Research Laboratories, California

We report on a systematic study of energetic electron spectra in the inner magnetosphere. The observations were made from the low-altitude satellite S81-1 during the period June–November 1982. The electron spectrometers covered the energy range 6 keV to 1 MeV. In most geographic areas the electron energy spectra are smooth, but in the region of the South Atlantic Anomaly the spectra often consist of a series of broad peaks. The number of peaks is typically three, but may be as many as eight, or in some cases there may be none. The peak-to-valley ratios are often an order of magnitude or more. Peaks in the spectra of electrons from 100 keV to above 1 MeV at higher altitudes have been reported earlier in conjunction with geomagnetic storms. At the 250-km nominal altitude of the S81-1 observations, peaks in the energetic electron spectra are observed on most days and at all levels of geomagnetic activity.

INTRODUCTION

Electron energy spectra observed in the South Atlantic Anomaly region by low-altitude satellites have been reported to exhibit strong peaks. The first report of a single peak in the electron spectrum at 1.5 MeV came from 1963 observations [*Imhof and Smith*, 1966], for which a detailed model of acceleration by drift loss resonance was developed [*Cladis*, 1966]. Additional observations of single and double peaks in the electron spectrum below 1 MeV were made in 1972 [*Imhof et al.*, 1973]. In 1979 the satellite P78-1 observed double, and rarely, multiple, peaks in the spectrum from 68 keV to 1.2 MeV [*Imhof et al.*, 1981*a*]. All of these observations were made in the region of the South Atlantic Anomaly at altitudes of 800 km and below.

We report here on detailed observations of the electron spectrum observed by the S81-1 satellite, which was also part of the Stimulated Emission of Energetic Particles (SEEP) experiment. These measurements were made in the South Atlantic Anomaly region, from L = 1.2 to 2.0. A unique feature of this satellite is the low altitude, a nominal height of 250 km for the data we present here. The observations were made throughout the time span from June to December 1982.

In this region the observed spectrum was typically a series of peaks, with peak-to-valley ratios of an order of magnitude. We report here, for the first time, on the basis of several hundred passes that a series of peaks in the spectrum was normally observed in this region, and that a smooth exponential spectrum was rare. The multiplicity, or number of peaks in the spectrum, was typically three, although as many as eight have been seen. This multiplicity is much greater than previously reported. We have also investigated how the energy of the peaks varies with L and longitude of the observations.

Copyright 1985 by the American Geophysical Union.

Paper number 5A8488
0148-0227/85/005A-8488$05.00

INSTRUMENTATION

These observations were made by energetic electron detectors in the S81-1 payload. The data were taken over a 6-month span from June through December 1982. The orbital inclination was 97.7°, which is a sun synchronous polar orbit. Most of these observations were made at an altitude of about 250 km.

The payload carried an array of instrumentation, but the measurements reported here were made by three solid-state electron spectrometers, in the range 6–1000 keV [*Imhof et al.*, 1983*a*]. The detectors were passively cooled to achieve high resolution. Other characteristics are summarized in Table 1.

The satellite was three-axis stabilized, and the detectors were arranged so that one (ME1) looked upward away from the earth and the second (ME2) looked downward toward the earth. The third detector (TE) was mounted perpendicular to the others, with its axis approximately along the E-W horizontal direction. In most cases the central axis of the TE detector looked at 90° local pitch angle, while the pitch angle of the ME1 (ME2) varied from 0° (180°) at the magnetic poles to 90° at the magnetic equator. For most of the data presented here, the TE detector measured locally mirroring particles. The ME1 and ME2 measured primarily trapped electrons mirroring somewhat below the satellite, but also recorded precipitating and backscattered electrons. At these low altitudes the observed fluxes are not far from the 100-km atmospheric absorbing layer so that local pitch angles near 90° correspond to equatorial pitch angles within a few degrees of the loss cone. In addition, observations in the South Atlantic Anomaly are made where the drift shells come closest to the 100-km level. Therefore we assume that electrons which do not precipitate here will not precipitate at other longitudes and are drifting around the earth with periods in the range of 1 to 3 hours.

Some coordinated observations have been made with one of the electron spectrometers on the P78-1 satellite. This instrument uses a room temperature solid state detector covering the range 68–1170 keV. The detector is on the spinning section of the satellite, obtaining a pitch angle distribution each spin. The orbit is also sun synchronous polar, but at an altitude of approximately 600 km. It began operations in February 1979 and is still returning data.

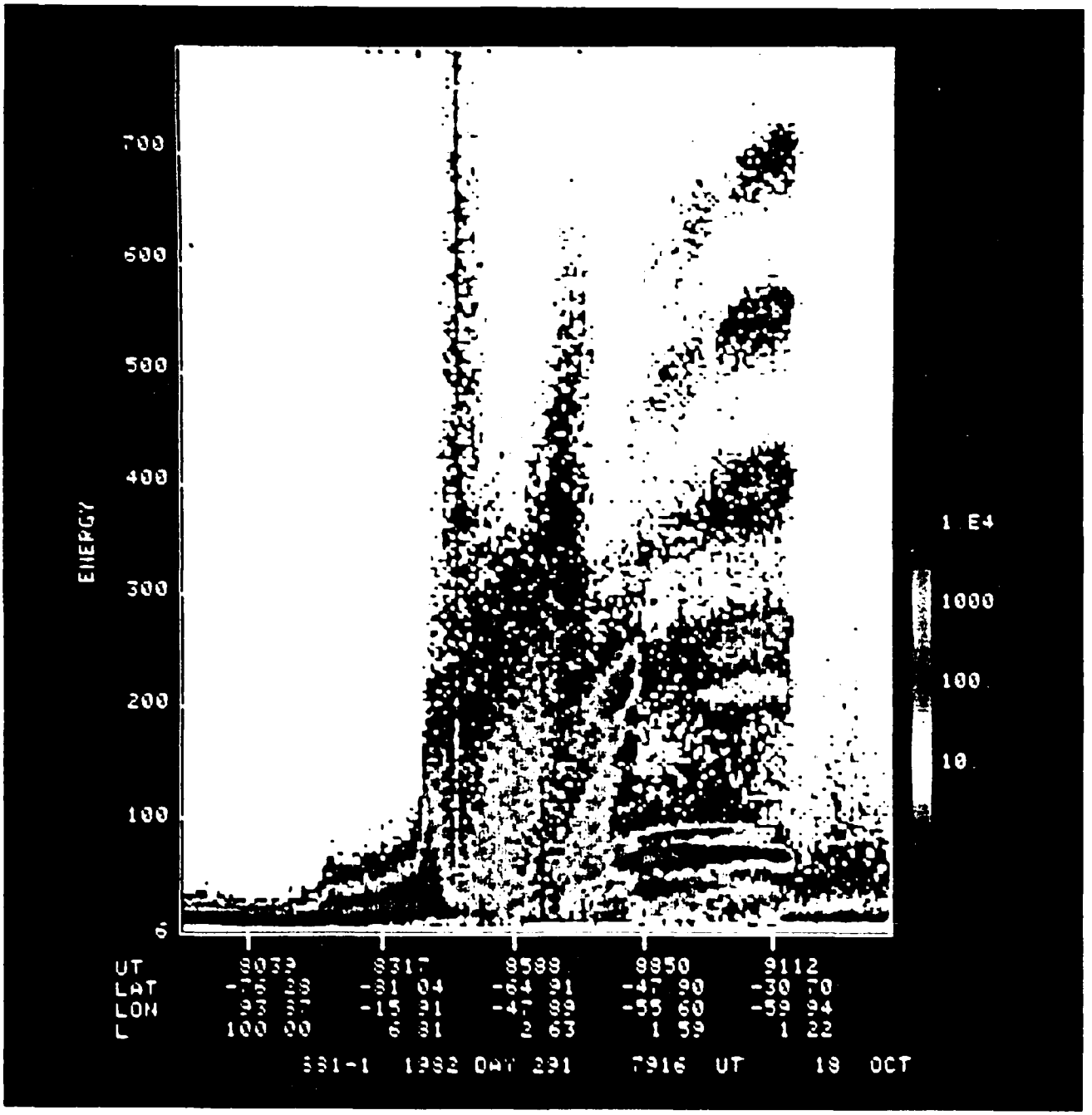

Plate 1. Two-dimensional display of the HE electron spectra versus time. Energies run from 6 keV (bottom) to 1 MeV (top), and time runs from left to right. The electron counting rate is indicated by colors. The approximate conversion from color to electron flux is indicated on the right, but efficiency and dead-time corrections are not included in plotting this figure.

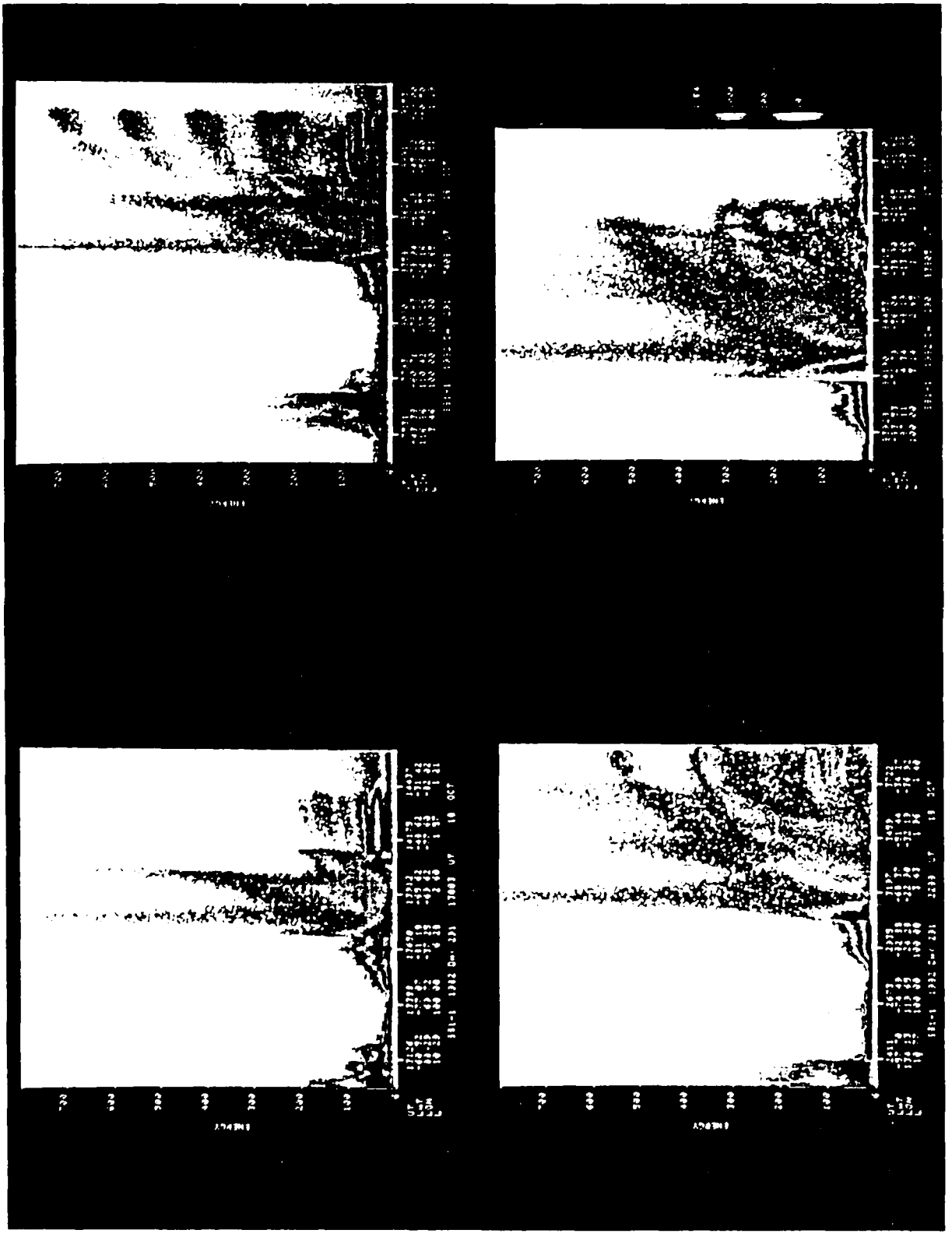

Plate 2. Variation of the observed electron spectra with longitude. The approximate longitudes are 285°, 300°, 320°, and 340°. The upper right frame covers the same time interval as Plate 1.

TABLE 1. Spectrometer Characteristics

Satellite	Detector	Energy Range, keV	Aperture, deg	Geometric Factor cm^2 sr	Zenith Angle, deg
S81-1	TE	6–1000	±20	0.17	90
S81-1	ME1	45–1000	±30	2.47	0
S81-1	ME2	45–1000	±30	2.47	180
P78-1	EEM	68–1120	±15	0.69	spinning

OBSERVATIONS

Because of the high orbit inclination the S81-1 passed over most areas of the earth twice per day. We restrict this discussion to spectra observed in the general region of the South Atlantic Anomaly, but more specifically in the longitude range 300°–360°E and at small L values and southern latitudes. Figure 1 illustrates the basic characteristics of these spectra. The upper set of points comes from the TE detector, while the lower group shows both the ME1 and ME2 points, which overlap. The electron spectra have a series of peaks at 80 keV, 220 keV, 270 keV, 380 keV, 550 keV, and 660 keV. The spectra of electrons mirroring at the altitude of the satellite (TE) have maxima which are an order of magnitude more intense than the neighboring minima, and the electrons mirroring below the satellite have slightly less prominent peaks.

The range of L values over which the peak structures were observed in the anomaly is 1.2 to 2.0. Figure 2 gives a sampling of spectra in this range for the same pass through the region. In this figure, only the detector looking at 90° local pitch angle is shown, to simplify the presentation. It is clear from the figure that peaks can be correlated from one spectrum to the next and that the energy of a given peak increases with decreasing L.

The dependence of the energies of the peaks on L is best displayed by a color-coded display. In Plate 1 the peaks are blue, and the valleys take on the background color. The vertical scale represents energy from 6 keV to 1 MeV, and the horizontal scale is linear in time. Each "spectrum" is an 8-s average, and the total time covered is 25 min. On the left side the satellite is over the south polar cap, a region of very soft spectra. The vehicle moves into the outer belt, a region of hard spectra, with counts being recorded over the entire energy range. The satellite proceeds northward through the slot region and into the South Atlantic Anomaly. In this region the spectrum is seen to split into six branches, with the separation of the peaks increasing with decreasing L. Figure 1 shows a vertical cut through this display at L = 1.31, nearly the northernmost limit of the peaked spectra. At L = 1.20 the electron intensity drops sharply, and equatorward, only detector background is observed.

On a typical observing day, peaks of this type were observed at L = 1.2 over the longitude range 270–345°E. Plate 2 shows the four passes through that region on October 18, 1982. The passes are sequenced from west to east, which is the direction of drift of the energetic electrons, but the time order of the observations runs from latest to earliest. At

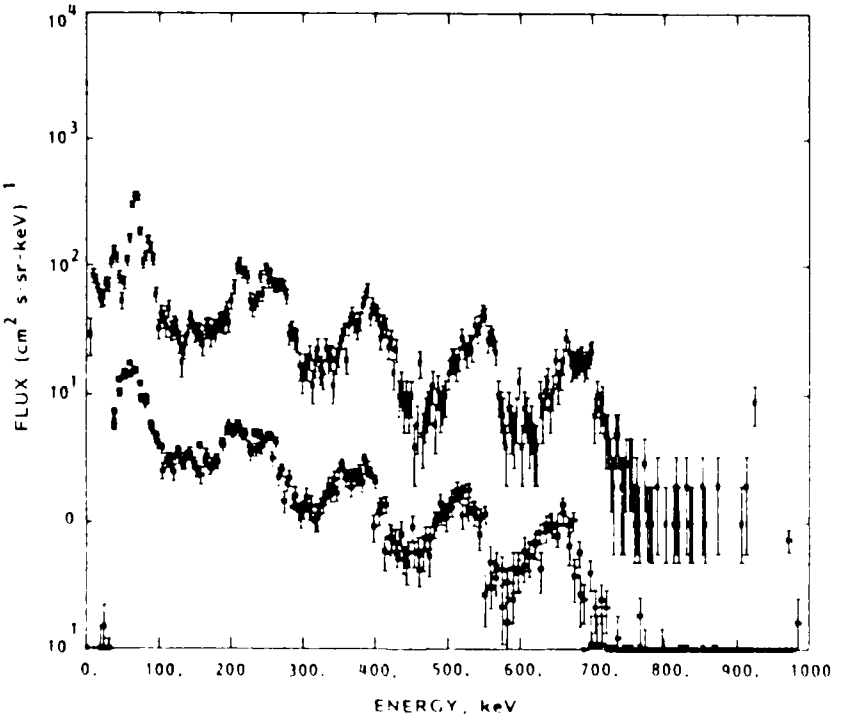

Fig. 1. S81-1 electron spectrum on October 18, 1982. The accumulation was for 30.72 s, starting at 0330:21 UT, covering a range in L of 1.31 to 1.28 (36.6°S to 34.5°S latitude). At that time the satellite was at a longitude of 301°E and an altitude of 285 km, moving northward over the equator. The upper trace gives TE data points. The ME1 and ME2 data points fall on top of each other and appear to be a single trace below.

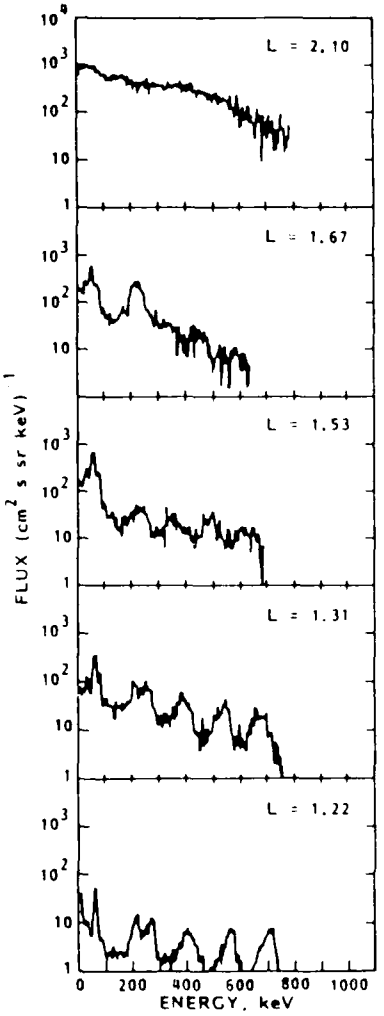

Fig. 2. S81-1 electron spectra at five different L values representative of the range over which the peaks are observed. For clarity, only data from the IE spectrometer are plotted, and the statistical errors are not shown.

the western side of the region the peaks are closely spaced and extend only to 200 keV. Moving 22.5° eastward, the peaks are most distinct and extend to the highest energies, in this case 700 keV (Figures 1 and 2 show data from this pass). At 22.5° farther eastward the separation of the peaks is the largest, but the highest-energy peaks are not seen. In the fourth frame, at about 340° longitude, the peaks are still evident, but the overall structure is irregular. This sequence is typical of the data recorded by the satellite in the South Atlantic Anomaly at L values from 1.2 to 2.0 and at the typical observing altitude of 250 km.

During the course of the S81-1 mission, data from over 600 passes through the South Atlantic Anomaly region at ~250 km were recorded and transmitted. Spectra of this type, with multiple branches, were observed in almost every case. We emphasize that the normal trapped electron spectrum in this region consists of a series of broad peaks.

Isolated cases of spectra of this type have been observed by the P78-1 satellite [*Imhof et al.*, 1981*a*]. In these data, taken at 600 km, the peaks are less prominent. Often spectra observed at this altitude in the anomaly show no peaks, and when they are observed, the peaks are only single or double. The largest number of peaks in a single spectrum ever noted in the P78-1 data is four, on July 15, 1982, after a large geomagnetic storm.

To display the variation of the peak energy with L, we have plotted the center of the four most energetic peaks in Figure 2 as a function of L in the left panel of Figure 3. A satisfactory fit to a linear dependence is obtained. However, we point out that the range of L values and energies is small and that the peaks are broad, so that other functional dependences are possible. The behavior shown here is typical for the peaks we have studied; however, the slope of the fit is different in each case.

One potentially important characteristic of the electron spectral peaks is whether or not the energies of the peaks in a single spectrum are evenly spaced or harmonically related. The peaks in Figure 1 have the appearance of uniform spacing, but the actual values of the energies of the peaks are

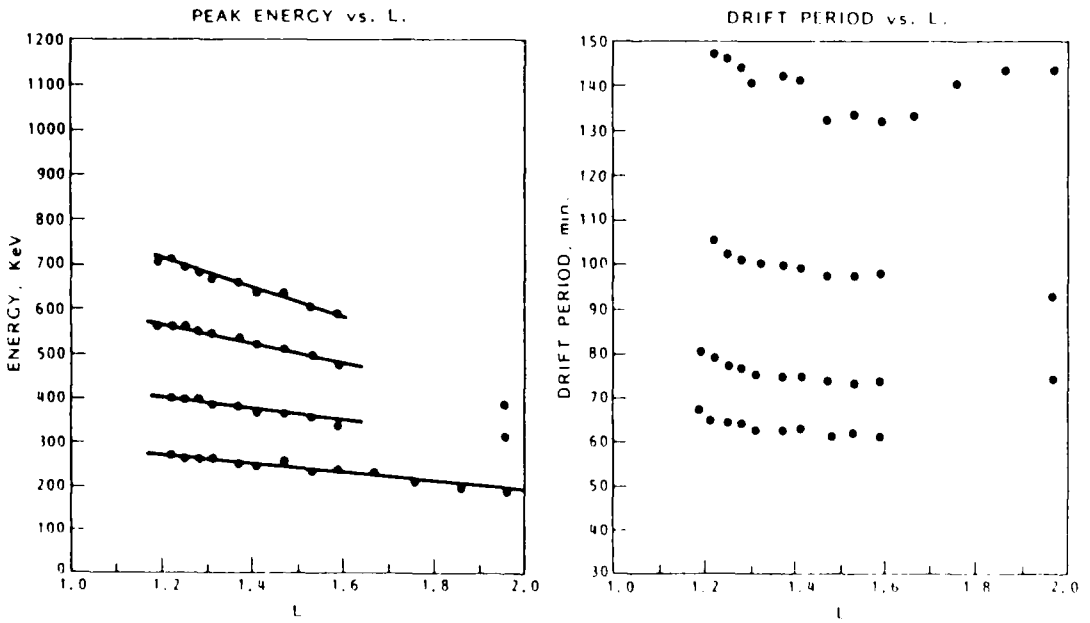

Fig. 3. (Left) The energy of the electron peaks in keV versus L. Each data point is a 30.72 s average. (Right) The calculated drift period for the electrons in the peaks as a function of L.

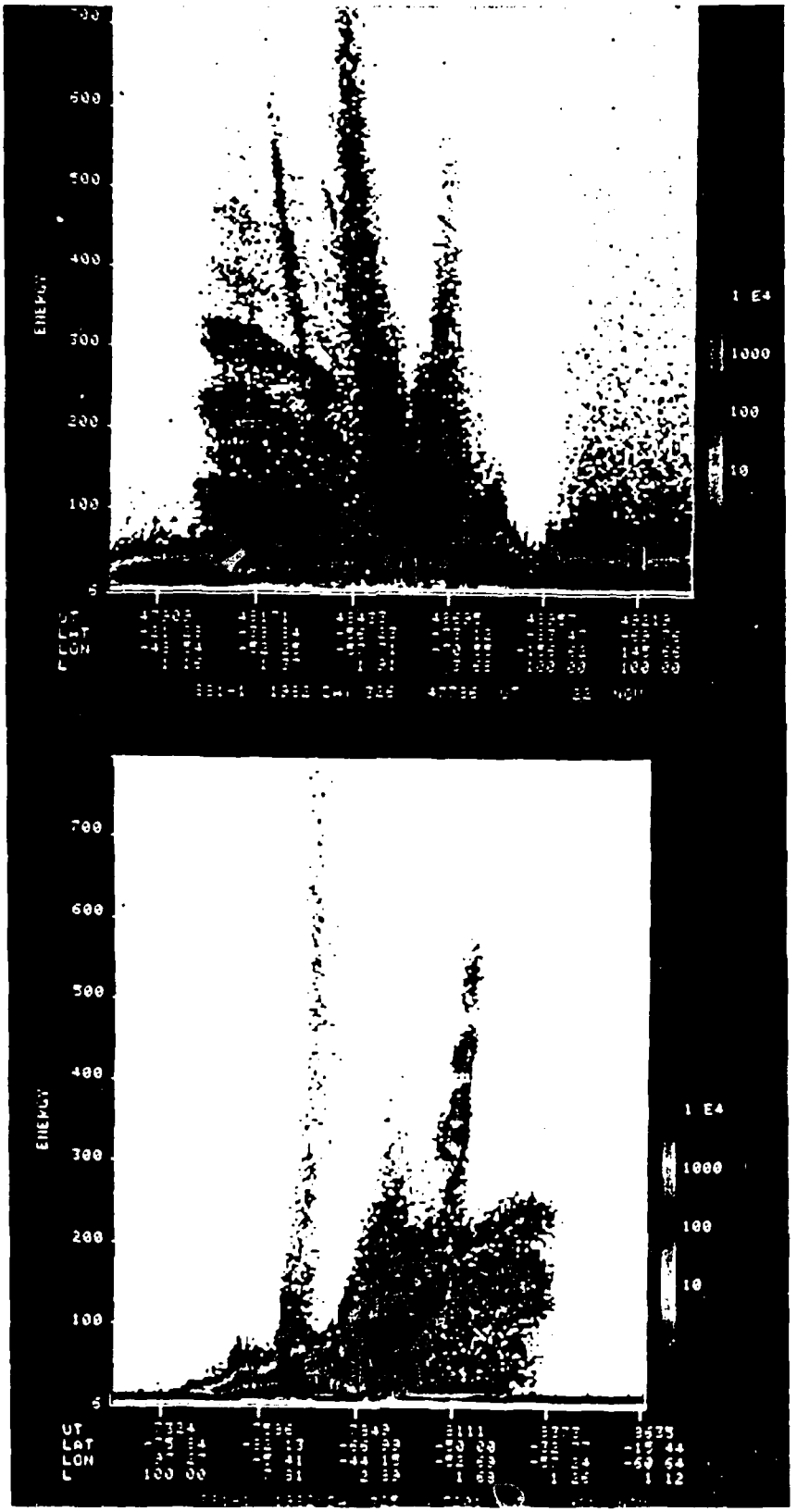

Plate 3 Examples of spectra which show the interplay between the cyclotron resonance loss peak and the multiple peaks. (Top) November 22, 1982, at 48300 s UT. (Bottom) November 21, 1982, at 8200 s UT.

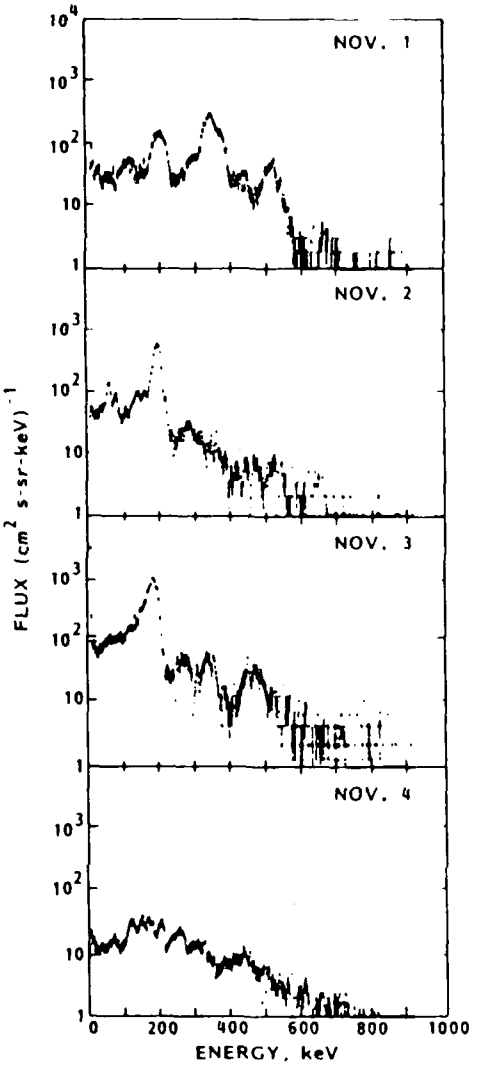

Fig. 4. Illustration of the persistence of peaks from day to day. Spectra from the S81-1 satellite were taken each day at $L = 1.29$. The observing times (all in 1982) were November 1 at 0236 (longitude 300°), November 2 at 0217 (longitude 304°), November 3 at 0200 (longitude 308°), and November 4 at 0141 (longitude 312°).

not evenly spaced. In addition, Plate 2 shows that at other longitudes the spacing between the peaks may be irregular. We have not found any simple relationship between the energies of the individual peaks.

The general characteristics of the peaks observed at one location may be preserved from day to day. Individual peaks increase or decrease in intensity in relation to others, but the energies change slowly. Figure 4 shows electron spectra observed on three successive days in as nearly as possible the same location. The peak at 180 keV becomes more prominent with time, while the peaks at 350 and 530 keV fade out.

In the region of $L = 1.6$–2.0, narrow peaks which vary rapidly with L have been observed previously [*Imhof et al.*, 1973; *Vampola and Kuck*, 1978; *Imhof et al.*, 1983*a*, *b*]. These peaks have been shown to be due to pitch angle scattering by cyclotron resonance interactions with monochromatic VLF waves from ground-based transmitters [*Imhof et al.*, 1981*b*]. Very narrow peaks of this type were observed 204 times by S81-1 in six months of observations.

Plate 3 shows the two types of peaks occurring in a single region. The illustration is in the same format as Plate 1. The top panel shows data from November 22 at ~1325 UT, and the bottom panel shows data from November 21 at ~0215 UT. The sharply rising structure near $L = 1.67$ is a peak in the electron spectrum with a variation in L which is the same as the L variation of the energy for cyclotron resonance at the equator. All of the electrons in the peak which vary rapidly with L can be accounted for as pitch angle scattering from a single frequency source.

The significant feature of this figure is that there appears to be an interplay between the two types of peak structures. In the top panel, note that the rapidly varying structure is intensified as it crosses the energies of the slowly varying

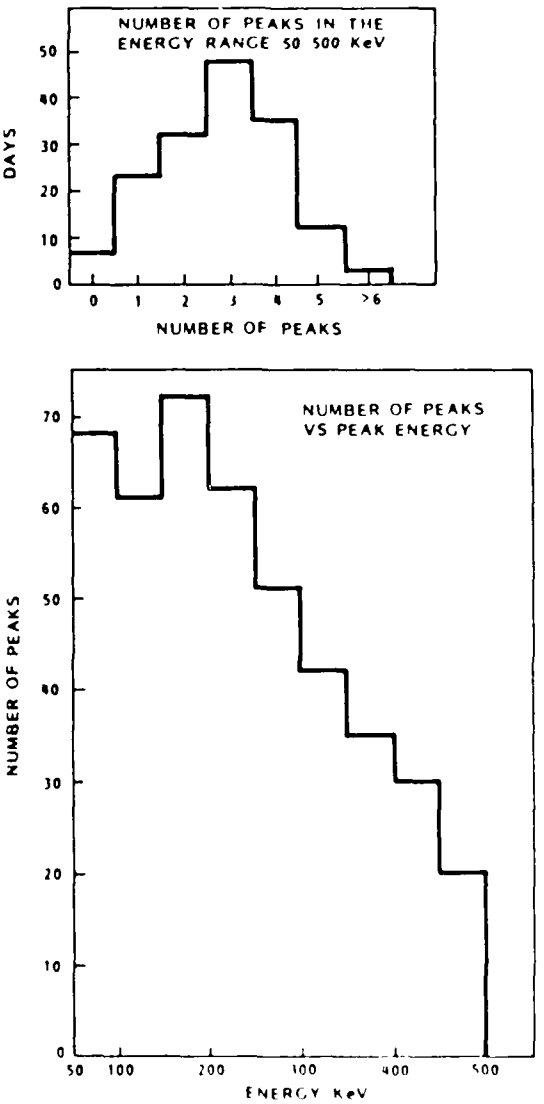

Fig. 5. The statistics of the observed electron energy peaks for each spectrum. For every observing day we have used one spectrum from longitude range 295°–316° and closest to $L = 1.30$. The range of energies runs from 50 keV to 500 keV. (Top) The number of peaks in the spectrum. (Bottom) The frequency of occurrence of a given peak energy in bins 50 keV wide.

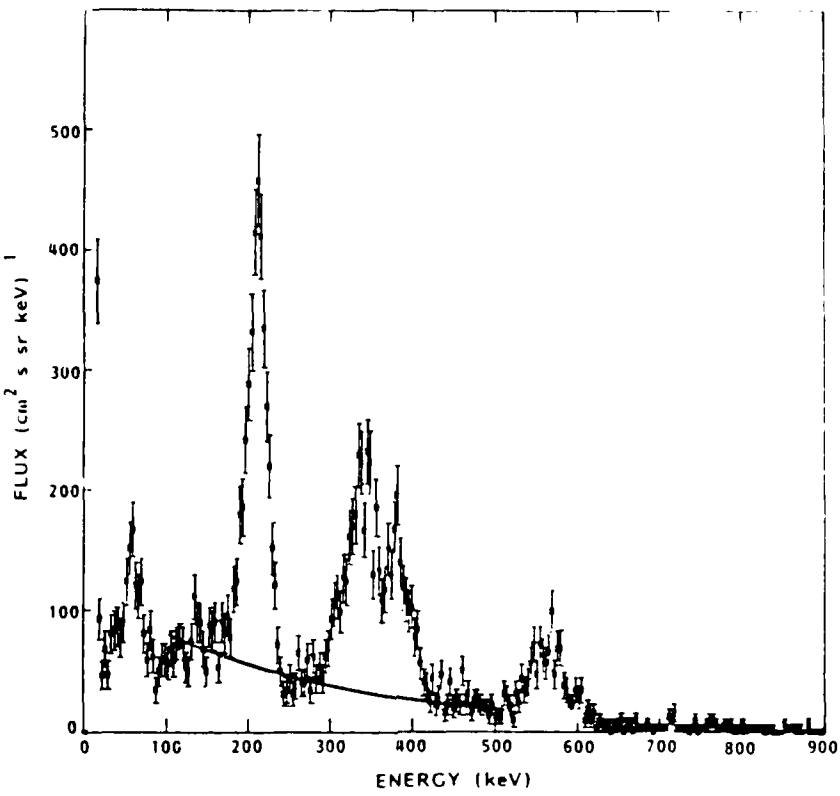

Fig. 6. Resolving the spectrum into peaks and an underlying background. The heavy solid curve represents the function Ae^{-E/E_0}, with E_0 = 200 keV. The data are from November 24, 1982, at 4993 s UT, L = 1.28, and the longitude was 317°E.

peaks. In the bottom panel there are intensifications of the rapidly varying peak which are at the presumed locations of slowly varying peaks which are so weak as to be below the threshold for detection by this instrumentation.

Time Variations in the Spectral Peaks

Since multiple peaks are a regular feature of the electron energy spectrum in the South Atlantic Anomaly, we can study their time variations. To remove spatial variations, we have selected the one nighttime pass per day in which the satellite ground track came closest to a fixed point on the earth. The reference point was at 305° longitude and at an L value of 1.30, with the observations spanning a range of +/−10° in longitude. Data coverage was obtained for 160 of the 176 days from June 13 to December 5, 1982.

For each pass, electron energy spectra up to 500 keV were accumulated for 30.72 s and plotted. Peaks in the plotted spectra were visually identified, and the energies measured. Figure 5 summarizes the results. The top panel shows the number of peaks observed on each of the 160 days. The energy range was 50–500 keV, and peaks above 500 keV were not counted. The distribution has a maximum at three. We observed that there were no peaks in seven cases and, in three cases, six or more were observed. The bottom panel of Figure 5 shows the distribution of the energies of the 449 peaks, plotted in bins 50 keV wide. The range 150–200 keV has the most (72), and the occurrence drops rapidly with increasing energy above that energy.

To separate the flux in the peaks from the flux in the smooth background, a best fit exponential was found for the total flux in the energy range 100–500 keV. The fitting procedure yields two parameters, a characteristic energy E_0 and the total flux over the energy range. The trend line was then lowered to intersect, as accurately as possible, the flux in the spaces between the peaks. The difference between the exponential and the observed spectrum gives a measure of the component of the flux in peaks.

Figure 6 illustrates how we have made quantitative estimates of the flux. Unlike previous illustrations, this figure uses a linear flux scale. The solid curve shows the best estimate of the background spectrum between 100 and 500 keV. The flux above this curve represents the flux attributed to the peaks. The appropriate trend line could be determined for 125 of the 160 days. The result is a time series of the flux in the peaks on a daily basis over the observing period.

Figure 7 shows the flux of electrons in the peaks at L = 1.3 as a function of time; each data point is equivalent to the area above the background in a plot like Figure 6. For comparison, Dst is also plotted. Most of the six large changes in Dst can be matched to an increase in the area under the peaks, as for example on days 195 and 252. However, the flux in the peaks may also be large at times when geomagnetic activity is relatively low, as on day 306. For this reason there is no simple association between geomagnetic storms and the flux in the peaks.

Significant peaks in the electron spectrum from 100 to 500 keV are observed at times of high geomagnetic activity, a point which has been noted by earlier papers. We have shown here, on the basis of a systematic survey of all of the S81-1 coverage, that significant peaks are also seen during

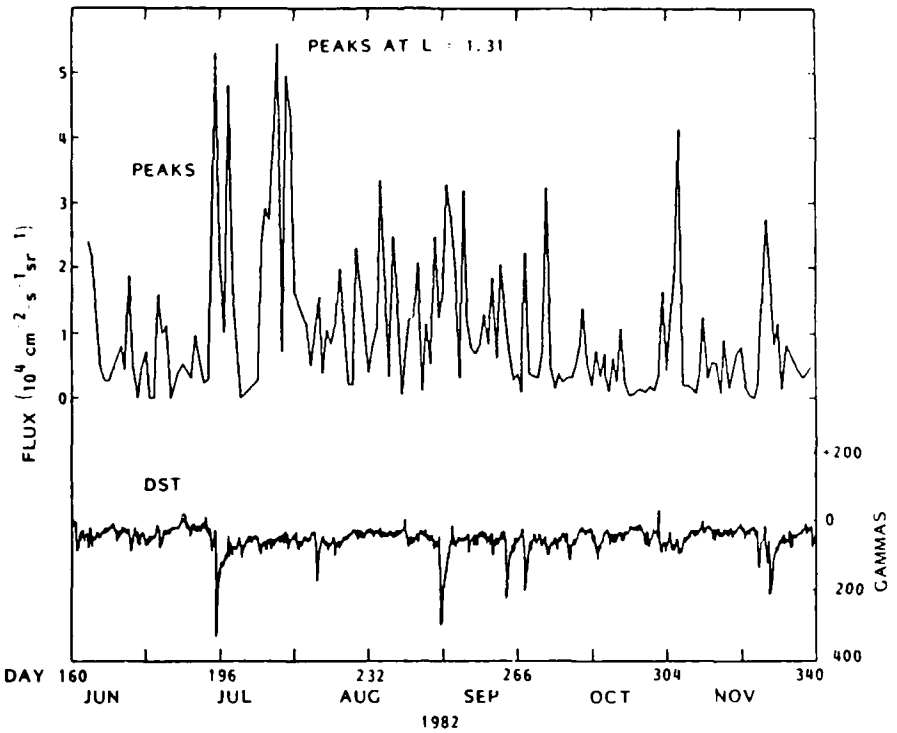

Fig. 7. The time series of the flux in the peaks at L = 1.31 for the data set, with the linear flux scale given at the left. Also plotted along the bottom is the *Dst* for the same time period, with the scale on the right axis.

geomagnetically quiet times and in fact on most days when observing in the South Atlantic Anomaly at an altitude of 250 km. Therefore large geomagnetic storms are not the primary origin of this phenomenon.

Discussion

One model for the formation of these peaks is the drift loss resonance model of *Cladis* [1966]. The time for these observed electrons to drift once around the earth, because of magnetic field curvature and gradients, is in the range of 1 to 3 hours. If there are changes in the equatorial current, as seen in the terrestrial surface field at low latitude, which are resonant with these drift periods, acceleration is expected. The resulting energy redistribution might produce these peaks. Agreement between the peaks observed by the P78-1 satellite in the range L = 1.2–1.4 and the power spectrum of the low-latitude field according to the predictions of this model were reported by *Imhof et al.* [1981*a*].

In the second panel from the top of Figure 4 we have plotted the calculated drift period for an electron with an energy equal to each of the peaks in Plate 1 as a function of L. The magnetic field and electron angular drift rate were calculated using the model of *Olson and Pfitzer* [1974] and scaled to the observed electron energy. The drift period was taken to be 2π divided by the angular drift rate; no longitude variations or accelerations were taken into account.

The result in the second panel of Figure 4 is that the period has a variation of about 5% over the range L = 1.2–1.6. This is not a constant but is much smaller than the variation of peak energy with L. In the other cases we have examined, the drift period deviates from a constant value by about this magnitude. The variations in drift rate are comparable to the P78-1 observations of *Imhof et al.* [1981*a*] over the range L = 1.2–1.5.

A serious problem for this model is the very small energy gain per circuit of the earth, which coupled with the long drift periods gives long acceleration times. The driving fluctuations in the equatorial current are required to maintain coherence over many cycles for this mechanism to be effective. *Williams and Frank* [1984] have considered this same process for the acceleration of medium energy ions observed by ISEE 1. They rejected the process on the grounds that it is too slow, in their case because the acceleration time is long in comparison to the loss of ions by charge exchange.

The S81-1 satellite, with a nominal altitude of 250 km, observed electron spectral peaks at the magnetic minimum, which is the minimum altitude for electrons at a given drift shell value and equatorial pitch angle. Satellites observing at higher altitude should intersect these peaks at the same drift shell and equatorial pitch angle at other longitudes around the world. A crucial test for this model is the longitude distribution of this type of peak at other altitudes. A comprehensive survey of this type is under way using data from the 600-km orbit of the P78-1 satellite.

Summary

1. A series of broad peaks is a prominent feature of the spectrum of energetic electrons near the edge of the loss cone in the region of the South Atlantic Anomaly. The geographic location where we have observed this phenomenon is in the longitude range 270–360°, at L from 1.2 to 2.0, and at a nominal altitude of 250 km.

2. The number of peaks in the energy range 50 keV to

500 keV may be as many as six, although on a few occasions we have observed that there were none. In some cases, peaks up to 1 MeV have been observed.

3. The prediction of constant drift period agrees approximately but not in detail with the observations.

Acknowledgments. This experiment was sponsored by the Office of Naval Research (contract N00014-79-C-0824), and additional support for this investigation came from the Lockheed Independent Research program. The work of S. J. Battel, the payload system engineer, is much appreciated. Thanks also go to B. Beck, K. Van Stone, and J. McGlennon for their efforts in the data reduction.

The Editor thanks A. Vampola and another referee for their assistance in evaluating this paper.

REFERENCES

Cladis, J. B., Resonance acceleration of particles in the inner radiation belt, in *Radiation Trapped in the Earth's Magnetic Field*, edited by B. M. McCormac, pp. 112–115, D. Reidel, Hingham, Mass., 1966.

Imhof, W. L., and R. V. Smith, Low altitude measurements of trapped electrons, in *Radiation Trapped in the Earth's Magnetic Field*, edited by B. M. McCormac, pp. 100–111, D. Reidel, Hingham, Mass., 1966.

Imhof, W. L., E. E. Gaines, and J. B. Reagan, Dynamic variations in intensity and energy spectra of electrons in the inner radiation belt, *J. Geophys. Res.*, *78*, 4568, 1973.

Imhof, W. L., E. E. Gaines, and J. B. Reagan, High-resolution spectral features observed in the inner radiation belt trapped electron population, *J. Geophys. Res.*, *86*, 2341, 1981*a*.

Imhof, W. L., R. R. Anderson, J. B. Reagan, and E. E. Gaines, The significance of VLF transmitters in the precipitation of inner belt electrons, *J. Geophys. Res.*, *86*, 11,225, 1981*b*.

Imhof, W. L., J. B. Reagan, H. D. Voss, E. E. Gaines, D. W. Datlowe, J. Mobilia, R. A. Helliwell, U. S. Inan, J. Katsufrakis, and R. G. Joiner, Direct observation of radiation belt electrons precipitated by the controlled injection of VLF signals from a ground-based transmitter, *Geophys. Res., Lett.*, *10*, 361, 1983*a*.

Imhof, W. L., J. B. Reagan, H. D. Voss, E. E. Gaines, D. W. Datlowe, J. Mobilia, R. A. Helliwell, U. S. Inan, J. Katsufrakis, and R. G. Joiner, The modulated precipitation of radiation belt electrons by controlled signals from VLF transmitters, *Geophys. Res. Lett.*, *10*, 615, 1983*b*.

Olson, W. P., and K. A. Pfitzer, A quantitative model of the magnetospheric magnetic field, *J. Geophys. Res.*, *79*, 3739, 1974.

Vampola, A. L., and G. A. Kuck, Induced precipitation of inner zone electrons, *J. Geophys. Res.*, *83*, 2543, 1978.

Williams, D. J., and L. A. Frank, Intense low-energy ion populations at low equatorial altitudes, *J. Geophys. Res.*, *89*, 3903, 1984.

D. W. Datlowe, E. E. Gaines, W. L. Imhof, and H. D. Voss, Lockheed Missiles and Space Co., Inc., Department 91-20, Building 255, 3251 Hanover Street, Palo Alto, CA 94304

(Received January 21, 1985;
revised April 22, 1985;
accepted April 23, 1985.)

JOURNAL OF GEOPHYSICAL RESEARCH, VOL. 91, NO. A3, PAGES 3077–3088, MARCH 1, 1986

Relativistic Electron and Energetic Ion Precipitation Spikes Near the Plasmapause

W. L. IMHOF, H. D. VOSS, J. B. REAGAN, D. W. DATLOWE, E. E. GAINES, AND J. MOBILIA

Lockheed Palo Alto Research Laboratory, Palo Alto, California

D. S. EVANS

National Oceanic and Atmospheric Administration, Boulder, Colorado

An investigation has been made of electron and associated ion precipitation spikes near the plasmapause that are narrow in L shell and in which relativistic electrons are favored. The electron energy spectra during the spikes sometimes had equivalent e fold energies in excess of 500 keV. In approximately 31% of these spike events observed from the low-altitude polar orbiting satellites P72-1, P78-1, and S81-1, nearly simultaneous precipitation was measured in energetic ions above ~30 keV at about the same L value. Several of the precipitation spikes occurred primarily in the drift loss cone, but in some cases, significant precipitation ($\sim 10^{-2}$ ergs/cm^2 s) was also observed in the bounce loss cone. The electron spikes occurred preferentially in the evening sector, and all of the associated narrow ion spikes were in that local time interval. Narrow relativistic electron spikes were observed on less than 1% of the crossings of the plasmapause. From the set of S81-1 events a search was made for those also observed on the NOAA 6 spacecraft. On rare occasions, nearly simultaneous (< 2000 s) narrow spikes with hard electron spectra were found at approximately the same L value from both spacecraft and at longitudes differing by 8°–47°. These findings suggest a patchy profile, sometimes with an arc structure which may extend over longitude intervals as great as 25° and time intervals as long as 2000 s. From consideration of the AE index for 17 events, 12 were found to occur close to the times of substorms. The spike precipitation is interpreted in terms of cyclotron resonance wave-particle interactions involving radiation belt particles, the narrow widths being associated with fine structure in the cold plasma density profiles near the plasmapause and the energy selectivity associated with an upper frequency cutoff in the waves.

INTRODUCTION

The possibility that relativistic electrons can undergo a cyclotron resonance with electromagnetic ion cyclotron waves that are associated with proton precipitation was first suggested by *Thorne and Kennel* [1971]. They indicated that relativistic electron precipitation may be parasitic, i.e., driven by waves generated by the precipitation of ring current protons. One of the predictions of this mechanism is that relativistic electron precipitation should be correlated with more intense low-energy (5–50 keV) proton precipitation fluxes along the bulge region of the plasmapause. However, such precipitation processes may only apply to highly relativistic electrons when finite temperatures are considered, as shown by *Davidson* [1978].

Relativistic electron precipitation phenomena in conjunction with ion precipitation might best be studied when confined to a narrow latitude interval. Narrow L shell bands of electron precipitation in the outer radiation belt were reported by *Koons et al.* [1972], and simultaneous wave measurements indicated that the electrons were pitch angle scattered in the presence of intense ELF electrostatic waves. The precipitating electrons were several hundred keV in energy, but associated proton measurements were not presented. Narrow zones of preferentially relativistic electron precipitation were first reported by *Imhof et al.* [1977], but no attempt was made to correlate the phenomenon with ion precipitation. Relativistic electron precipitation events that occur over a narrow latitudinal zone embedded within a broader region of intense energetic ion precipitation were presented by *Thorne and Andreoli* [1980]. In that study, four events were found with a well-defined threshold energy for electron precipitation which they attributed to electromagnetic ion cyclotron waves. Single and multiple peaks in precipitating protons of > 120 keV having a narrow distribution in L above a smooth continuum were reported by *Reagan et al.* [1975]. Spiky structures in proton precipitation were also observed by *Koons* [1975].

In the present paper we specifically address only events involving the preferential precipitation of high-energy electrons over a narrow range in L shell and look for associated ion precipitation in those events. We avoid the preferential high-energy precipitation near the trapping boundary, which often displays hard spectra with shapes that vary strongly with L [*Imhof et al.*, 1979]. In addition to finding nearly simultaneous ion precipitation during two of the relativistic electron events previously published by *Imhof et al.* [1977], we report the results of a study of this class of events with data acquired on the P78-1, the S81-1, and the NOAA 6 spacecraft. From the data presented it is concluded that many of the spikes may have resulted from wave-particle interactions between radiation belt particles and low-frequency waves. The narrowness of the spikes may be associated with fine structure in the cold plasma densities near the plasmapause where many of the events occurred.

DESCRIPTION OF THE INSTRUMENTATION

In this paper, use is made of data acquired on four polar orbiting satellites. The pertinent instrumentation in each of these is listed in Table 1. In the data analysis, L values were calculated using the Goddard Space Flight Center (GSFC 12/66) geomagnetic field model [*Cain et al.*, 1967] for the epoch 1972 (P72-1 data) or the epoch 1980 (P78-1, S81-1, and NOAA 6)

Copyright 1986 by the American Geophysical Union.

Paper number 5A8827
0148-0227/86/005A-8827$05.00

TABLE 1. Electron/Proton Detectors

Satellite				Particle Detectors					
Name	Altitude, km	Local Time	Spinning (Period) or Oriented	Name	Type	Threshold Energy	Geometric Factor, cm^2 sr	Acceptance Angle, deg	Mirroring or Precipitating
P72-1	736–761	Noon, midnight	Spinning (5 s)	EEM 001	Electrons	160 keV	0.36	±20	Both
				LEP 001	Ions	120 keV	0.09	± 8	Both
				Anti for Ge spectrometer	Electrons	3–4 MeV	...	Omni	Both
P78-1	550–625	Noon, midnight	Spinning (5.5 s)	EEM 002	Electrons	68 keV	0.69	±15	Both
				LEP 002	Ions	60 keV	0.1	± 16	Both
				Anti for Ge spectrometer	Electrons	3–4 MeV	...	Omni	Both
S81-1	170–280	1030, 2230	Oriented	ME 1	Electrons	45 keV	2.47	±30	Precipitating (zenith)
				TE 2	Electrons	6 keV	0.17	±20	Mirroring (90° to zenith)
				LE 4	Ions	50 keV	0.1	±10	Both (50° to zenith)
				Anti for ME 1 spectrometer	Electrons	1–6.5 MeV	...	Omni	Both
NOAA 6	800–830	0730, 1930	Oriented	Electron spectrometer	Electrons	30 keV	0.0095	±15	Precipitating (zenith)
				Electron spectrometer	Electrons	30 keV	0.0095	±15	Mirroring (81° to zenith)
				Proton spectrometer	Protons	30 keV	0.0095	±15	Precipitating (zenith)
				Proton spectrometer	Protons	30 keV	0.0095	±15	Mirroring (83° to zenith)

All of the particle spectrometers contained silicon solid state sensors except for the EEM 001 instrument, which consisted of a plastic scintillator. Each provided energy spectral information through pulse height analysis. The electron spectrometers on the P72-1 and P78-1 spacecraft are described by *Imhof et al.* [1979] and *Imhof et al.* [1981], respectively. The proton spectrometer on the P72-1 satellite was described by *Reagan et al.* [1975]. Each of the payloads on the P72-1 and P78-1 satellites also contained large-volume anticoincidence scintillator shields which responded to electrons above a relatively high threshold energy. These anticoincidence counters provided no spectral information but had a high sensitivity and were therefore suitable for detecting relativistic electron precipitation spikes. The anticoincidence counter surrounding the Germanium spectrometer on the P72-1 satellite consisted of a plastic scintillator and is described by *Nakano et al.* [1974], whereas those in the Germanium spectrometers on the P78-1 spacecraft consisted of sodium iodide (polyscin) and are described by *Nakano et al.* [1980].

The payload in the SEEP (Stimulated Emission of Energetic Particles) experiment on the S81-1 spacecraft contained an array of cooled silicon solid state detectors to measure electrons and ions directly with high-sensitivity and fine energy resolution [*Voss et al.*, 1982]. The anticoincidence counter surrounding the ME 1 spectrometer consisted of a plastic scintillator.

The Space Environment Monitor on the NOAA 6 satellite includes a set of silicon solid state detectors which measure the intensity of electrons and ions above 30 keV. Two electron and two proton detector systems are mounted in pairs, one of each type oriented to view zenith, the other two viewing at 83° (protons) and 81° (electrons) to the first pair in a plane perpendicular to the orbit plane. For the events studied here the detector pair which viewed zenith was measuring precipitating particles, whereas the other pair detected particles with local pitch angles near 90°.

PRESENTATION OF DATA

Examples of Events Observed From Single Spacecraft

Data from three satellites, P72-1, P78-1, and S81-1, were individually surveyed to find narrow spikes (less than 10 s observing time) in the fluxes of electrons above energies of ~4 MeV, ~3.5 MeV, or 1–6.5 MeV, respectively. The number of events was 9, 8, and 24, from 8, 14, and 7 months of survey in 1972–1973, 1979–1980, and 1982, respectively. In all cases the selection criteria required that the flux enhancements were not associated with the isotropic pitch angle distribution commonly present at the trapping boundary.

The narrow energy selective electron precipitation events reported here are uncommon in that only 41 events in the P72-1, P78-1, and S81-1 data were found from a survey of many orbits. A quantitative assessment of the frequency of onset of events and intercomparisons between the occurrence rates observed by the vehicles during various time periods is limited by the unavoidably different event criteria used in each case and the varying portions of the complete data sets that were analyzed. The threshold energies and geometric factors for detecting events in the anticoincidence counters were not the same, and two vehicles (P72-1 and P78-1) were spinning, whereas the S81-1 satellite was oriented. However, one can state that the narrow ($\lesssim$10 s duration in the spacecraft frame) relativistic electron precipitation spikes were observed to occur on less than 1% of the crossings of the plasmapause. Accordingly, this particular class of precipitation does not represent a major contribution to the losses of particles from the radiation belts. However, they are important to study, because the electron and ion precipitation enhancements are often nearly simultaneous and narrow in time or L shell and therefore present a unique opportunity to study the precipitation processes.

Out of the total of 41 narrow energy selective electron precipitation events reported here in the P72-1, P78-1, and S81-1

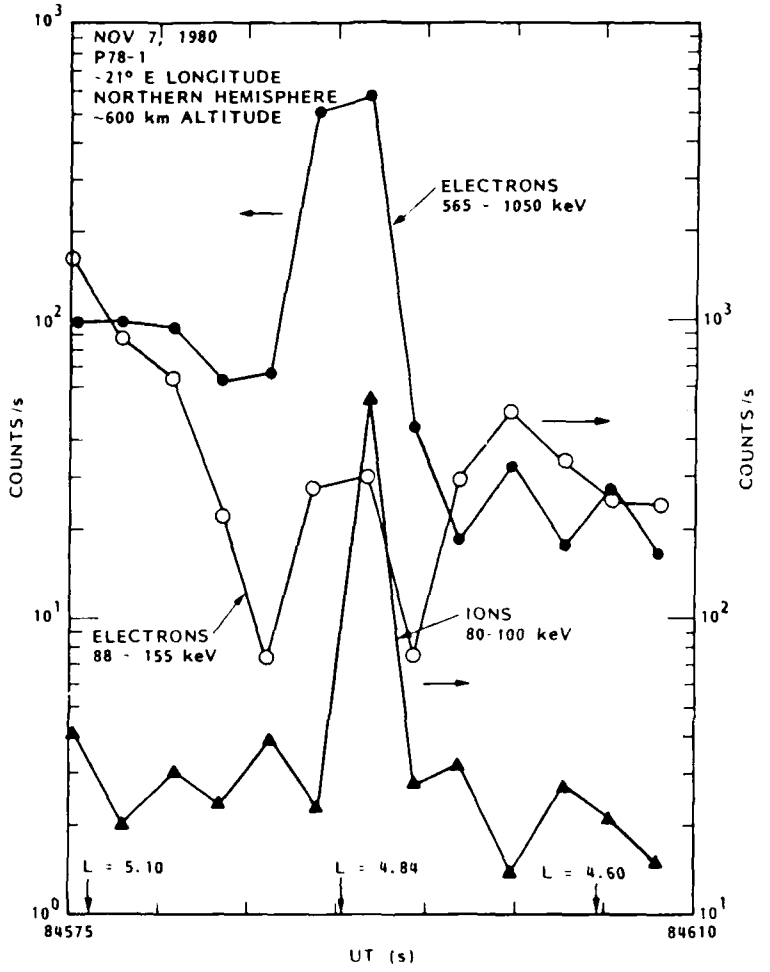

Fig. 1. The counting rates observed with the EEM 002 and LEP 002 spectrometers on the P78-1 satellite for electrons and ions in selected energy intervals and at local pitch angles near 90°. Arrows indicate the applicable vertical scale in each case.

data, nine of these events also contained a narrow zone of energetic ion precipitation at nearly the same time and L shell. However, in these nine cases, small but distinct differences in the observed L shell widths and/or positions were often present. In regard to the frequency of occurrence of simultaneous ion and electron precipitation events it should be realized that in 12 of the 24 S81-1 events the instrumentation was not in a mode suitable for detecting ions. Since these narrow precipitation events are rare, the near-coincidence of 9 out of 29 or 31% of the cases seems to be far more common than accidental. On the other hand, coincident precipitation did not occur in 20 cases, and this might reflect the absence of waves at the appropriate frequency to precipitate the ions.

An example of an event found in the P78-1 data is shown in Figure 1. Here are plotted the average counting rates of locally trapped electrons and ions in selected energy intervals. The high-energy electrons (565-1050 keV) increase by a large factor at ~84590 s UT whereas lower-energy (88-155 keV) electrons show little increase at that time along with a pronounced decrease just before and just afterward. The ions also show a strong spike which is even narrower in time and/or L shell. Most of the particles observed in the event are not directly precipitating in the bounce loss cone, but because of the high B value at their mirror points they will be lost due to atmospheric interactions sometime during their longitude drift around the world. Since the observation point was just a few degrees east of the anomaly in the northern hemisphere, the electrons must have been injected within a few degrees west of the point of observation. The protons, which drift westward, could have been injected far east of the point of observation, but the close agreement with the electron spike makes that seem less likely. Each point in the plot represents the average of approximately twenty-five 0.032-s summation intervals for pitch angles 65°-115° during a half-spin of the satellite. Based on the relative fluxes of the ions and electrons and the observed differences in the flux versus time profiles, it can be shown that the ion enhancements during this and other events cannot be attributed to an instrument response to the higher-energy electrons. Another feature of this event, unlike many of the others, is that the lower-energy electrons showed a pronounced decrease in flux just before and just after the hard spectrum spike.

The preferential enhancement of the higher-energy electrons during the November 7, 1980, event is best illustrated with the energy spectra shown in Figure 2. Here the spectrum during the spike is plotted for comparison with the average of the spectrum before and after the event. Clearly, the higher energy electrons increased by a much larger factor than did the lower-energy electrons.

An event of the same type was observed by the S81-1 satellite on July 11, 1982. Figure 3 shows the counting rate versus time profile for electrons in the bounce loss cone in two differ-

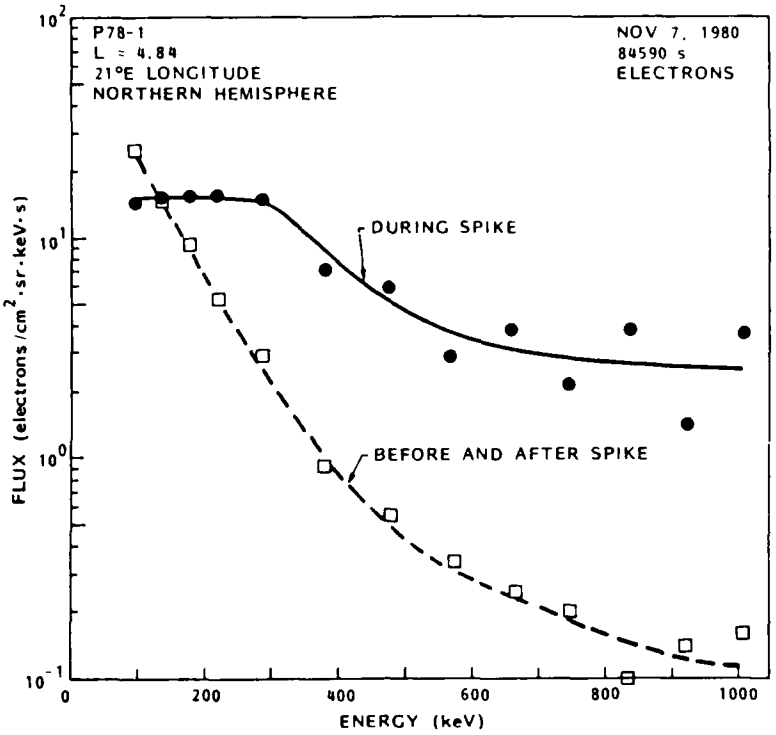

Fig. 2. Energy spectrum measured with the EEM 002 spectrometer during a spike event and the average of that recorded before and after the spike. The channels have been grouped to reduce the statistical uncertainties.

ent energy ranges. As with the pattern of the P78-1 events, the fluxes of electrons of >300 keV increased by a larger factor than did the lower-energy electrons. This tendency is illustrated with the energy spectra measured in ME 1 as shown in Figure 4. One can see that the spectrum is much harder during the spike than before and afterward.

During the event shown in Figure 3 an ion enhancement was observed in the LE 4 spectrometer at nearly the same time as the higher-energy electron flux increase but with a somewhat different time profile and at a slightly different L value. In this regard the event was similar to the one presented in Figure 1 based on the P78-1 data.

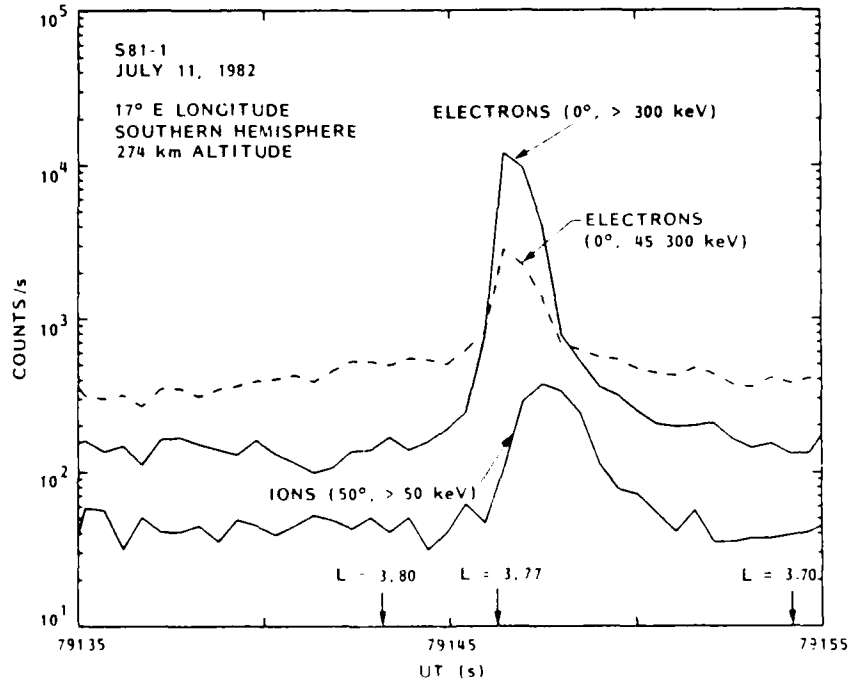

Fig. 3. The counting rates observed with the ME 1 and LE 4 spectrometers in the SEEP payload on the S81-1 spacecraft at local zenith angles of 0° and 50°, respectively, are plotted as a function of time.

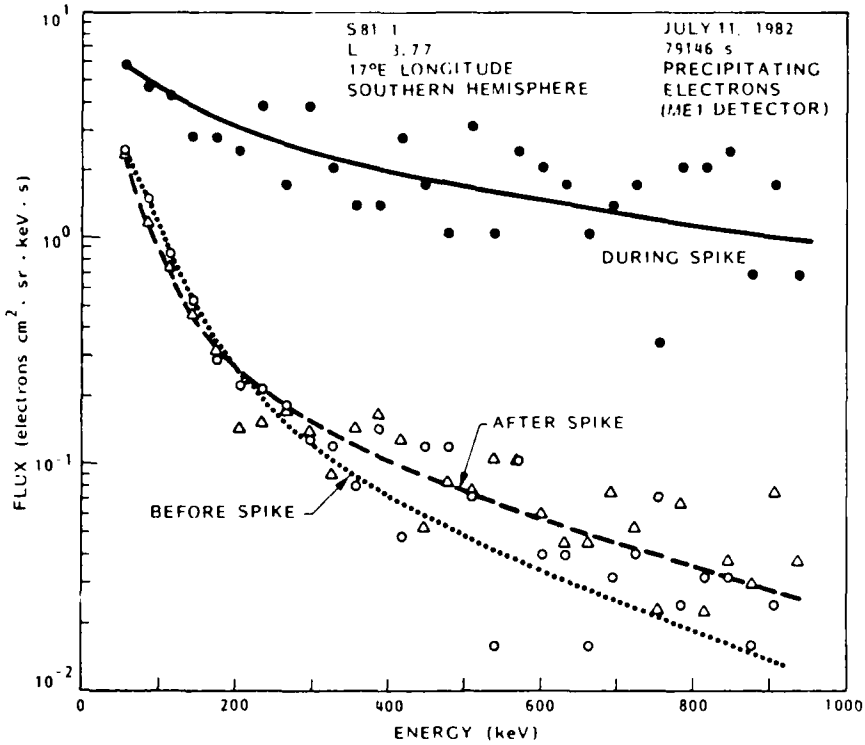

Fig. 4. Energy spectrum measured with the ME 1 spectrometer during a spike event and the spectra recorded before and after the spike. The channels have been grouped to reduce the statistical uncertainties.

Several relativistic electron precipitation spikes over very narrow L shell intervals were previously reported [*Imhof et al.*, 1977] on the basis of data acquired from the P72-1 satellite during an 8-month time period, October 1972 to May 1973. During those events the fluxes of electrons of $\gtrsim 4$ MeV underwent pronounced and narrow enhancements lasting less than 10 s, whereas the lower-energy electrons were not significantly affected. Only electrons were considered in the initial study of energy selective precipitation mechanisms using these data. More recently, having observed ion precipitation simultaneously with energy selective electron precipitation in the P78-1 and S81-1 data sets, the older data were examined for the simultaneous occurrence of ion precipitation. On two of the nine events previously studied, narrow zones of ion precipitation were found at nearly the same location on successive orbits. The electron and ion data from these two passes are shown in Figure 5. Clearly, the ions at 250–400 keV show enhanced fluxes over a narrow L shell region at approximately the same time and position as the relativistic electrons with energies of >4 MeV. The close association between the electron and ion spikes makes it less likely that either had been injected far away in longitude and just drifted to the point of observation. From the entire set of on-orbit data as well as the laboratory calibrations it can be shown that the ion spectrometer was not simply responding to relativistic electrons. During the remaining seven relativistic electron precipitation events observed in 1972–1973, narrow and pronounced ion precipitation did not occur, although in some of the cases the ion fluxes were enhanced in the general vicinity of the relativistic electron precipitation.

Events in Both the S81-1 and the NOAA 6 Data

Since the NOAA 6 instrument provided no means of monitoring the fluxes of electrons above energies exceeding 300 keV, a search for relativistic electron precipitation events could not be performed based on the detection of electrons in the MeV range, as done with the P72-1, P78-1, and S81-1 spacecraft. Instead, in the NOAA 6 instruments, electron and proton responses were studied at times within 3 hours of the observation of narrow relativistic electron spikes in the S81-1 spacecraft. The criteria for correlation were further restricted by requiring the NOAA 6 event to be within 60° in longitude and 0.11 units in L value of the S81-1 event.

Examples of relativistic electron precipitation spikes observed in both the S81-1 and NOAA 6 data are shown in Figure 6. In each of the events the spikes consisted of significant enhancements in the fluxes of >300-keV electrons in both the drift and bounce loss cones. The listed angles refer to the zenith viewing directions rather than pitch angles. The central pitch angles for electrons observed by the 0° detectors in the NOAA 6 and S81-1 payloads are all within 27° of being parallel to the magnetic field lines. The pitch angles for the 90° detectors are all within 15° of being perpendicular to the magnetic field lines. On each of these events the fluxes of precipitating electrons above 300 keV increased by larger factors than did those of trapped electrons. Detailed analyses of the precipitating to trapped ratios and comparisons between the NOAA 6 and S81-1 data are limited by an alternation of the 1-s accumulation intervals between the precipitating and trapped particles in the NOAA 6 measurements. In the plots of the latter data the counting rates on successive 1-s intervals are connected by straight lines.

The energy spectra of the precipitating electrons from the S81-1 measurements during the two foregoing events are illustrated in Figure 7. Clearly, the spectra were significantly harder during the spikes than before or after. There is no well-defined energy threshold for flux enhancement, but the fluxes of electrons show a marked increase at energies up to at least 1 MeV. The equivalent e fold energies are sometimes in

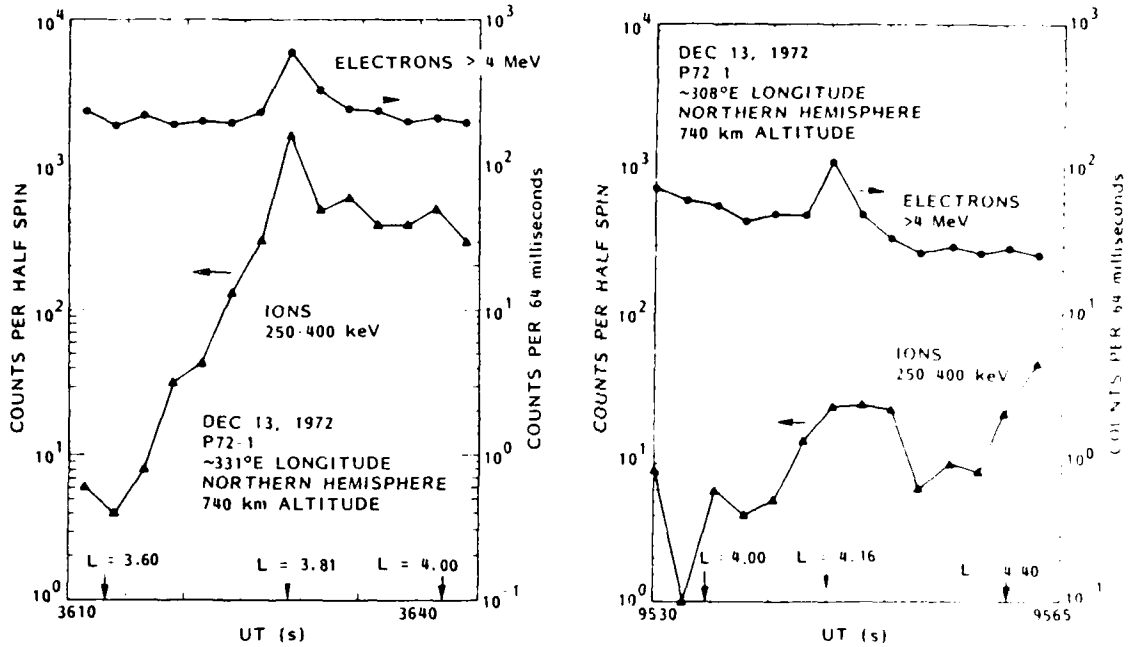

Fig. 5. The counting rate of electrons of >4 MeV observed with the anticoincidence counter surrounding one of the *Germanium* spectrometers on the P72-1 spacecraft and the rates of ions of 250–400 keV at nearly 90° pitch angle measured in the LEP 001 spectrometer on the same satellite.

excess of 500 keV. During the spikes on September 2, 1982, and November 17, 1982, the energy deposition rates corresponding to the spectra measured in the bounce loss cone were 2.4×10^{-2} and 2.7×10^{-2} ergs/cm^2 s, respectively.

It should be noted that events with large fluxes of high-energy electrons in the bounce loss cone were not observed from the P72-1 and P78-1 satellites, but this measured difference in character of the events may result from the oriented condition of the S81-1 and NOAA 6 experiments in contrast with the spinning nature of the other two satellites and the differences in geometric factors of the various detectors. Also, selecting events observed from two satellites at somewhat different times and positions may have generally favored stronger wave-particle interactions.

Nearly coincident ion spikes appeared in all seven of the NOAA 6 passes in which high-energy electron enhancements occurred at nearly the same L value as in the S81-1 data. However in two of these events the electron and ion spikes were somewhat wider than 10 s in the spacecraft frame. At the times of these events the ion detector in the S81-1 payload was not in the proper mode for measuring ions, so it is not known whether an ion spike occurred at the time of the SEEP observations. When the S81-1 ion detector was in the correct mode for counting ions and they were detected, corresponding electron spikes in both the S81-1 and the NOAA 6 data were not observed.

The longitude and time differences when similar events were observed in the NOAA 6 and S81-1 data are shown in Figure 8. For all of the plotted points a relativistic electron spike was observed in the S81-1 detector oriented at 0° zenith angle. Different symbols are used to indicate whether or not an electron spike was observed in the NOAA 6 data within 0.1 of the same L value. A shading encompasses electron precipitation events that extend less than 25° in longitude and less than 2000 s in time. Five of seven events observed from both spacecraft fell within these limits. These findings suggest a patchy profile, sometimes with an arc structure which may extend over longitude intervals as great as 25° and time intervals as long as 2000 s. The plot in Figure 8 is consistent with the general lack of occurrence of the energy selective precipitation spikes on successive orbits, differing by ~6000 s in time and about 25° in longitude.

Morphology of the Events

All the narrow electron spikes reported here occurred in the outer radiation belt. The invariant latitude and MLT values are plotted in Figure 9, with different symbols for those that involved only electrons and for those in which the ion fluxes also showed an enhancement. The events are plotted at the local time of observation. Those electrons in the drift loss cone could have been injected at an earlier time, but in most of the cases, electrons are also in the bounce loss cone, and a long longitude drift interval seems less likely. Also shown are the four events presented by *Thorne and Andreoli* [1980] as electromagnetic ion cyclotron wave events. Data coverage on the P72-1 and P78-1 spacecraft was approximately equal near noon and midnight (within about 2 hours), and for the S81-1 satellite it was almost equal near 1030 and 2230 local time (within about 2 hours). At low L values the NOAA 6 measurements covered MLT values of 0630–0900 and 1830–2130. The premidnight hours were clearly the most favored for occurrence of energy selective electron precipitation spikes. This preference was particularly strong for events with nearly simultaneous ion and energy selective relativistic electron precipitation. The concentration of events prior to local midnight is a noteworthy finding, but additional information is needed to establish the source of the spikes.

Since the equatorial plasma densities and hence the wave-particle resonant energies are known to undergo major changes near the plasmapause, it is of interest to consider the locations of these events with respect to that position. In Figure 10 the locations in L of the energy selective spikes are plotted as a function of the position of the plasmapause based on Kp [*Carpenter and Park*, 1973]. This formalism used a

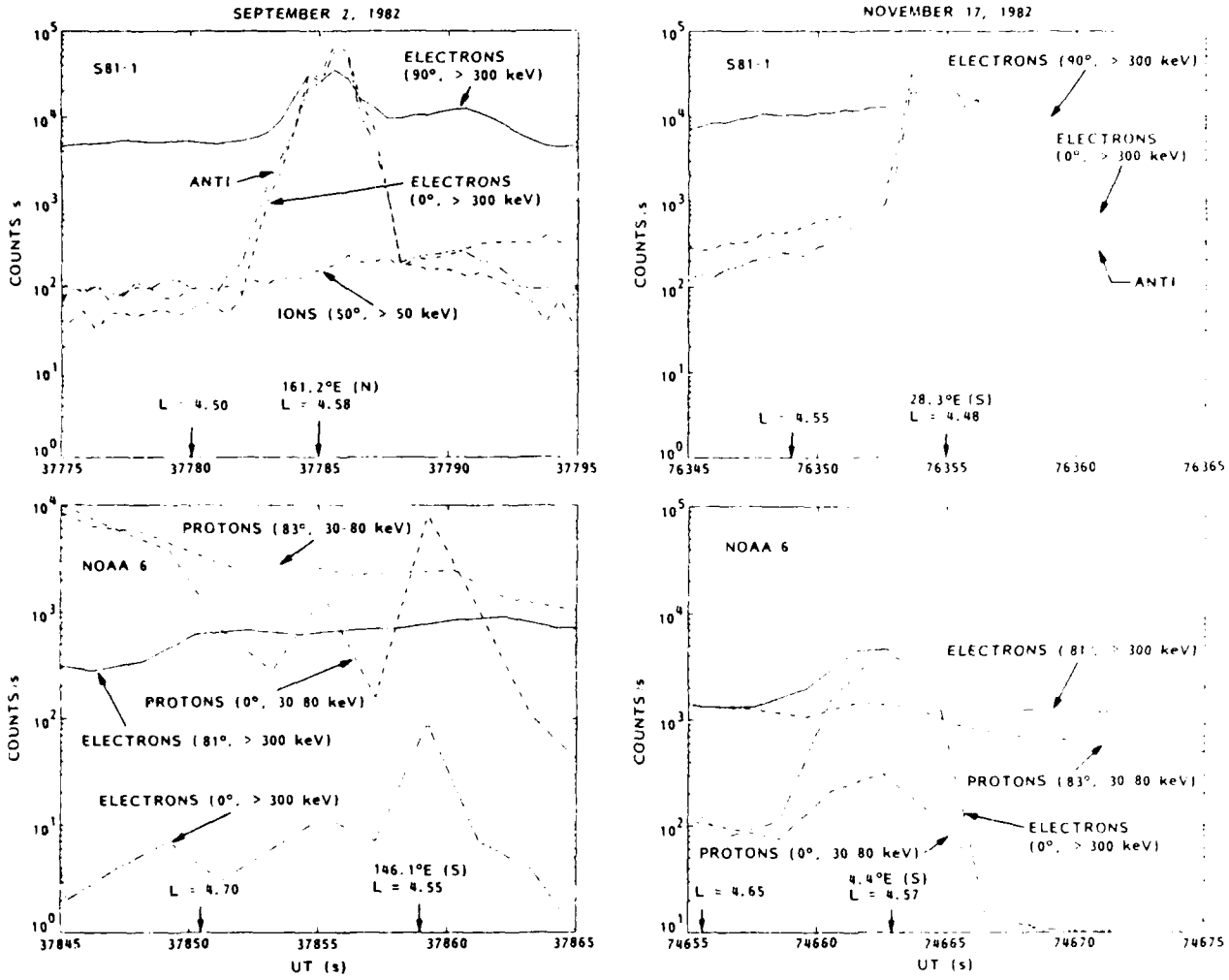

Fig. 6. In the top sections the counting rates observed with ME 1, TE 2, and LE 4 spectrometers in the SEEP payload on the S81-1 spacecraft at local zenith angles of 0°, 90°, and 50°, respectively, are plotted as a function of time for events on (left) September 2, 1982, and (right) November 17, 1982. Also plotted are the counting rates in the anticoincidence counter. In the bottom sections are plotted the counting rates of electrons of > 300 keV measured at 0° and at 81° zenith angle and of protons of 30–80 keV measured at 0° and at 83° zenith angle on the NOAA 6 spacecraft. After the longitude values, (N) or (S) indicates whether the observations were made in the northern or southern hemisphere, respectively.

simple dipole model, and consideration of the differences in magnetic field model for the calculation of L value is beyond the scope of this formalism. The formula applies to all magnetic local times, but at MLT values near 2100 the actual L values of the plasmapause may be slightly higher (D. L. Carpenter, private communication, 1985). The L values for the plasmapause location based on the Carpenter and Park formalism are not intended to be accurate representations, but are given mainly to illustrate the general location of the events with respect to the plasmapause position. A Kp scale is provided on the right-hand side. A line is drawn to indicate positions of equal value in L for the spike and the plasmapause. It can be seen that many of the spikes occurred in the vicinity of the plasmapause.

DISCUSSION

It should be emphasized that many of the electron precipitation events reported here were observed in the drift loss cone. Even for the majority of events observed in the bounce loss cone with the S81-1 and NOAA 6 instruments the pitch angle distributions were far from isotropic, with the fluxes near 90° pitch angle often being an order of magnitude greater than those near 0°. In contrast, the energy selective precipitation events reported by *Thorne and Andreoli* [1980] were all measured in the bounce loss cone. The four events with isotropy over the upward looking hemisphere had energy selective properties similar to those reported here. However, those events were discovered from more than 14 months of data, and they occurred in the dusk meridian, a time interval not covered well in the present observations.

The spikes reported by *Koons et al.* [1972] appear similar to those considered in the present paper, but here we have analyzed many electron events and have considered the frequency of occurrence of associated narrow ion spikes. The spikes might also be related to the relativistic electron precipitation (REP) event at $L = 4.5$ reported by *West and Parks* [1984]. Bremsstrahlung X rays and ELF emissions were measured simultaneously. The X ray fluxes had a hard energy spectrum, and the authors concluded they were due to precipitation of relativistic electrons. West and Parks interpreted the event as being the result of electron cyclotron interaction with whistlers. However, the data were limited to one event, so it is

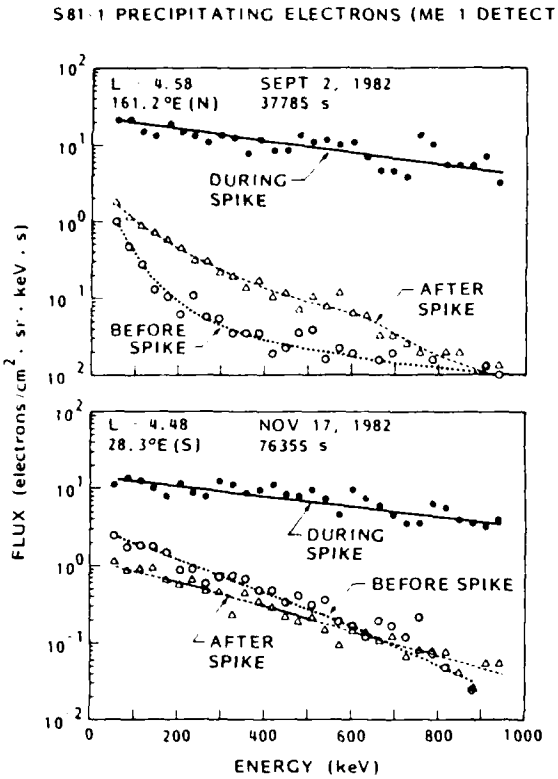

Fig. 7. Energy spectra measured with the ME 1 spectrometer during two different spike events. Also shown are the spectra recorded before and after the spike.

difficult to establish how it might relate to the events presented here.

Many electron and ion precipitation processes are believed to be associated with wave-particle interactions. For simplicity and because a large portion of the length of a field line is near the equator, that region is often taken to be the location where the interactions take place. It is therefore logical to consider the frequencies of the waves that might be responsible for first-order cyclotron resonance at the equator. For this purpose the resonance frequencies were calculated using a program supplied by G. T. Davidson (private communication, 1984). The frequencies for the case on November 7, 1980, are plotted in Figure 11 as a function of the near-equatorial cold plasma density. Cyclotron resonance was assumed for waves traveling parallel to the magnetic field lines, and the wave-particle interactions were all taken to occur at the equator. However, various modes of wave-particle interactions are possible, and therefore the wave frequencies for a given plasma density may be somewhat different than shown. Many of the events occurred in the neighborhood of $L = 4$–5, and the cold plasma densities in the equatorial region were therefore generally in the vicinity of 100 cm^{-3}. The frequencies of the waves responsible for the electron precipitation were probably in the range 10–100 Hz. An upper frequency cutoff in the waves could account for the observed energy selectivity. The nearly simultaneous precipitation of ions would require that the waves extend to lower frequencies, 1 Hz or less. Waves of such low frequencies could be associated with whistlers, and because of the dispersion the waves might last for several seconds. On the ground it is difficult to follow the whistlers to low frequencies, but from satellites, proton whistlers have been measured at frequencies down to ~100 Hz [*Shawhan*, 1966]. However, few studies have addressed this frequency portion of whistlers. In fact, the extent to which waves in the 10- to 100-Hz range occur at high altitudes in the near-equatorial region of outer radiation belt L shells is not well known. These data indicate the need for further measurements of low-frequency waves.

It would have been desirable to have measured the low-frequency wave environment near the equator simultaneously with the particle observations at low altitudes. However, waves at the appropriate position are measured only infrequently, and the probability of having performed such a measurement in coincidence with the rare events reported here is quite low. It is possible that the wave-particle interactions took place at low altitudes, as reported by *Koons et al.* [1972], where the frequency of any responsible waves would be much higher, but low-altitude measurements of the waves were also not available at the times of the events. Lacking one-to-one coordinations between wave and particle measurements, we might compare the times of occurrence of the events with the

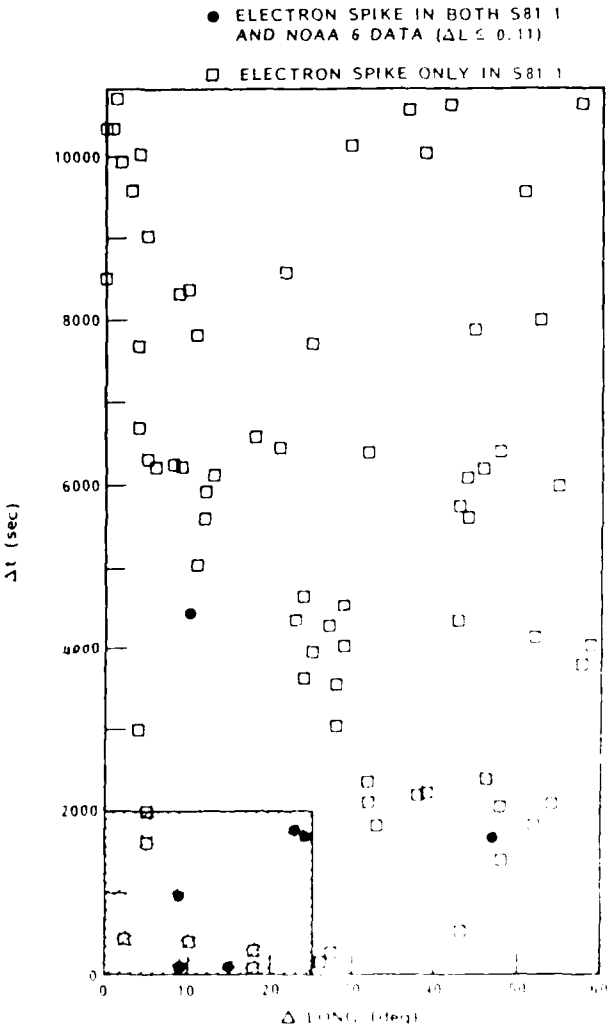

Fig. 8. Differences in longitude and time for events observed both the S81-1 and the NOAA 6 payloads. The solid circles repre events when a narrow electron spike was observed in both the and the NOAA 6 data, but in two of these cases the spike NOAA 6 data had an observed duration somewhat greater th Five of the seven coincident events are within the shaded box

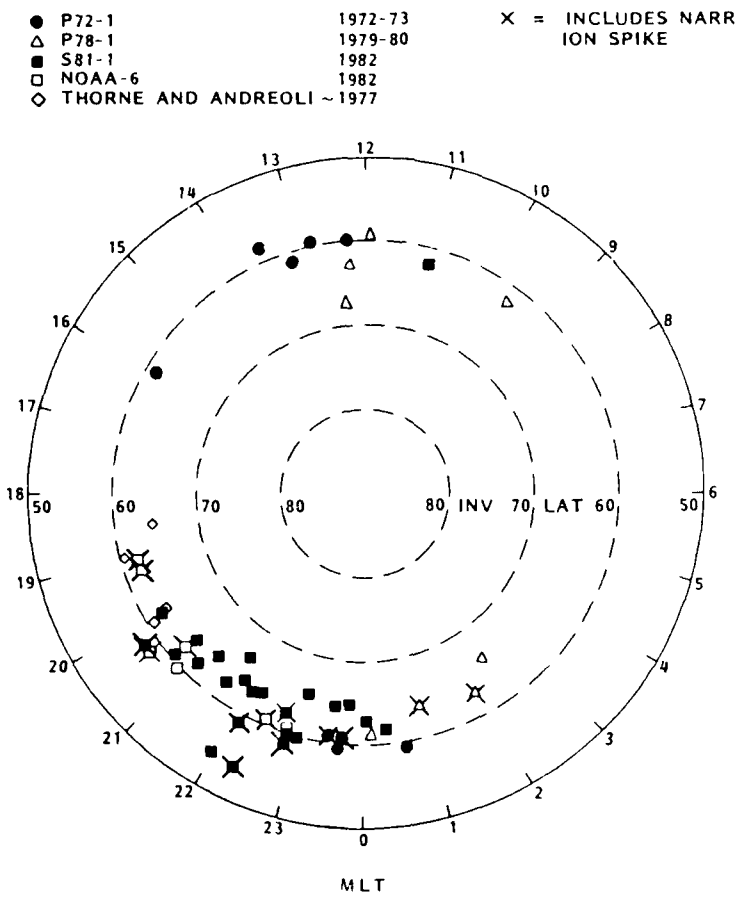

Fig. 9. An invariant latitude/magnetic local time plot of the events observed on the P72-1, the P78-1, and the S81-1 spacecraft as well as the four electromagnetic ion cyclotron wave events reported by *Thorne and Andreoli* [1980]. Events observed on the NOAA 6 spacecraft within 3 hours in time and 0.11 units in L of those measured on the S81-1 satellite are also shown. All of the events from the P72-1, P78-1, and S81-1 vehicles were observed over a period of less than 10 s, as were the proton events from NOAA 6. Two of the electron events measured on NOAA 6 were somewhat longer than 10 s. The principal data coverage was in the MLT intervals 1000–1400 and 2200–0200 on the P72-1 and P78-1 satellites and in the intervals 0830–1230 and 2030–0030 on the S81-1 spacecraft, and for NOAA 6 the range of coverage for low L values was 0630–0900 and 1830–2130.

expected times of the presence of low-frequency waves. *Bossen et al.* [1976] have reported PC 1 events at synchronous orbit to have an increased occurrence rate within $1\frac{3}{4}$ hours of a substorm expansion onset. In Figure 12 the times of the spike events are indicated on plots of the *AE* index. It can be seen that six of the eight events in 1980 occurred very close to the times of substorms and likewise for six of the nine events in 1972–1973. Therefore during many of the events it is likely that low-frequency waves were enhanced in the near-equatorial region.

The narrow L shell confinement of the relativistic precipitation spikes may reflect fine structure in the cold plasma density profiles and hence in the cyclotron resonance energies. Narrow regions of enhanced or depleted plasma density near the plasmapause have been reported by *Anderson* [1984]. Fine structure in the plasma density profiles might also explain the pronounced and narrow depletions of the lower-energy electrons just before and after the spike on November 7, 1980. The nearby spikes in electron and ion precipitation might be attributed to fine spatial structure in the plasma density profiles combined with the presence of waves spanning a sufficiently broad frequency range. Minor displacements in the electron and ion spikes might be attributed to details of the plasma density profiles and the wave intensity-frequency distributions.

In addition to the cyclotron resonance energies being strongly localized, the waves might also be confined to narrow spatial regions. Many years ago it was suggested by *Smith et al.* [1960] that whistler mode waves could be trapped in plasma ducts aligned with the earth's magnetic field lines. Subsequently, observations have supported this concept, and recently, *Beghin et al.* [1984] observed density structures containing ducted waves. These structures were called "ELF plasma ducts." The typical horizontal sizes of these plasma ducts were found to lie in the range 5–50 km. Such dimensions are not inconsistent with the sizes of the spikes reported here, which are typically in the neighborhood of 5 s or ~35-km distance. Plasma densities were measured in the SEEP payload on the S81-1 satellite [*Voss et al.*, 1985], and in several of the passes a density depletion was observed in the plasma trough near the relativistic electron spikes.

SUMMARY

Data have been presented on rare relativistic electron and energetic ion precipitation events with the characteristics of a

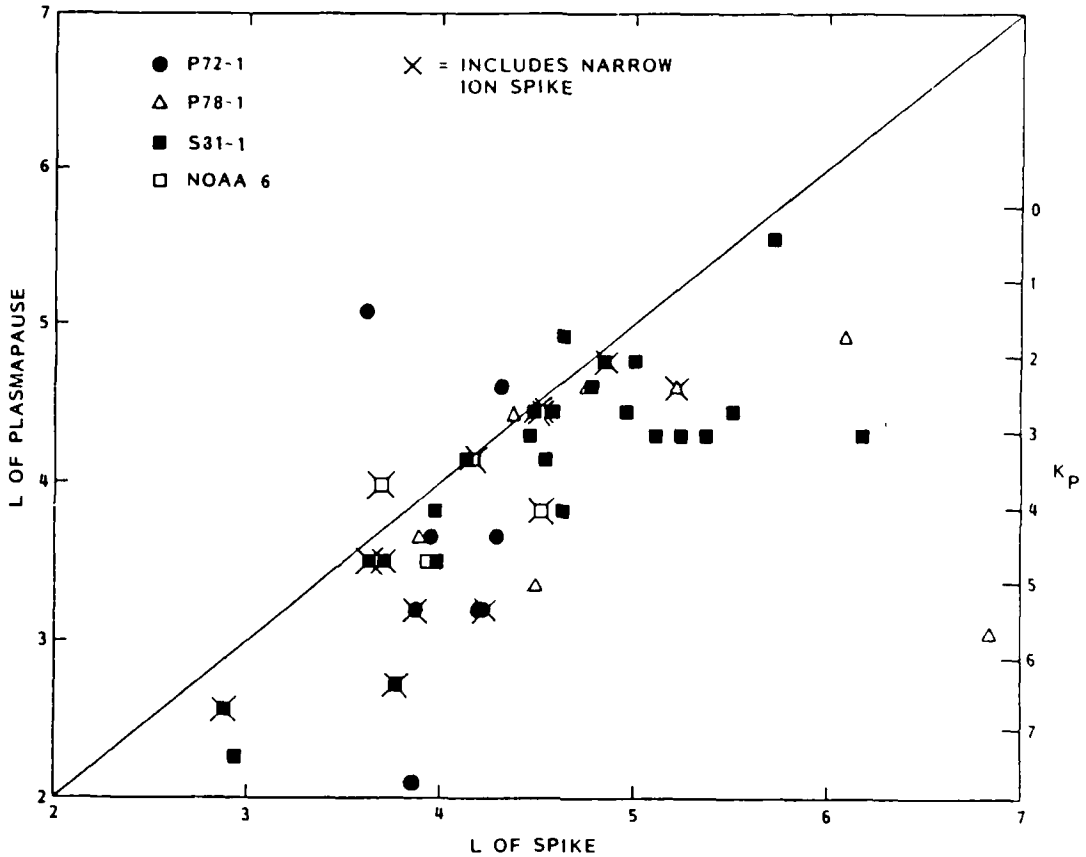

Fig. 10. The locations in L of the preferential high-energy spikes plotted as a function of the plasmapause positions based on Kp [*Carpenter and Park*, 1973]. L of plasmapause is equal to $5.7 - 0.47 \times$ (maximum Kp in previous 12 hours). All of the events from the P72-1, P78-1, and S81-1 vehicles were observed over a period of less than 10 s, as were the proton events from NOAA 6. Two of the electron events measured on NOAA 6 were somewhat longer than 10 s.

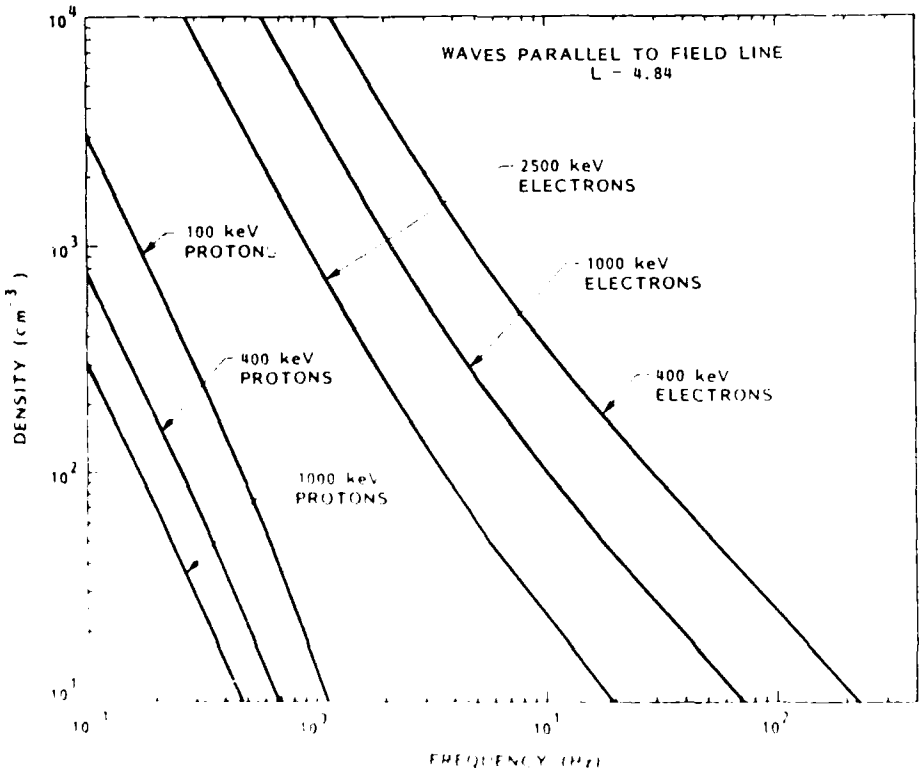

Fig. 11. The calculated resonance frequencies at the equator for electrons and protons of selected energies traveling parallel to the magnetic field line plotted as a function of the near-equatorial cold plasma density. The selected L value corresponds to the spike observed on November 7, 1980. These calculations were performed using a computer program supplied by G. T. Davidson (private communication, 1984).

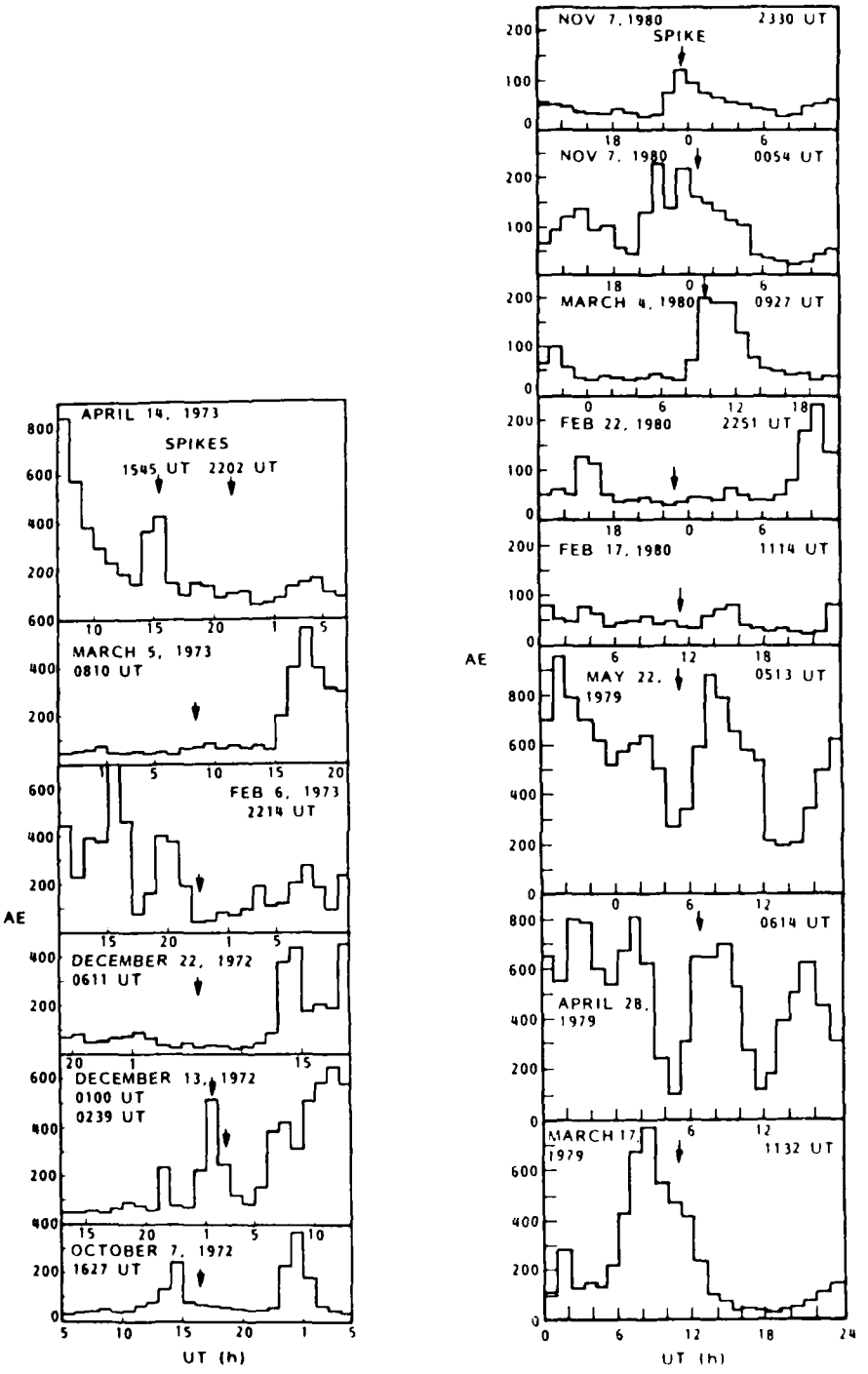

Fig. 12. The *AE* index plotted as a function of time. Arrows indicate the times of the precipitation spike events. The arrow near 0100 UT on December 13, 1972, represents two spike events.

very hard spectrum and narrow spatial extent. The most promising explanation is wave-particle interactions within fine structures in the cold plasma.

Acknowledgments. The development of the P72-1 and P78-1 satellite payloads and the performance of the experiments were supported by the Defense Advanced Research Project Agency through the Office of Naval Research (contracts N00014-69-C-0372 and N00014-78-C-0070, respectively). The SEEP payload on the S81-1 spacecraft was sponsored by the Office of Naval Research (contract N00014-79-C-0824). For all three of these satellite experiments, launch and orbital support were provided by the Air Force Space Test Program Office. Much of the data analysis presented here was sponsored by the Lockheed Independent Research Programs. Appreciation is extended to J. P. McGlennon and C. K. Chalmers for their efforts in processing the data. We also acknowledge the contribution of V. J. Hill who wrote the program which reduced and archived the NOAA 6 data.

The Editor thanks the two referees for their assistance in evaluating this paper.

REFERENCES

Anderson, R. R., Plasmapause location and structure as deduced from the ISEE 1 plasma wave experiment data (abstract), *Space Res.*, XXIV, 37, 1984.

Beghin, C., J. C. Cerisier, J. L. Rauch, J. J. Berthelier, F. Lefeuvre, R. Debrie, O. A. Maltseva, and N. I. Massevitch, Experimental evidence of field-aligned LHF plasma ducts in the ionospheric trough and in the auroral zone, paper presented at the International Con-

ference on the Results of the ARCAD 3 Project and of the Recent Programs in Magnetospheric and Ionospheric Physics, Toulouse, France, Centre Natl. d'Etudes Spatiales, Toulouse, France, May 1984.

Bossen, M., R. L. McPherron, and C. T. Russell, A statistical study of Pc 1 magnetic pulsations at synchronous orbit, *J. Geophys. Res.*, *81*, 6083, 1976.

Cain, J. C., S. J. Hendricks, R. A. Langel, and W. V. Hudson, A proposed model for the International Geomagnetic Reference Field, *J. Geomagn. Geolectr.*, *19*, 335, 1967.

Carpenter, D. L., and C. G. Park, On what ionospheric workers should know about the plasmapause-plasmasphere, *Rev. Geophys.*, *11*, 133, 1973.

Davidson, G. T., Relativistic electron precipitation and resonance with ion cyclotron waves, *J. Atmos. Terr. Phys.*, *40*, 1085, 1978.

Imhof, W. L., J. B. Reagan, G. H. Nakano, and E. E. Gaines, Narrow spikes in the selective precipitation of relativistic electrons at mid-latitudes, *J. Geophys. Res.*, *82*, 117, 1977.

Imhof, W. L., J. B. Reagan, G. H. Nakano, and E. E. Gaines, Studies of the sharply defined *L* dependent energy threshold for isotropy at the midnight trapping boundary, *J. Geophys. Res.*, *84*, 6371, 1979.

Imhof, W. L., E. E. Gaines, and J. B. Reagan, Observations of multiple, narrow energy peaks in electrons precipitating from the inner radiation belt and their implications for wave-particle interactions, *J. Geophys. Res.*, *86*, 1591, 1981.

Koons, H. C., Proton precipitation by a whistler-mode wave from a VLF transmitter, *Geophys. Res. Lett.*, *2*, 281, 1975.

Koons, H. C., A. L. Vampola, and D. A. McPherson, Strong pitch-angle scattering of energetic electrons in the presence of electrostatic waves above the ionospheric trough region, *J. Geophys. Res.*, *77*, 1771, 1972.

Nakano, G. H., W. L. Imhof, and R. G. Johnson, A satellite-borne high resolution Ge (Li) gamma-ray spectrometer system, 1, Description of the instruments and gamma-ray backgrounds in earth orbit, *IEEE Trans. Nucl. Sci.*, *21*, 159, 1974.

Nakano, G. H., W. L. Imhof, and J. B. Reagan, High resolution gamma-ray spectroscopy on the P78-1 satellite, *IEEE Trans. Nucl. Sci.*, *27*, 405, 1980.

Reagan, J. B., W. L. Imhof, S. K. Lew, and J. D. Matthews, Observations of quasi-trapped protons at mid latitudes (abstract), *Eos Trans. AGU*, *56*, 1047, 1975.

Shawhan, S. D., Experimental observations of proton whistlers from INJUN 3 VLF data, *J. Geophys. Res.*, *71*, 29, 1966.

Smith, R. L., R. A. Helliwell, and I. W. Yabroff, A theory of trapping of whistlers in field-aligned columns of enhanced ionization, *J. Geophys. Res.*, *65*, 815, 1960.

Thorne, R. M., and L. J. Andreoli, Mechanisms for intense relativistic precipitation, in *Exploration of the Polar Upper Atmosphere, Proceedings of the NATO Advanced Study Institute Held at Lillehammer, Norway*, May 5–16, 1980, p. 381, D. Reidel, Hingham, Mass., 1980.

Thorne, R. M., and C. F. Kennel, Relativistic electron precipitation during magnetic storm main phase, *J. Geophys. Res.*, *76*, 4446, 1971.

Voss, H. D., J. B. Reagan, W. L. Imhof, D. O. Murray, D. A. Simpson, D. P. Cauffman, and J. C. Bakke, Low temperature characteristics of solid state detectors for energetic x-ray, ion, and electron spectrometers, *IEEE Trans. Nucl. Sci.*, *29*, 164, 1982.

Voss, H. D., J. Mobilia, D. W. Datlowe, and S. N. Roselle, The ground support computer and in-orbit survey data analysis program for the SEEP experiment, *IEEE Trans. Nucl. Sci.*, *32*, 168, 1985.

West, R. H., and G. K. Parks, ELF emissions and relativistic electron precipitation, *J. Geophys. Res.*, *89*, 159, 1984.

D. W. Datlowe, E. E. Gaines, W. L. Imhof, J. Mobilia, J. B. Reagan, and H. D. Voss, Lockheed Palo Alto Research Laboratory, Palo Alto, CA 94304.

D. S. Evans, National Oceanic and Atmospheric Administration, Boulder, CO 80303.

(Received August 8, 1985;
revised November 8, 1985;
accepted November 11, 1985.)

JOURNAL OF GEOPHYSICAL RESEARCH, VOL. 91, NO. A8, PAGES 8883-8894, AUGUST 1, 1986

Slot Region Electron Precipitation by Lightning, VLF Chorus, and Plasmaspheric Hiss

W. L. IMHOF, H. D. VOSS, M. WALT, E. E. GAINES, J. MOBILIA, D. W. DATLOWE, AND J. B. REAGAN

Lockheed Palo Alto Research Laboratory, Palo Alto, California

Energetic electrons are precipitated from the slot region of the radiation belts by a variety of mechanisms, including short duration wave bursts associated with lightning and chorus and more slowly varying plasmaspheric hiss. Characteristics of the nightside short duration precipitation events, including their favored occurrence at certain longitudes in the northern hemisphere, indicate that they are predominantly associated with lightning. The dayside events seem to relate primarily to VLF chorus. Here a study is made of various characteristics of the short duration precipitation bursts, namely, the longitude and L shell variations, the day/night differences, the energies of spectral maxima, and the rapid spectral variations with time. In addition, the total loss rates of electrons from the radiation belts are obtained from the measured energy spectra and pitch angle distributions. An assessment is made of the relative importance of the bursts as a loss mechanism for slot region electrons in comparison to the more slowly varying precipitation processes. The assessment is based on a comparison of the energies of the peaks often observed in the energy spectra of both classes of precipitation. The slowly varying electron fluxes observed in the drift loss cone frequently display peaks in the energy spectra which indicate that they are precipitated by plasmaspheric hiss and that this process therefore represents a major loss mechanism. Well-defined bursts, which appear to be associated with lightning at nighttime and perhaps chorus in the daytime, were observed on only about 2% of the satellite passes and are generally of lower energy than the general population in the drift loss cone, suggesting that the bursts are not the dominant loss mechanism. There is some overlap between the distributions in peak energy, and lightning may play a role in precipitating electrons from the slot region primarily at nighttime, with its greatest contribution at low L shells.

INTRODUCTION

The importance of various mechanisms for precipitating electrons from the "slot region" of the radiation belts ($L \approx$ 2–3.5) is still not well understood. Many years ago it was shown that atmospheric scattering is not an important loss mechanism for electrons trapped on L shells above ~ 1.3 [*Walt*, 1964]. The significance of plasmaspheric hiss as a loss mechanism for slot region electrons was suggested by *Lyons et al.* [1972]. The coordinated measurements of *Imhof et al.* [1982], which simultaneously observed electron precipitation and VLF hiss, were consistent with this hypothesis. The precipitation of energetic electrons from the slot region by off-equatorial interactions with VLF transmitter waves has been invoked by *Vampola* [1977] to explain his observed longitude variations in electron precipitation. Throughout much of the slot region the lack of a pronounced diurnal variation in the electron precipitation has been used to argue against the importance of waves from ground-based VLF transmitters, since the transmission of the ionosphere to these waves is much reduced during the daytime [*Imhof et al.*, 1984].

Lightning was first suggested by *Dungey* [1963] and then discussed by *Cornwall* [1964] as a source of waves for precipitating electrons. This loss mechanism was later discarded as being unimportant [*Roberts*, 1966]. The possible importance of electron precipitation associated with lightning has been reopened with the measurements of Trimpi events [*Carpenter et al.*, 1984], in which the amplitude or phase of a subionospherically propagating VLF signal is perturbed at the time of reception of a magnetospheric whistler. Recent related activities include the direct observations from a satellite of electrons precipitated by lightning [*Voss et al.*, 1984]. In the latter investigation, discrete lightning-induced electron precipitation events (LEP) were observed within the bounce loss cone in synchronization with whistlers observed at ground stations. *Voss et al.* [1984] found that a single LEP burst at $L = 2.3$ emptied about 0.001% of the radiation belt in the region encompassing the burst magnetic field lines. The data also suggested that a single lightning flash can precipitate electrons at locations separated by 2000 km. Although well-defined isolated LEP events are infrequent, lightning could still play a dominant role, since it may also greatly enhance the pitch angle diffusion process but not be detectable as isolated events.

Evidence exists for electron precipitation by VLF chorus, since bursts of precipitating electrons were always accompanied by chorus emissions [*Oliven and Gurnett*, 1968]. It has also been shown that radiated power line harmonics (PLH) in the kilohertz range can on occasion dominate VLF activity in the magnetosphere [*Helliwell et al.*, 1975; *Park and Helliwell*, 1977; *Luette et al.*, 1979]. The foregoing authors have suggested that PLH may enhance the precipitation of energetic particles in the magnetosphere.

Based on the measured pitch angle distributions, it will be shown that the drift loss cone electrons represent a significant portion of the loss rate into the atmosphere. Hence mechanisms which populate the drift loss cone will be important in determining the overall loss rates. Here we attempt to assess relative contributions in the slot region of lightning whistlers and of chorus bursts to the injection of electrons into the drift loss cone. This assessment is based on the energies of peaks observed in the electron energy spectra. We have compared the electron spectra observed in the drift loss cone with the spectra of electrons precipitated by well-defined bursts. From these comparisons one can set limits on the importance of the various loss mechanisms.

DESCRIPTION OF SATELLITE INSTRUMENTATION

The data presented here were acquired with energetic electron spectrometers placed on two low-altitude polar orbiting

Copyright 1986 by the American Geophysical Union.

Paper number 5A8312
0148-0227/86/005A-8312$05.00

TABLE 1. Characteristics of Electron Spectrometers

Satellite	Electron Spectrometer	Energy Threshold, keV	Geometric Factor, cm^2 sr	Central Viewing Zenith Angle	Acceptance Angle, deg
P78-1	EEM 002	68	0.69	spinning	±15
P78-1	PRM 004	59	1.0×10^{-3}	spinning	±3.5
S81-1	ME 1	45	2.47	0°	±30
S81-1	TE 2	6	0.17	90°	±20

satellites. On one of the satellites, P78-1, electrons were measured from 68 keV to 1 MeV over the time period 1979–1985. The observations from the other satellite (S81-1) were more restricted in time (May–December 1982), but the electron measurements extended to lower energies, 6 keV.

The P78-1 satellite was launched into orbit on February 24, 1979. The spacecraft was in a sun synchronous, noon-midnight, nearly circular orbit at ~600-km altitude with an inclination of 96.7°. The satellite traveled northward during the daytime. The section of the satellite containing the electron spectrometers spun about an axis perpendicular to the orbit plane with a period of 5.5 s.

The instrument from which the energy spectra of electrons above 68 keV were obtained was a high-sensitivity, high-resolution (0.69 cm^2 sr geometric factor, ~20 keV full width at half maximum) spectrometer with the designation EEM 002. The center axis of the collimator was oriented at 90° to the spin axis. It employed a 1000-μm-thick silicon solid state detector surrounded by a plastic scintillator anticoincidence shield for background reduction. The collimator entrance aperture was covered by a 3.2-mg/cm^2 aluminum and Kapton window that prevented protons with less than 1-MeV energy from reaching the detector. A detailed description of this instrument is provided elsewhere [*Imhof et al.*, 1981].

Fine resolution electron pitch angle measurements were made with a second spectrometer designated PRM 004, having a threshold energy of 59 keV. This instrument, designed to measure high fluxes of electrons, had a 3.5° half-angle collimator and a 1000-μm-thick silicon surface barrier detector with 0.07-cm^2 area resulting in a geometric factor of 1.0×10^{-3} cm^2 sr. A 13-μm-thick silicon detector ahead of the main detector and in anticoincidence with it provided rejection of low-energy protons. A third silicon detector, 1000 μm thick and 0.50 cm^2 in area and positioned behind the other

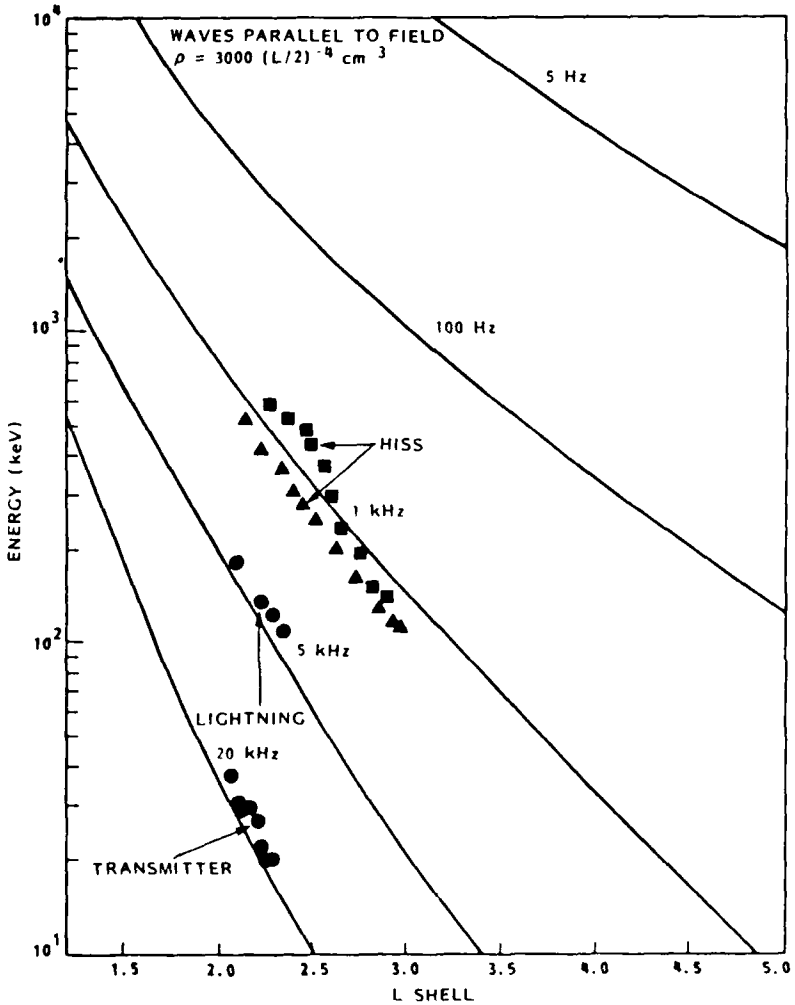

Fig. 1. The electron energies calculated for first-order cyclotron resonant interactions near the equator for waves traveling parallel to the magnetic field lines. The plasma densities were taken to be 3000 $(L/2)^{-4}$ cm^{-3}. The central energies of observed peaks are also plotted for selected cases identified as being due to VLF waves from a ground-based transmitter [*Imhof et al.*, 1983], to waves associated with lightning [*Voss et al.*, 1984], or to plasmaspheric hiss [*Imhof et al.*, 1982].

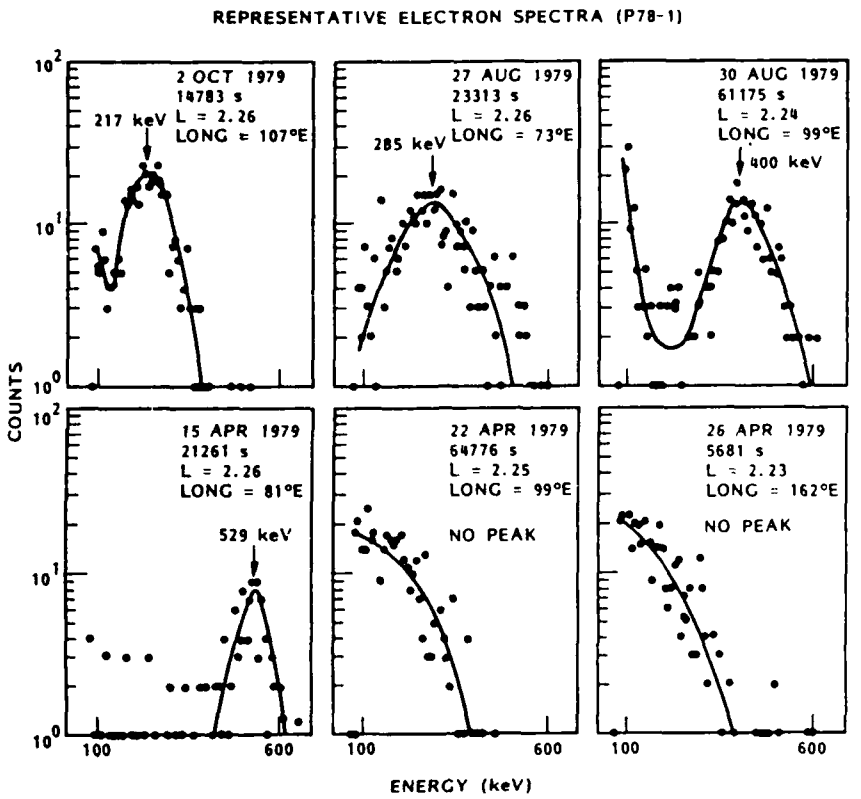

Fig. 2. Representative examples of the energy spectra of electrons observed in the drift loss cone from the P78-1 satellite. Best fit curves to the data points are shown.

two, was sensitive to electrons with energies greater than ~1 MeV. The stack of detectors was surrounded on all but the collimator side by a minimum of 0.5 cm of tungsten shielding to reduce background.

The satellite payload in the Stimulated Emission of Energetic Particles (SEEP) experiment on the three-axis stabilized S81-1 spacecraft contained an array of cooled silicon solid state detectors to measure electrons and ions directly with high-sensitivity and fine energy resolution [*Voss et al.*, 1982]. The electron spectrometers were oriented at various angles to the local vertical. In this paper, use is made of two electron spectrometers. The instrument ME 1 at a zenith angle of 0° had an acceptance angle of ±30°, a threshold energy of 45 keV, and a geometric factor of 2.47 cm² sr. The spectrometer TE 2 at 90° zenith angle had an acceptance angle of ±20°, a threshold of 6 keV, and a geometric factor of 0.17 cm² sr. The S81-1 spacecraft was in a sun synchronous 1030 and 2230 local time polar orbit at 170–280 km, traveling southward during the daytime. The inclination was 96.3°. The characteristics of the electron spectrometers used in the present study are summarized in Table 1.

PRESENTATION AND INTERPRETATION OF DATA

Electrons are precipitated from the slot region of the radiation belts by VLF waves originating from various sources and spanning a broad range of frequencies. The energies of electrons resonating at the equator with waves of selected frequencies traveling parallel to the magnetic field lines are plotted as a function of L in Figure 1. Equatorial plasma densities of 3000 $(L/2)^{-4}$ cm^{-3} have been assumed [*Chappell et al.*, 1970]. For comparison the central energies of peaks observed in the energy spectra of electrons at various L values and mirroring at low altitudes are plotted for representative passes of a satellite when the interactions were identified as being due to VLF waves from transmitters [*Imhof et al.*, 1983], to waves associated with lightning [*Voss et al.*, 1984], or to plasmaspheric hiss [*Imhof et al.*, 1982]. The curves are calculated under the assumption that the particle scattering occurs primarily at the equator with field-aligned waves. Although this assumption is subject to question, a detailed treatment of off-equatorial interactions with waves propagating at finite angles to the magnetic field is beyond the scope of this paper. However, the strong tendency of data such as those plotted in Figure 1 to align with the theoretical curves suggests that the major interaction occurs as assumed here. In any case, in this paper we are directly comparing the spectra observed in the drift loss cone with those observed during bursts, and the detailed nature of the precipitation mechanism should not have a major impact on the conclusions.

Examples of the energy spectra of locally trapped electrons observed near $L = 2.25$ in the drift loss cone are shown in Figure 2. These spectra were all taken from the P78-1 satellite at central pitch angles of 65°–115° and at B values such that the electrons precipitate into the atmosphere before drifting all the way around the earth. Many of these spectra with pronounced peaks are typical of those observed in the drift loss cone in association with plasmaspheric hiss [*Imhof et al.*, 1982]. For completeness, two examples of spectra without peaks are also given. Best fit curves to the data points are shown. From the P78-1 satellite, peaked energy spectra were observed in 62% of the cases, although this percentage is only approximate due to the subjective nature of the criteria for establishing the presence of a peak.

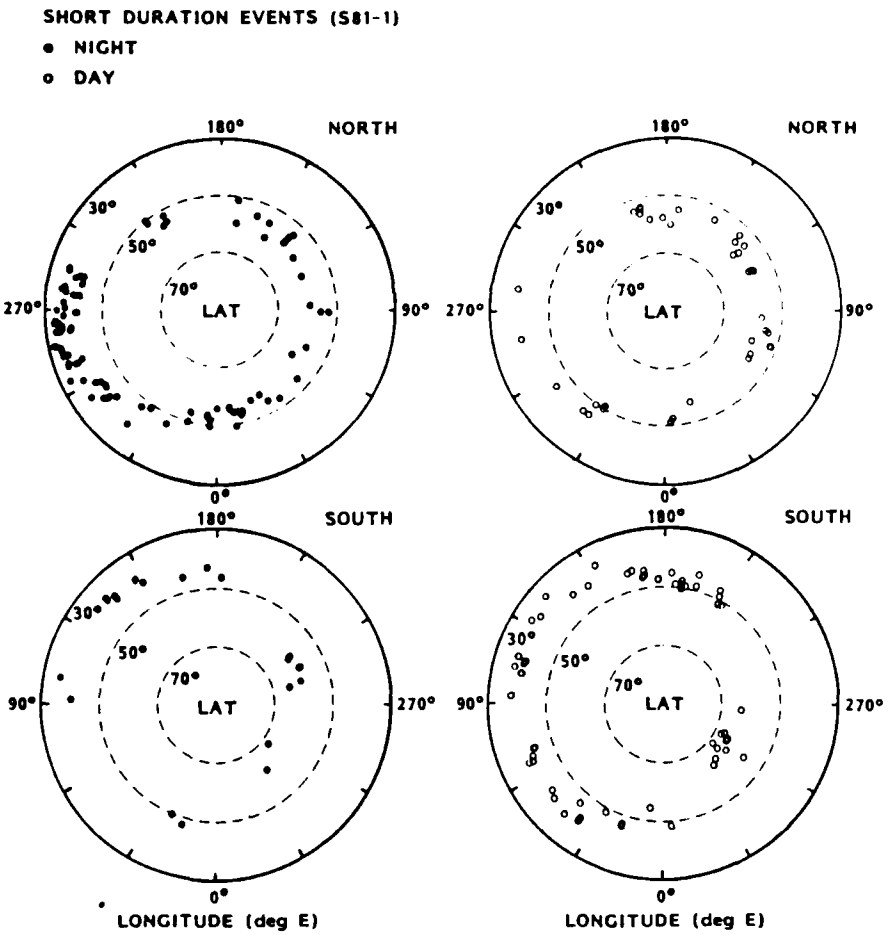

Fig. 3. The geographic latitude/longitude coordinates of short duration electron precipitation events. Separate plots are provided for those observed in the daytime and nighttime and the north and south, respectively.

We now wish to compare the electron energy spectra normally observed in the drift loss cone with those associated with short bursts of electron precipitation. The time structures of the latter events are similar to those of the lightning-induced electron precipitation events presented by *Voss et al.* [1984] or to the precipitation patterns that might be associated with chorus bursts [*Oliven and Gurnett*, 1968]. The LEP events observed by *Voss et al.* [1984] had the following features: (1) a rapid rise of electron flux (<0.2 s), (2) the subsequent and relatively slow decay of the flux (~2 s), (3) repetitive pulses of constant period (~0.3 s) within the overall 2-s decay, (4) the greater intensity of the near-90° pitch angle flux compared with the near-0° pitch angle flux, and (5) the peaked energy spectra (~150 keV). The electron microbursts reported by *Oliven and Gurnett* [1968] were characterized by fast fluctuations on a time scale of ~0.5 s. The microbursts were always accompanied by a group of VLF chorus emissions which consisted of closely spaced discrete bursts, usually rising in frequency in the range ~0.5–6 kHz, with individual bursts typically having a duration of a few tenths of a second. Events in which the fluxes of electrons display a rapid increase with time (about 1 s or less) are probably not associated with plasmaspheric hiss, which typically has much slower temporal variations.

Extremely narrow peaks of the type produced by VLF transmitters [*Vampola and Kuck*, 1978; *Imhof et al.*, 1983] have not been found in the S81-1 slot region data. However, those spectra in which no peaks were present might have been produced by transmitters if the interaction region was broad and not near the equator, as suggested by *Vampola* [1977].

We have compiled energy spectra recorded from the S81-1 satellite in the slot region during precipitation events which have the following characteristics: (1) at least a factor of 2 increase in counting rate of the ME 1 spectrometer, (2) a fast rise time (1 s or less), and (3) a decay time of less than 3 s. These events were most efficiently observed from the oriented satellite S81-1, as the 5.5-s spin period of P78-1 obscured time variations of a few seconds' duration. Short duration events meeting the foregoing criteria were observed from the S81-1 spacecraft in both the bounce and drift loss cones. To obtain the energy spectra of the burst electrons, a subtraction was made of the backgrounds taken just before or after the events. Some of the spectra showed well-defined maxima, whereas others decreased monotonically with energy.

From a survey of the data taken in the range $L = 2$–3 on the S81-1 satellite a total of 222 electron precipitation events of short duration were found that met the above-mentioned criteria. Of these, 102 occurred on the dayside, and 120 on the nightside. Since the satellite was in a 1030 and 2230 local time orbit, the magnetic local time crossings of the $L = 2$–3 region were confined to the near neighborhood of those times. Plots of the geographic coordinates of the dayside and nightside events are shown in Figure 3, where data from the northern and southern hemispheres are plotted separately. The number

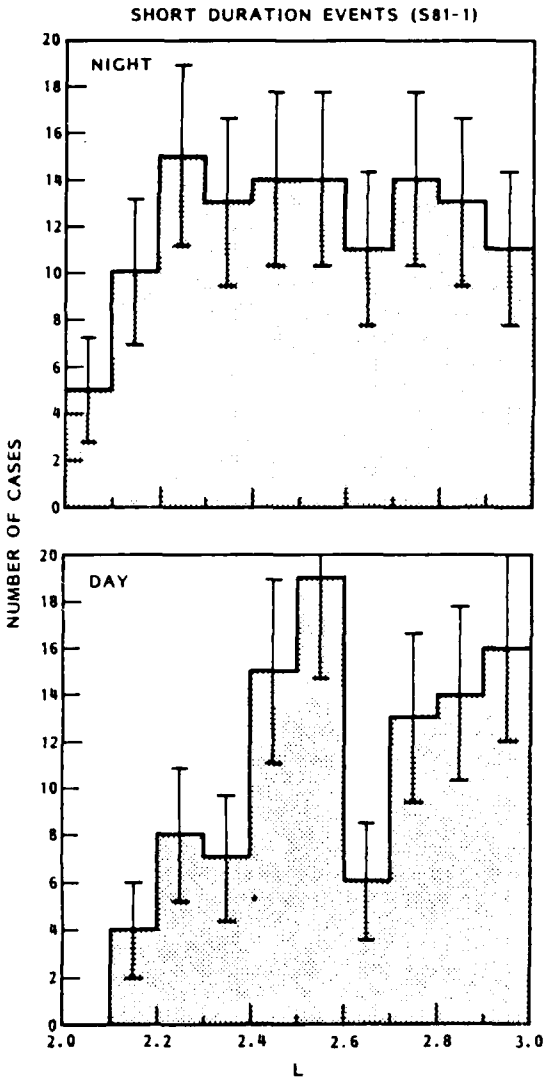

Fig. 4. Distributions in L of the short duration events, separately at night and in the daytime.

of dayside and nightside passes examined in the data set was 4854 and 4773, respectively, and their distribution in longitude was nearly uniform. The plots in Figure 3 therefore represent to a reasonable degree the distribution in occurrence frequency of short duration precipitation events. The nightside events occurred preferentially in the northern hemisphere at longitudes between ~250 E and ~320 E, a region of known lightning-induced electron precipitation activity [*Voss et al.*, 1985*a*]. This enhancement may reflect both the spatial distribution in the occurrence frequency of lightning strokes during the summer and fall months, when most of the data were acquired, and the altitude offset of the magnetic field lines and the associated lower detector backgrounds. For the higher frequency waves associated with lightning (~5 kHz) the transmission through the ionosphere is known to be greater on the nightside by as much as 5 8 dB [*Helliwell*, 1965]. One therefore expects the lightning-induced electron precipitation to be primarily a nightside phenomenon, unless the occurrence frequency were much greater in the daytime or the wave growth were so strong that the input wave intensity was not very important. The diurnal variation of lightning on a worldwide basis is not well known, but in central Europe the probability of thunderstorm activity at 2230 local time is lower than that at 1030 local time by a factor of about 2 [*Israel*, 1973]. Assuming the same diurnal variation to apply to other continents, the higher transmission through the ionosphere at nighttime leads to a domination of the lightning-induced electron precipitation at nighttime.

VLF chorus occurs predominantly between midnight and 1600 local time [*Tsurutani and Smith*, 1977]. The abrupt onset of chorus in the postmidnight sector would not contribute significantly to the nightside data from the S81-1 spacecraft, since these observations occurred at about 2230. It is therefore suspected that many of the dayside events are associated with chorus bursts. Although chorus emissions occur predominantly outside the plasmapause, they have been observed at invariant latitudes below 45° or at L shells below 2 [*Oliven and Gurnett*, 1968]. The short duration electron bursts are assumed not to be caused by hiss, which generally shows no substantial change in its spectrum or intensity for periods of minutes or even hours. "Impulsive" hiss with marked variations in amplitude over periods of the order of 1 s occurs only occasionally [*Helliwell*, 1965]. Of course, for present purposes the terminology applied to short duration wave events is unimportant.

In Figure 4 the number of events have been divided into L shell intervals of 0.1 unit each. The fractional occurrence of events in each interval can be obtained from dividing the number plotted by 4854 for daytime or 4773 for nighttime passes, respectively. The statistical uncertainties are indicated in each case. It can be seen that within the interval $2 < L < 3$ the dayside events tended to occur more often on higher L shells, whereas the nightside events spanned that region more uniformly. The predominance of the dayside events at the higher end of the region $L = 2$ 3 is consistent with the origin being chorus, which is very common beyond the plasmapause [*Burtis and Helliwell*, 1975; *Tsurutani and Smith*, 1977]

Corresponding to the peaks observed in the energy spectra, the equivalent wave frequencies have been calculated for waves traveling parallel to the magnetic field lines. First-order cyclotron resonance interactions have been assumed to occur at the equator with a cold plasma density taken to be $3000\ (L/2)^{-4}\ \mathrm{cm}^{-3}$. The distributions of the equivalent frequencies are shown in Figure 5 with the statistical uncertainties indicated. The dayside and nightside distributions are similar, although the fast rise events at night appear to show a greater concentration near 4 kHz.

The rising frequency character of chorus should manifest itself in the electron spectra as a peak energy that decreases with increasing time. This property of the electron energy spectra has been investigated by considering the time dependence of the ratios of electron fluxes above various threshold energies. In Figure 6 the ratios of flux above 100 keV to flux above 45 keV are plotted as a function of time for three nightside and three dayside events. To achieve better statistical accuracies, the spectral ratios were taken from the TE 2 spectrometer at 90° zenith angle, but the short events were observed in both the TE 2 and ME 1 spectrometers and hence in both the bounce and drift loss cones. The spectral variations with time are therefore believed not to result from drift dispersion effects. These events were selected from 69 cases with high-intensity enhancements in the TE 2 detector and hence good statistical accuracies in the ratios. From that group, 16 had well-defined trends for either hardening or softening over a time interval spanning the maximum counting rate. Eight of the nine nightside cases had a ratio increasing with time, and

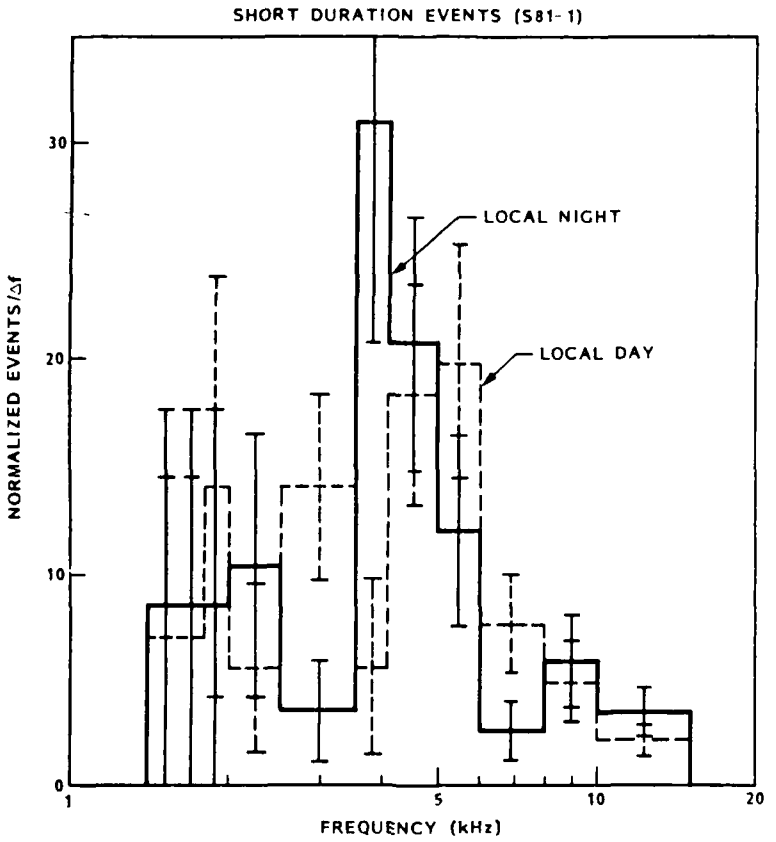

Fig. 5. Distributions in equivalent frequencies of the waves responsible for the observed peaks in the electron spectra. The waves are assumed to be traveling parallel to the magnetic field lines, and a plasma density of $3000\ (L/2)^{-4}$ cm^{-3} has been used.

all seven of the dayside cases had a ratio decreasing with time. In each section of the figure the counting rates of electrons above 45 keV are plotted below the ratios. The statistical uncertainties associated with each ratio are indicated, but they are not shown for the counting rates, since the errors fall within the data point symbols. For the dayside events the decreasing ratio with increasing time is consistent with a rising frequency, as observed in most chorus events. This trend is relatively small but nonetheless beyond the statistical uncertainties. On the other hand, the nightside events often show an increasing ratio with increasing time, which indicates a falling frequency with time. The latter pattern is a characteristic of whistlers. The dynamic spectra of precipitating electrons associated with lightning events have been studied in detail [*Voss et al.*, 1985*a*] and a spectral hardening from 100 to 350 keV with increasing time was clearly present. For all of the examples presented here the dayside events showed a softening with time, whereas a hardening was observed in the nighttime cases, as expected for chorus and lightning events, respectively. However, for 53 of the 69 cases, or approximately 77%, there appeared no significant spectral trend in either direction over the time interval of concern.

A statistical study has been performed of the energy spectra of electrons measured in the drift loss cone. At low altitudes such electrons are observed at most longitudes, as illustrated in Figure 7. In this figure the fluxes of locally mirroring electrons of > 68 keV in the range $2.5 < L < 2.6$ and at an altitude of ~ 600 km are plotted as a function of longitude, separately in the northern and southern hemispheres. These values are averages recorded over each longitude interval. The value of B at the point of observation is shown in the upper section of the figure. When B is greater than 0.31, the minimum drift altitude of the observed electrons is less than 0 km, and the electrons precipitate into the atmosphere sometime during their longitude drift. All such electrons are in the drift loss cone. From the figure it is clear that at these I values significant fluxes of drift loss cone electrons are observed at most longitudes. Only in the northern hemisphere at points conjugate to the South Atlantic Anomaly are the average fluxes very low.

To examine whether the drift loss cone electrons represent a significant portion of those being precipitated from the radiation belt, we have calculated the total loss rates into the atmosphere. Knowing the detailed pitch angle distributions and energy spectra of electrons at 600-km altitude, one can compute the instantaneous loss rate of electrons into the atmosphere. The measurements used for this purpose were performed with the PRM 004 instrument, which has a 3.5° collimator half angle and a $\sim 2°$ spin accumulation interval, leading to an overall angular resolution of $\pm 4°$. The geometric factor of this spectrometer is relatively small (~ 0.001 cm^2 sr), and it was generally necessary to combine data from several spins and from more than one satellite pass through a region of interest to obtain adequate statistical accuracies. Typical pitch angle distributions obtained by these means are shown in Figure 8 for three longitude intervals in the southern hemisphere. Two of the distributions are at local noon, whereas the fluxes at longitudes east of the anomaly were measured at night. Each of these distributions is taken from five to eight satellite passes. Clearly, the pitch angle distributions are wider

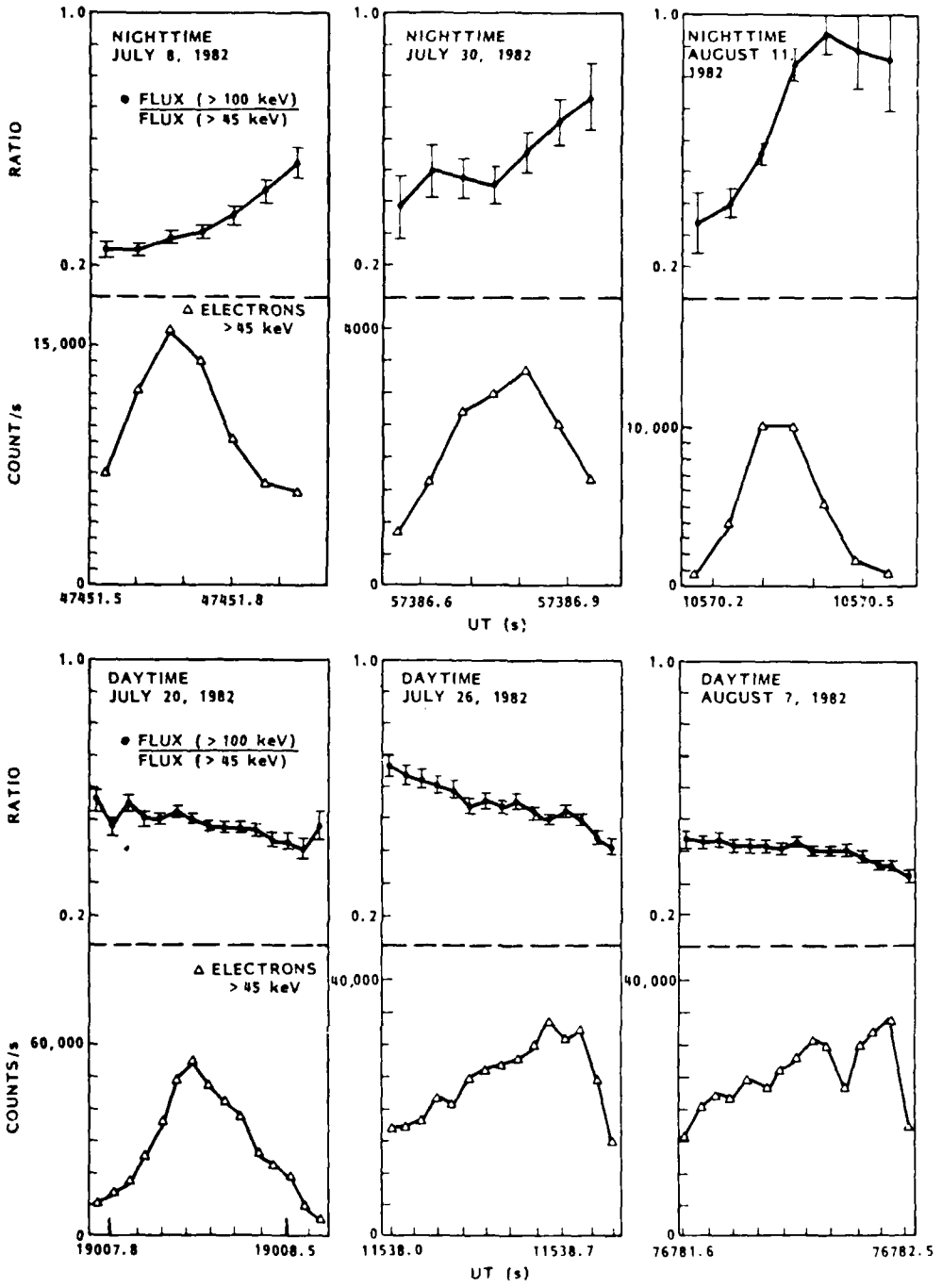

Fig. 6. Ratios of the fluxes of electrons above 100 keV to those above 45 keV in the TE 2 spectrometer plotted as a function of time for representative dayside and nightside events. Also plotted in each section are the counting rates of electrons above 45 keV.

for electrons in the drift loss cone at the western edge of the anomaly than for the more stably trapped electrons observed in the heart of the anomaly.

The observed pitch angle distributions at several longitudes were combined with the absolute intensities and energy spectra extrapolated to 10 keV to calculate the total loss rates of electrons into the atmosphere [*Walt et al.*, 1968]. These loss rates at $L = 2.5$ are plotted in Figure 9 as a function of longitude for electrons precipitating in the southern hemisphere. For each longitude interval, data were taken from a variety of satellite passes (six on the average) during both magnetically active and quiet conditions. The error bars represent the range of energy depositions corresponding to the limits of the pitch angle distributions for individual passes at a given longitude. Although the present results exhibit large variations, the derived electron loss rates are consistent with the measured lifetimes. Since the pitch angle distributions are peaked at 90°, the loss rates in Figure 9 are primarily due to electrons near the edge of the loss cone. The loss rates from electrons well within the bounce loss cone make only a small contribution to

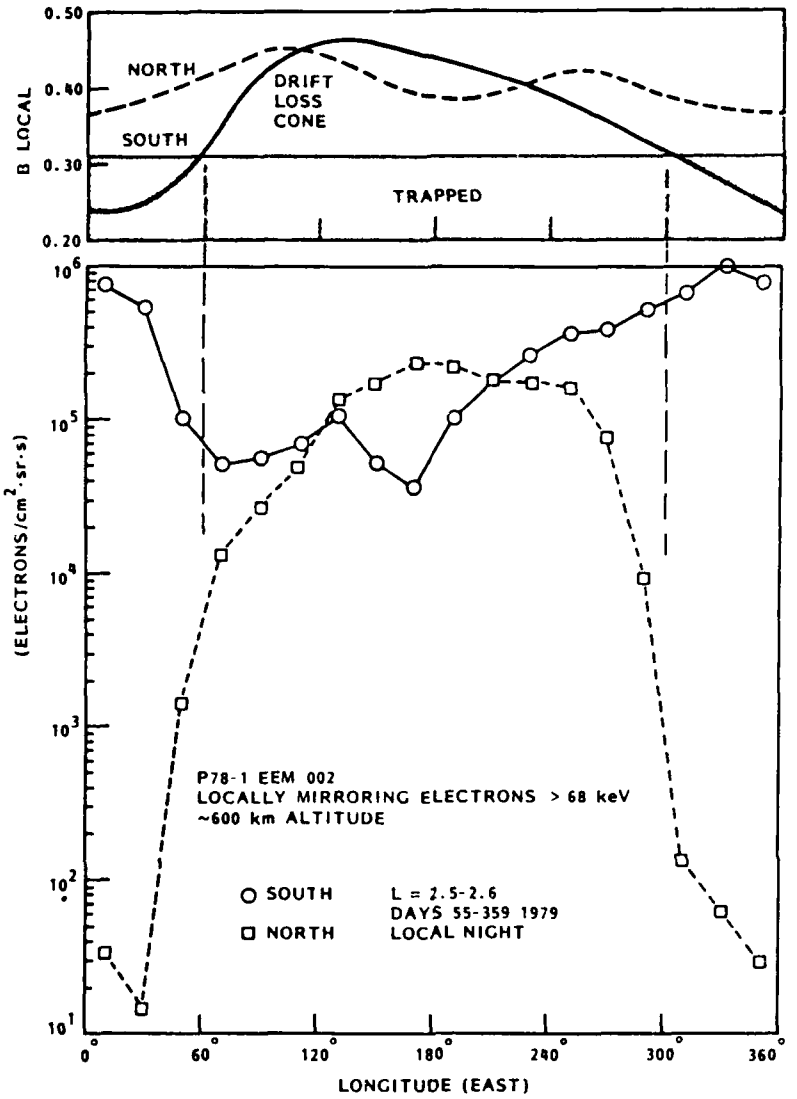

Fig. 7. Fluxes of electrons >68 keV from the P78-1 satellite at $L = 2.5$–2.6 plotted as a function of longitude. The points shown are average values recorded over each longitude interval.

the longitude and hemisphere averages, the greatest loss rates occurring in the south at longitudes near the South Atlantic Anomaly.

The energy deposition rate averaged over all longitudes in the southern hemisphere at $L = 2.5$ is 10^{-3} ergs/cm^2 s, whereas the rate in the north is much less. Equivalently, the average loss rate for electrons in the southern hemisphere is 6×10^3 el/cm^2 s. Taking an equatorial flux of 1.7×10^8 el/cm^2 s at $L = 2.5$, the number of electrons in the tube of unit area at the top of the atmosphere is 10^9 el/cm^2. A loss rate of 6×10^3 el/cm^2 s therefore implies a lifetime of 1.9 days. With allowance for the uncertainties this value is consistent with measured lifetimes of ~5 days at $L = 2.5$ for electrons in the few hundred keV range as measured by Vampola [*Lyons et al.*, 1972] or the return of poststorm fluxes to their prestorm levels within a few days [*Lyons and Williams*, 1975]. *West et al.* [1981] measured lifetimes of ~(5–11) days at $L = 2.5$. Subsequent to the flux buildup associated with magnetic activity the mid-latitude electron flux was observed by *Voss et al.* [1985*b*] to decrease with an *e*-folding time of about 5 days. These comparisons indicate that the electrons observed in the drift loss cone represent a major fraction of those being lost from the slot region. Electron energy deposition rates at various longitudes have also been derived by *Vampola and Gorney* [1983] based on measurements from the S3-2 satellite of locally precipitating electrons. Their energy depositions, which apply to 36- to 317-keV electrons, show less variation with longitude than Figure 9 and are a factor of about 5 lower.

The distributions of the central energies of the spectral peaks observed under various conditions at $L = 2.25$ are shown in Figure 10. Similar plots are provided in Figures 11 and 12 for $L = 2.50$ and 2.75, respectively. These L values have been selected to span the range $L = 2$–3, which is representative of the slot region. For either the daytime or nighttime distributions the median peak energies in the drift loss cone decrease somewhat with increasing L value, although the decrease is not as rapid as the decrease in resonant energy with L for constant frequency. This observation may reflect a greater importance of lower frequency waves at higher L values. For intercomparison the distributions in peak energies are shown separately for short duration precipitation events

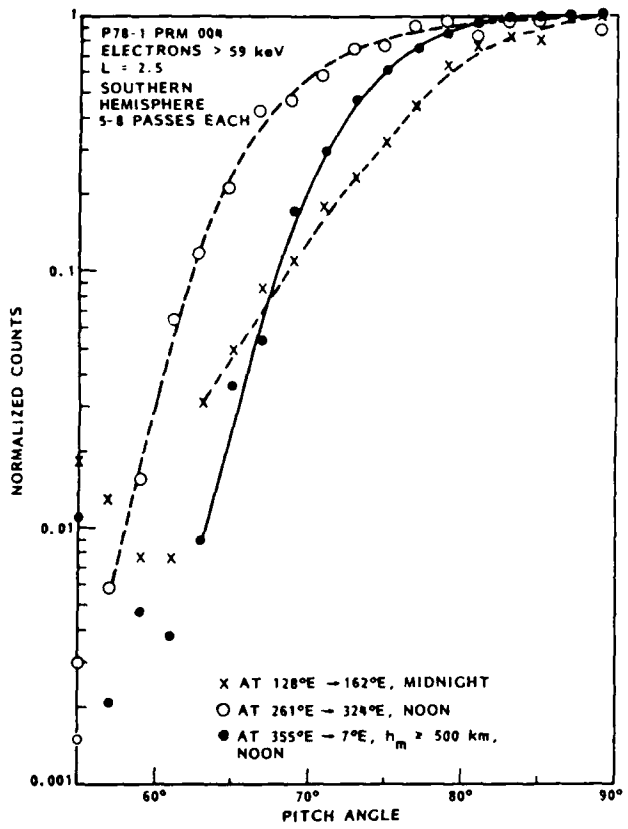

Fig. 8. Pitch angle distributions observed from the P78-1 satellite at ~600-km altitude over each of three different longitude intervals.

observed at 170–280 km altitude and for the more persistent drift loss cone electrons observed at similar altitudes from the S81-1 satellite or at 600 km from the P78-1 spacecraft. The short duration events, which are in both the bounce and drift loss cones, are plotted only for data taken on the oriented spacecraft, since they could not be observed efficiently from the spinning satellite. The spectra for short duration events were summed over time intervals of 1–3 s, the exact duration selected on the basis of the amplitude profile. The peak energies were obtained empirically from the spectra, and no special effort was devoted to distinguishing the equatorial and off-equatorial contributions. Clearly, at each of the L shells, most of the peaks associated with short duration events tend to be at lower energies than most of those observed in the drift loss cone, although there is some overlap. This difference in energy is more pronounced at the higher L shells. These spectral differences are consistent with the importance of the plasmaspheric hiss mechanism for producing the drift loss cone electron distribution, since hiss typically is of lower frequency than whistlers and will resonate with higher energy electrons. In all of the drift loss cone examples in Figures 10, 11, and 12, peaks were observed in 57% of the nighttime and 64% of the daytime energy spectra. For the short duration bursts the equivalent fractions were 47% and 70% of the nighttime and daytime cases, respectively.

When comparing the distributions of peak energies in Figures 10, 11, and 12, one should note that the P78-1 data have a threshold of 68 keV, while the S81-1 data correspond to a threshold of 6 keV. This threshold difference could lead to an apparent higher average energy for the P78-1 distribution. *However, using only S81-1 data for burst fluxes and the drift loss cone fluxes leads to the conclusions mentioned above.*

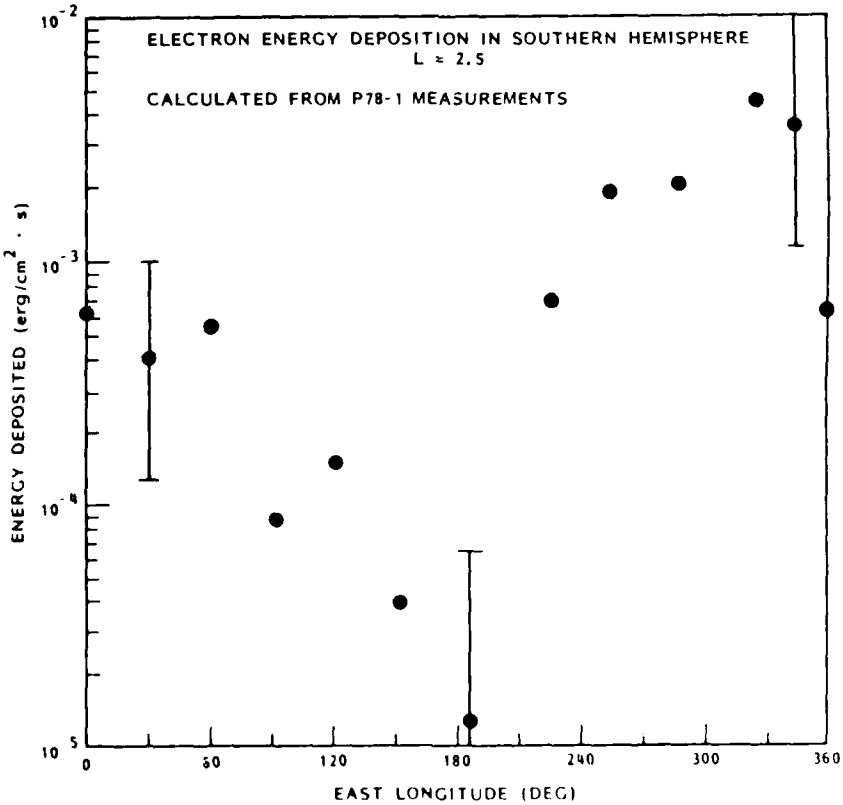

Fig. 9. The average rate of deposition of energy into the atmosphere in the southern hemisphere plotted as a function of longitude at $L = 2.5$. For each longitude interval, data were taken during both active and quiet conditions. The error bars are estimated uncertainties.

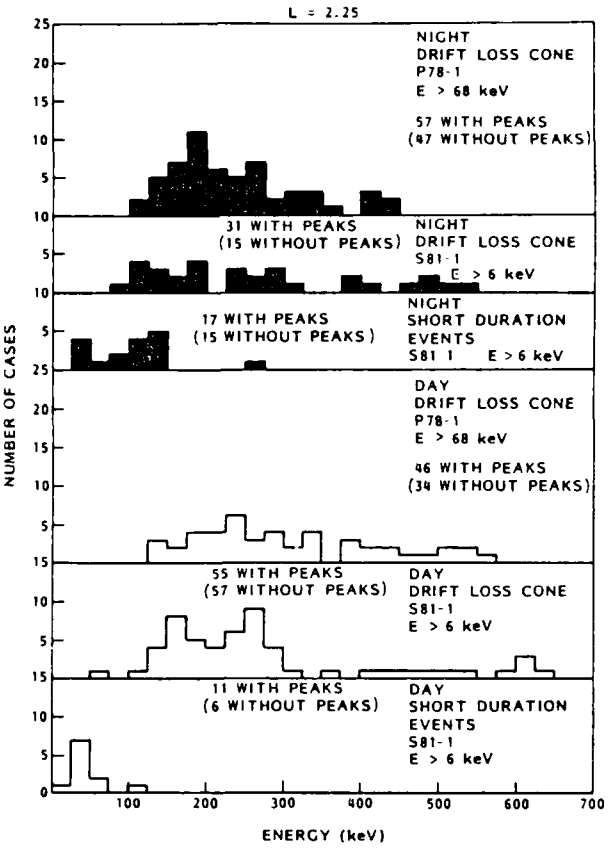

Fig. 10. The distributions in central peak energies observed from the EEM 002 spectrometer on the P78-1 spacecraft and the TE 2 spectrometer on the S81-1 satellite under various conditions at $L = 2.126$–2.375.

One characteristic of the peaks in the energy spectra of electrons in the drift loss cone is that the median energies are higher on the dayside than at nighttime. This difference could reflect diurnal variations in the cold plasma densities. However, from a statistical study of a large body of whistler data *Park et al.* [1978] found that for $L > 3$, diurnal effects are obscured by relatively large day-to-day variations in the plasma density due to storm and substorm effects.

The diurnal variation in the occurrence frequency of spectral peaks in the drift loss cone has been investigated based on the distributions shown in Figures 10, 11, and 12. For each energy interval the day-to-night ratio of the percentage of passes with peaks has been derived. These ratios are presented in Figure 13, where the energy intervals have been converted to equivalent wave frequency intervals for first-order cyclotron resonance taking place near the equator. Again it has been assumed that the waves are traveling parallel to the magnetic field lines and that the cold plasma density is given by the empirical value $3000\,(L.2)^{-4}$ cm^{-3}. The data from each of the two satellites P78-1 and S81-1 clearly indicate a trend for the day-to-night ratio to decrease with increasing frequency. A ratio less than 1.0 at frequencies above ~ 3 kHz is consistent with the lower transmission of such waves through the daytime ionosphere and therefore suggests that these waves may have originated below the ionosphere, as in the case of lightning or transmitter-generated waves. At lower frequencies the diurnal variation in the ionospheric transmission becomes very small, and one would therefore expect the day-to-night ratio to be close to unity if the occurrence rate of the source were independent of local time. Since the ratio is greater than unity at frequencies near 1 kHz, it is concluded that such waves occur more often in the daytime. Although the diurnal variations of ELF/VLF waves near the equator are not well known, existing observations suggest that their intensities increase in the early daylight hours [e.g., *Barrington et al.*, 1971; *Dunckel and Helliwell*, 1969]. The present data are consistent with such a diurnal variation. An increased intensity in the daytime also applies to VLF chorus emissions, which may contribute significantly to the drift loss cone fluxes at $L \geq 2.5$. Chorus has been found to favor strongly times near 1030 MLT in comparison to 2230 MLT [*Luette*, 1983]. On the other hand, from the S81-1 data the short duration events at $L \leq 2.5$ have been found to occur less often in the daytime than nighttime. This suggests that the nightside events are more associated with lightning than chorus.

Summary

From a survey of short duration precipitation events it has been found that the nightside events occurred primarily in the northern hemisphere and preferentially at longitudes between about 250 E and about 320 E. This interval is a region of

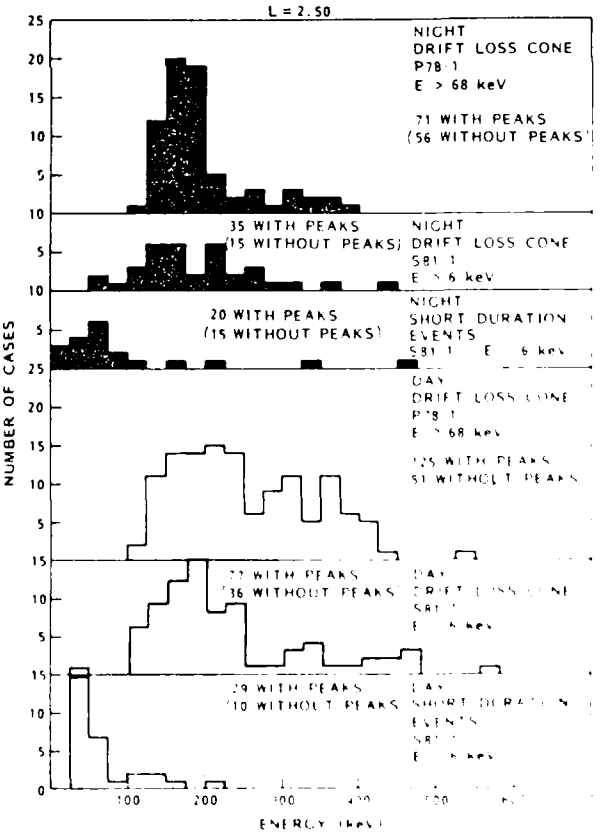

Fig. 11. The distributions in central peak energies observed from the EEM 002 spectrometer on the P78-1 spacecraft and the TE 2 spectrometer on the S81-1 satellite under various conditions at $L = 2.376$–2.625.

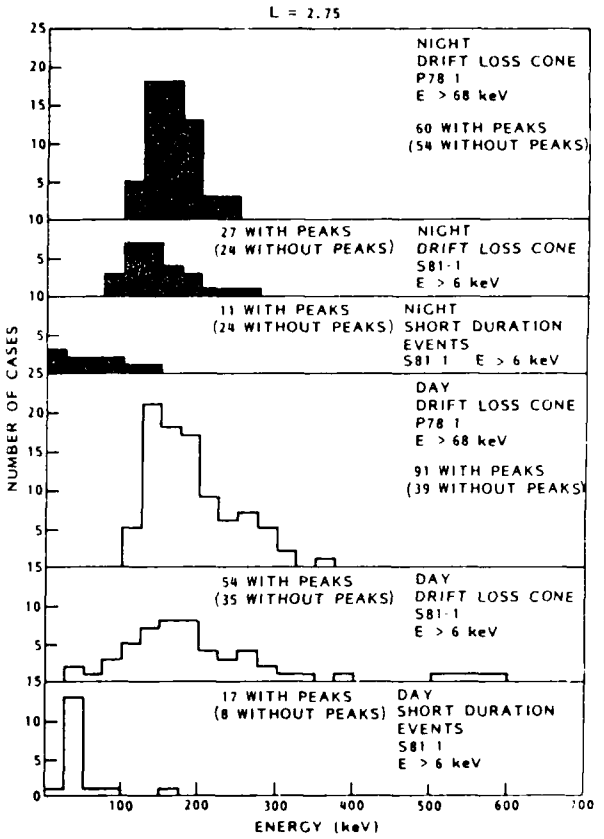

Fig. 12. The distributions in central peak energies observed from the EEM 002 spectrometer on the P78-1 spacecraft and the TE 2 spectrometer on the S81-1 satellite under various conditions at $L = 2.626$–2.875.

preferred lightning activity, especially in the summer and fall months, when most of the data were acquired. Although in this longitude interval, short duration events were observed much more often at nighttime than was true at other longitudes, the frequency of occurrence of dayside events was not enhanced. This behavior is consistent with a low transmission of lightning-induced waves through the ionosphere in the daytime. Other diurnal differences were clearly present, such as the higher L shell preference within the range $2 < L < 3$ for dayside events and the more uniform distribution of nightside events. The combined diurnal, longitude, and L shell variations of the short duration bursts are consistent with the nightside events being predominantly associated with lightning and the dayside events being caused by chorus.

From calculations of the total loss rates of electrons in the drift loss cone based on pitch angle distribution and energy spectrum measurements we conclude that electrons in the drift loss cone represent a significant fraction of those lost from the slot region. Within the slot region the peaks associated with drift loss cone electrons tend to be at higher energies than those observed in short duration events. Barring unexpected and pronounced differences between these classes of precipitation in the position of interaction relative to the equator or the propagation angles of the waves, this finding suggests that most of the precipitating electrons injected into the drift loss cone by wave-particle interactions involve waves of lower frequencies and hence higher resonant electron energies than do the waves associated with the short duration lightning or chorus. Such waves are probably predominantly associated with plasmaspheric hiss. On the other hand, there is some overlap between the two distributions in peak energy, and lightning may play a role in precipitating electrons in the slot region primarily at nighttime. Its greatest contribution appears to be at low L shells.

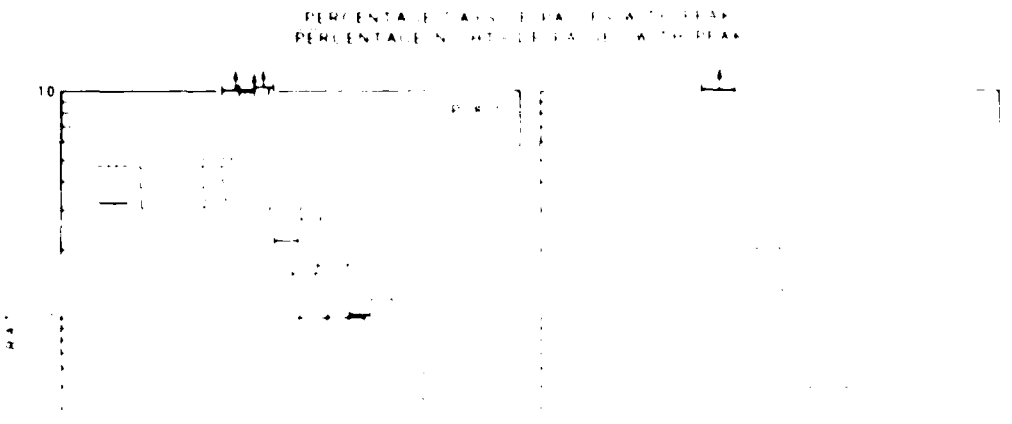

AD-A188 724 STIMULATED EMISSION OF ENERGETIC PARTICLES (SEEP)(U) 3/3
LOCKHEED MISSILES AND SPACE CO INC PALO ALTO CA PALO
ALTO RESEARCH LAB W L IMHOF ET AL. 30 NOV 87
UNCLASSIFIED LMSC/D068456 N00014-79-C-0824 F/G 4/1 NL

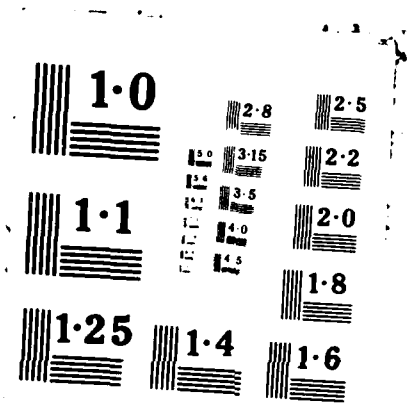
1·0
2·8
2·5
3·15
2·2
3·5
1·1
2·0
1·8
1·25
1·4
1·6

Acknowledgments. The development of the P78-1 satellite payload and the performance of the experiment was supported by the Defense Advanced Research Project Agency through the Office of Naval Research (contract N00014-78-C-0070). The SEEP payload on the S81-1 spacecraft was sponsored by the Office of Naval Research (contract N00014-79-C-0824). For both of these satellite experiments, launch and orbital support were provided by the Air Force Space Test Program Office. Much of the data analysis presented here was sponsored by the Lockheed Independent Research Program. Appreciation is extended to J. P. McGlennon, K. Van Stone, and C. K. Chalmers for their efforts in processing the data. Helpful discussions with R. A. Helliwell and U. S. Inan are appreciated.

The Editor thanks R. M. Thorne and another referee for their assistance in evaluating this paper.

REFERENCES

Barrington, R. E., T. R. Hartz, and R. W. Harvey, Diurnal distribution of ELF, VLF, and LF noise at high latitudes as observed by Alouette 2, *J. Geophys. Res.*, *76*, 5278, 1971.

Burtis, W. J., and R. A. Helliwell, Magnetospheric chorus: Amplitude and growth rate, *J. Geophys. Res.*, *80*, 3265, 1975.

Carpenter, D. L., U. S. Inan, M. L. Trimpi, R. A. Helliwell, and J. P. Katsufrakis, Perturbations of subionospheric LF and MF signals due to whistler-induced electron precipitation bursts, *J. Geophys. Res.*, *89*, 9857, 1984.

Chappell, C. R., K. K. Harris, and G. W. Sharp, The morphology of the bulge region of the plasmasphere, *J. Geophys. Res.*, *75*, 3848, 1970.

Cornwall, J. M., Scattering of energetic trapped electrons by very-low-frequency waves, *J. Geophys. Res.*, *69*, 1251, 1964.

Dunckel, N., and R. A. Helliwell, Whistler mode emissions on the OGO 1 satellite, *J. Geophys. Res.*, *74*, 6371, 1969.

Dungey, J. W., Loss of Van Allen electrons due to whistlers, *Planet. Space Sci.*, *11*, 591, 1963.

Helliwell, R. A., *Whistlers and Related Ionospheric Phenomena*, Stanford University Press, Stanford, Calif., 1965.

Helliwell, R. A., J. P. Katsufrakis, T. F. Bell, and R. Raghuram, VLF line radiation in the earth's magnetosphere and its association with power system radiation, *J. Geophys. Res.*, *80*, 4249, 1975.

Imhof, W. L., E. E. Gaines, and J. B. Reagan, Observations of multiple, narrow energy peaks in electrons precipitating from the inner radiation belt and their implications for wave-particle interactions, *J. Geophys. Res.*, *86*, 1591, 1981.

Imhof, W. L., R. R. Anderson, J. B. Reagan, and E. E. Gaines, Coordinated measurements of slot region electron precipitation by plasmaspheric wave bands, *J. Geophys. Res.*, *87*, 4418, 1982.

Imhof, W. L., J. B. Reagan, H. D. Voss, E. E. Gaines, D. W. Datlowe, J. Mobilia, R. A. Helliwell, U. S. Inan, J. Katsufrakis, and R. G. Joiner, Direct observation of radiation belt electrons precipitated by the controlled injection of VLF signals from a ground-based transmitter, *Geophys. Res. Lett.*, *10*, 361, 1983.

Imhof, W. L., J. B. Reagan, E. E. Gaines, and D. W. Datlowe, The *L* shell region of importance for waves emitted at ground level as a loss mechanism for trapped electrons >68 keV, *J. Geophys. Res.*, *89*, 10,827, 1984.

Israel, H., *Atmospheric Electricity*, vol. II, *Fields, Charges, Currents*, p. 365, Israel Program for Scientific Translations, Jerusalem, 1973.

Luette, J. P., Power line radiation in the magnetosphere, Ph.D. dissertation, Stanford University, Stanford, Calif., March 1983.

Luette, J. P., C. G. Park, and R. A. Helliwell, The control of the magnetosphere by power line radiation, *J. Geophys. Res.*, *84*, 2657, 1979.

Lyons, L. R., and D. J. Williams, The storm and poststorm evolution of energetic (35-560 keV) radiation belt electron distributions, *J. Geophys. Res.*, *80*, 3985, 1975.

Lyons, L. R., R. M. Thorne, and C. F. Kennel, Pitch angle diffusion of radiation belt electrons within the plasmasphere, *J. Geophys. Res.*, *77*, 3455, 1972.

Oliven, M. N., and D. A. Gurnett, Microburst phenomena, 3. An association between microbursts and VLF chorus, *J. Geophys. Res.*, *73*, 2355, 1968.

Park, C. G., and R. A. Helliwell, Whistler precursors: A possible catalytic role of power line radiation, *J. Geophys. Res.*, *82*, 3234, 1977.

Park, C. G., D. L. Carpenter, and D. B. Wiggin, Electron density in the plasmasphere: Whistler data on solar cycle, annual, and diurnal variations, *J. Geophys. Res.*, *83*, 3137, 1978.

Roberts, C. S., Electron loss from the Van Allen zones due to pitch angle scattering by electromagnetic disturbances, in *Radiation Trapped in the Earth's Magnetic Field*, edited by B. M. McCormac, p. 403, D. Reidel, Hingham, Mass., 1966.

Tsurutani, B. T., and E. J. Smith, Two types of magnetospheric ELF chorus and their substorm dependences, *J. Geophys. Res.*, *82*, 5112, 1977.

Vampola, A. L., VLF transmission induced slot electron precipitation, *Geophys. Res. Lett.*, *4*, 569, 1977.

Vampola, A. L., and D. J. Gorney, Electron energy deposition in the middle atmosphere, *J. Geophys. Res.*, *88*, 6267, 1983.

Vampola, A. L., and G. A. Kuck, Induced precipitation of inner zone electrons, 1, Observations, *J. Geophys. Res.*, *83*, 2543, 1978.

Voss, H. D., J. B. Reagan, W. L. Imhof, D. O. Murray, D. A. Simpson, D. P. Cauffman, and J. C. Bakke, Low temperature characteristics of solid state detectors for energetic x-ray, ion and electron spectrometers, *IEEE Trans. Nucl. Sci.*, *NS-19*, 164, 1982.

Voss, H. D., W. L. Imhof, M. Walt, J. Mobilia, E. E. Gaines, J. B. Reagan, U. S. Inan, R. A. Helliwell, D. L. Carpenter, J. P. Katsufrakis, and H. C. Chang, Lightning-induced electron precipitation, *Nature*, *312*, 740, 1984.

Voss, H. D., W. L. Imhof, M. Walt, J. Mobilia, E. E. Gaines, U. S. Inan, R. A. Helliwell, and D. L. Carpenter, Energy and time structure of lightning-induced electron precipitation, (abstract), *Eos Trans. AGU*, *66*, 350, 1985*a*.

Voss, H. D., W. L. Imhof, J. Mobilia, E. E. Gaines, and J. B. Reagan, Energetic particles in the nighttime middle and low latitude ionosphere, *Adv. Space Res.*, *5*(4), 175-178, 1985*b*.

Walt, M., The effects of atmospheric collisions of geomagnetically trapped electrons, *J. Geophys. Res.*, *69*, 3947, 1964.

Walt, M., W. M. McDonald, and W. E. Francis, Penetration of auroral electrons into the atmosphere, in *Physics of the Magnetosphere*, edited by R. L. Carovillano, J. F. McClay, and H. R. Radoski, D. Reidel, Hingham, Mass., 534, 1968.

West, H. I., Jr., R. M. Buck, and G. T. Davidson, The dynamics of energetic electrons in the earth's outer radiation belt during 1968 as observed by the Lawrence Livermore National Laboratory's spectrometer on OGO 5, *J. Geophys. Res.*, *86*, 2111, 1981.

D. W. Datlowe, E. E. Gaines, W. L. Imhof, J. Mobilia, J. B. Reagan, H. D. Voss, and M. Walt, Lockheed Palo Alto Research Laboratory, Palo Alto, CA 94304.

(Received November 19, 1985;
revised April 7, 1986;
accepted April 17, 1986.)

JOURNAL OF GEOPHYSICAL RESEARCH, VOL. 92, NO. A5, PAGES 4515-4524, MAY 1, 1987

Electron Precipitation Bursts in the Nighttime Slot Region Measured Simultaneously From Two Satellites

W. L. IMHOF, H. D. VOSS, J. MOBILIA, AND E. E. GAINES

Lockheed Palo Alto Research Laboratory, Palo Alto, California

D. S. EVANS

National Oceanic and Atmospheric Administration, Boulder, Colorado

Based on data acquired in 1982 with the Stimulated Emission of Energetic Particles payload on the low-altitude (170–280 km) S81-1 spacecraft and the Space Environment Monitor instrumentation on the NOAA 6 satellite (800–830 km), a study has been made of short-duration nighttime electron precipitation bursts at $L = 2.0$–3.5. From 54 passes of each satellite across the slot region simultaneously in time, 21 bursts were observed on the NOAA 6 spacecraft, and 76 on the S81-1 satellite. Five events, probably associated with lightning, were observed simultaneously from the two spacecraft within 1.2 s, providing a measure of the spatial extent of the bursts. This limited sample indicates that the intensity of precipitation events falls off with width in longitude and L shell but individual events extend as much as 5° in invariant latitude and 43° in longitude. The number of events above a given flux observed in each satellite was found to be approximately inversely proportional to the flux. The time average energy input to the atmosphere over the longitude range 180°E to 360°E at a local time of 2230 directly from short-duration bursts spanning a wide range of intensity enhancements was estimated to be about 6×10^{-6} ergs/cm^2 s in the northern hemisphere and about 1.5×10^{-5} ergs/cm^2 s in the southern hemisphere. In the south, this energy precipitation rate is lower than that from electrons in the drift loss cone by about 2 orders of magnitude. However, on the basis of these data alone we cannot discount weak bursts from being a major contributor to populating the drift loss cone with electrons which ultimately precipitate into the atmosphere.

INTRODUCTION

Electrons are known to be precipitated from the radiation belts in short-duration bursts by lightning-induced waves based on theory [*Dungey*, 1963; *Cornwall*, 1964; *Roberts*, 1966], rocket measurements [*Rycroft*, 1973; *Goldberg et al.*, 1986], Trimpi events [*Carpenter et al.*, 1984], and satellite measurements [*Voss et al.*, 1984; *Imhof et al.*, 1986]. Chorus events [*Oliven and Gurnett*, 1968] also play a role in precipitating electrons. Important characteristics of a given event are the intensity, the energy spectrum, the pitch angle scattering, and the spatial extent in L shell and longitude. This information is needed for assessing the total number of electrons precipitated, for studying the propagation in longitude or L shell of the responsible waves, and for assessing the effects on radio wave propagation of the associated ionospheric changes. The intensities and energy spectra of a few events identified with lightning were measured by *Voss et al.* [1984]. In that paper, some indications were obtained of the spatial extents, since the events were recorded on the ground level as whistlers and the precipitating electrons were observed 2000 km away in longitude on a satellite. However, precise knowledge of the spatial extents of the events was limited by the fact that the precipitation was measured directly at only one location. Information on the intensities and spatial extents of lightning-induced electron precipitation can, in principle, be obtained from study of Trimpi events [*Carpenter et al.*, 1984], but generally, there are uncertainties involved in the interpretation of those data. The most direct approach for obtaining this information is to measure the precipitating electrons directly.

Copyright 1987 by the American Geophysical Union.

Paper number 6A8744
0148-0227/87/006A-8744$05.00

The energy spectra of short-duration events were recently studied, using data from the SEEP experiment on the S81-1 satellite [*Imhof et al.*, 1986]. The objective of that investigation was to assess the importance of such events as a loss mechanism for slot region electrons based on the presence of L-dependent peaks in the spectra. The observable bursts were found not to account for the bulk of the precipitation. Evaluations of the importance of short-duration bursts can also be made on the basis of the measured occurrence frequency, spatial size, and electron flux distributions. In this paper we have studied the spatial sizes of electron bursts by analyzing particle measurements performed simultaneously from the S81-1 and NOAA 6 satellites at local night and at times when both spacecraft were in the L shell range where such events are most commonly observed, $L = 2.0$–3.5. These bursts are probably associated with lightning [*Voss et al.*, 1984; *Imhof et al.*, 1986]. This study has encompassed weaker events than those considered in the earlier investigation, and for the first time the intensity distribution of the short-duration bursts has been obtained.

DESCRIPTION OF INSTRUMENTATION

The data presented here were acquired in the time period June–December 1982 with electron spectrometers placed on the S81-1 and the NOAA 6 satellites. The S81-1 spacecraft was three-axis stabilized in a sun-synchronous polar orbit at low altitude (170–280 km), which was phased so that the satellite crossed the equator northbound at a local time of approximately 2230. It carried the Stimulated Emission of Energetic Particles (SEEP) experiment, which contained an array of cooled silicon solid state detectors to measure electrons and ions directly with high sensitivity and fine energy resolution [*Voss et al.*, 1982]. The electron spectrometers were oriented at various angles to the local vertical and covered energies up

to about 1 MeV. In this study, use is made of three electron spectrometers. The instrument ME 1 at a zenith angle of 0° had an acceptance angle of ±30°, a threshold energy of 45 keV, and a geometric factor of 2.47 cm² sr. The spectrometer TE 2 at 90° zenith angle had an acceptance angle of ±20°, a threshold of 6 keV, and a geometric factor of 0.17 cm² sr. The spectrometer LE 5 was oriented at a zenith angle of 50°, had an acceptance angle of ±20°, a threshold energy of about 2 keV, and a geometric factor of 0.17 cm² sr. The SEEP counting rates were accumulated during successive 0.064-s intervals.

The NOAA 6 satellite is three-axis stabilized in a 800- to 830-km-altitude polar orbit, which is phased so that the satellite crosses the equator northbound at a subsatellite local time of approximately 1930. The Space Environment Monitor (SEM) on this spacecraft includes a set of solid state detectors which measure the intensity of electrons and ions over the energy range from 30 keV to >1000 keV (for electrons) and 30 keV to >2500 keV (for protons). The geometric factor of these detectors is 9.5×10^{-3} cm² sr for both the electron and proton detector systems. The fields of view are ±15°. One of the electron detector systems is oriented to view zenith, the other viewing at 81° to the zenith in a plane perpendicular to the orbit plane. The latter detector measures trapped electrons at most locations in the orbit. Counting rates from the NOAA 6 detectors were accumulated with a 50% duty cycle for 1-s intervals; there was a multiplexing of data between the zenith viewing and 81° detectors. Therefore the observations from a single detector were not continuous but rather 1-s samples available every other second.

In each of the electron spectrometers on both satellites some counts were lost from scattering of electrons in the entrance foil and the sensor. The fractional loss of counts is dependent upon the pitch angle distributions and the energy spectra of the electrons. No corrections for this decrease in detection efficiency were made. The magnitude of the effect in terms of electron flux or energy deposition rate was always less than a factor of 2, and its inclusion would have had a relatively small effect on the derived rates of energy deposition into the atmosphere from short-duration bursts in comparison to that from electrons in the drift loss cone; that ratio was about 10^{-2}. The recognition of coincidence events at both satellites and the derivation of the spatial extent of individual bursts would be virtually unaffected.

EXPERIMENTAL RESULTS

Previously, a study was made of the energy spectra of fast rise events observed from the S81-1 spacecraft [*Imhof et al.*, 1986]. These events were identified by requiring that the counting rate in the ME 1 spectrometer increased by at least a factor of 2 in less than 1 s and the subsequent decay be such that the flux remained high for no longer than 3 s. Three examples of such events, as observed in the ME 1 and the TE 2 spectrometers, are shown in Figure 1. Characteristics of the nightside short-duration bursts, including their favored occurrence at certain longitudes in the northern hemisphere, indicate that they are predominantly associated with lightning [*Voss et al.*, 1984; *Imhof et al.*, 1986]. In the initial survey performed for $L = 2$–3 a total of 222 bursts were found, 102 in the daytime and 120 at night.

Data were being acquired in the electron spectrometers on the NOAA 6 spacecraft at the times when most of the bursts were observed from the S81-1 spacecraft. Because of different orbital parameters there was considerable variation in the relative positions of the two satellites at the times when short-duration events were identified in the S81-1 data. For that subset of events observed by the SEEP payload which occurred during the local night and for which the NOAA 6 spacecraft was simultaneously at L values between 2 and 3 (a longitudinal separation between the spacecraft of about 45°) there were no coincident bursts observed in the NOAA 6 spectrometers [*Imhof et al.*, 1985]. The lack of coincident bursts under these selection criteria may have partly reflected the much lower sensitivity of the NOAA 6 instruments combined with the initial selection of events that were strong in the SEEP data and therefore probably centered close to that spacecraft. In some cases the negative response may have indicated that the precipitation event did not occur on the L shell locations of both spacecraft or that it occurred during the alternate 1-s off period of the NOAA 6 0° spectrometer.

This paper reports the results of a study which includes short-duration events that are weaker than the intense ones selected for the initial study of the S81-1 data. In the present investigation, both the NOAA 6 and the S81-1 data were surveyed for any statistically significant events that appeared in the nightside data when both spacecraft were in the range $L = 2.0$–3.5. The survey of S81-1 data was limited to the longitude interval 180° E to 360 E and to the northern hemisphere, since far fewer nighttime events were observed in the south during the previous study [*Imhof et al.*, 1986]. Simultaneous data from the NOAA 6 satellite were taken from both hemispheres at longitudes between 150 E and 345 E. Under these conditions a total coincident observation time of 6094 s in 54 passes of each satellite was examined. On 44 of these passes the NOAA 6 spacecraft was in the south, leaving 10 passes in the north.

Initially, counting rate versus time plots from the zenith detectors on the two satellites were surveyed at times for which both were in the range $L = 2.0$–3.5. Events were selected when (1) the counting rate increased in a time of about 2 s or less by at least 4 standard deviations in a normal error distribution of the peak rate (S81-1 data) or 2.65 standard deviations of the peak rate (NOAA 6 data) above a "background" rate taken from 1 536 s (S81-1) or 6 s (NOAA 6) before the event, (2) the enhanced counting rate was at least 10 counts/s and did not persist for longer than 3 s, and (3) the counting rate then decreased back to a level comparable to that present before the event. It was required that the "background" counting rate in the zenith detectors be less than 5000 counts/s (S81-1) or 400 counts/s (NOAA 6) to avoid identifying as events small fractional increases in the "background" rate. No coincidence events between the two satellites were prevented by these criteria. In general, the statistical uncertainties did not permit inclusion in the selection criteria of fine time scale variations characteristic of strong lightning-induced electron precipitation events [*Voss et al.*, 1984]. Under these conditions, at local nighttime, 21 NOAA 6 events and 76 S81-1 events were found. The smaller number of NOAA 6 events may result from the higher altitude and lower signal to background ratios for that vehicle, and it is certainly a consequence of the smaller geometric factor or 50% duty cycle and hence lower sensitivity of that instrument. The lower counting rates also led to the need for a lower standard deviation criterion for the NOAA 6 data. The total elapsed times for which the counting rates fell within acceptable limits for events were 3990 s and 5961 s in the NOAA 6 and S81-1 data, respectively. Based on these times and the requirement that there be at least two samples before and after an event, the number of events that might have resulted solely from statistical vari-

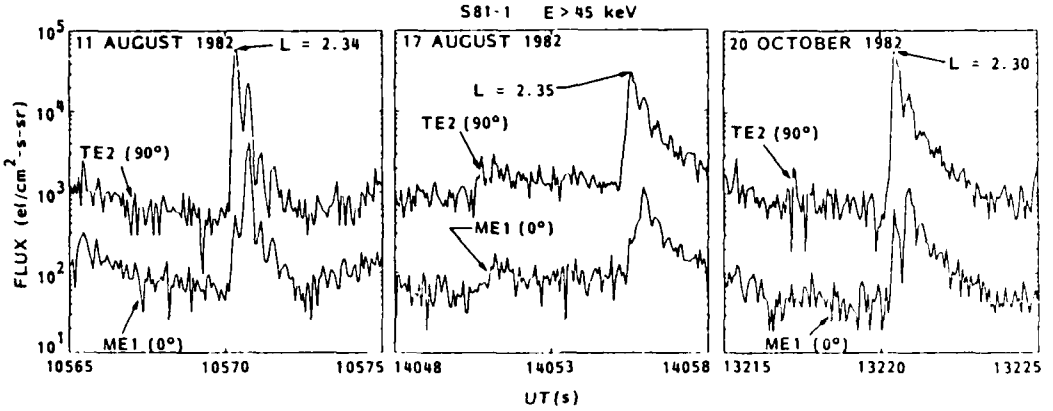

Fig. 1. Electron flux >45 keV versus time for three fast rise events observed at 90° and 0° zenith angles from the S81-1 spacecraft.

ations of the counting rate is calculated to be approximately 7 in the NOAA 6 data base and 0.4 in the S81-1 data. Of the 21 NOAA 6 events with more than 2.65 standard deviations, nine had more than 3.25 standard deviations and four had more than 4.0 standard deviations. For a normal distribution with 21 cases having more than 2.65 standard deviations the number of cases with more than 3.25 and more than 4.0 standard deviations would be 3.0 and 0.2, respectively. One concludes that many of the NOAA 6 bursts and virtually all of the S81-1 events are real and not merely due to statistical variations.

Many weaker events were included in the S81-1 data that were not considered in the previous study of fast rise events. The inclusion of nighttime events with smaller flux increases is illustrated in Figure 2. Here are shown the distributions in the factor of increase in counting rate during each event, separately for the cases studied in the previous investigation [*Imhof et al.* 1986] and those in the present compilations. The histogram labeled "S81-1 events (×2 criterion)" refers to events found in the previous survey, where it was required that the counting rate in the ME1 spectrometer increase by at least a factor of 2. The one labeled "S81-1 events" covers the bursts found in the

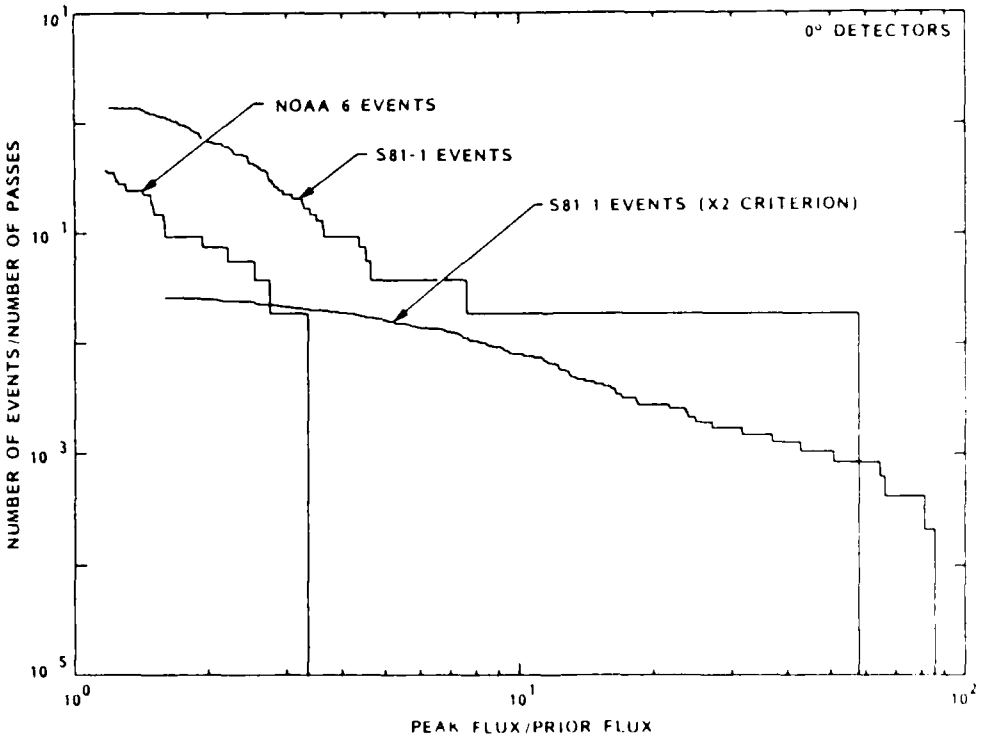

Fig. 2. The distributions in the factor increase of counting rate during short-duration bursts from surveys of the S81-1 data with two different criteria, and the survey of NOAA 6 data. The label "S81-1 events (×2 criterion)" refers to events found in the previous survey, where it was required that the ME 1 counting rate increased by at least a factor of 2. The label "S81-1 Events" covers events found in the recent survey.

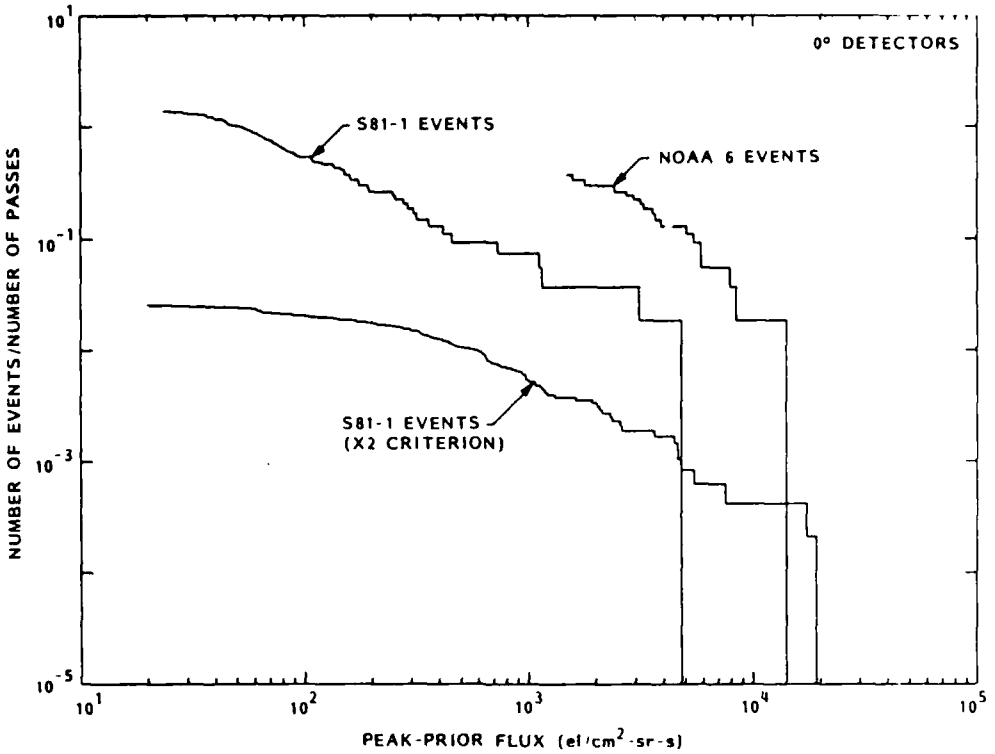

Fig. 3. The probability of the electron intensity in a short-duration event exceeding a given intensity plotted as a function of that intensity. The net precipitating electron fluxes are above an energy threshold of 45 keV (S81-1) or 30 keV (NOAA 6). The S81-1 events found with different selection criteria are plotted separately and are labeled as in Figure 2. The shapes of these integral event probability versus electron intensity curves closely follow an inverse electron flux curve, although there is a tendency for the distribution to flatten for very low intensity events.

recent survey using the criteria presented in the previous paragraph. By including weaker bursts it is now possible to study over a broader range the distributions in intensity and spectrum of events observed from both the S81-1 and the NOAA 6 spacecraft. This figure shows that when selecting only events in which the flux increased by at least a factor of 2 the distribution in peak flux/prior flux spanned larger values than when this criterion was not invoked.

The integral distributions in the net increase in precipitating fluxes of electrons above 45 keV (the S81-1 data) or above 30 keV (the NOAA 6 measurements) for those short-duration events occurring at nighttime are shown in Figure 3. In the previous survey of the S81-1 data, labeled "S81-1 events ($\times 2$ criterion)," for the selection of events it was required that the counting rate increase by at least a factor of approximately 2. In the present survey, labeled "S81-1 events," it was only necessary that the counting rate increase by 4 standard deviations. As one might expect, the distribution in net flux increases tends to favor larger values with the more demanding selection criteria. Each of the distributions has been normalized by dividing the number of events by the number of passes. In the previous study of short-duration bursts using the S81-1 observations [*Imhof et al.*, 1986] the primary interest was in the electron energy spectra, specifically the presence or absence of L-dependent peaks, the energies of the peaks when they appeared, and the comparisons with the peaks observed in the drift loss cone. Here we are concerned with other factors: the spatial extents of the bursts and the frequency of occurrence as a function of the absolute electron flux of the events. Previously, only rather strong bursts were selected from S81-1 observations taken over both the northern and southern hemispheres and at all longitudes. In the present study, all statistically significant events were selected from the S81-1 data, but only when the satellite was in the northern hemisphere at longitudes between 180°E and 360°E. Between the previous and present surveys the rates of occurrence of the stronger events in the S81-1 data are not inconsistent, although in the latter case the total time sampled was much smaller and the statistical uncertainties larger.

Because of the much smaller geometric factor of the NOAA 6 instruments one might expect to measure fewer events from that satellite. However, the upper ends of the flux distributions should be comparable between NOAA 6 and S81-1 when proper account is taken of the differing geographical positions and altitudes of sampling from the two satellites. Differences in the flux observed at the two satellites will result from significant differences in the equatorial pitch angles of the electrons being sensed by the zenith viewing detectors. For the satellite passes considered here, fluxes observed by NOAA 6 during an event are expected to be higher than those seen by S81-1. This difference is due to the fact that NOAA 6 at a higher altitude views electrons with larger equatorial pitch angles. Additional differences in the responses of NOAA 6 and S81-1 to the same event may occur because the two satellites were often in opposite hemispheres.

For various investigations, including calculations of the total precipitation rates of electrons associated with short-duration bursts, it is necessary to consider the relationship

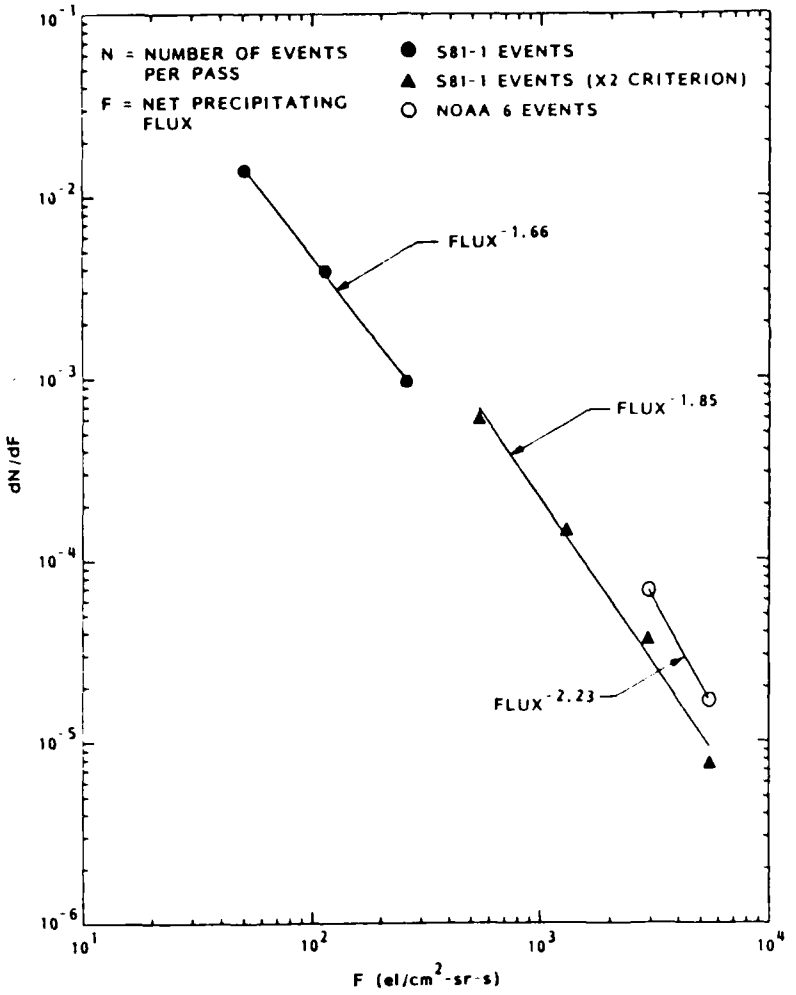

Fig. 4. Plot of dN/dF versus F, where N is the number of events per pass and F is the net precipitating flux. The net precipitating electron fluxes are above an energy threshold of 45 keV (S81-1) or 30 keV (NOAA 6). The two classes of S81-1 events are labeled as in Figure 2. The distributions are shown only for the larger events to exclude effects associated with the threshold criteria for classifying events. The ordinate for the S81-1 events with a factor of 2 criterion is arbitrarily normalized. Least squares fit power law distributions are also shown.

between the frequency of occurrence of events of a given intensity and the electron intensity. These data are shown in Figure 4 together with least squares fit slopes to the distributions for all of the measured values in the interval $L = 2.0$–3.5. The ordinate is dN/dF, where N is the number of events per pass and F is the net precipitating flux. The ordinate for the S81-1 events with a factor of 2 criterion, previous survey, is arbitrarily normalized. Points are only shown for the larger events to exclude effects associated with the threshold criteria for classifying events. The fits are close to an inverse square relationship for all three sets of data points. This relationship also holds for the low as well as for the high L shell portions of the interval. With the number of events per unit electron flux interval inversely proportional to the square of the flux, the energy input to the atmosphere per unit flux becomes inversely proportional to the flux. The upper limit to the electron flux clearly cannot exceed the maximum equatorial fluxes observed in other experiments over the L shell range of interest, nor can it exceed the average trapped fluxes observed in the present measurements. Therefore the best fit power law dependences between the event occurrence frequency and the event flux cannot be integrated over all fluxes without special consideration at both very low and very high fluxes.

The ratios between the electron flux at energies of >100 keV and >45 keV (>30 keV for the NOAA 6 data) for all the nighttime burst observed by the two satellites are plotted in Figure 5 as a function of the flux of >45 keV electrons (or >30 keV for NOAA 6). The two classes of S81-1 events are labeled the same as in the previous figures. This plot shows considerable scatter, and there is no evidence for a significant dependence of spectral hardness upon electron flux. This finding is consistent with that expected for wave-particle interactions involving whistlers having a given frequency distribution independent of wave intensity.

The ratio between the net increase in the precipitating electron flux and the flux of locally trapped electrons at the peak of the event for these nighttime events is plotted in Figure 6 as a function of the net increase of precipitating fluxes (at energies of >45 keV for the S81-1 cases and >30 keV for the NOAA 6 cases). The value of the locally trapped fluxes at the

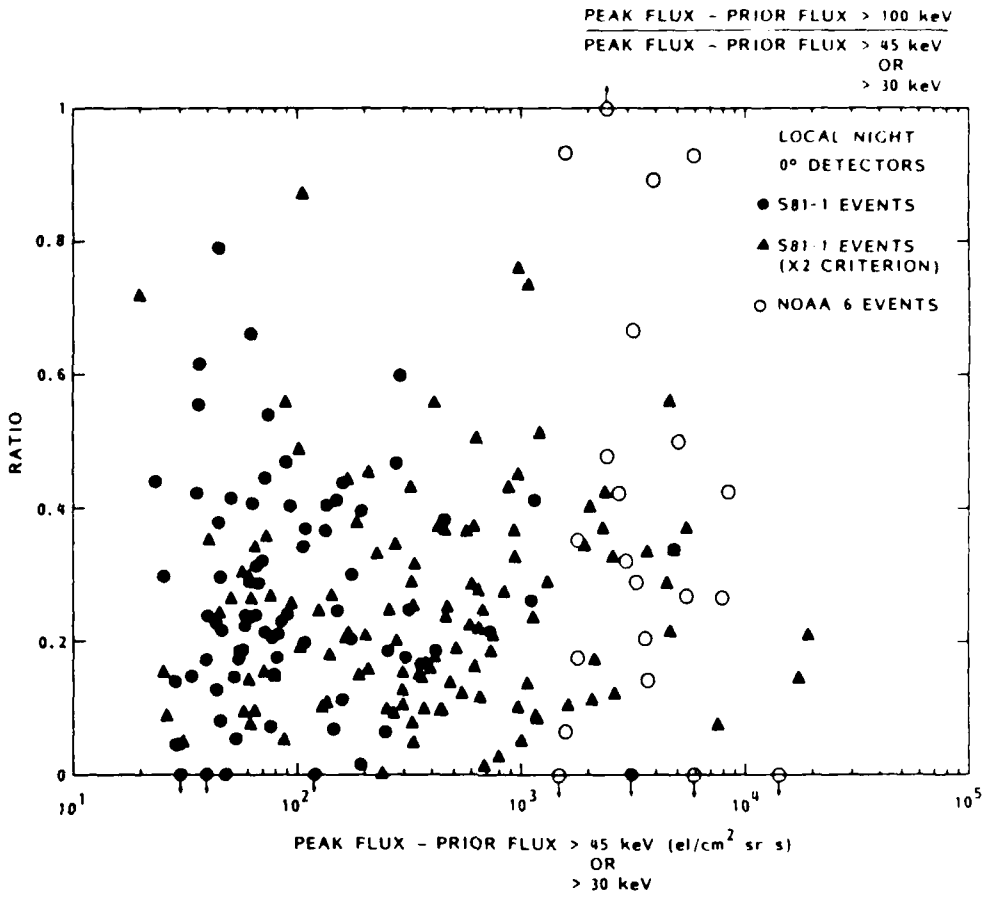

Fig. 5. The hardness of the precipitating electron energy spectrum, expressed as the ratio of the net precipitating electron flux at energies above 100 keV to that at energies above 45 keV (for S81-1) or 30 keV (for NOAA 6) plotted as a function of the peak electron intensity within an event. The two classes of S81-1 events are labeled as in Figure 2. There is no systematic relationship between the spectral hardness and the event intensity

peak of an event is used in preference to the net increase, because the fractional increase in trapped fluxes is generally very small during an event. One concludes from this plot that for the identifiable bursts the degree to which the loss cone is filled during a short-duration event is not strongly dependent upon the intensity of precipitating flux at energies above 45 keV (30 keV for the NOAA 6 events).

In order to obtain a measure of the spatial extents of the events we considered those that were observed simultaneously from both the S81-1 and the NOAA 6 spacecraft. An example of a good coincident event is shown in Figure 7. Within less than 1 s a short-duration burst was observed in both zenith-oriented instruments. At this time the spacecraft were on comparable L shells and separated by 42° geographic longitude, with both in the northern hemisphere.

There were a total of five instances when an event was observed simultaneously, to within 1.2 s, by the two spacecraft. For each of the NOAA 6 bursts the time differences between the NOAA 6 and S81-1 nighttime events are shown in histogram form in Figure 8. For eight NOAA 6 events, no bursts were observed on S81-1, and yet for these events both spacecraft were in the range $L = 2.3$-5 for a time interval of at least 18 s before and after the NOAA 6 burst. These cases are not included in the histogram. Five coincident events are simultaneous within ± 1.2 s. It should also be noted that there is a concentration of events at near coincidence. The favored occurrence of bursts at close times but not in coincidence may reflect electron precipitation associated with different lightning strokes at nearby times from the same storm. Based upon the frequency of events observed by the two spacecraft and the total simultaneous observation time of 6094 s, the number of accidental coincidences to within ± 1.2 s is calculated to be 0.6. Therefore most of the events observed simultaneously by both spacecraft are true coincidences rather than random.

Although the number of NOAA 6 events is limited, the data base permits one to estimate the lower limit of the extent of short-duration bursts. The differences in geographic longitude and invariant latitude between the location of S81-1 and NOAA 6 at the instant that an event was observed by NOAA 6 or by both of the satellites are shown in Figure 9, the solid circles being those nighttime events that were coincident within ± 1.2 s at both satellites. Other points are indicated by open circles. Each of the NOAA 6 events is represented by the positions of the two spacecraft at that time. Since all of the S81-1 events were selected to be in the northern hemisphere, the longitude differences are based upon the NOAA 6 location if that satellite was in the north or based upon the magnetic conjugate to NOAA 6 if that satellite was in the south. The

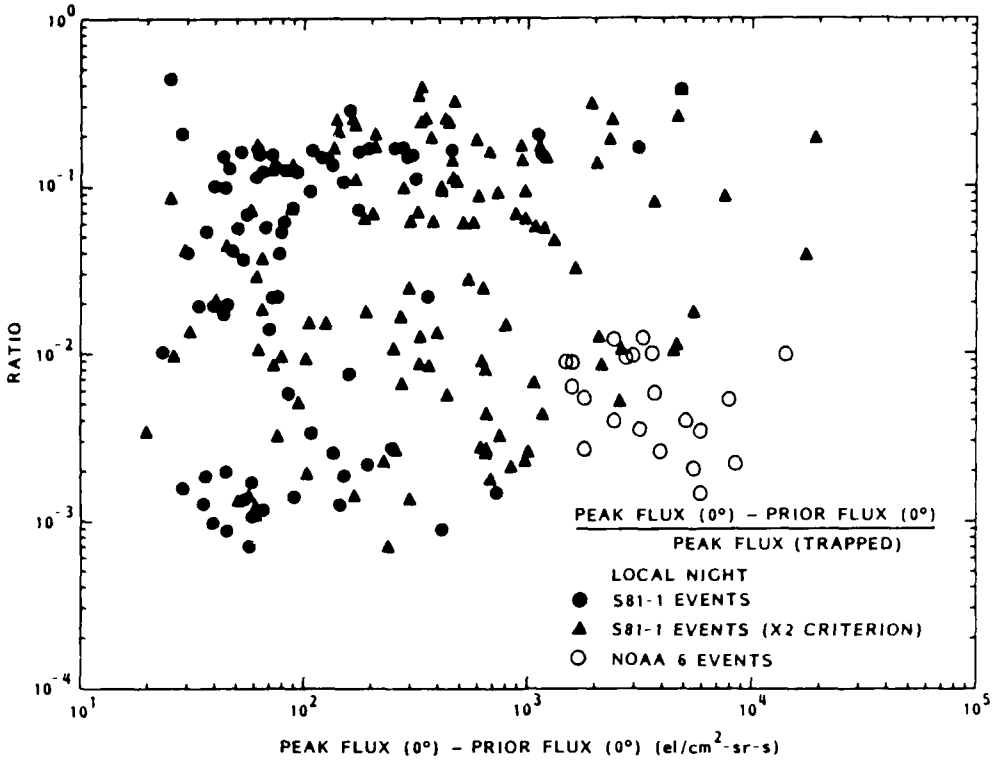

Fig. 6. A measure of the electron pitch angle distribution, expressed as the ratio between the net precipitating fluxes at energies above 45 keV (for S81-1) or 30 keV (for NOAA 6) and the locally trapped fluxes at the peak of the event, plotted as a function of the net precipitating fluxes during an event. The two classes of S81-1 events are labeled as in Figure 2. There is no systematic relationship between this intensity ratio and the intensity of the event.

preferred negative sign for the invariant latitude differences may reflect the known cutoff in whistler activity at L values below approximately 2, but it may also be merely a statistical variation in view of the small number of coincidence events. From Figure 9 one concludes that individual events can extend in longitude over as much as 43° and in invariant latitude over as much as 5°.

For each of the five events which were observed in coincidence by the two satellites the energy fluxes into the atmosphere were calculated using the observed energy spectra and pitch angle distributions of the precipitating electrons. The energy spectra were measured by both spacecraft with adequate resolution for this purpose. The pitch angle distributions were obtained with only coarse angular resolution, so it was not possible to include the contributions from electrons at the edge of the bounce loss cone in this calculation, as was done previously for electrons in the drift loss cone [*Gaines et al.*, 1986]. For the S81-1 data, use was made of the electron measurements at three different zenith angles (0°, 50°, and 90°) to construct a pitch angle distribution. The 81° detector on the NOAA 6 satellite generally measured trapped electrons and showed no clear response to a burst event, because the trapped electron intensities were relatively high. Hence the shape of the electron pitch angle distribution was taken to be identical to that of S81-1 during the same coincident event. The calculated energy depositions obtained from the measurements on each of the spacecraft during the five coincident events are summarized in Table 1. Some uncertainty in this tabulation results from the on-off cycling of the NOAA 6 instruments.

Discussion

The measurements presented here provide a basis for deriving the total loss rate of electrons from the radiation belts by short-duration bursts. The energy inputs to the atmosphere can be calculated, from which the associated riometer absorption and the effects on radio wave propagation can be estimated. However, the absorption effects detected by riometers would be relatively weak and not evident in available data. The energy deposition rates into the atmosphere from short-duration electron bursts have been calculated based on the observed distributions in flux, and for a representative pitch angle distribution and energy spectrum. The latter were taken from the measurements on day 291 at 10,080 s.

In order to be observed by the S81-1 spacecraft at altitudes of 170–280 km, electrons must have suffered a pitch angle scatter within one bounce period, which would range between a change of very nearly 0° to more than 1° in the equatorial plane, depending upon the longitude of the observation. The S81-1 data thereby included cases where observed electrons had undergone a very small scatter in pitch angle. Such a perturbation would appear to resemble the small angle scatterings that cause electrons to populate the drift loss cone. However, at locations where a pitch angle scatter of nearly 0° is sufficient to place an electron into the loss cone the background count rates are very high, and so only very strong burst events can be observed, and the contribution of very low intensity events to the precipitation cannot be evaluated. For this reason the frequency of occurrence of weak events and their relative importance to strong bursts events is beyond the

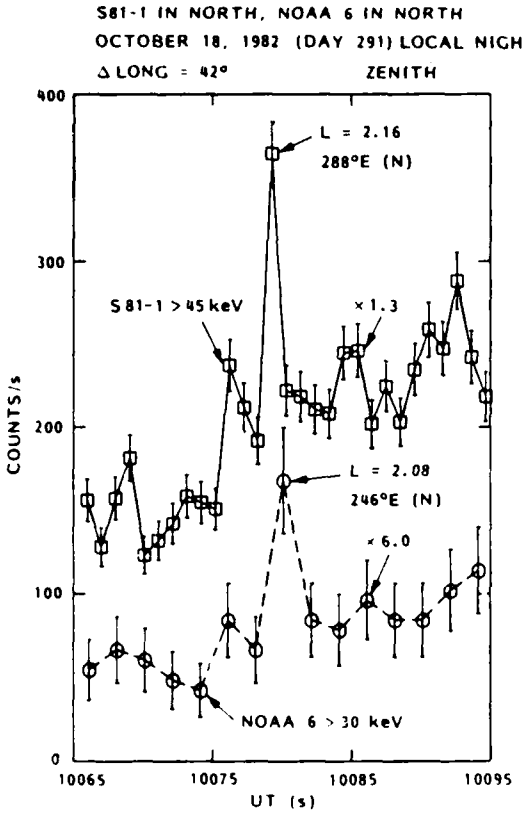

Fig. 7. An example of a coincident event observed in both the S81-1 and the NOAA 6 zenith instruments. The S81-1 points represent average counts per second in successive 1-s intervals, and these are interconnected by solid lines to indicate continuous coverage. The NOAA 6 points represent the counts recorded in alternate 1-s intervals and are interconnected by dashed lines to represent the 50% duty cycle for data coverage.

scope of the current observations. For the bursts observed from the NOAA 6 spacecraft at altitudes of 800–830 km the required pitch-angle scatterings were quite small. The S81-1 events were subdivided into different intervals for the equatorial pitch angle corresponding to the satellite position minus that at 100-km altitude in the conjugate hemisphere. For each of these groups of data the number of events above a given flux was found to be approximately inversely proportional to the flux as was the frequency of occurrence of bursts, although the statistical sample sizes of the groups were quite limited. This analysis indicated that the frequency of occurrence versus flux curve is not strongly dependent upon the minimum pitch angle scattering required for observation of an event. A careful assessment of the contributions from pitch angle scatterings of various magnitudes is not undertaken here, but the data suggest that the results of calculations of energy deposition into the atmosphere from burst events may not be altered in a major way by the inclusion of small angle scatterings.

From the S81-1 bursts the average rate of deposition of energy into the northern nightside atmosphere in the period June–December 1982 at a local time of ~2230 and over the longitude range 180°E to 360°E was found to be about 6×10^{-6} ergs/cm^2 s. In the southern hemisphere the average rate as measured from the NOAA 6 spacecraft was found to be about 1.5×10^{-5} ergs/cm^2 s. The latter energy deposition rate is small in comparison to the worldwide average of 10^{-3} ergs/cm^2 s at $L = 2.5$ in the southern hemisphere from precipitating electrons [*Imhof et al.*, 1986]. However, on the basis of the data presented here alone we cannot discount a major contribution from weak precipitation bursts to populating those electrons in the drift loss cone which ultimately precipitate into the atmosphere. Accurate estimates of this contribution are difficult to make, since extrapolation of the data presented here to weak bursts involves many unknowns, including the pitch angle distributions of very weak events. In central Europe, thunderstorms are known to occur more often in the early afternoon hours by perhaps a factor of 5 [*Israel*, 1973] than during the S81-1 nighttime observations at 2230. Nonetheless, such a local time variation is small in comparison to the aforementioned differences of a factor of 10^2. If the $1/\text{flux}^2$ relationship in Figure 4 holds true over a much wider flux range than shown, in addition to the number of bursts per second being higher, the total energy input to the atmosphere could be significantly greater. With a $1/\text{flux}^2$ dependence for the number of events per unit flux the number times the flux of bursts varies as $1/\text{flux}$, and the integral flux above a given level varies logarithmically. The number of events times their flux can at most approach the observed average fluxes. It is possible that the rather steady input to the atmosphere from electrons in the drift loss cone could result primarily from many weak precipitation bursts, but the data presented here do not extend to such events.

To obtain the average total rates of energy input to the atmosphere from short-duration bursts, it is not necessary to know the area of precipitation during each individual event, but one need only measure the average inputs to the atmosphere at positions of interest. However, for studies of the

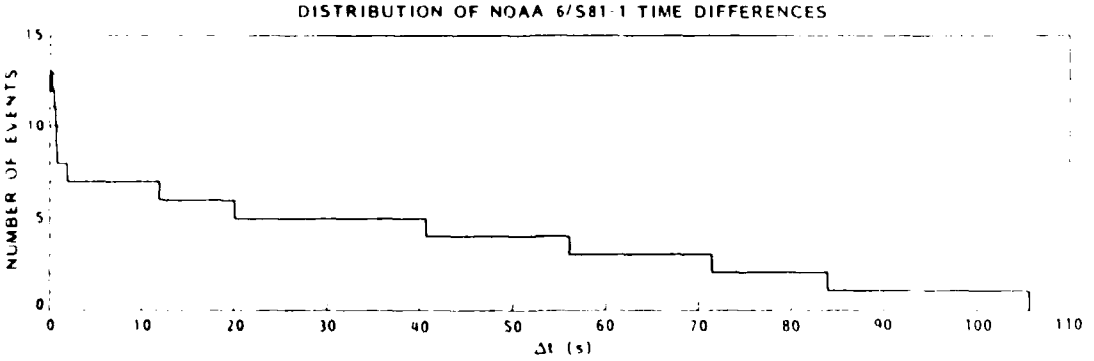

Fig. 8. Integral distribution of the time differences between events observed from the NOAA 6 and the S81-1 satellites.

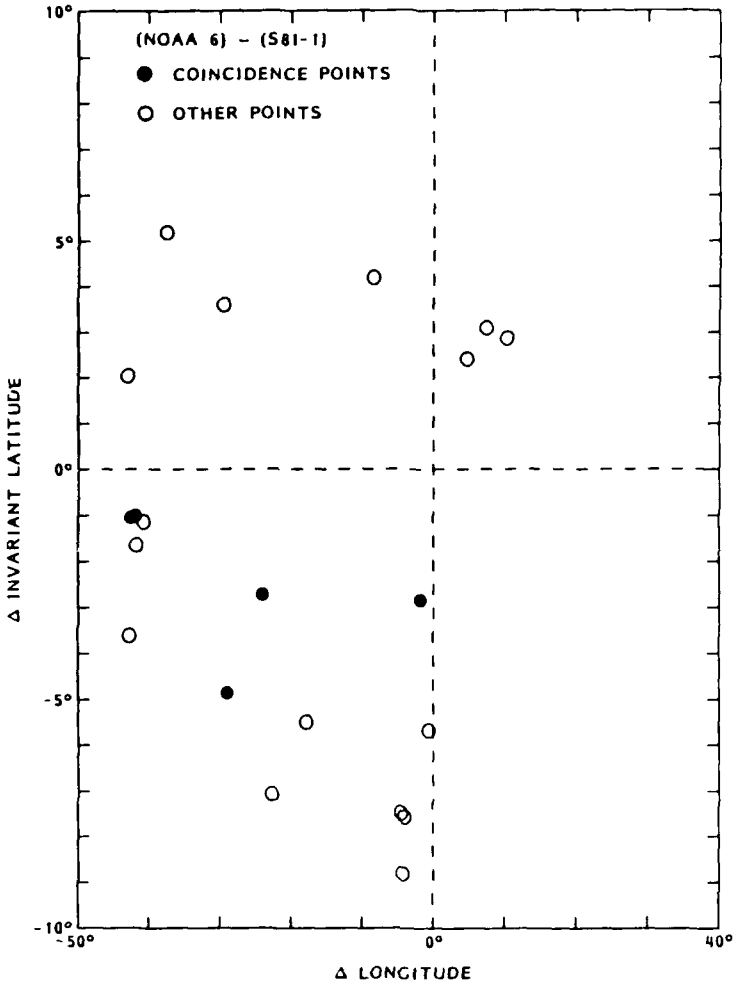

Fig. 9. The longitude and invariant latitude differences between the S81-1 and the NOAA 6 positions for coincident events and for cases in which a burst was not observed in the S81-1 data. Each of the NOAA 6 events is represented by the positions of the two spacecraft at the time of the event.

physics of the precipitation phenomena and of the effects of electron precipitation events on radio wave propagation, such as in the Trimpi effect [*Carpenter et al.*, 1984] it is necessary to know the spatial extent of individual precipitation events. Fewer electron precipitation bursts that are very widespread may have a larger impact on subionospheric wave propagation than would more bursts that are very localized but with the same total energy input to the atmosphere. The two-satellite measurements presented here are useful for such studies, but clearly, better statistics and more detailed measurements of the extent separately in longitude and L shell are needed. A two-position measurement leaves partially unanswered both the spatial extent and the intensity profile of the precipitation during individual events.

Information on the spatial extents of individual precipitation events can be obtained from detailed analysis of Trimpi events [*Carpenter et al.*, 1984]. A more straightforward approach would be through use of remote imaging techniques

TABLE 1. Energy Deposition

Day Number, 1982	Time, s	Hemisphere		L Value		NOAA 6 Longitude in the North, °E	Longitude Difference,* deg	At Position of S81-1 Satellite, ergs/cm²	At Position of NOAA 6 Satellite ergs cm²	S81-1 / NOAA 6
		S81-1	NOAA 6	S81-1	NOAA 6					
220	25,000	N	S	2.48	2.22	223	1	1.7×10^{-3}	6.8×10^{-3}	0.25
249	80,637	N	S	2.26	2.19	308	43	6.1×10^{-5}	4.8×10^{-3}	0.013
267	281	N	S	2.59	2.14	297	30	1.2×10^{-4}	2.8×10^{-3}	0.043
291	10,080	N	N	2.16	2.08	246	42	1.3×10^{-4}	1.4×10^{-3}	0.09
309	824	N	S	3.37	2.96	298	25	2.7×10^{-4}	3.0×10^{-3}	0.09

*S81-1 longitude in the north minus NOAA 6 longitude in the north.

such as bremsstrahlung X ray mappings performed from a satellite. The latter technique has been repeatedly demonstrated for high-latitude phenomena [*Imhof et al.*, 1974; *Mizera et al.*, 1978; *Voss et al.*, 1983], but burst events in the slot region are relatively weak compared to auroral fluxes. However, the rapid rise and short duration of burst precipitation events can be used to aid discrimination against background, and it should be possible to map the precipitation region with this technique.

Acknowledgments. The SEEP payload on the S81-1 spacecraft was sponsored by the Office of Naval Research (contract N00014-79-C-0824). Launch and orbital support were provided by the Air Force Space Test Program Office. The data analysis presented here was supported by the Office of Naval Research and by the Lockheed Independent Research Program. Appreciation is extended to D. W. Datlowe for his contributions and to J. P. McGlennon for his effort in processing the data. We also acknowledge the contribution of V. J. Hill, who wrote the program which reduced and archived the NOAA 6 data. Helpful discussions with M. Walt are greatly appreciated.

The Editor thanks A. Saint-Marc and P. Tanskanen for their assistance in evaluating this paper.

REFERENCES

Carpenter, D. L., U. S. Inan, M. L. Trimpi, R. A. Helliwell, and J. P. Katsufrakis, Perturbations of subionospheric LF and MF signals due to whistler-induced electron precipitation bursts, *J. Geophys. Res.*, *89*, 9857, 1984.

Cornwall, J. M., Scattering of energetic trapped electrons by very-low-frequency waves, *J. Geophys. Res.*, *69*, 1251, 1964.

Dungey, J. W., Loss of Van Allen electrons due to whistlers, *Planet. Space Sci.*, *11*, 591, 1963.

Gaines, E. E., W. L. Imhof, W. E. Francis, M. Walt, and T. J. Rosenberg, Correlated electron and X ray measurements of quiet time electron precipitation: A comparative study of bremsstrahlung production and transport in the atmosphere, *J. Geophys. Res.*, *91*, 13,455, 1986.

Goldberg, R. A., J. R. Barcus, L. C. Hale, and S. A. Curtis, Direct observation of magnetospheric electron precipitation stimulated by lightning, *J. Atmos. Terr. Phys.*, *48*, 293, 1986.

Imhof, W. L., G. H. Nakano, R. G. Johnson, and J. B. Reagan, Satellite observations of bremsstrahlung from widespread energetic electron precipitation events, *J. Geophys. Res.*, *79*, 565, 1974.

Imhof, W. L., H. D. Voss, J. Mobilia, and D. S. Evans, The spatial extent of lightning and chorus electron precipitation bursts in the slot region (abstract), *Eos Trans. AGU*, *66*, 1039, 1985.

Imhof, W. L., H. D. Voss, M. Walt, E. E. Gaines, J. Mobilia, D. W. Datlowe, and J. B. Reagan, Slot region electron precipitation by lightning, VLF chorus, and plasmaspheric hiss, *J. Geophys. Res.*, *91*, 8883, 1986.

Israel, H., *Atmospheric Electricity*, vol. II, *Fields, Charges, Currents*, p. 365, Israel Program for Scientific Translations, Jerusalem, 1973.

Mizera, P. F., J. G. Luhmann, W. A. Kolasinsky, and J. B. Blake, Correlated observation of auroral arcs, electrons, and X rays from a DMSP satellite, *J. Geophys. Res.*, *83*, 5573, 1978.

Oliven, M. N., and D. A. Gurnett, Microburst phenomena, 3, An association between microbursts and VLF chorus, *J. Geophys. Res.*, *73*, 2355, 1968.

Roberts, C. S., Electron loss from the Van Allen zones due to pitch angle scattering by electromagnetic disturbances, in *Radiation Trapped in the Earth's Magnetic Field*, edited by B. M. McCormac, p. 403, D. Reidel, Hingham, Mass., 1966.

Rycroft, M. J., Enhanced energetic electron intensities at 100 km altitude and a whistler propagating through the plasmasphere, *Planet. Space Sci.*, *21*, 238-251, 1973.

Voss, H. D., J. B. Reagan, W. L. Imhof, D. O. Murray, D. A. Simpson, D. P. Cauffman, and J. C. Bakke, Low temperature characteristics of solid state detectors for energetic x-ray, ion and electron spectrometers, *IEEE Trans. Nucl. Sci.*, *NS-19*, 164, 1982.

Voss, H. D., W. L. Imhof, J. B. Reagan, R. R. Vondrak, M. Walt, J. Mobilia, D. W. Datlowe, D. P. Cauffman, W. Calvert, and R. G. Joiner, SEEP X-ray imagery of the earth's aurora (abstract), *Eos Trans. AGU*, *64*, 792, 1983.

Voss, H. D., W. L. Imhof, M. Walt, J. Mobilia, E. E. Gaines, J. B. Reagan, U. S. Inan, R. A. Helliwell, D. L. Carpenter, J. P. Katsufrakis, and H. C. Chang, Lightning-induced electron precipitation, *Nature*, *312*, 740, 1984.

D. S. Evans, National Oceanic and Atmospheric Administration, Boulder, CO 80303.

E. E. Gaines, W. L. Imhof, J. Mobilia, and H. D. Voss, Lockheed Palo Alto Research Laboratory, Palo Alto, CA 94304.

(Received September 10, 1986;
revised November 19, 1986;
accepted December 4, 1986.)

END

FILMED

MARCH, 1988

DTIC